NASA CR-165310
VOUGHT REPORT 2-53020/1R-52726

ADDITIONAL TESTING OF THE INLETS DESIGNED FOR A TANDEM FAN V/STOL NACELLE

ANDRES H. YBARRA

Contract NAS3-21468
June 1981

VOUGHT CORPORATION

NASA

NASA CR-165310
VOUGHT REPORT 2-53020/1R-52726

ADDITIONAL TESTING OF THE INLETS DESIGNED FOR A TANDEM FAN V/STOL NACELLE

by
Andres H. Ybarra

June 1981

Prepared Under Contract No. NAS3-21468
by
Vought Corporation
Dallas, Texas
75265

for
Lewis Research Center
National Aeronautics and Space Administration
Cleveland, Ohio
44135

TABLE OF CONTENTS

LIST OF FIGURES

LIST OF TABLES

1.0 Summary

An approximately 0.25 scale model of a Tandem Fan nacelle designed for a Type A (Subsonic Cruise) V/STOL aircraft configuration has been tested in the NASA Lewis Research Center 10-by-10 foot (3.048 by 3.048 meter) wind tunnel. Twelve-inch (.3048 meter) tip driven turbofans were used to provide the suction source for the front and aft inlets. A series of three tests have been conducted - isolated front inlet, isolated aft inlet, and combined front and aft inlets. The performance for the isolated aft inlet has been reported previously, Reference 2. The performance for the isolated front inlet and for the combined front and aft inlets is reported herein. Model variables include front and aft inlets with aft inlet variations of short and long aft inlet cowls, with a shaft simulator and diffuser vortex generators, cowl lip fillets and nacelle strakes. Inlet pressure recovery, distortion, and inlet angel-of-attack separation limits were evaluated at tunnel velocity from 0 to 240 knots (123.5 m/s), angles-of-attack from -10 to +40 degrees and inlet flow rates corresponding to throat Mach number from 0.0 to 0.6. Combined nacelle pitch and yaw runs up to 30^{0} were also made.

High efficiency inlet performance and stable operation were verified at all design forward speed and angle-of-attack conditions. The interference effects between front and aft inlet were minimal and favorable. The clean long aft inlet total pressure recovery is approximately 99% at zero degrees angle-of-attack throughout the transition speed range (0 - 135 knots). The recovery level decreases about 1% at 40^{0} angle-of-attack and 135 knots. With the shaft simulator and vortex generators present, the performance levels are approximately 0.5% lower. The clean short aft inlet total pressure recovery is approximately 100% at zero degrees angle-of-attack through the transition speed range. At 135 knots and 40^{0} angle-of-attack the recovery level is still at 98%. Addition of fillets at the lower corners reduces the performance levels. However, with the nacelle strakes installed, the high speed, high angle-of-attack recovery is still 98%.

2.0 Introduction

V/STOL aircraft require propulsion system inlets which can operate over a wide range of flight speeds, mass flow and angles-of-attack and yaw. In addition, these configurations require nozzles which can provide high thrust coefficients and efficient turning over a wide range of deflection angles. Requirements placed on the inlets and nozzles can be especially severe due to the operating environment on board various types of combat ships. Thus considerable research and configuration development is required to design inlets and nozzles for such an application.

The V/STOL aircraft being developed by the Vought Corporation for Navy Type A (Subsonic Cruise) applications employs a tandem fan propulsion system arranged in two nacelles, integrated structurally with the fuselage. Each nacelle contains a complete propulsion unit consisting of a core engine, two fixed pitch fans with variable inlet guide vanes, and associated inlets and nozzles (Figure 1). The fans are located ahead of the core engine and are mounted co-axially with the engine. Small fan diameters result from the use of two fans in each nacelle. A vectoring nozzle for the front fan and an inlet for the aft fan are incorporated between the two fans. Flow through the two fans is maintained separate at all times. The core engine is located immediately behind the aft fan and is supercharged by it. The core and aft fan flows are mixed and discharged through a vectoring nozzle.

Flow paths through the Tandem Fan nacelle are shown in Figure 2. During conventional flight, fan flows are vectored directly aft. For VTOL, nozzles are repositioned as shown to vector thrust vertically. Intermediate thrust vector angles are achieved by corresponding intermediate positions of each nozzle. Thrust vector response is rapid and smooth transitions are achieved by the control forces achievable through combined thrust modulation and vectoring.

The inlets have been designed to provide good performance and low distortion in a minimum length. Large inlet lip radii are used for good takeoff and V-Mode performance and to reduce inlet flow distortion. The front inlet incorporates a close coupled inlet, fan, and nose cap for improved crew visibility. The aft inlet has been arranged to benefit from the favorable

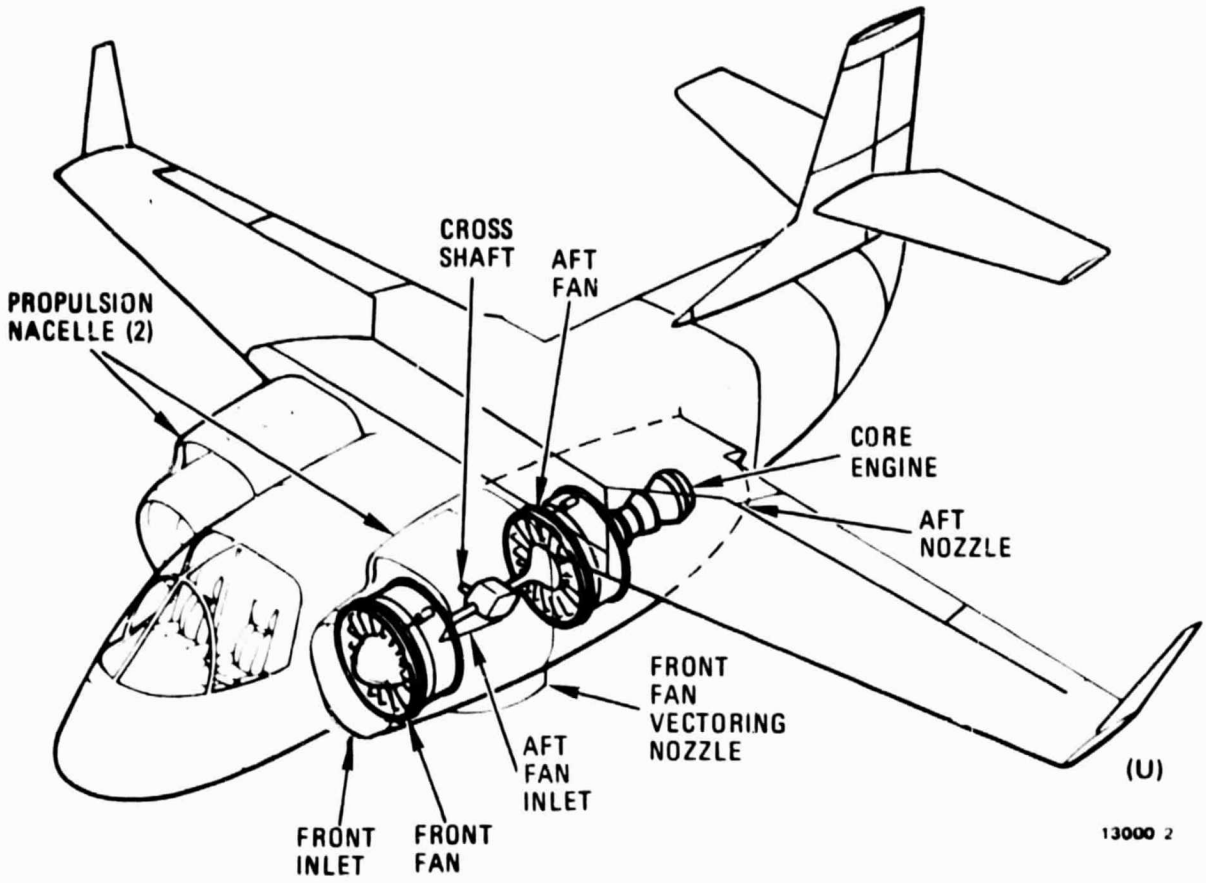

FIGURE 1 V/STOL TYPE "A" TANDEM FAN POWERED AIRCRAFT

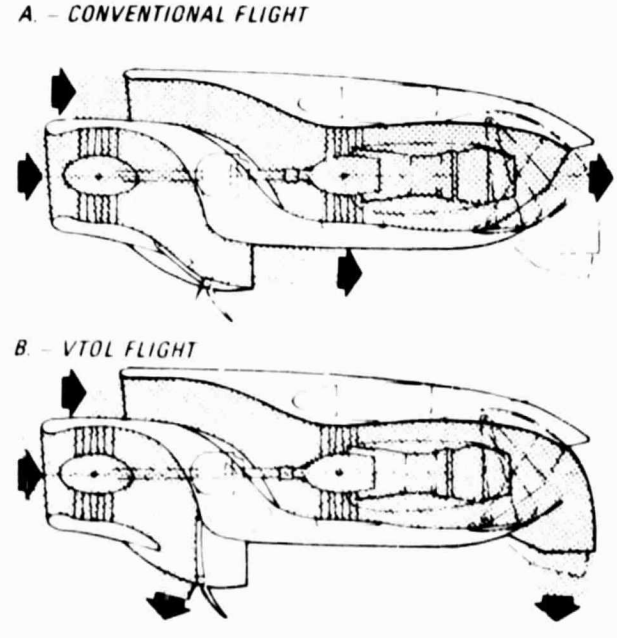

FIGURE 2 SINGLE STAGE TANDEM FAN NACELLE

flow field of the front inlet and to integrate well into the nacelle. Low difussion rates and high turning of the flow through the bend to the aft fan has been provided to reduce losses and flow distortion.

The nozzles are designed to provide high thrust coefficients and efficient turning of the flow over a range of deflection angles from 0^0 (cruise) to 110^0 (V/STOL). The forward nozzle, which is two-dimensional for good integration with the nacelle and ease in vectoring, uses a simple two-piece deflector to vector thrust. Variation of nozzle area in cruise is achieved with a small flap mounted on the nacelle surface. The aft nozzle, which vectors mixed flow from the core engine and the aft fan, is two-dimensional for ease in vectoring the flow. The nozzle deflector is hinged along the lower portion of the nacelle and is rotated downward for V/STOL. A rotating lower flap is used to achieve the nozzle areas required for cruise.

Several years ago NASA Lewis Research Center (LeRC) and the Vought Corporation began a research effort to develop a broad data base for the design of the inlet and nozzle systems that will contribute to an effective, efficient, lightweight low drag Tandem Fan propulsion system that operates satisfactorily at the conditions applicable to the Navy Type A V/STOL aircraft.

This Vought report covers, under contract NAS3-21468 (Reference 1), the performance evaluation of the combined inlet model by NASA Lewis in the 10-by-10 foot (3.048-by-3.048 meter) wind tunnel. The aft inlet model is described in Reference 2.

3.0 SYMBOLS AND ABBREVIATIONS

A_{CAP}	Capture area
A_E	Fan exit area
A_{HI}	Hilite area
A_{MAX}	Area at maximum cowl diameter
A_{TH}	Throat area
BID	Blow-in door
DC60	Inlet Distortion Index (Ref. 9)
D_{HI}	Hilite equivalent diameter
D_{MAX}	Maximum inlet equivalent diameter
D_{PT}	Maximum inums minimum total pressure at fan rake station
D_{SPILL}	Inlet spillage drag
D_{TH}	Throat equivalent diameter
H.L.	Hilite
IDC	Inlet distortion index (Ref. 9)
IDR	Inlet distortion index (Ref. 9)
KD_2	Inlet distortion index (REf. 9)
$K\theta$	Inlet distortion index (Ref. 9)
LeRC	National Aeronautics and Space Administration Lewis Research Center

LNG	Long
$\dot{m}$	Inlet airflow
$\dot{m}_o$	Airflow based on free stream conditions
M_{AF}	Aft Fan Mach number
MAX-MIN	Inlet distortion index. PTMAX-PTMIN/PTAV
M_{FAN}	Fan face Mach number
M_{FF}	Front Fan Mach number
M_o	Freestream Mach number
M_{TH}	Throat Mach number (MTHROAT)
P_s	Individual tap static pressure
P_T	Individaul probe total pressure
P_{TAV}	Average total pressure at fan rake station
P_{TFAN}	Fan face total pressure
P_{TMAX}	Maximum total pressure probe reading at fan face
P_{TMIN}	Minimum total pressure probe reading at fan face
P_{TO}	Free stream total pressure
q_o	Free stream dymanic pressure
REC	Inlet total pressure recovery, PTAV/PTO
RMS	Root mean square pressure level

RPMC	Fan corrected RPM, $N/\sqrt{\theta}$
S	Surface distance along inlet wall measured from hilite
SHF	Shaft Simulator
VG	Vortex generator
V_o	Free stream velocity
W	Inlet airflow to fan
X	Inlet axial distance
Y	Inlet vertical distance
α	Angle-of-attack, also ALPHA, degrees
δ	Ratio of total pressure to sea level static pressure
θ	Ratio of total temperature to standard data temperature, or equivalent diffuser conical half angle, degrees
ψ	Angle of yaw, degrees

SUBSCRIPTS

dd	Drag divergence
FAN	Fan
HI	Hilite
MAX	Maximum
0	Freestream
S	Static
T	Total
TH	Throat
2	Fan Discharge

4.0 Program Objectives and Description

The objectives of this test program were to develop a broad data base for the design of aft inlet systems that will contribute to an efficient, light weight, low drag tandem fan propulsion system that operates satisfactorily at the conditions applicable to the U.S. Navy Type A V/STOL aircraft. The primary area of investigation was to determine the interference effects between front and aft inlets and to verify the isolated front inlet performance.

The model hardware was designed to be compatible with installation in the NASA Lewis Research Center wind tunnels. Inlet testing was conducted using a government-furnished twelve-inch (.3048 meter) diameter Tech Development tip turbine fan.

The isolated front inlet model was tested over a range of flight speeds from 0 to 135 knots (69.5 m/s). Angle-of-attack was varied from -10^0 to 40^0. Inlet flow rates corresponding to throat Mach number up to 0.5 were evaluated at the above tunnel conditions.

Isolated aft inlet model was tested over a range of flight speeds from 0 to 240 knots. Angle-of-attack was varied from -10^0 to 40^0. Inlet flow rates corresponding to throat Mach numbers up to 0.5 were evaluated at the above tunnel conditions. Configuration variables included a fan shaft simulator, duct vortex generators and blow-in doors. These results are reported in Reference 2.

The combined inlet model was tested over a range of flight speeds from 0 to 240 knots (124 m/s) with angle-of-attack variation from 10 to + 40 degrees, also. Inlet flow rates for front and aft inlet were varied from 0 to 0.6 throat Mach number, with both matching and non-matching flow rates. Some combined pitch and yaw runs up to 30^0 were also conducted to evaluate the effect of cross flow upon aft inlet performance.

The inlet configurations were evaluated in terms of engine face total pressure recovery and distortion, inlet angle-of-attack and separation limits. Recovery and distortion were evaluated with a multitube total pressure rake located at the fan face station with the twelve-inch (.3048 meter) fan located downstream of the fan face station. Both steady state and dynamic pressure measurements were obtained.

5.0 Test Apparatus

This section describes the Tandem Fan nacelle model and the associated instrumentation. In addition, the NASA Lewis wind tunnel test facility, test conditions, procedures, and data reduction requirements are also described.

5.1 Model Description

The nacelle model is an approximately 0.25 scale geometric representation of the full scale Tandem Fan nacelle and consists of both front and aft-mounted inlets and a tip turbine drive turbofan for each inlet duct. Appropriate cowlings and fairings were designed and fabricated into a wind tunnel test article. A photograph of the complete nacelle is shown in Figure 3.

Inlets

The inlet models for this program were designed by Vought to conform to the Vought V-530 Tandem Fan configuration. The inlet configurations were designed to produce maximum performance during vertical take-off, while minimizing drag penalties during cruise and loiter. The inlet design conditions corresponding to take-off, landing, and transition are presented in Table I.

TABLE I INLET DESIGN CONDITIONS

	Vertical Operation	Transition Flight
M_{FAN}	0.5	0.2 - 0.6
α_{MAX}	---	30^0
ψ_{MAX} (35 kt. crosswind	90^0	90^0
V_0	---	0 - 150 kts. (0 - 77.2 m/s)

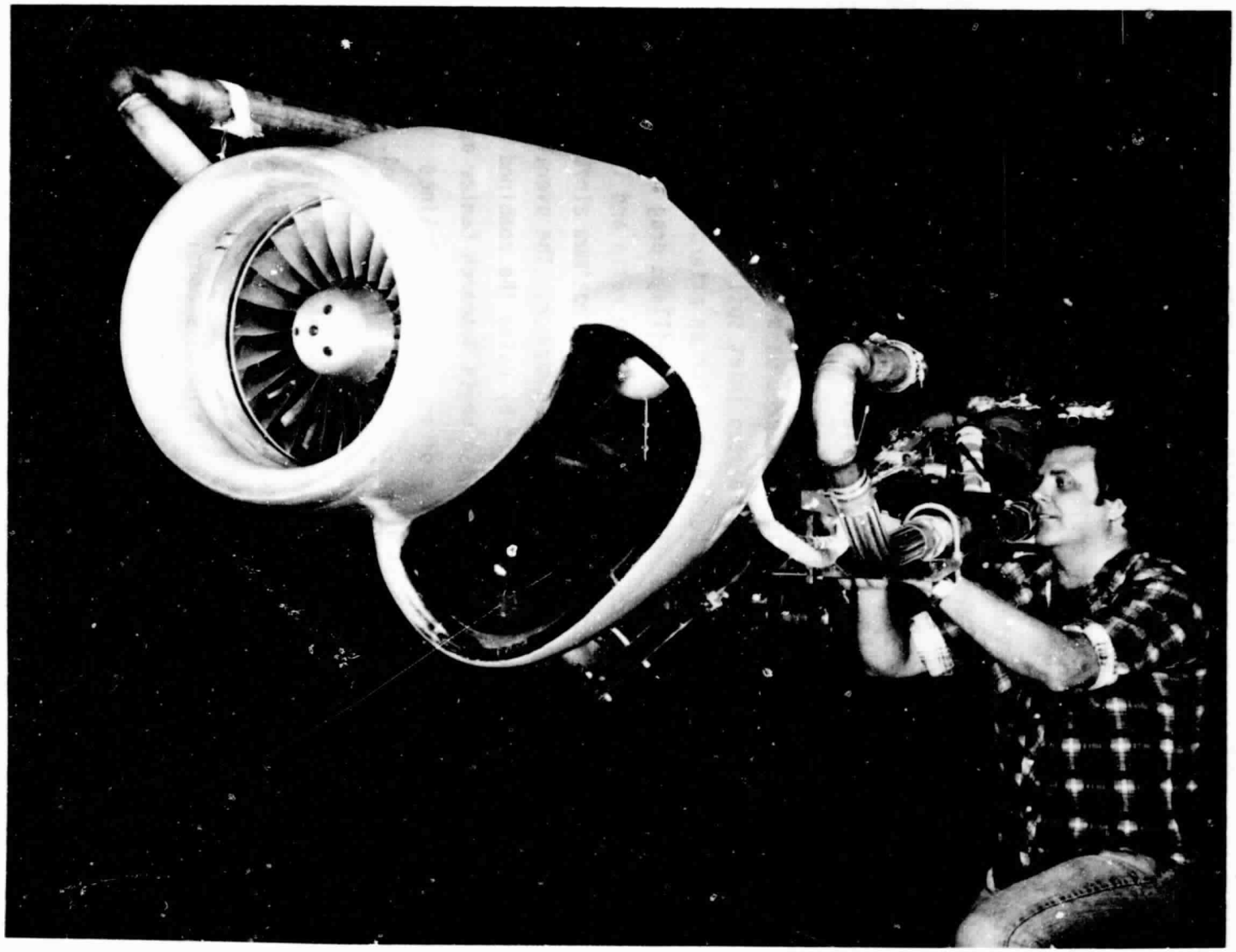

FIGURE 3. TANDEM FAN FRONT AND AFT INLET MODEL INSTALLED IN NASA LEWIS RESEARCH CENTER 10-BY-10 FOOT WIND TUNNEL.

Front Inlet

To meet the design conditions of Table I, the Front inlet shape was defined in terms of contraction ratio, lip geometry and shape, and throat area. Preliminary inlet design studies, using existing test data of reference 3 and 4 indicated a contraction ratio (A_{HI}/A_{TH}) of 1.46 was required to satisfy the low speed requirements, specifically the cross-wind conditions of Table I. However, for high speed operation a lower contraction ratio, and thinner lip, was desired to minimize inlet cruise and loiter drag. Lip shape studies were next performed using the test data of References 3 and 4. Several selected lip shapes meeting the V/STOL requirements of Table I were then evaluated in terms of high speed cruise and loiter drag levels based on the data in references 5 and 6.

Figure 4 identifies the external lip area ratio (A_{MAX}/A_{HI}) of 1.22, forebody diameter ratio (D_{HI}/D_{MAX}) of 0.91 and forebody length ratio (X/D_{MAX}) of 0.3 selected and their relation to high speed mass flow and drag divergence levels. Figure 5 illustrates the predicted inlet spillage drag levels as a function of mass flow ratio and Mach number for an external lip area ratio of 1.22. The cruise power mass flow ratio and spillage drag are shown in the figure for reference. With the inlet contraction ratio and lip geometry selected, the inlet throat area was sized to provide maximum airflow during cruise flight at approximately a 0.65 throat Mach number. The overall diffuser lines were then established through analysis by using the combined potential and viscous flow routine developed by NASA Lewis Research Center and Vought (Reference 7). Figure 6 shows a schematic of the basic inlet lines while Figure 7 shows the diffuser area distributions selected for the model.

A photograph of the front inlet (isolated) nacelle model installed in the NASA Lewis Research Center 10-by-10 foot wind tunnel is shown in Figure 8.

Figure 9 shows a schematic of the front inlet nacelle model assembly. For the first test entry the fan face total pressure rake was located in the front inlet airstream to measure front inlet performance. In the second test entry, the front inlet was replaced by a forebody cap so that the performance of the aft inlet alone could be obtained. And in the current test entry the performance of the aft inlet with both front and aft inlets in operation was measured.

Forebody Length Was Compromised to
Allow for 1.5 in. Cylindrical Spacer.

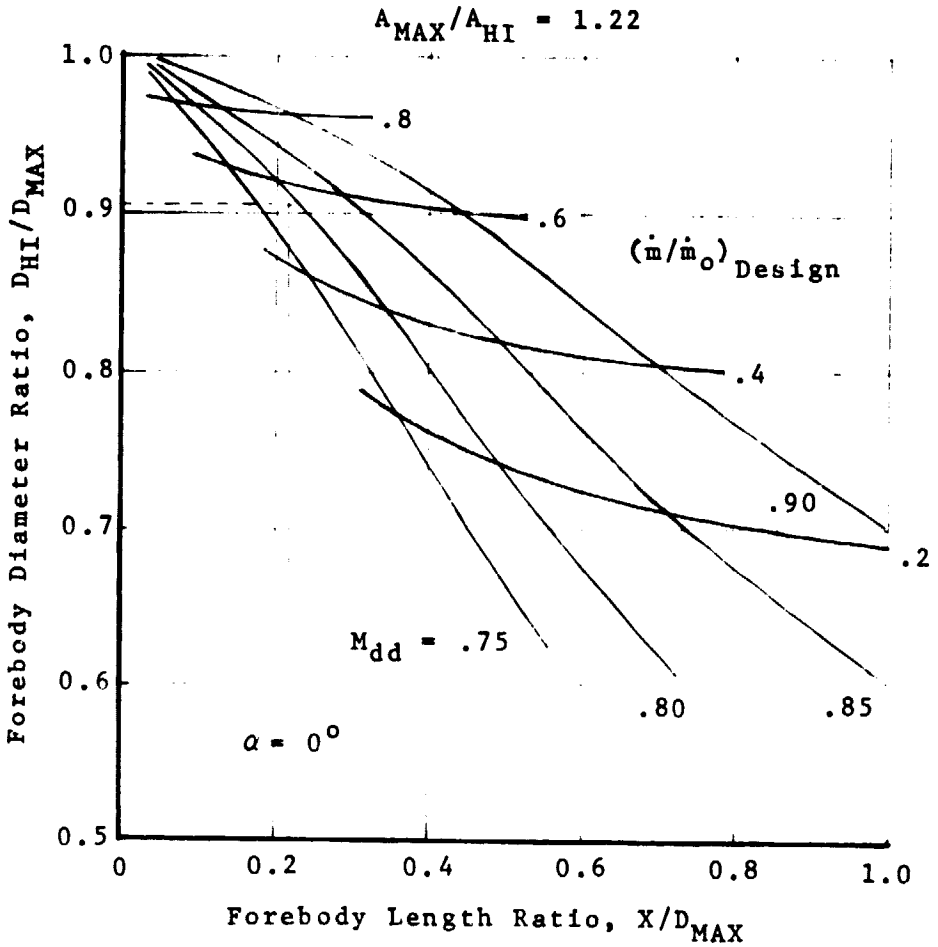

FIGURE 4. FRONT INLET EXTERNAL LIP CHARACTERISTICS.

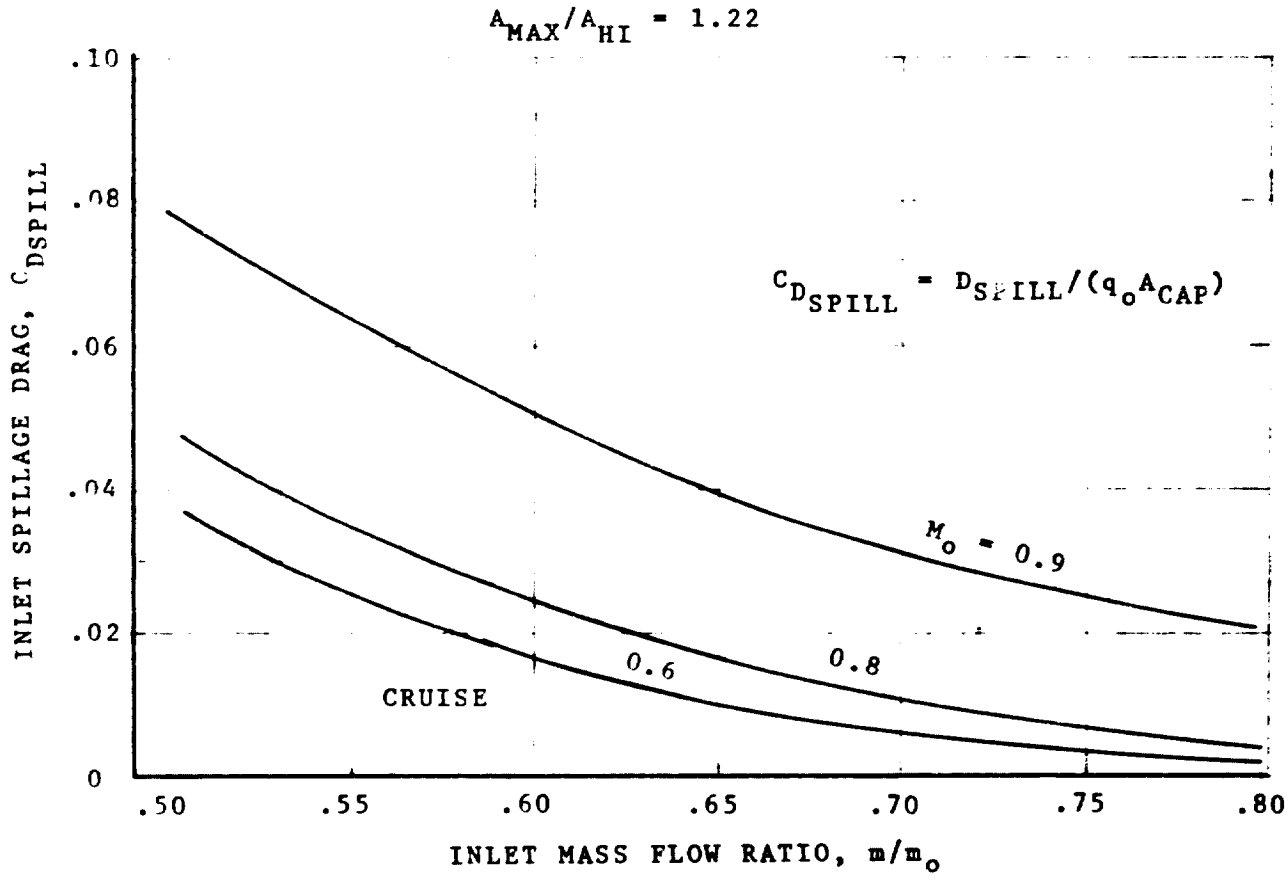

FIGURE 5. FRONT INLET SPILLAGE DRAG CHARACTERISTICS.

Aft Inlets

The aft inlet was also designed to the operating conditions defined in Table I. Details of the inlet design and model description are given in Reference 2, for both the Long and Short Aft Inlets.

Figure 10 shows a schematic of the combined front and aft inlets nacelle model assembly. Both the Long and Short aft inlets are shown. The front fan drive shaft simulator and diffuser vortex generators (Reference 2) also are shown, together with the short aft inlet lip fillets and nacelle strakes, see sketch below. The horizontal strakes were installed 5 cm below the corners of the short aft inlet. The strakes were triangular pieces of 1.5 mm thick stainless steel metal, resembling highly swept delta wings, and were 15 cm wide by 36 cm long.

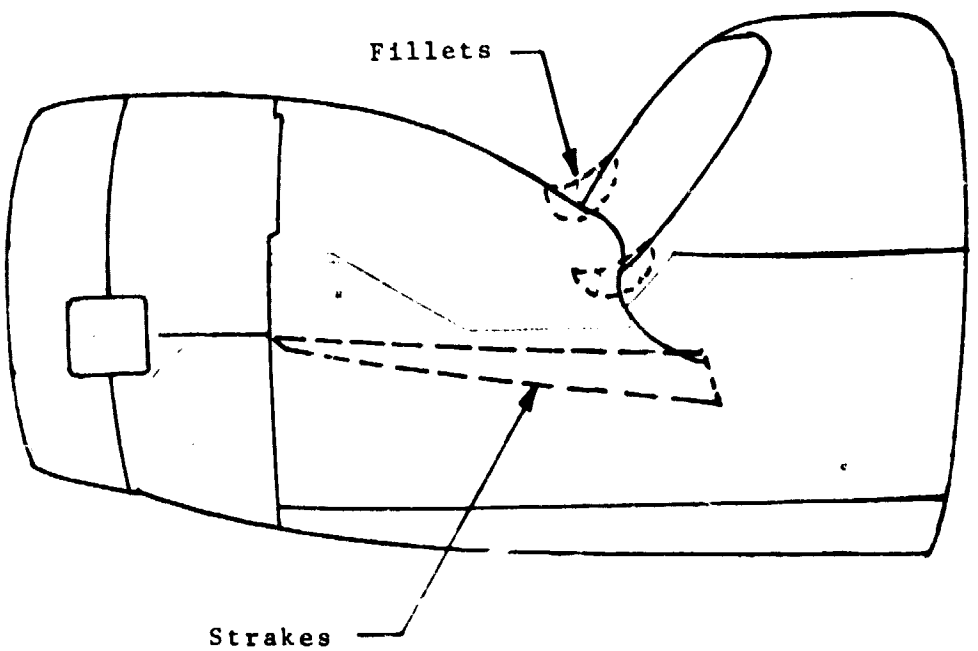

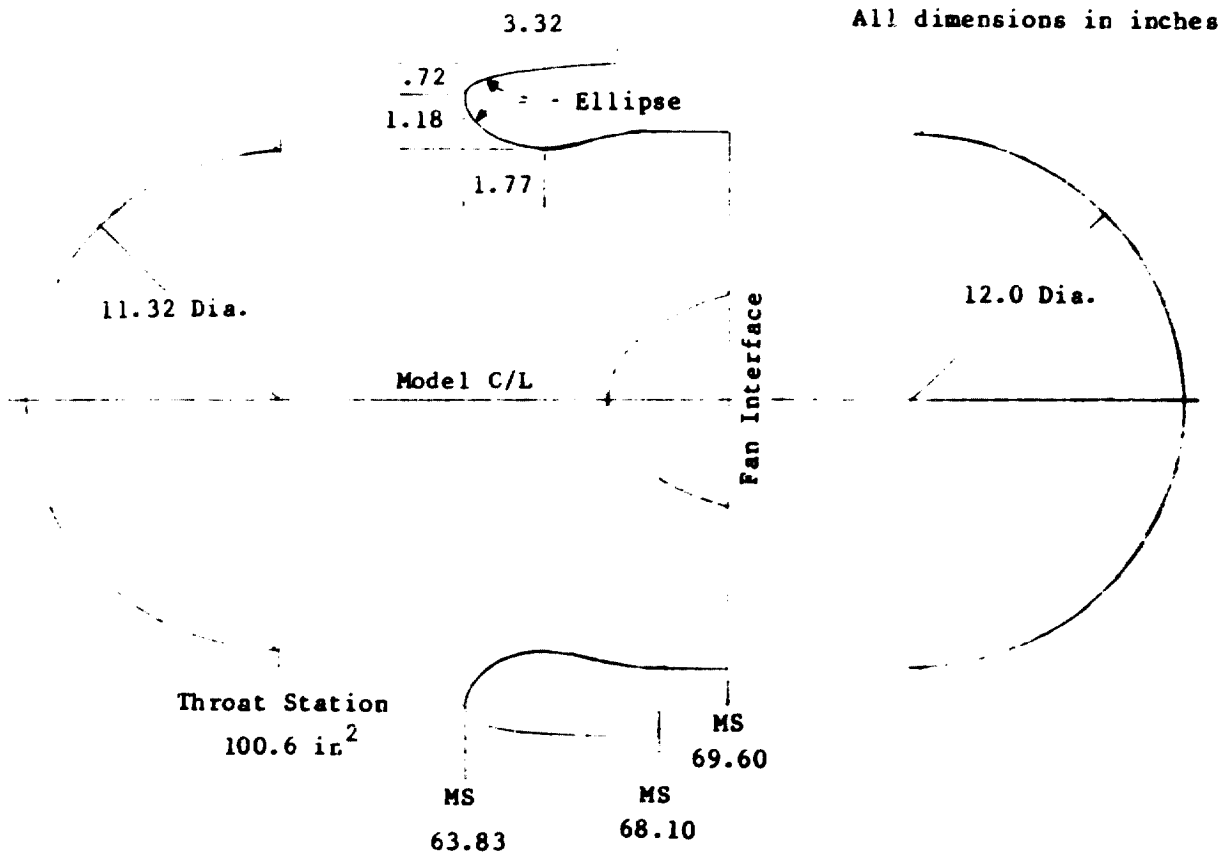

FIGURE 6. FRONT INLET LINES.

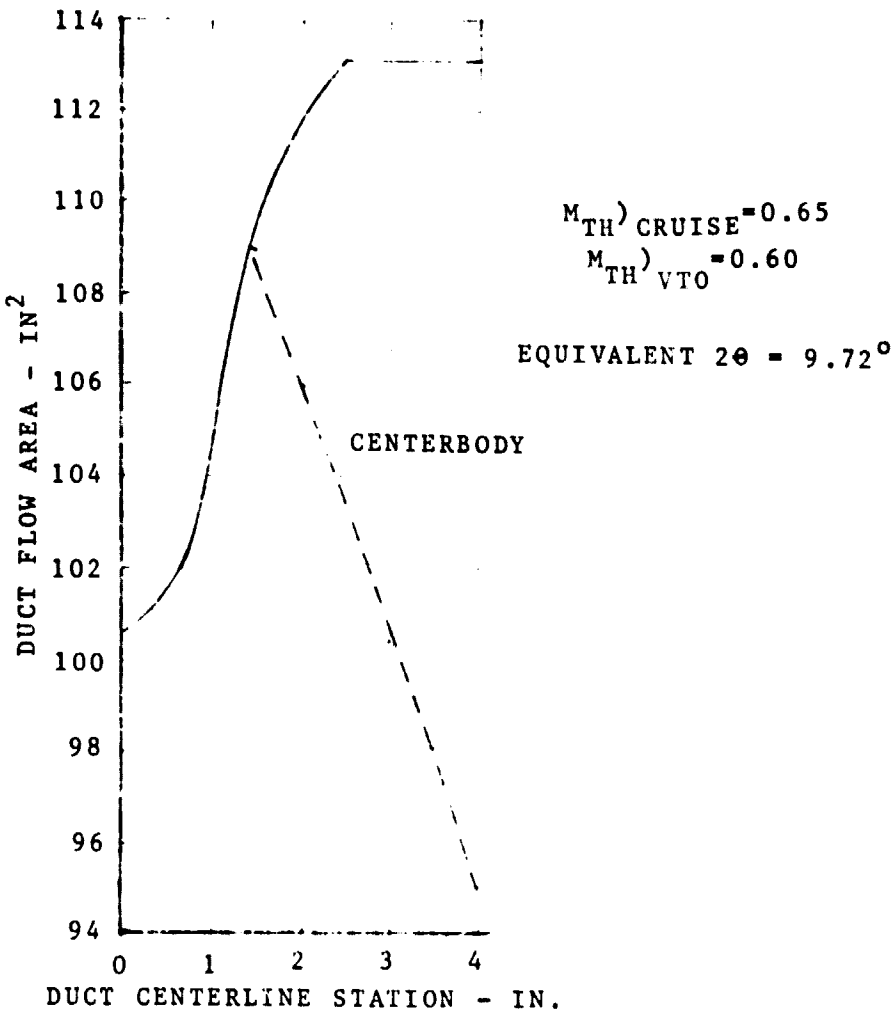

FIGURE 7. FRONT INLET DIFFUSER DESIGN.

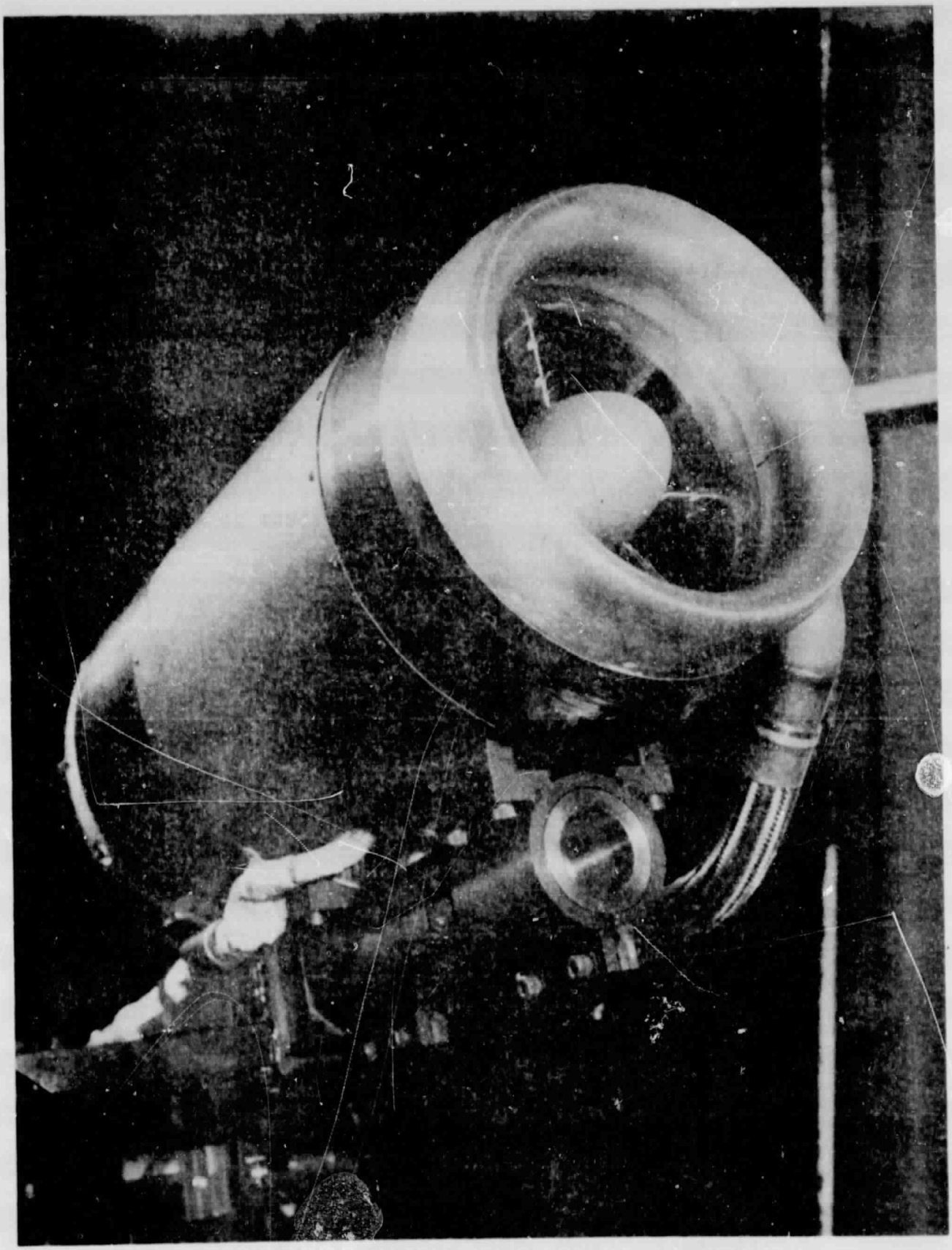

FIGURE 8. TANDEM FAN FRONT INLET MODEL INSTALLED IN NASA LEWIS RESEARCH CENTER 10-BY-10 FOOT WIND TUNNEL.

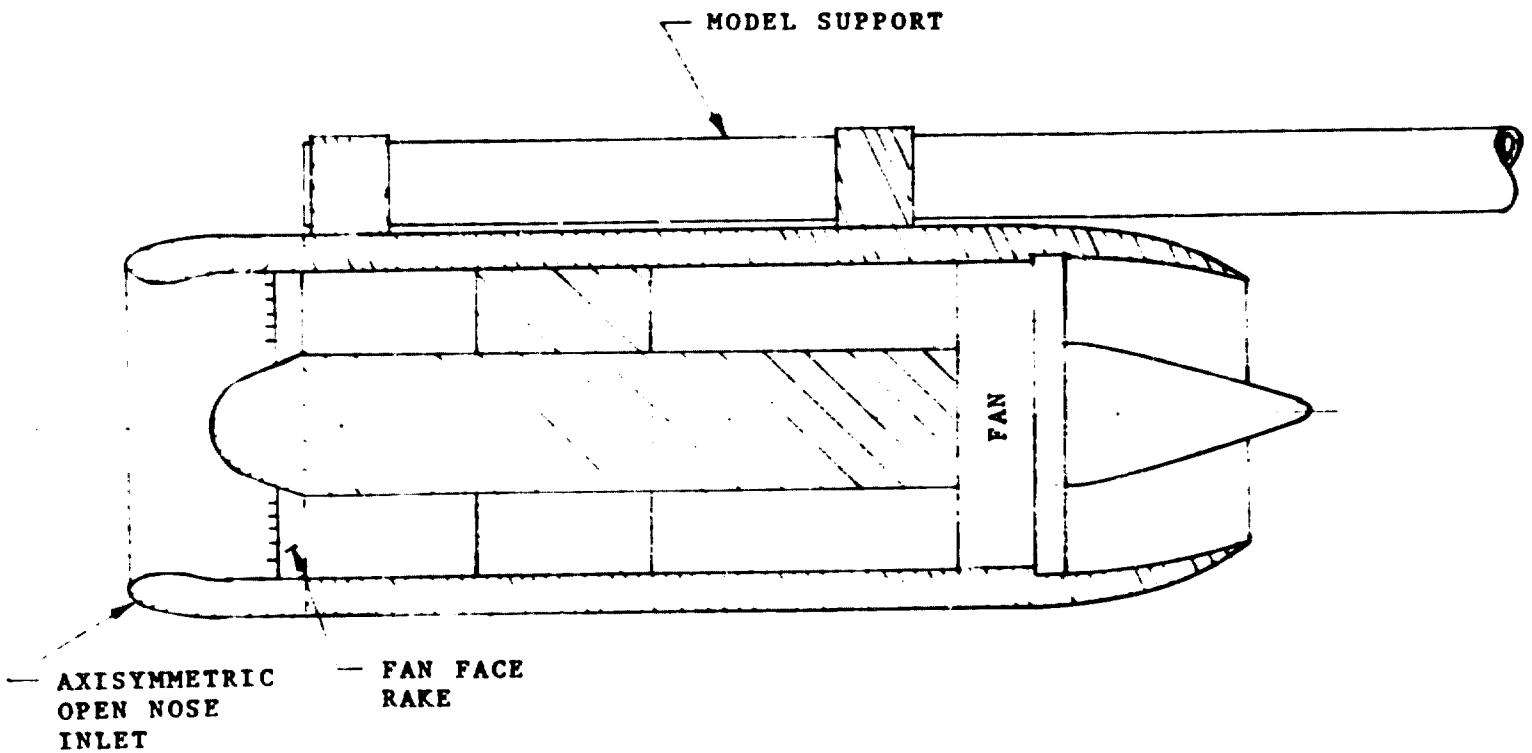

FIGURE 9. TANDEM FAN FRONT INLET MODEL ASSEMBLY.

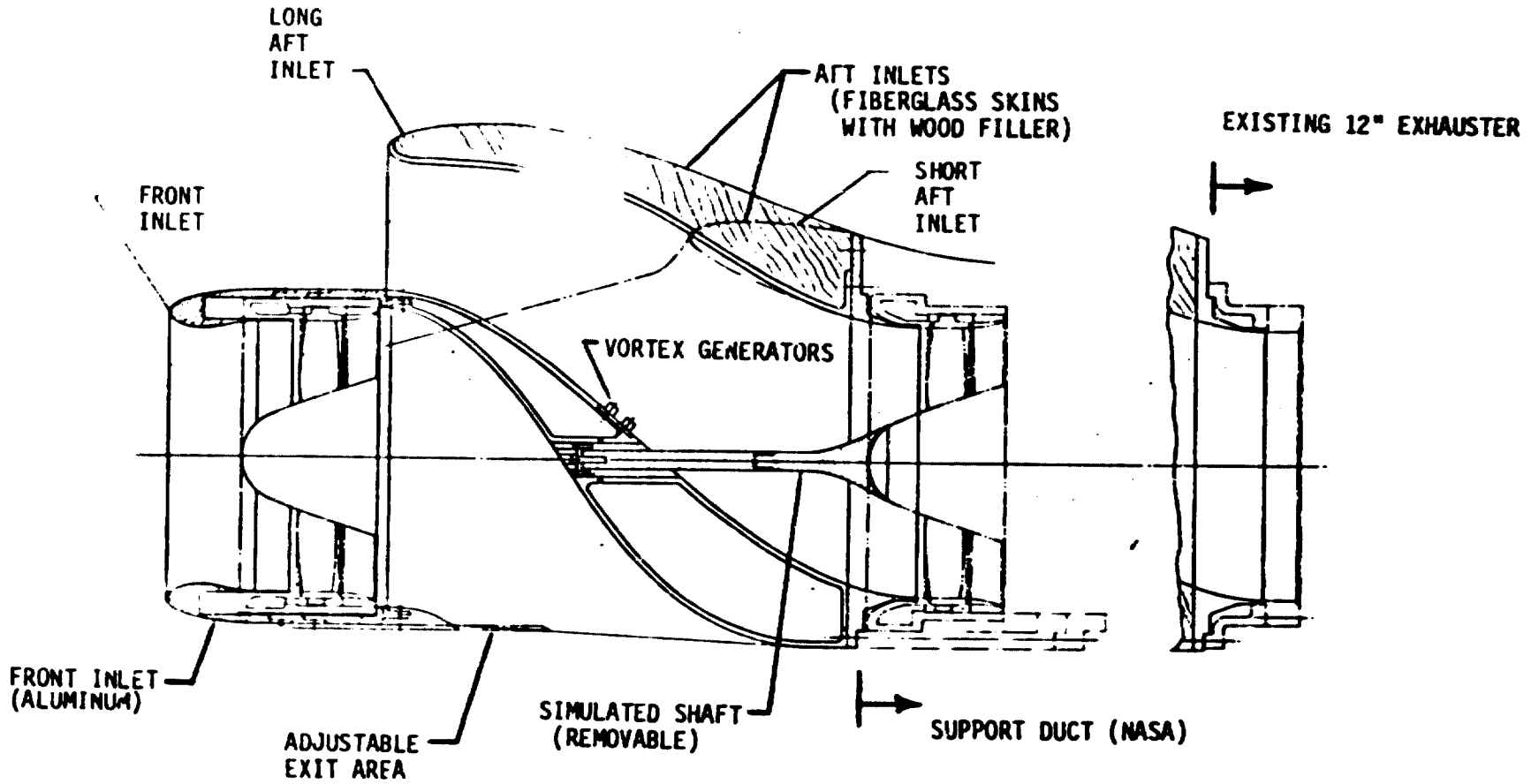

FIGURE 10. TANDEM FAN COMBINED INLET MODEL ASSEMBLY.

The front fan of the V/STOL Type A Tandem fan powered aircraft is to be driven by a shaft that extends from the aft fan, through the aft inlet duct, to the front fan assembly. To test the influence of such a shaft, a stationary shaft was installed in the aft inlet model duct. The diameter of the shaft simulator was .08 the diameter of the aft fan simulator or 1 inch (2.54 cm). The size of the shaft was scaled from the full size shaft dimensions which were developed during the V/STOL A tandem fan transmission sizing studies.

Configuration Definition

The various model configurations tested by NASA Lewis Research Center are listed in Table II. The isolated front inlet model is identified as Configuration 0. Performance for the isolated aft inlet test model configuration 1, 2, 3, 4, and 5 was reported in Reference 2. The baseline geometry for the combined inlet test is composed of front inlet and "clean" long aft inlet, Configuration 01.

TABLE II Model Configuration Definition

CONFIG. NO.	FRONT INLET	LONG AFT INLET				SHORT AFT INLET		
		BASIC	SHAFT	V.G.	B.I.D.	BASIC	FILLETS	STRAKES
0	X							
1		X						
01A	X[1]	X						
01B	X[5]	X						
2		X			X			
3		X		X				
4		X	X	X				
04	X[T]	X	X	X				
5						X		
05A	X[1]					X		
05B	X[5]					X		
06	X[1]							
07	X[1]							

[1] Fan drive air supply duct on top

[5] Fan drive air supply duct on side.

Turbofan

Fan engine airflow simulation was provided to the model by a 12 inch (.3048 meter) diameter, tip-driven, warm-air powered, turbofan which was designed and fabricated by Tech Development Inc. (Reference 8). Fan speed is controlled by the drive air to each tip turbine. Aft fan back pressure is controlled by a variable exit area consisting of a hydraulically translated conical plug inside a fixed nozzle ring. The front inlet nozzle is provided with several plates to vary the exit area and control the back pressure. The turbofan, shown in Figure 11, was calibrated in the 10-by-10 foot (3.048-by-3.048 meter) wind tunnel during March of 1979. Figure 12 shows the fan performance as a function of fan pressure ratio, fan flow rate, fan corrected speed, and exit area.

To conduct the aft inlet testing in the 10-by-10 foot (3.048-by-3.048 meter) tunnel an exit area (A_e) of 85 square inches (548.39 cm^2) was selected. Variations in fan flow rate (and inlet throat mach number) were obtained by varying fan corrected speed.

The front inlet nozzle model was provided with several plates to vary the exit area. In the combined inlet model configuration, preliminary results indicated that the front fan would operate at a point similar to the aft fan with no plate installed. Therefore, all combined inlet testing was conducted with the front inlet exit nozzle full open.

5.2 Instrumentation

The test model was instrumented extensively to provide detailed inlet aerodynamic performance data and to ensure safe operation of the propulsive nacelle. This section describes the model performance instrumentation which includes inlet and turbofan simulator parameters.

5.2.1 Inlet Instrumentation

The front inlet lip is provided with the following surface static pressure taps. There are two rows of nine each external taps at 0^0 and 20^0. There are three rows (8 each) of lip static taps at 0^0, 90^0, and 180^0. Also there are three rows (5 each) of static taps in the diffuser at

COURTESY TECH DEV (REF 8)

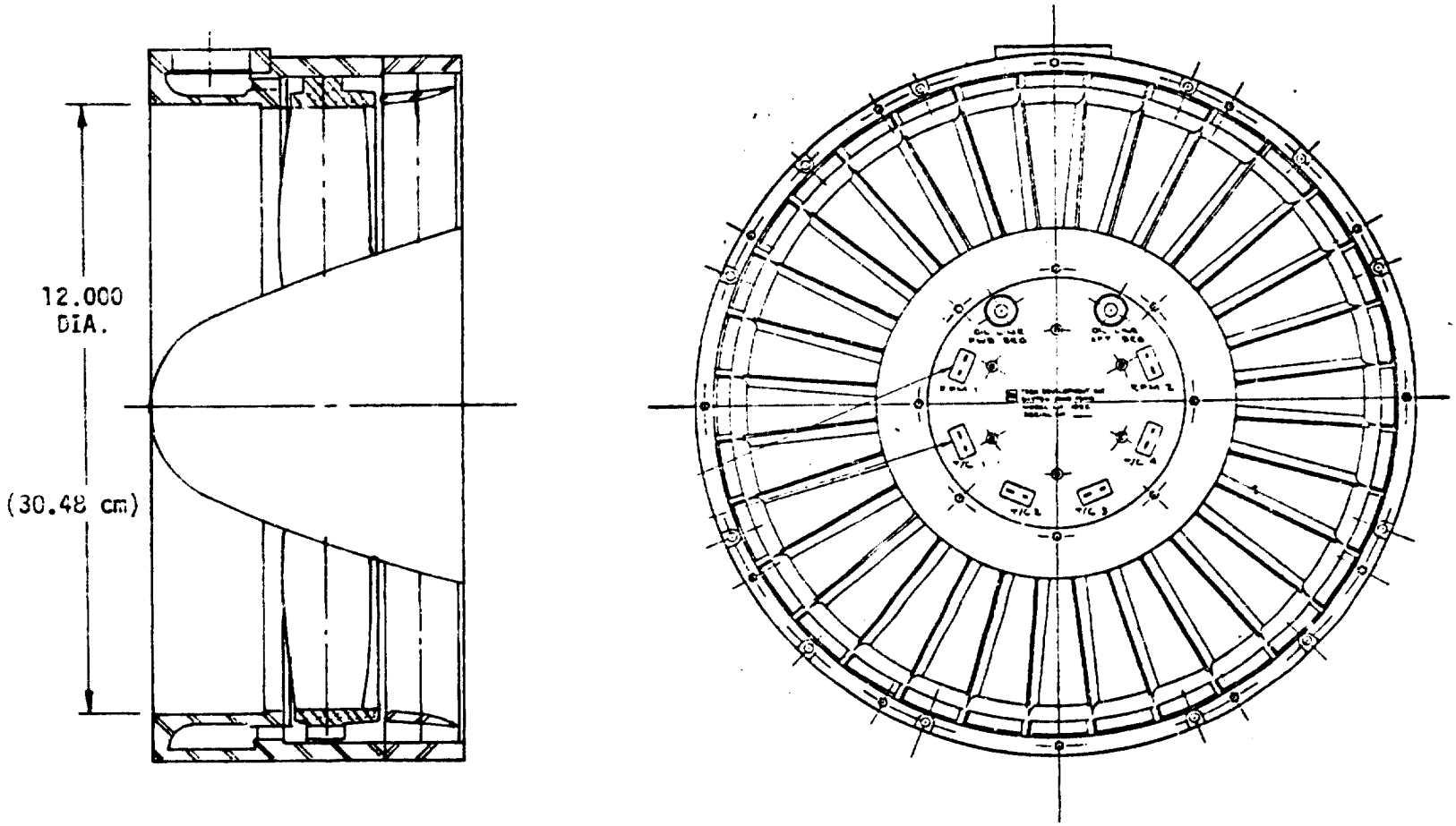

FIGURE 11 TWELVE-INCH POWERED SIMULATOR ASSEMBLY

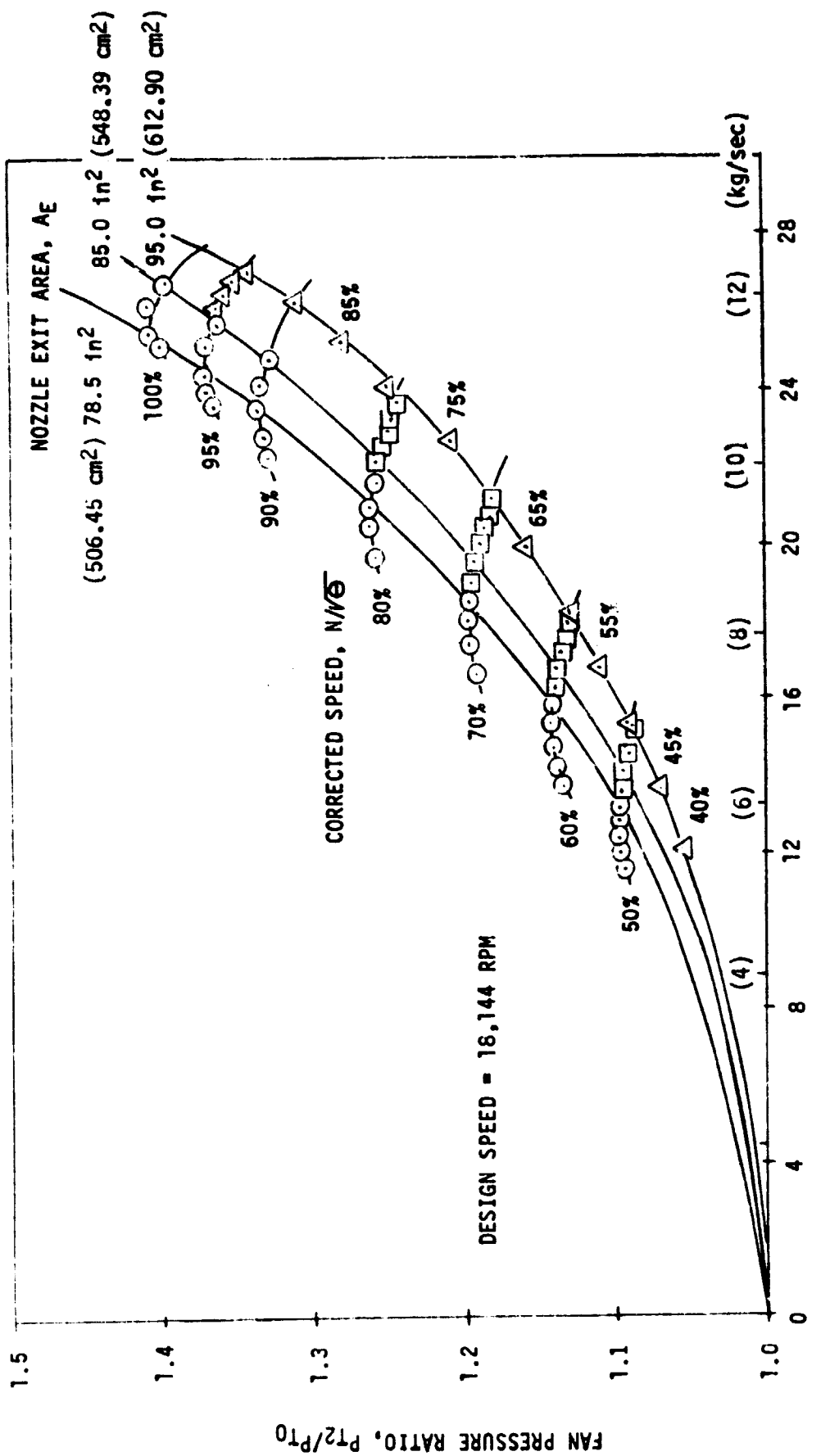

FIGURE 12 TWELVE-INCH POWERED FAN SIMULATOR CALIBRATION

0^0, 90^0, and 180^0. And, there are seven taps along the lip hilite, see Figure 13.

The aft inlet cowl lip is provided with seven surface static taps at the top (0^0) and seven along the side (90^0) as shown in Figure 14. Diffuser static pressure instrumentation includes three rows of static taps equally spaced from the throat to the fan face, at the top (0^0), on the side (90^0) and along the bottom (180^0). In addition, four static pressure taps are located on the inlet cowl lip hilite as shown in Figure 14.

The short aft inlet configuration is provided with eight surface static taps at the top (0^0) and eight along the side (90^0) as shown in Figure 15. Diffuser instrumentation includes one tap in the duct at the top (0^0), two taps in the duct at 90^0); instrumentation along the bottom (180^0) consists of 8 static taps (5 taps located ahead of inlet throat and 3 taps equally spaced from throat to the fan face.) Three additional pressure taps are located on the cowl lip highlight as shown in Figure 15.

5.2.2 Fan Instrumentation

The fan face rake has eight arms spaced 45 degrees apart. Each rake arm is provided with total pressure probes for measurement of steady state and dynamic pressures and flow angularity. Static pressure taps are located on the hub and tip surfaces alongside each rake arm. Figure 16 illustrates the fan face rake instrumentation for the 12-inch (30.48 cm) fan.

Other fan instrumentation recorded included fan exit total pressures and temperatures, fan exit static pressure and nozzle plug position, fan speed and stator pressure, fan drive air pressure and temperature. Turbine drive instrumentation included turbine exit total pressures, total temperature and static pressures.

5.3 Test Facility

The test program was conducted in the NASA Lewis Research Center 10-by-10 foot (3.048-by-3.048 meter) wind tunnel. A schematic of the model installed in the test section is shown in Figure 17. As shown in the figure, the model was cantilevered on the end of the support sting which in turn was

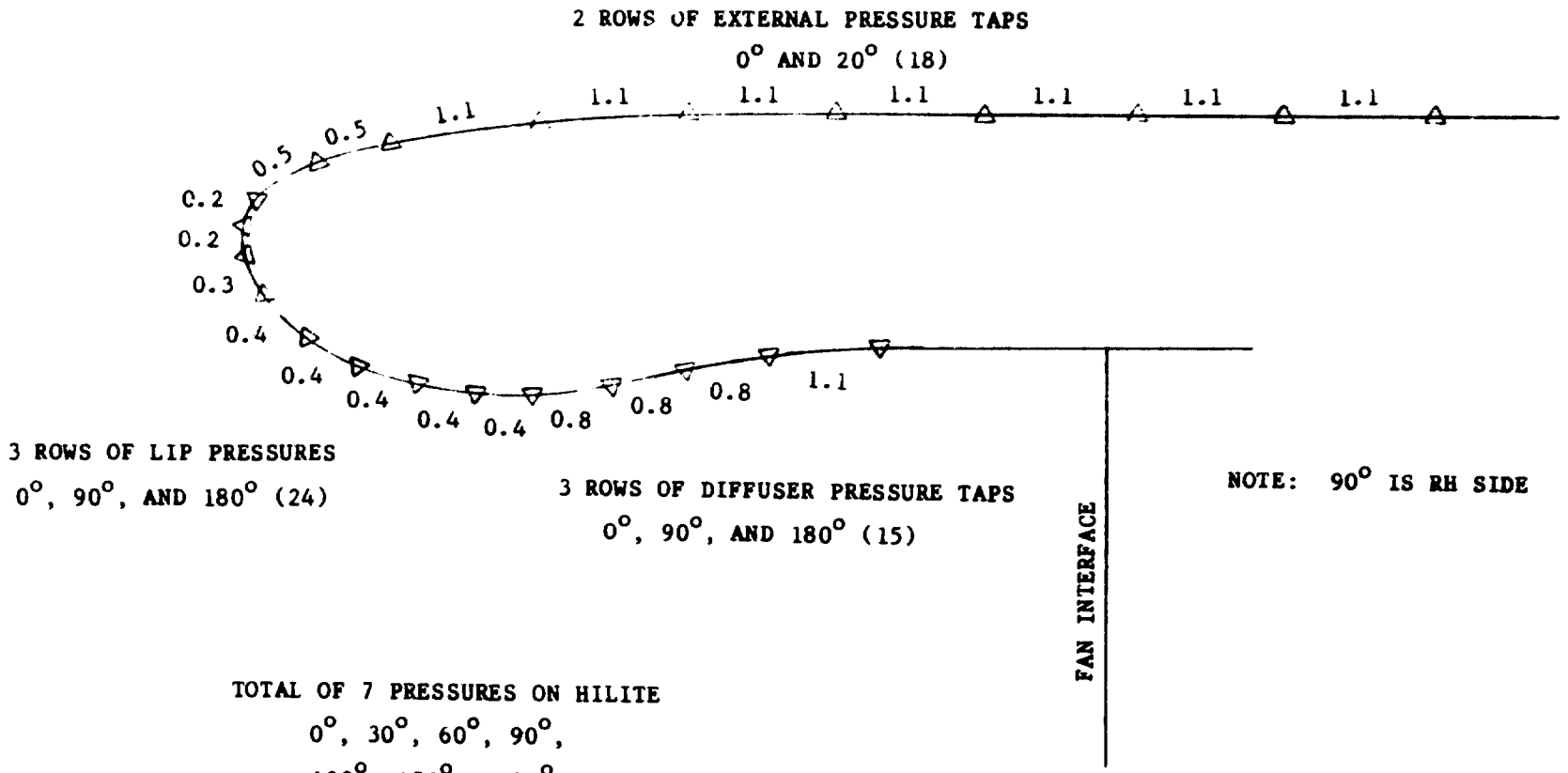

Figure 13. Front Inlet Pressure Tap Locations

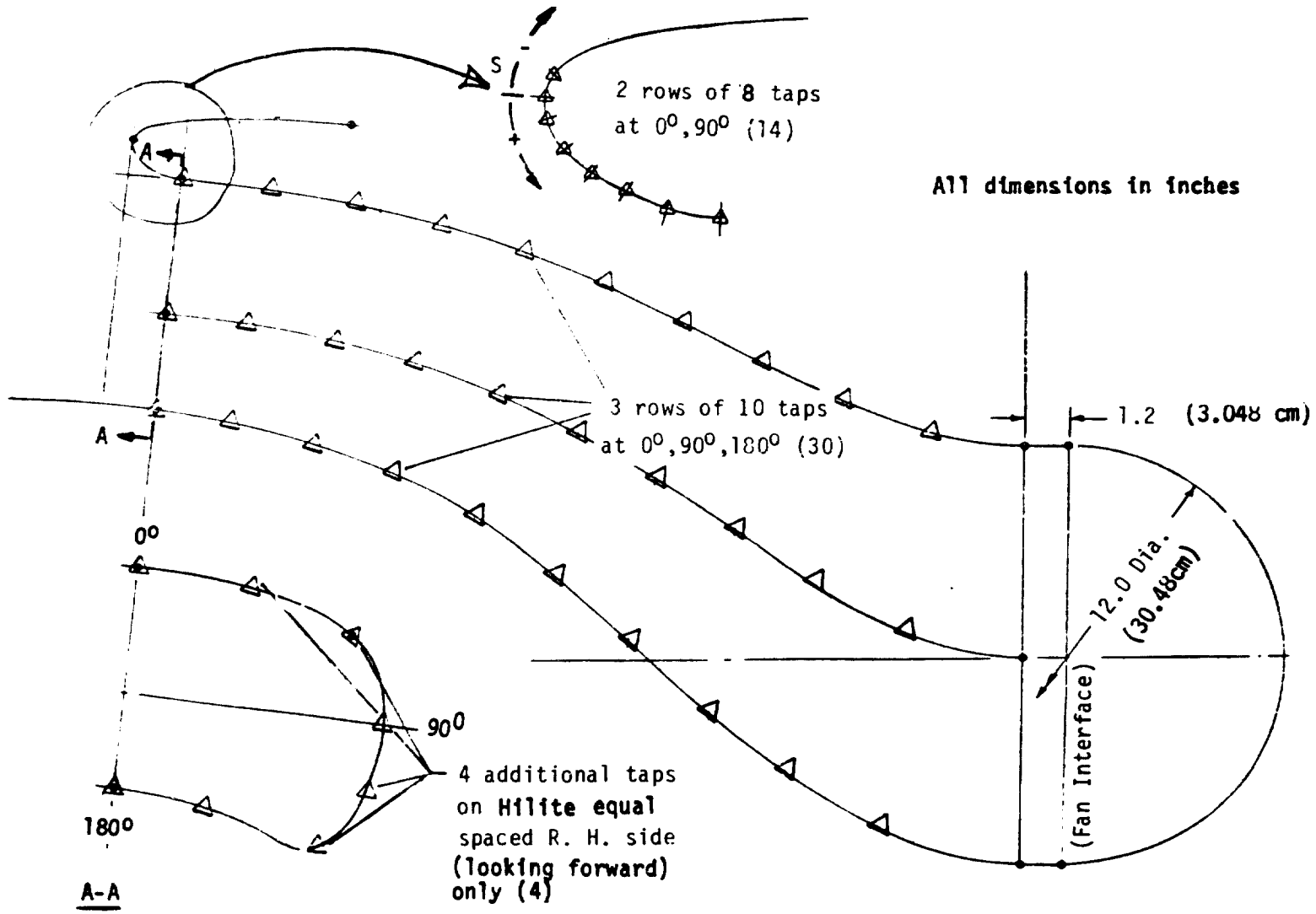

FIGURE 14 AFT INLET PRESSURE TAP LOCATIONS

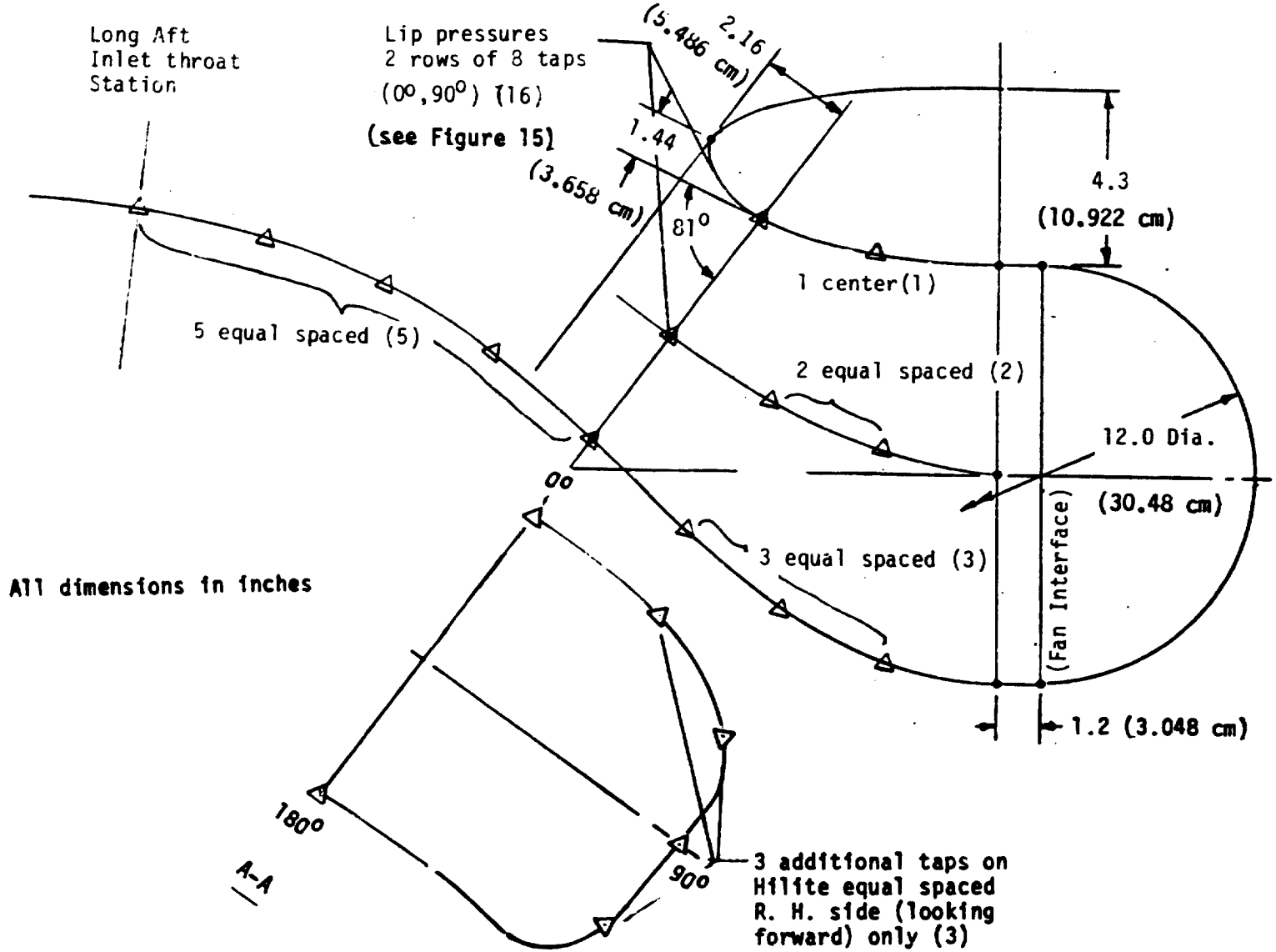

FIGURE 15 SHORT AFT INLET PRESSURE TAP LOCATIONS

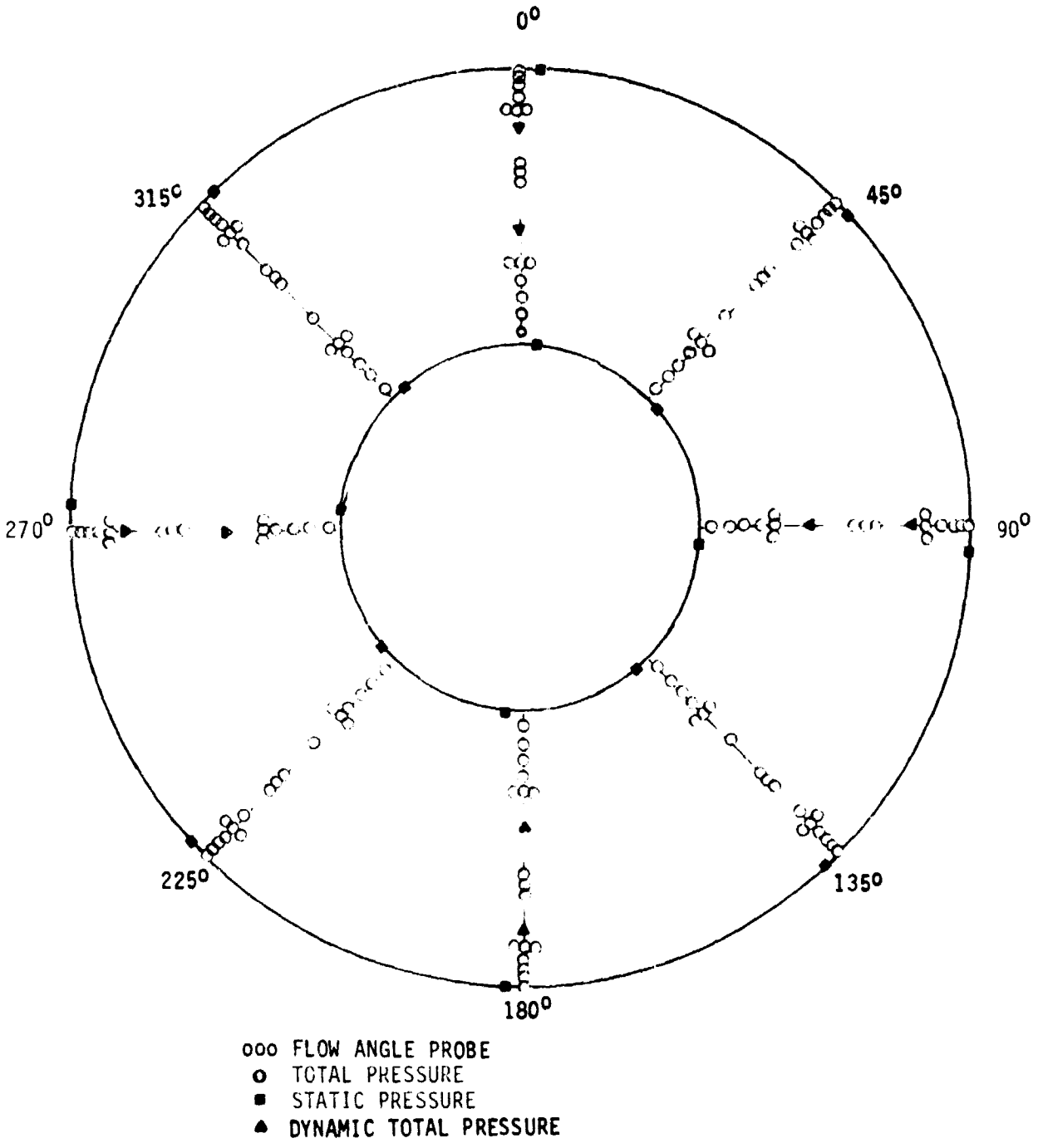

FIGURE 16 TWELVE-INCH FAN SIMULATOR INSTRUMENTATION RAKE AT FAN FACE

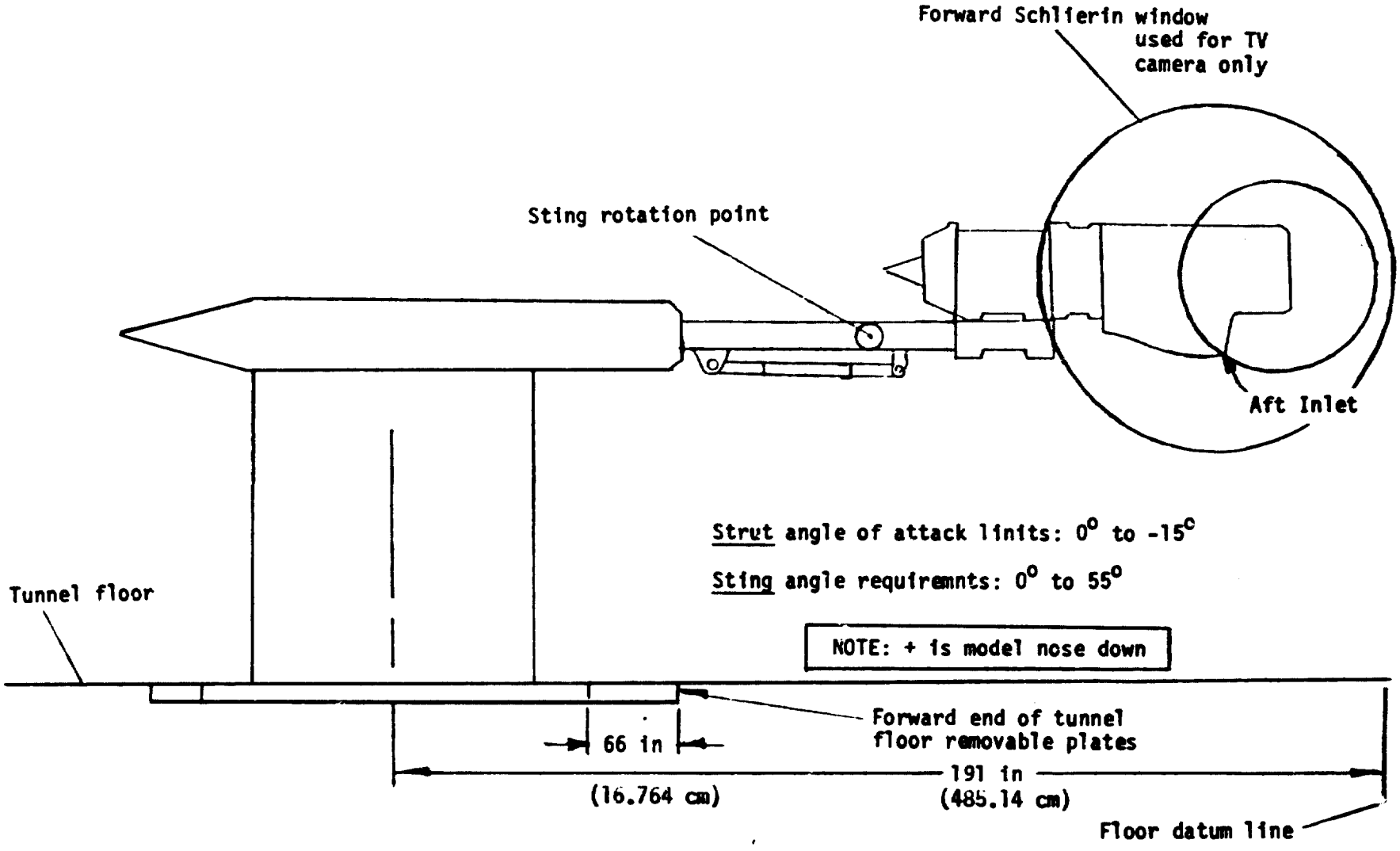

FIGURE 17 TANDEM FAN MODEL TUNNEL INSTALLATION

attached to the tunnel main support strut. The sting rotation point was located so that the forward part of the nacelle model was always visible, even at angle-of-attack. The nacelle model was mounted upside down for testing to utilize existing model support hardware.

5.4 Test Conditions and Procedures

Nacelle operating conditions simulated during this test are summarized in Table III in terms of configuration, tunnel velocity, nacelle angle-of-attack, and inlet throat Mach number (front and aft).

For model configuration 0, isolated front inlet model, the front inlet throat Mach number only is given. For the combined inlet test, the usual procedure was to run the aft inlet fan at full speed while increasing the front inlet fan speed; and then holding the front inlet fan at full speed while decreasing the aft inlet fan speed. For the cruise condition, V_o = 240 knots, extra points at intermediate fan speeds were also recorded.

The test was conducted using the following procedures:

(1) The Tandem Fan nacelle model was assembled to form a configuration as listed in Table III.
(2) The wind tunnel flow conditions were established.
(3) The model was pitched to an initial desired angle-of-attack.
(4) The turbofan simulators were operated at desired fan speeds and pressure ratios necessary to establish the desired inlet flow rates (throat Mach numbers, front and aft) and data was recorded.
(5) The model was pitched to the next angle-of-attack and Step (4), repeated.
(6) Steps (3), (4), and (5) were repeated at the next desired combination of front and aft fan speeds.
(7) Steps (2) through (6) were repeated at each wind tunnel flow condition required.
(8) Steps (1) through (7) were repeated for each model configuration desired.

TABLE III TANDEM FAN NACELLE TEST CONDITIONS

INLET MODEL CONFIGURATION	TUNNEL VELOCITY Vo - KTS	NACELLE ANGLE OF ATTACK	INLET THROAT MACH NUMBERS FRONT/AFT										
0	0	0	.13/-	.24/-	.28/-	.32/-	.36/-	.40/-	.44/-	.49/-	.53/-		
01A, 01B, 04, 05A, 05B, 06				0/.6		.4/.6		.6/.6		.6/.4		.6/0	
0	35	-10		.2/-		.3/-		.4/-		.5/-			
01A, 04, 05A		-10		0/.6		.4/.6		.6/.6		.6/.4		.6/0	
0		0		.2/-		.3/-		.4/-		.5/-		.6/-	
01A, 01B, 04, 05A, 05B, 06		0		0/.6		.4/.6		.6/.6		.6/.4		.6/0	
0		10		.2/-		.3/-		.4/-		.5/-		.6/-	
0		20		.2/-		.3/-		.4/-		.5/-		.6/-	
01A, 04, 05A		20		0/.6		.4/.6		.6/.6		.6/.4		.6/0	
0		30		.2/-		.3/-		.4/-		.5/-		.6/-	
0		40				.3/-		.4/-		.5/-		.6/-	
01A, 01B, 04, 05A, 05B, 06		40		0/.6		.4/.6		.6/.6		.6/.4		.6/0	
0	85	-10		.2/-		.3/-		.4/-		.5/-		.6/-	
01A, 01B, 05B, 06		-10		0/.6		.4/.6		.6/.6		.6/.4		.6/0	
0		0		.2/-		.3/-		.4/-		.5/-		.6/-	
01A, 01B, 04, 05A, 05B, 06		0		0/.6		.4/.6		.6/.6		.6/.4		.6/0	
0		10		.2/-		.3/-		.4/-		.5/-		.6/-	
0		20		.2/-		.3/-		.4/-		.5/-		.6/-	
01A, 01B, 04, 05A, 05B, 06		20		0/.6		.4/.6		.6/.6		.6/.4		.6/0	
0		30		.2/-		.3/-		.4/-		.5/-		.6/-	
0		40		.2/-		.3/-		.4/-		.5/-		.6/-	
01A, 01B, 04, 05A, 05B, 06		40		0/.6		.4/.6		.6/.6		.6/.4		.6/.6	
0	135	-10		.2/-		.3/-		.4/-		.5/-		.6/-	
01A, 01B, 04, 05A, 05B		-10		0/.6		.4/.6		.6/.6		.6/.4		.6/0	
0		0		.2/-		.3/-		.4/-		.5/-		.6/-	
01A, 01B, 04, 05A, 05B, 06		0		0/.6		.4/.6		.6/.6		.6/.4		.6/0	
0		10		.2/-		.3/-		.4/-		.5/-		.6/-	
0		20		.2/-		.3/-		.4/-		.5/-		.6/-	
01A, 01B, 04, 05A, 05B, 06		20		0/.6		.4/.6		.6/.6		.6/.4		.6/0	
0		30		.2/-		.3/-		.4/-		.5/-		.6/-	
0		40		.2/-		.3/-		.4/-		.5/-		.6/-	
01A, 01B, 04, 05A, 05B, 06		40		0/.6		.4/.6		.6/.6		.6/.4		.6/0	
01A, 04	240	0	.12/.32	.12/.45		.12/.56	.23/.56	.35/.56	.51/.56	.51/.45	.51/.32	.51/.14	.35/.13	.23/.14	.12/.13
05A		0				.12/.51		.35/.51	.51/.51	.51/.41		.51/.14		.23/.14	.12/.14
06				.23/.38		.23/.47	.30/.47	.40/.47	.54/.47	.54/.38	.54/.27	.54/.13	.39/.13	.23/.13	

5.5 Data Reduction and Presentation

Model and turbofan instrumentation data were recorded by the Lewis Research Center's Central Automatic Digital Data encoder and simultaneously recorded and analyzed by a time-sharing digital computer system. For the isolated inlet tests, a large amount of pressure data was recorded by the digital data encoder using eight automatic scanning valves each having 48 ports.

On-line data consisted digital displays to monitor and ensure safe operation of the fan.

Quick Look off-line data were processed on the Lewis computer to provide maximum test visibility and test performance. Final data and computer plots were processed at Lewis on the computer.

For the latter portion of the test program, the pressure measuring system and data reduction equipment at the LeRC 10x10 Wind Tunnel were modified as follows:

a. Mechanically scanned pressure units were replaced by electronically scanned pressure transducers (one for each pressure) which are electronically scanned at rates up to 10,000 per seond. Three point calibrations are performed automatically each 20 minutes to compensate for transducer drift due to changing tunnel air temperatures.

b. The LeRC "Escort" system replaced the Central Automatic Digital Data Encoder. The newer system allows better display of calculated values, as processed by a mimi-computer, and provides an upgraded display every 6 seconds.

c. IMB 370/3033 computer, in the new NASA Research Analysis Center, replaced the IBM 360, for faster processing of final data.

The data recorded from the test was reduced by the computer to the following parameters:

Inlet

- Surface static pressure ratio and Mach number distributions
- Weight flow and throat Mach number

Fan

- Fan face total pressure ratios and pressure recovery
- Fan face weight flow and Mach number
- Fan face total pressure distortion (MAX - MIN, KD_2, KO, IDC, IDR, DC60)
- Fan face flow angles
- Fan face total pressure contour plots
- Fan corrected speed, pressure ratio and horsepower

Turbine

- Turbine weight flow, pressure ratio and turbine horsepower.

6.0 Test Results

The following paragraphs present the inlet performance data obtained from the test. The first paragraph (6.1) describes the test results for the front inlet in terms of total pressure recovery, steady state pressure distortion, turbulence (RMS) pressure levels, fan face total pressure contour maps and diffuser static pressure distributions as functions of tunnel speed, model attitude, and inlet flow rate. Paragraph 6.2 compares the performance levels of the aft inlet when operating in an isolated environment to performance levels when operating in the presence of the front inlet. These comparisons are based on total pressure recovery, distortion and turbulence levels, fan face contour maps and static pressure distributions. Paragraphs 6.3 through 6.7 describe other combined inlet test results.

Summaries of the fan face pressure recovery and steady state distortion levels for the various inlet configurations are contained in Tables IV and V for isolated and combined inlet models, respectively.

6.1 Front Inlet

A summary of the fan face pressure recovery and steady state distortion levels for the various isolated inlet configurations is presented in Table IV, including the isolated front inlet.

Individual inlet performance levels for the front inlet configuration are presented in Figures 18 to 21. The total pressure recovery (P_{TAV}/P_{TO}) in the figures is the area weighted average pressure computed from the 40 probe rake at the fan face station (Section 5.2) divided by the freestream total pressure. The distortion level (DPT/PTAV) is computed as the difference between the maximum and minimum pressures in the 40 probe array divided by the average. The turbulence level (RMS/PTAV) is defined as the arithmetic average of root-mean-square values from the eight dynamic probes (Section 5.2) divided

TABLE IV DATA SUMMARY - RECOVERY/DISTORTION
FOR TANDEM FAN INLETS (ISOLATED)

FLIGHT CONDITION				LONG AFT INLET				
Freestream Velocity Kts	Angle of Attack Deg.	Throat Mach No.	Front Inlet (0)	Basic (1)	Blown-in Door (2)	Vortex Generator (3)	V. G. + Shaft (4)	Short Aft Inlet (5)
0	0	.5	.998/.004	.989/.048	.982/.061	.988/.049	.988/.049	.998/.013
(o m/s)	--	.3	.998/.003	.994/.019	.992/.025	.995/.019	.994/.020	.999/.004
35	0	.5	.998/.007	.988/.050	.983/.055	.989/.048	.988/.048	.997/.014
(18 m/s)	40	.5	.997/.013	.989/.048	.982/.056	.988/.055	.987/.056	.994/.041
85	0	.5	.998/.033	.984/.066*	.983/.055	.989/.049	.988/.046	.996/.030
(43.7 m/s)	40	.5	.997/.045	.987/.055	.982/.064	.986/.057	.985/.053	.985/.095
135	0	.5	.998/.023	.989/.045	.983/.053	.990/.050	.989/.046	.997/.025
(69.5 m/s)	40	.5	.997/.076	.981/.069	.977/.065	.978/.066	.978/.072	.979/.111
240 (123.5 m/s)	0	.4					.993/.037	.996/.042

*M_{TH} = .588

TABLE V -- DATA SUMMARY
RECOVERY/DISTORTION FOR TANDEM FAN AFT
INLET (COMBINED)

FLIGHT CONDITION			LONG AFT INLET		SHORT AFT INLET		
Velocity Kts.	Angle of Attack Deg.	Throat Mach No.	Basic (01A)	V. G. + Shaft (04A)	Basic (05A)	Fillets (06)	Strakes (07)
0	0	.6	.989/.067	.984/.074	1.000/.013	.999/.015	.998/.016
35	0	.6	.988/.069	.985/.072	.999/.018	.999/.015	
	40	.6	.989/.069	.983/.085	.998/.042	.993/.034	
85	0	.6	.988/.066	.987/.063	1.000/.021	.995/.021	.997/.032
	40	.6	.987/.064	.982/.074	.992/.061	.983/.077	.993/.041
135	0	.6	.988/.067	.988/.061	.999/.036	.986/.030	.996/.051
	40	.6	.978/.083	.974/.113	.979/.118	.961/.148	.984/.069
240	0	.6	.992/.066	.991/.058	.998/.043	.958/.053	

NOTE: All data for M_{FF} = 0.6

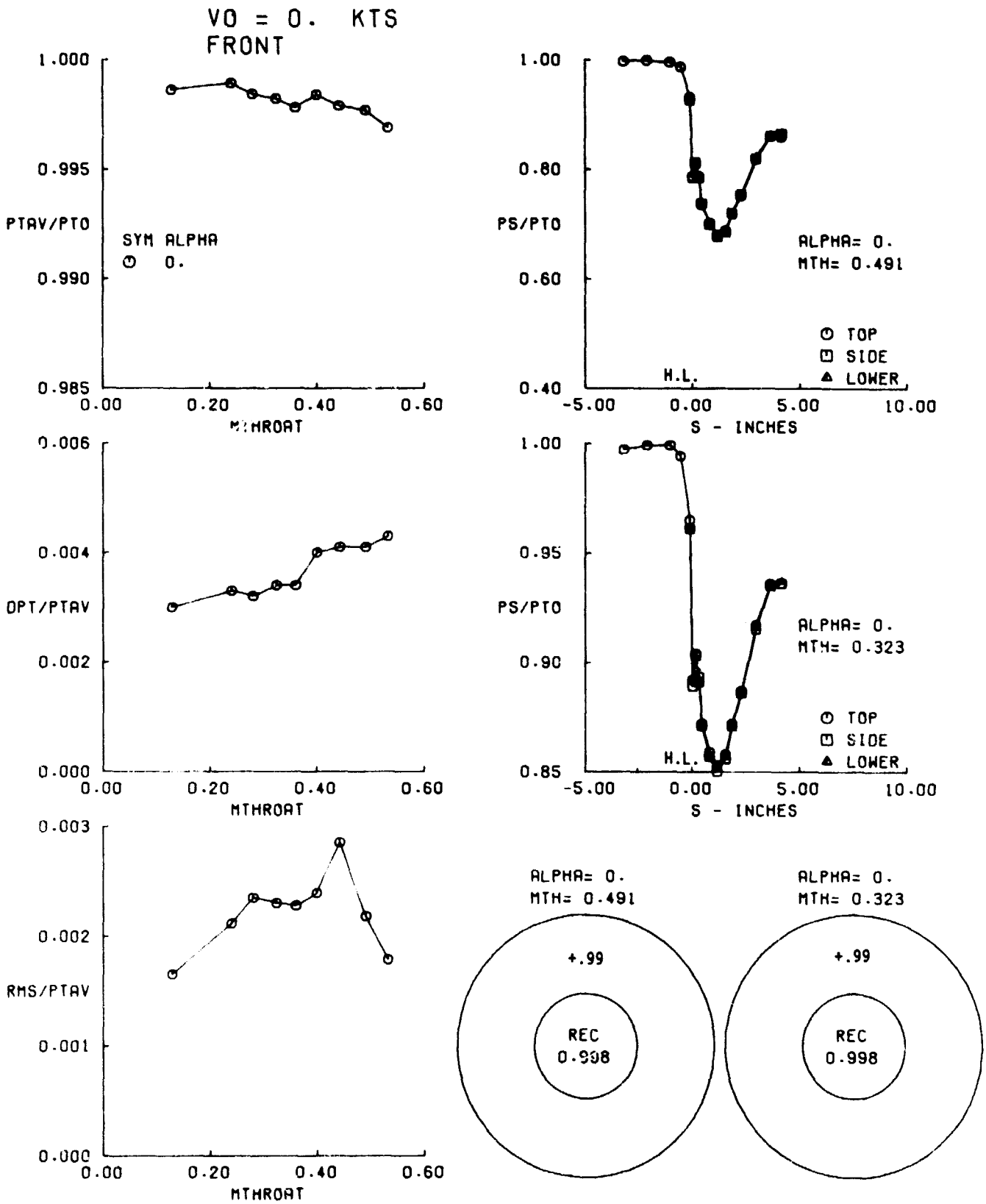

FIGURE 18. FRONT INLET PERFORMANCE AT V_o = 0 KNOTS.

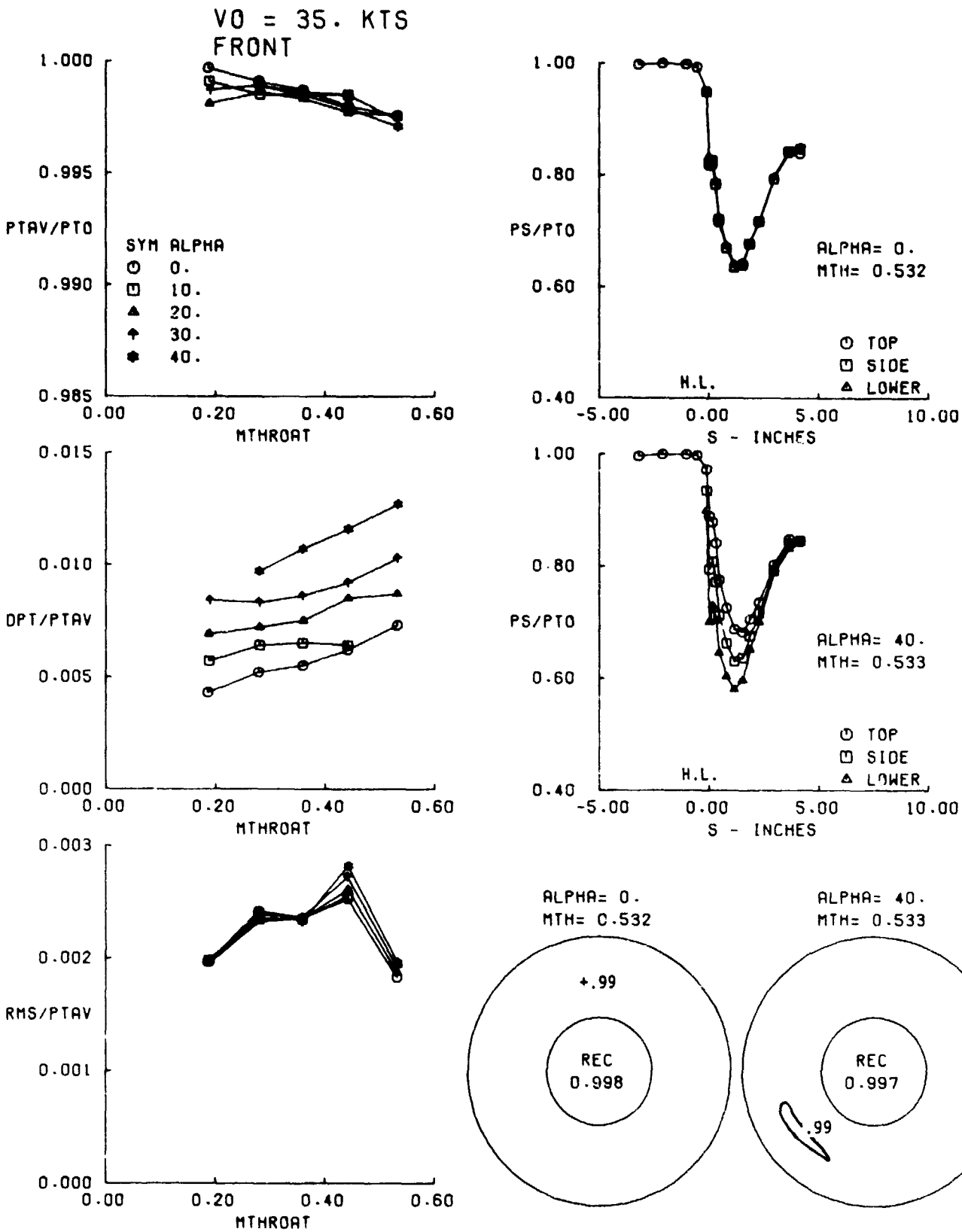

FIGURE 19. FRONT INLET PERFORMANCE AT V_o = 35 KNOTS.

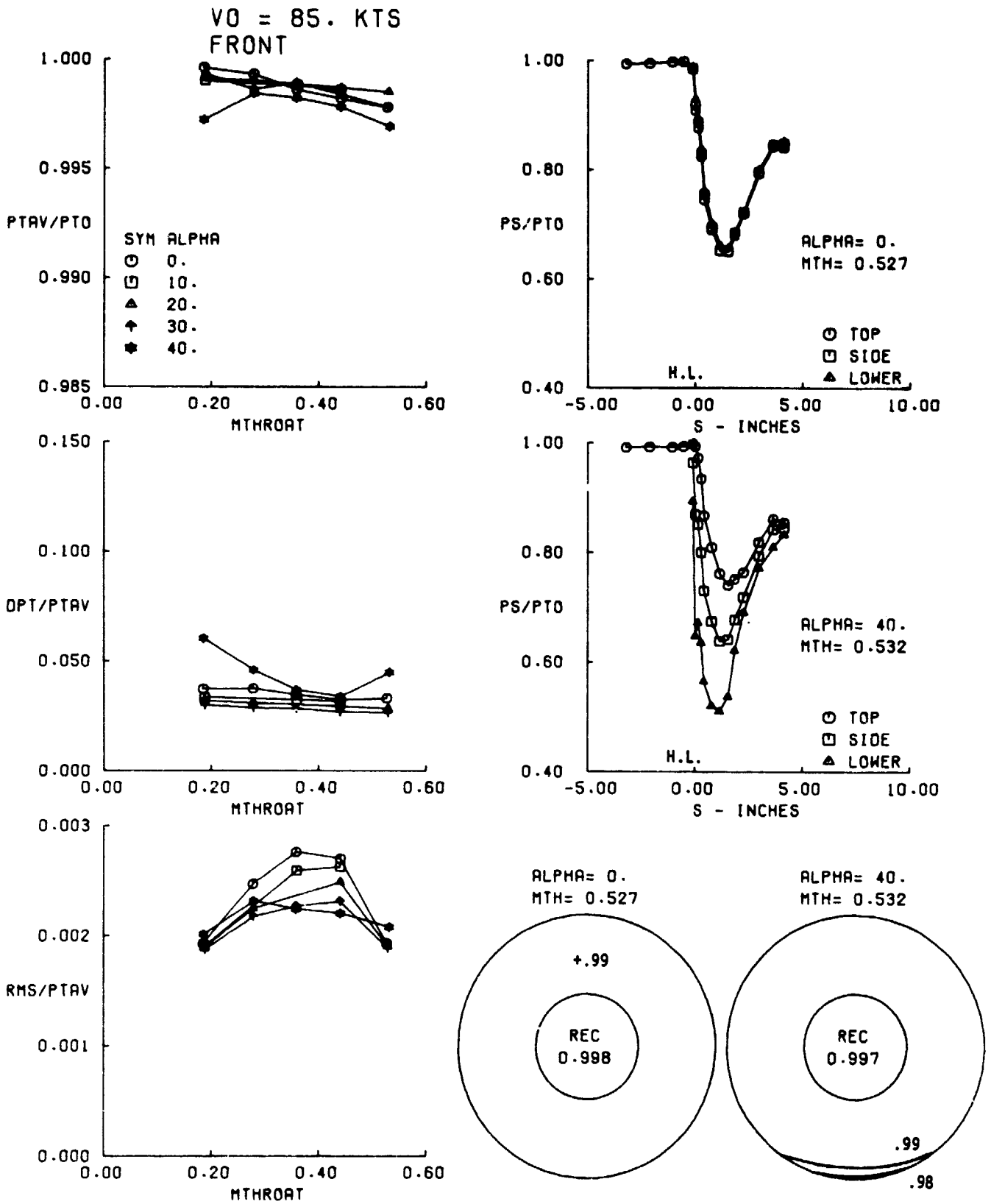

FIGURE 20. FRONT INLET PERFORMANCE AT V_o = 85 KNOTS.

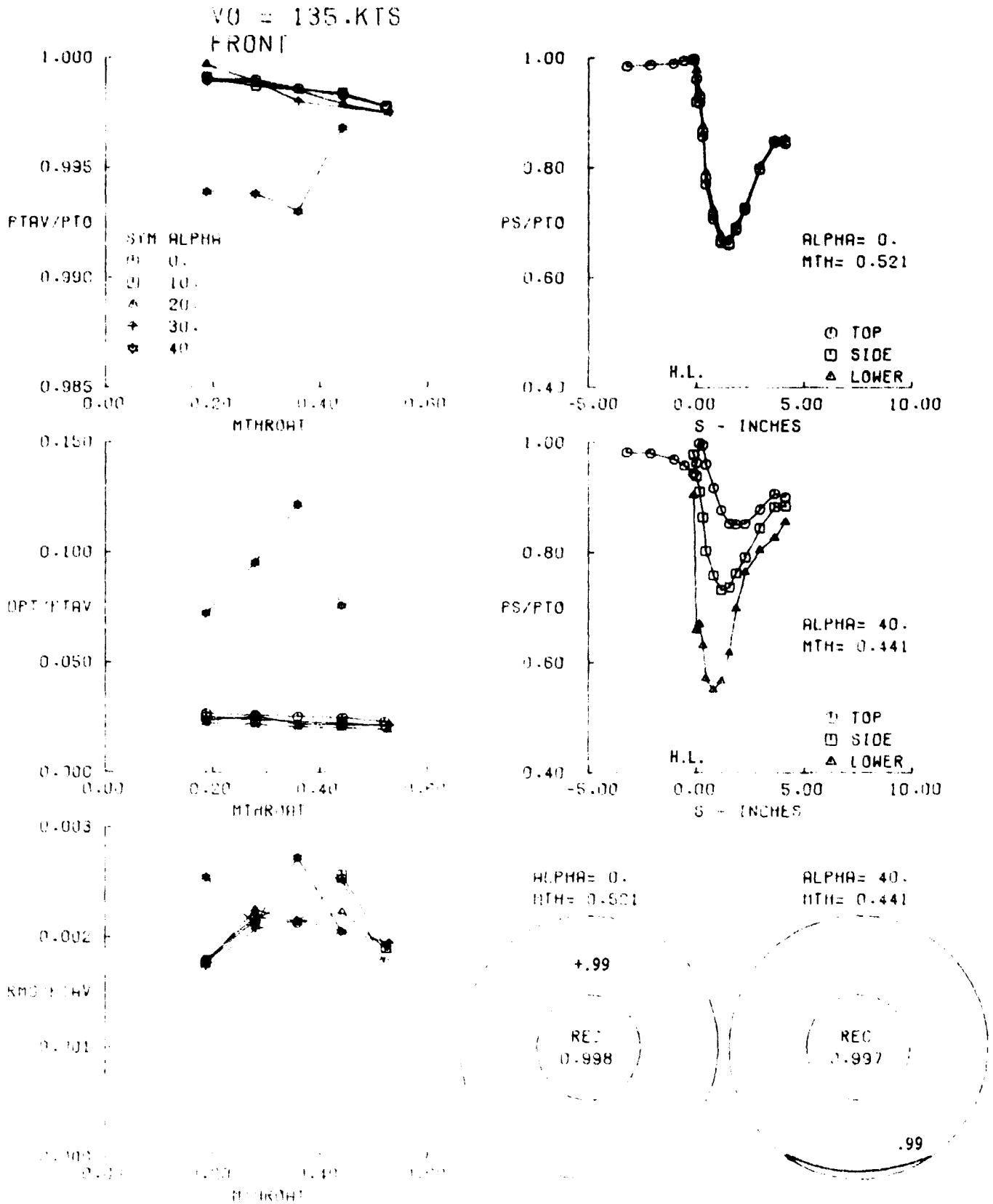

FIGURE 21. FRONT INLET PERFORMANCE AT V_o = 135 KNOTS.

by the average total pressure. These data are plotted as functions of inlet throat Mach number (inlet mass flow rate) which was controlled by the turbofan.

The static pressure distribution along three inlet "streamlines" are also presented for two inlet throat Mach numbers. The pressure ratio is formed by dividing the local static pressure by the freestream total pressure. The pressure ratios are plotted as a function of the surface distance from the inlet lip hilite, with positive being downstream. The three streamlines begin at the inlet top lip, the side lip, and along the lower lip surfaces.

Fan face station total pressure contour plots are presented for the same tunnel and inlet conditions as the static pressure distributions. These plots are oriented with the inlet on top looking downstream.

Fan face flow angularity data when plotted for the same inlet and tunnel conditions as the other data showed no particular trends and no plots are included in the reported results.

The inlet performance for the axisymmetric open nose front inlet design is presented in Figures 18 throug 21 for freestream velocities of 0, 35, 85, and 135 knots (0, 18, 43.7, and 69.5 m/s). Fan face pressure contours and inlet static pressure distributions are presented for throat Mach numbers of 0.49 and 0.323 in Figure 18 for the static case, Vo = 0 knots and $\alpha = 0^0$. Note the scale change in the static pressure distribution. The flow into the inlet is symmetrical as expected, with the highest local velocity occurring on the lip surface forward of the inlet throat plane. The fan face total pressure contours are essentially uniform at both low and high airflow rates.

The recovery levels remain essentially unchanged (at .998) as forward speed was increased to 35 knots (18 m/s), 85 knots (43.7 m/s) and 135 knots (69.4 m/s), Figures 19, 20 and 21, and angle-of-attack was increased to 10^0, 20^0 and then 30^0. At an angle-of-attack of 40^0 however, the pressure recovery decreases (to .997) and the distortion and turbulence level increase at forward speeds of 85 knots (43.7 m/s) and 135 knots (69.5 m/s), Figures 20 and 21.

Note also that at the $\alpha = 40^0$ condition the velocity at the inlet lip increases on the bottom surface and decreases on the top surface. The distortion pattern at the fan face remains essentially unchanged, increasing only slightly in pressure decay.

There is a discontinuity in static pressure distributions near the lip hilite. This characteristic was also found in analytical results obtained at LeRC, and are due to a slight discontinuity in the lip contour at the hilite.

6.2 Combined Inlets Comparisons

A summary of the fan face pressure recovery and steady state distortion levels for various combined aft inlet configurations is presented in Table V. Only aft inlet performance data are presented because the front inlet was not instrumented with a fan face rake.

Aft inlet performance levels for several configurations are presented in Figures 22 to 45. The total pressure recovery (P_{TAV}/P_{TO}) in the figures is the area weighted average pressure computed from the 40 probe rake at the fan face station (Section 5.2) divided by the freestream total pressure. The distortion level (DPT/PTAV) is computed as the difference between the maximum and minimum pressures in the 40 probe array divided by the average. The turbulence level (RMS/PTAV) is defined as the arithmetic average of root-mean-square values from the eight dynamic probes (Sectin 5.2) divided by the average total pressure. These data are plotted as functions of inlet throat Mach number. Each figure includes corresponding isolated aft inlet and combined aft inlet performance. For the combined model data, the total pressure recovery, distortion, and turbulence data are plotted for values of constant front inlet throat Mach numbers.

The static pressure distributions along three inlet "streamlines" are also presented for isolated aft inlet and combined aft inlet at approximately equal throat Mach numbers. The pressure ratio is formed by dividing the local static pressure by the freestream total pressure. The pressure ratios are plotted as a function of the surface distance from the inlet lip hilite, with positive being downstream. The three streamlines begin at the inlet outer (top) lip, the side lip, and along the lower ramp surface.

Fan face station total pressure contour plots are presented for the same tunnel and inlet conditions as the static pressure distributions. These plots are oriented with the inlet on top (looking downstream).

6.2.1 Long Aft Inlet

The long aft inlet isolated versus combined performance comparison data are given in Figures 22 through 33. These data are further divided into two major configurations -- clean long aft inlet (Figures 22 through 29) and long aft inlet with vortex generators and shaft simulator (Figures 30 through 33).

6.2.1.1 Clean Long Aft Inlet

Initially the front inlet fan hot-air supply pipe was located on the side of the nacelle. This location introduced an unsymmetrical distortion pattern on the aft fan face pressure contour maps. Therefore, the supply pipe was relocated to the top of the nacelle, Figure 3. Aft inlet performance with supply pipe at each location is presented next.

Supply Pipe on Top

Clean Long Aft Inlet performance with the front fan air supply pipe on top (in tunnel installation, actually across the front fan nozzle exit) is presented in Figures 22 to 25. These data are for tunnel operating conditions of Vo = 0, 35, 85, and 135 knots and angles-of-attack of -10, 0, 20, and 40^0. Generally, the presence of an operating front inlet improves the aft inlet performance. The static condition (Vo = 0 knots, $\alpha = 0^0$) is given in Figure 22.

At the static condition, Vo = 0 knots and $\alpha = 0^0$, the isolated long aft inlet pressure recovery is 0.989 and the distortion is .048, Table IV. The combined clean long aft inlet pressure recovery is 0.989 and the distortion is .067, Table V.

The pressure recovery is slightly better for the combined inlet model whereas the distortion levels are essentially identical. The turbulence levels also are equal except at the highest air flow. And both the static

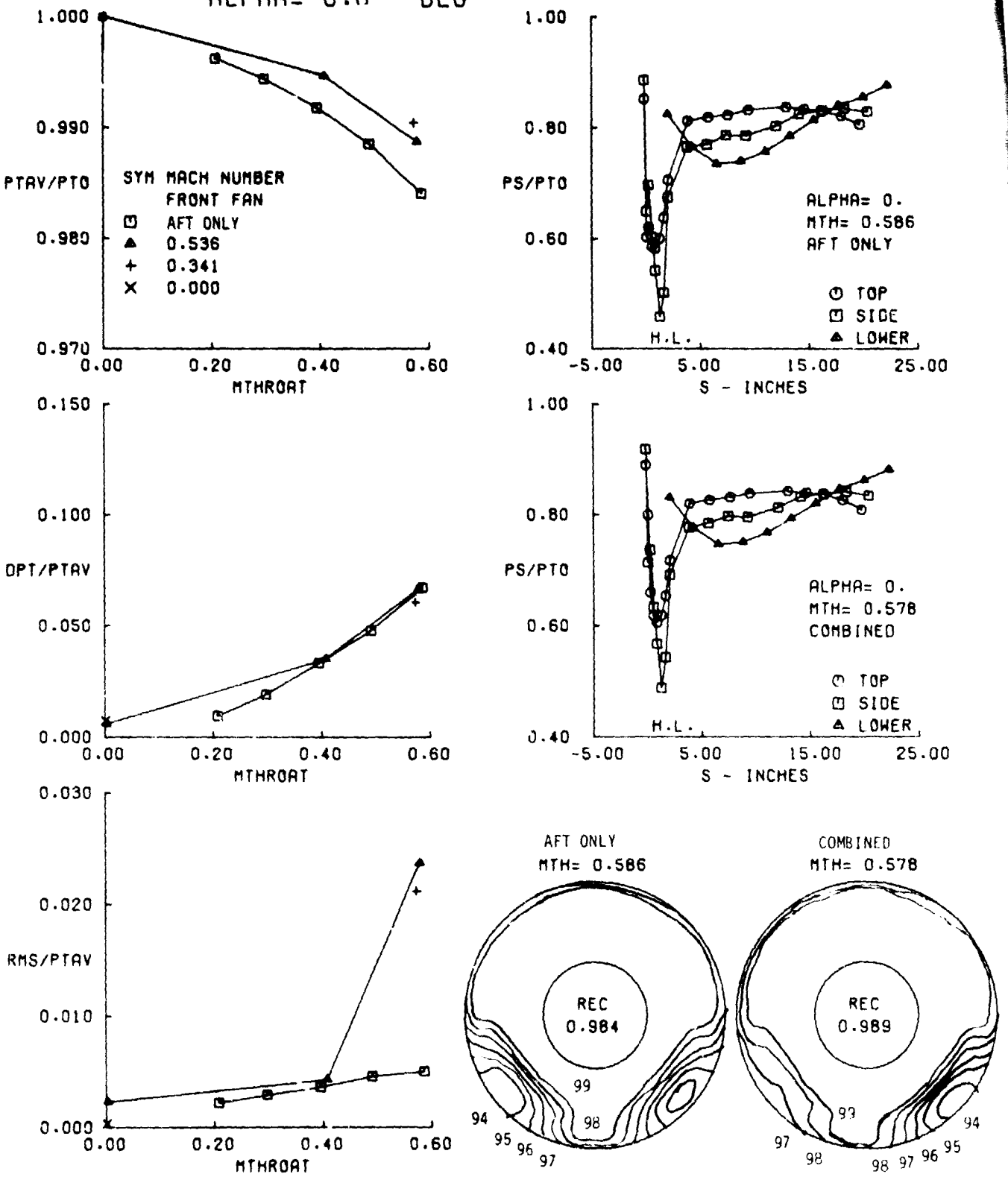

FIGURE 22. LONG AFT INLET PERFORMANCE AT V_0 = 0 KNOTS

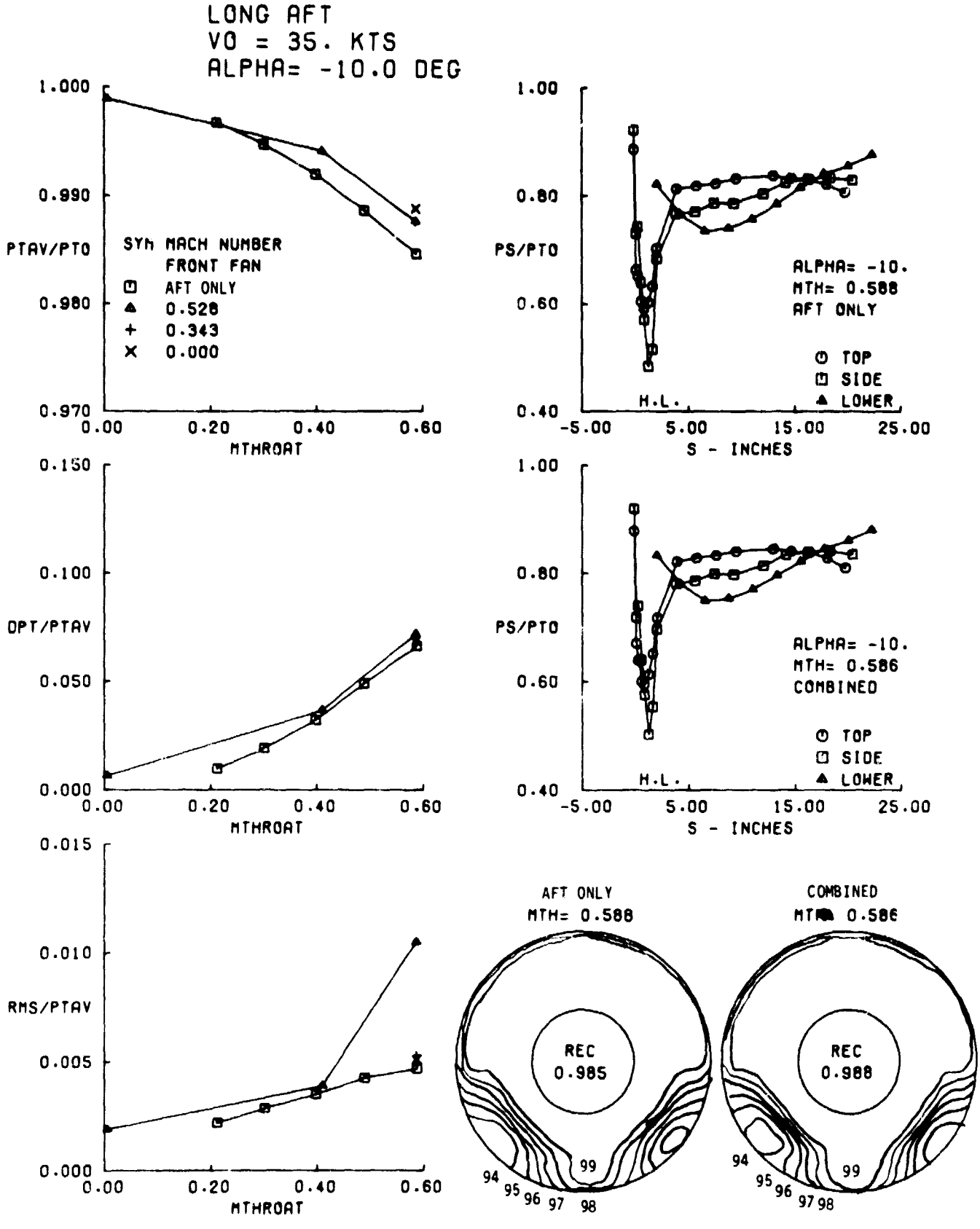

FIGURE 23a. LONG AFT INLET PERFORMANCE AT V_0 = 35 KNOTS, α = -10°.

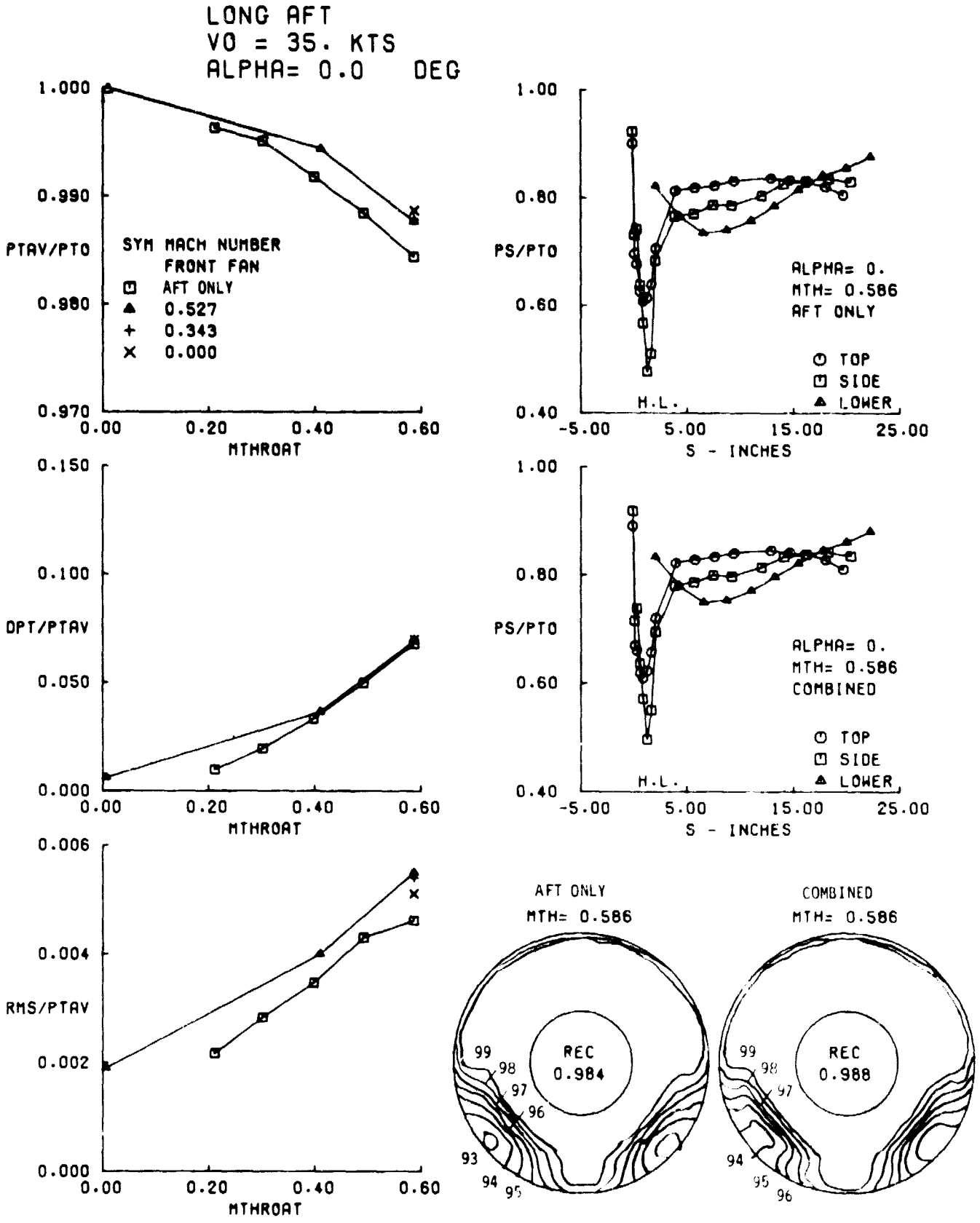

FIGURE 23b. LONG AFT INLET PERFORMANCE AT V_0 = 35 KNOTS, $\alpha = 0^0$.

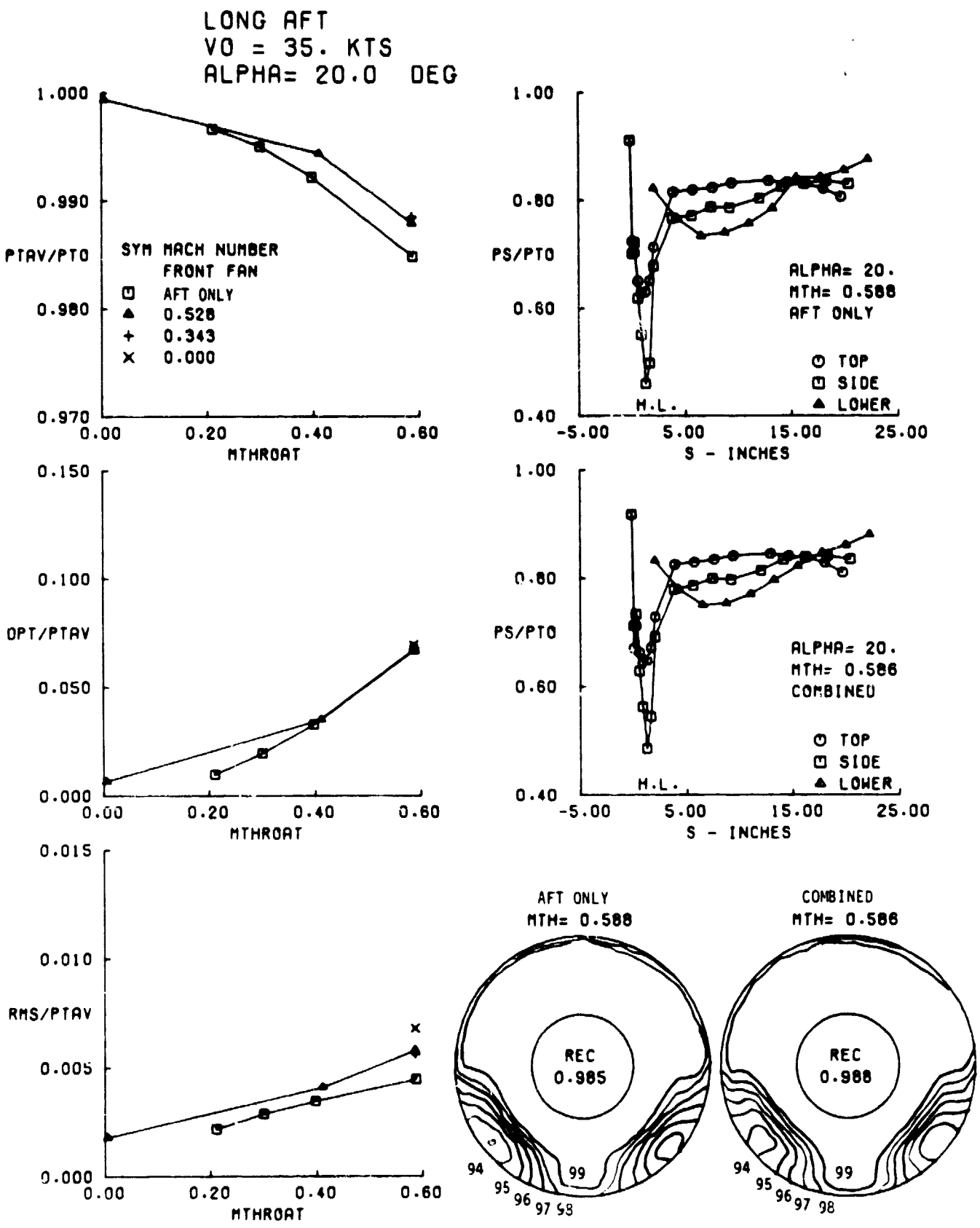

FIGURE 23c. LONG AFT INLET PERFORMANCE AT V_0 = 35 KNOTS, α = 20°.

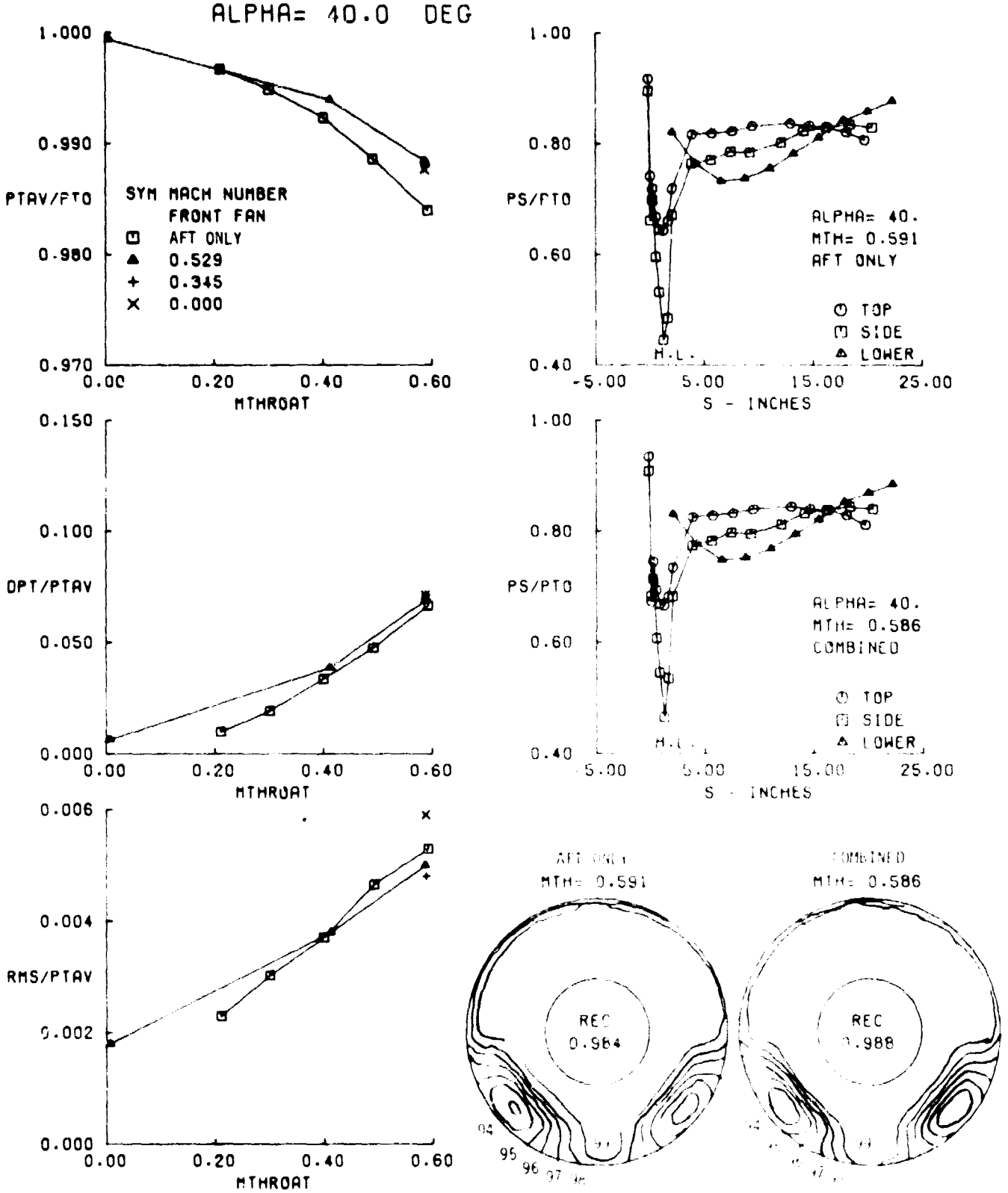

FIGURE 23d. LONG AFT INLET PERFORMANCE AT [illegible]

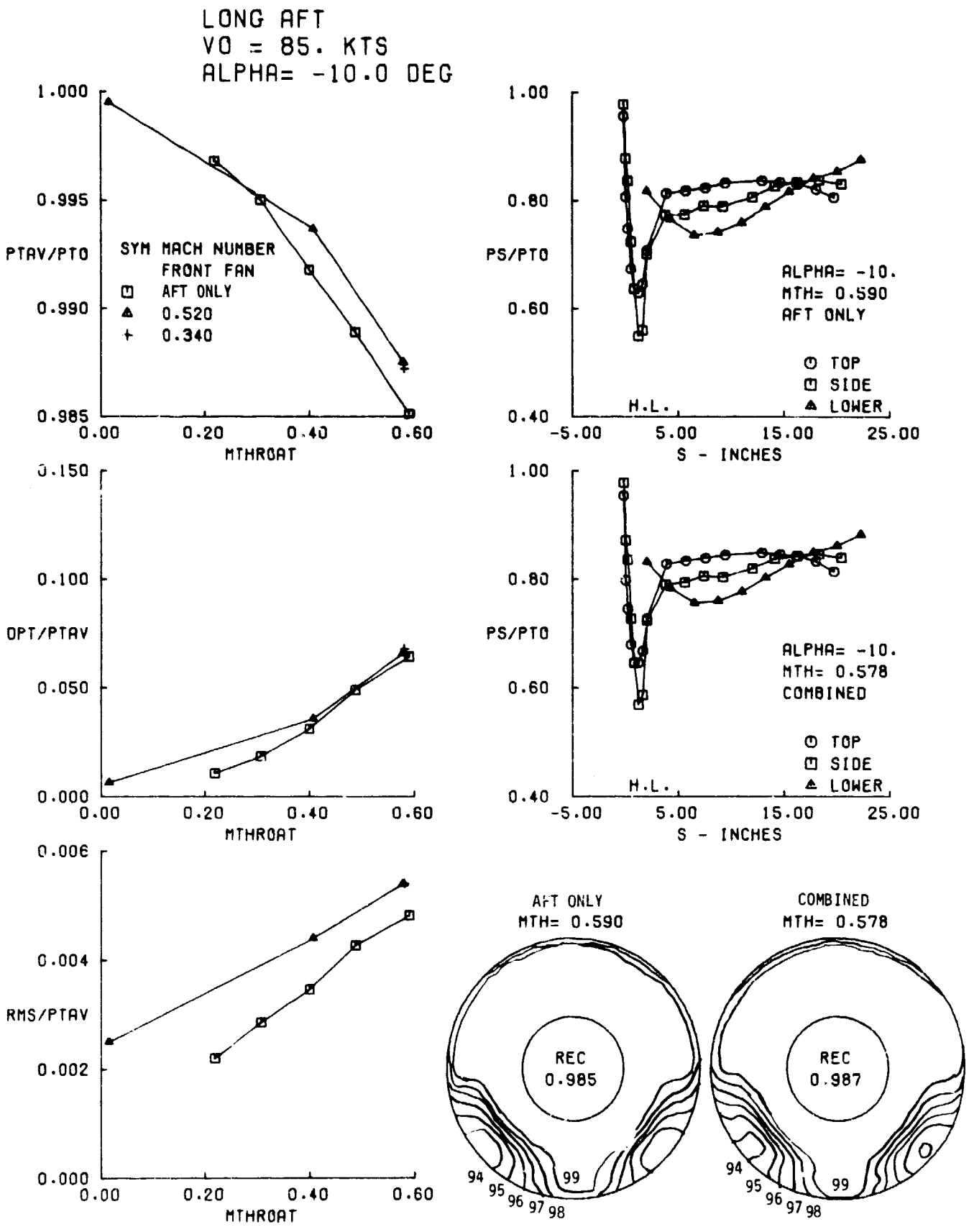

FIGURE 24a. LONG AFT INLET PERFORMANCE AT V_o = 85 KNOTS, α = -10°.

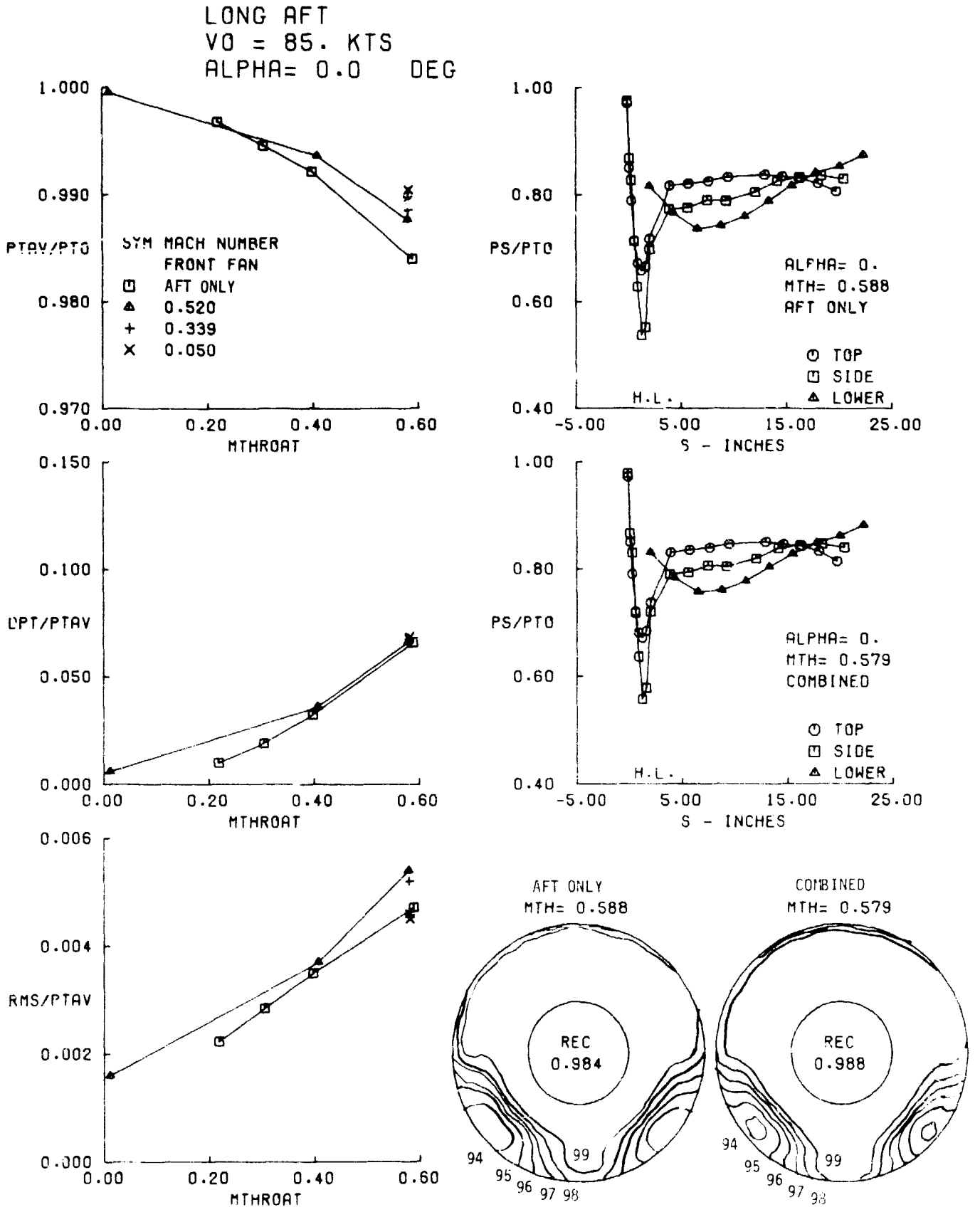

FIGURE 24b. LONG AFT INLET PERFORMANCE AT V_0 = 85 KNOTS, $\alpha = 0^0$.

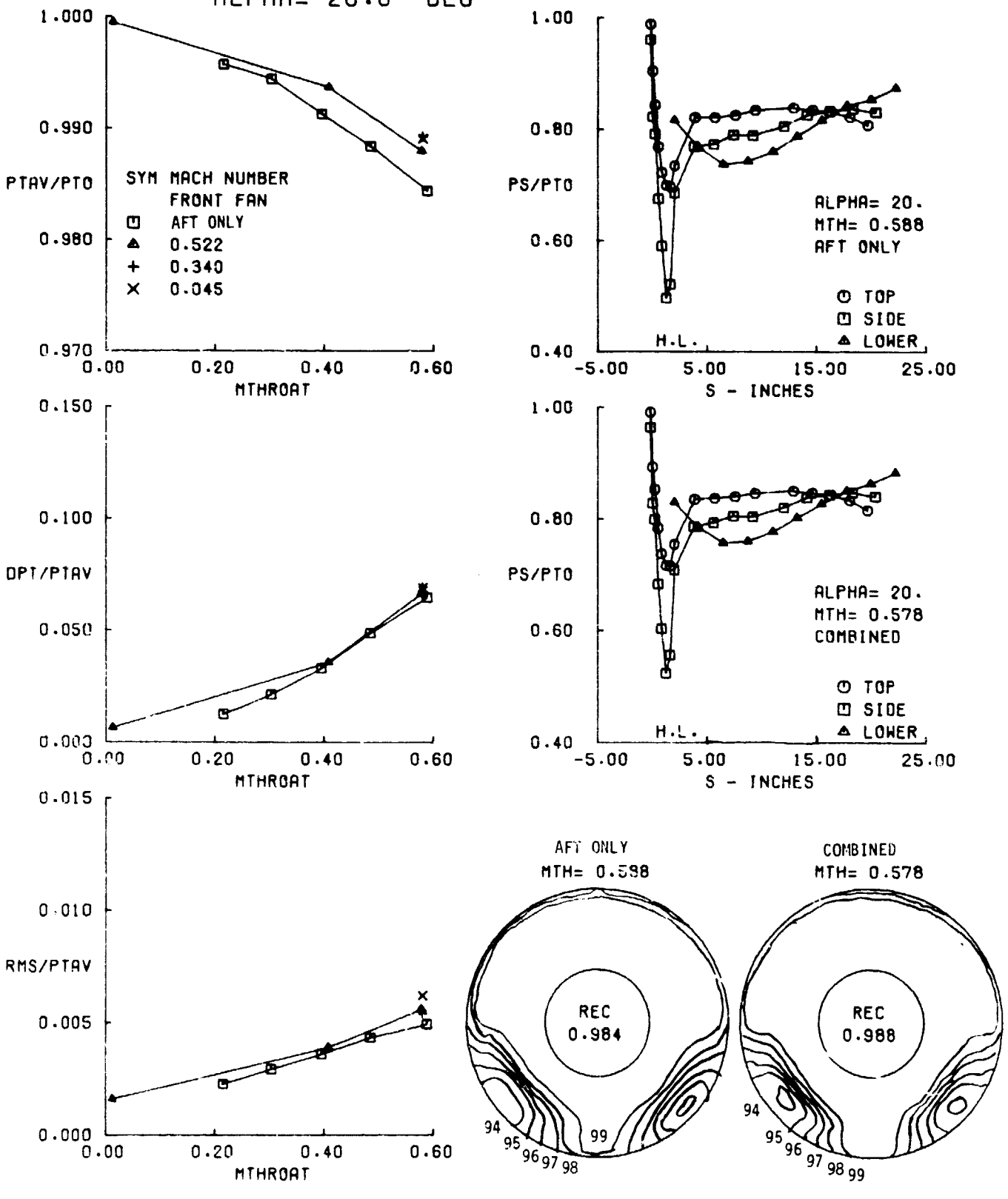

FIGURE 24c. LONG AFT INLET PERFORMANCE AT V_0 = 85 KNOTS, $\alpha = 20^0$.

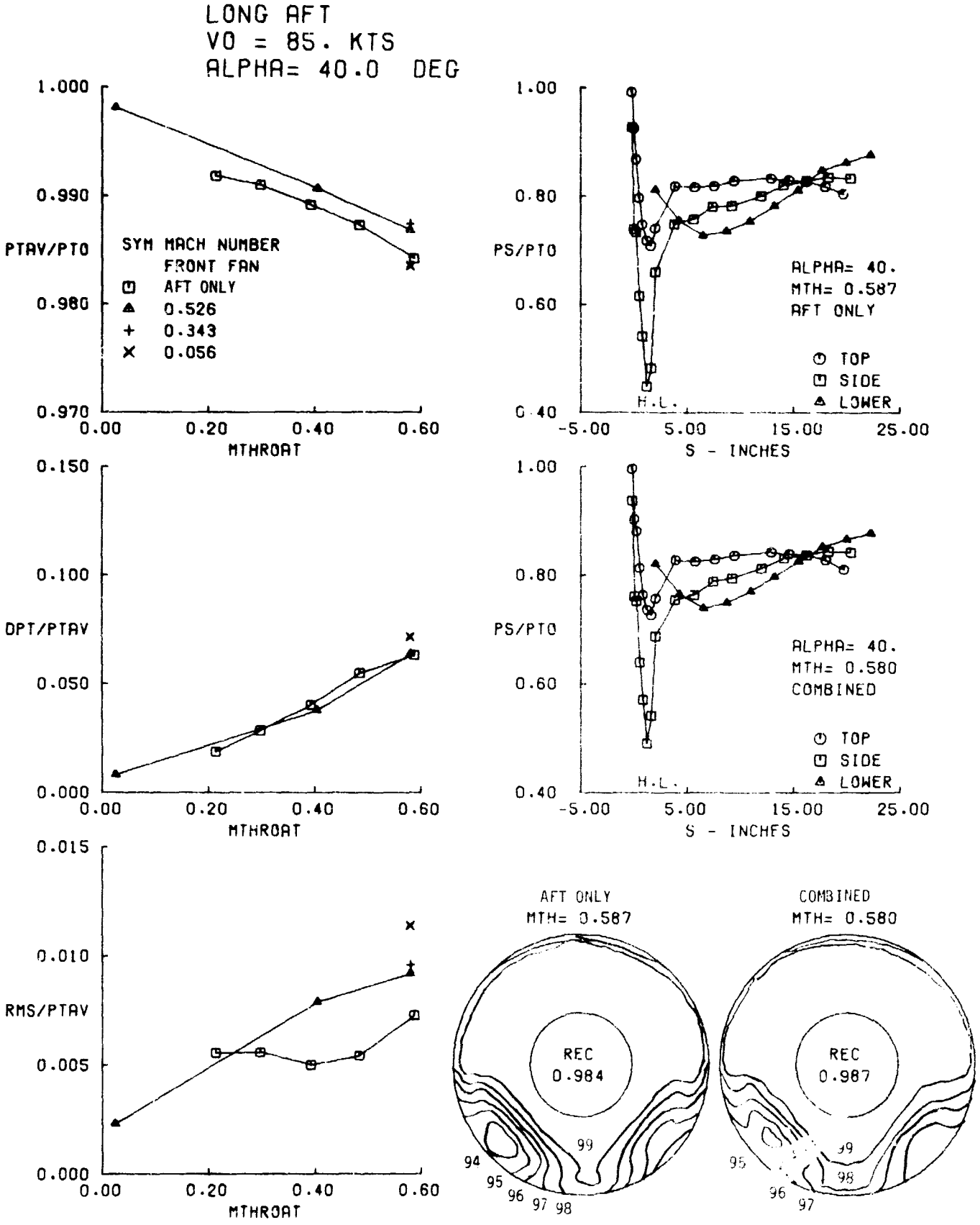

FIGURE 24d. LONG AFT INLET PERFORMANCE AT V_o = 85 KNOTS, Φ = 40°.

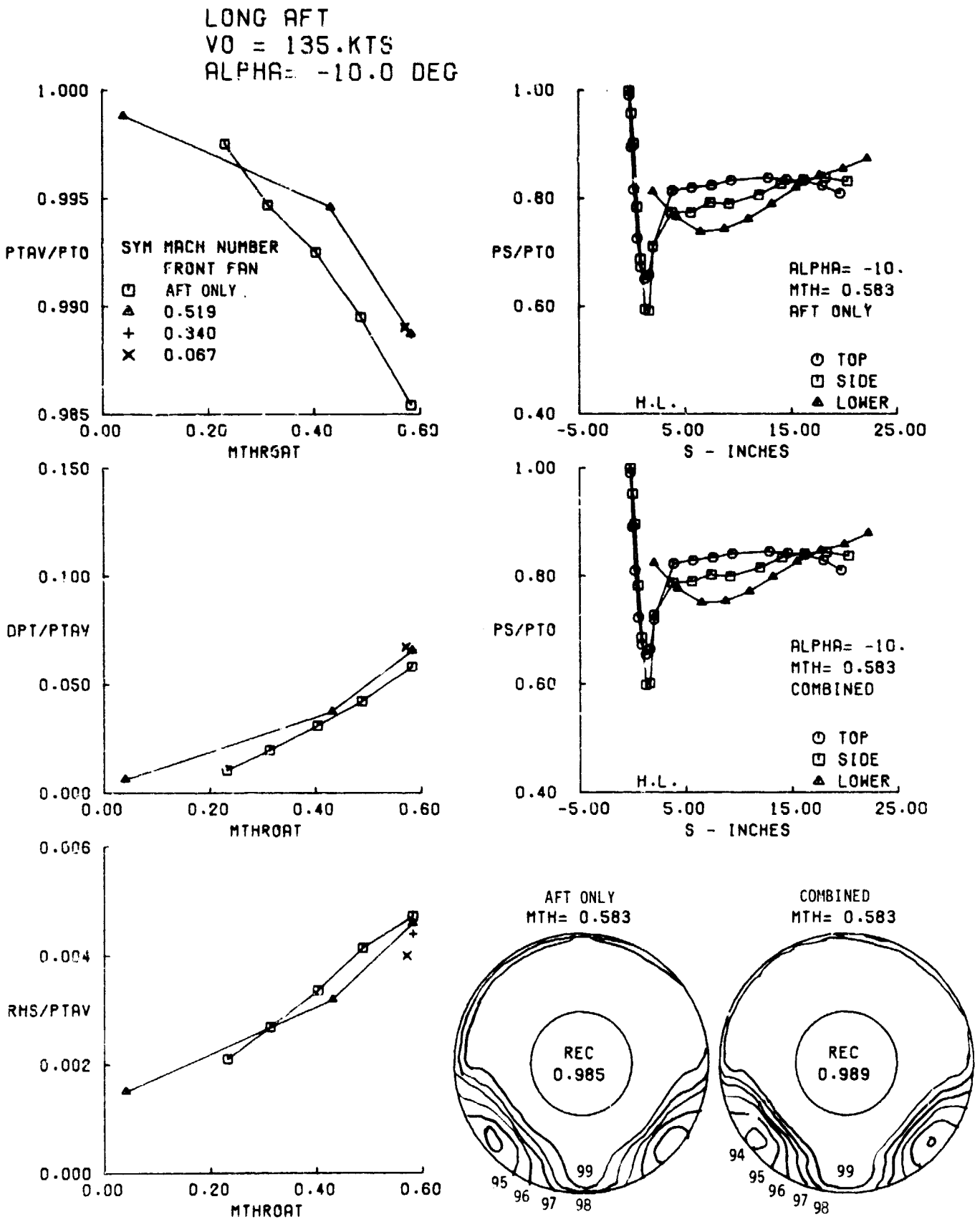

FIGURE 25a. LONG AFT INLET PERFORMANCE AT V_o = 135 KNOTS, α = -10°.

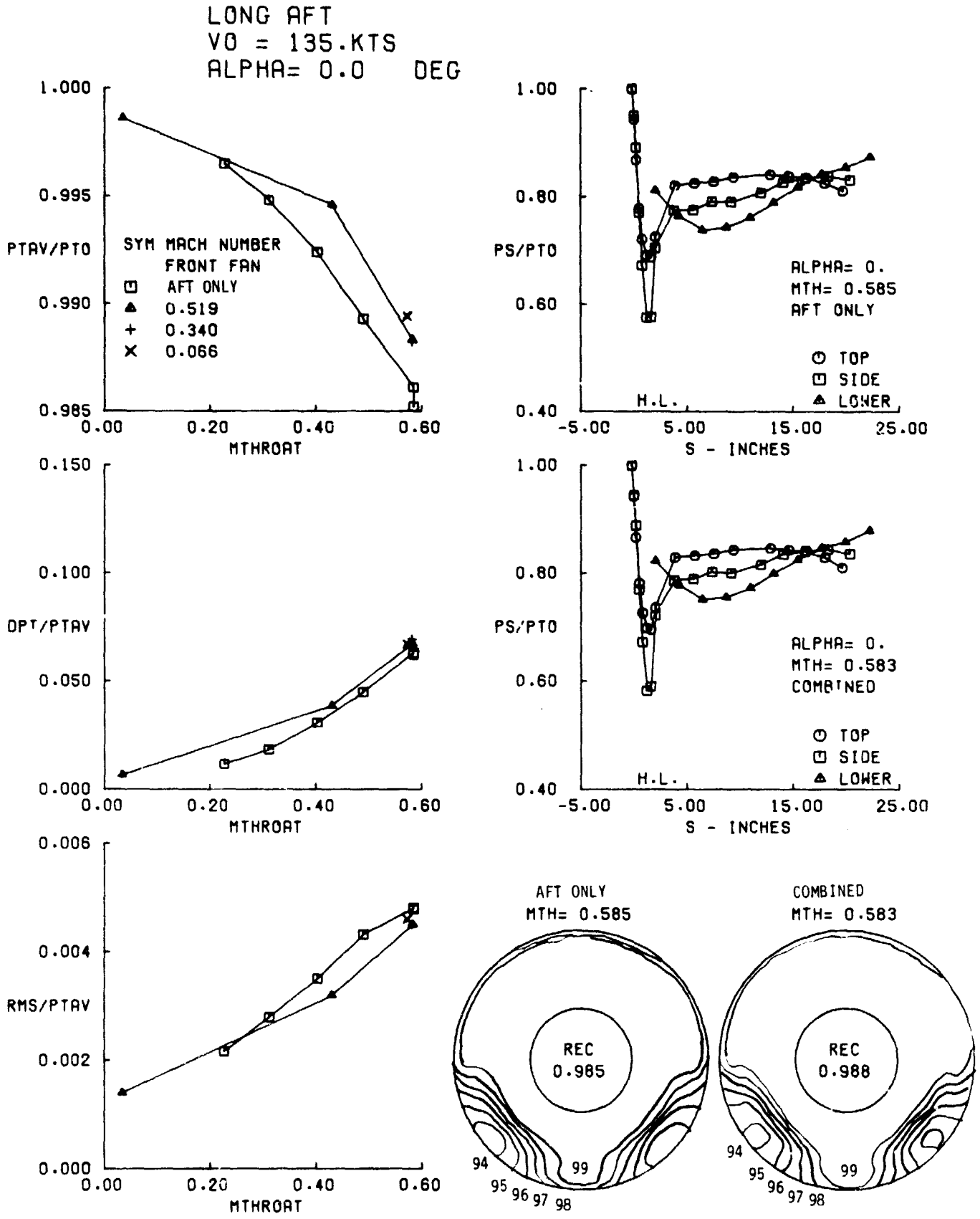

FIGURE 25b. LONG AFT INLET PERFORMANCE AT V_0 = 135 KNOTS, $\alpha = 0^0$.

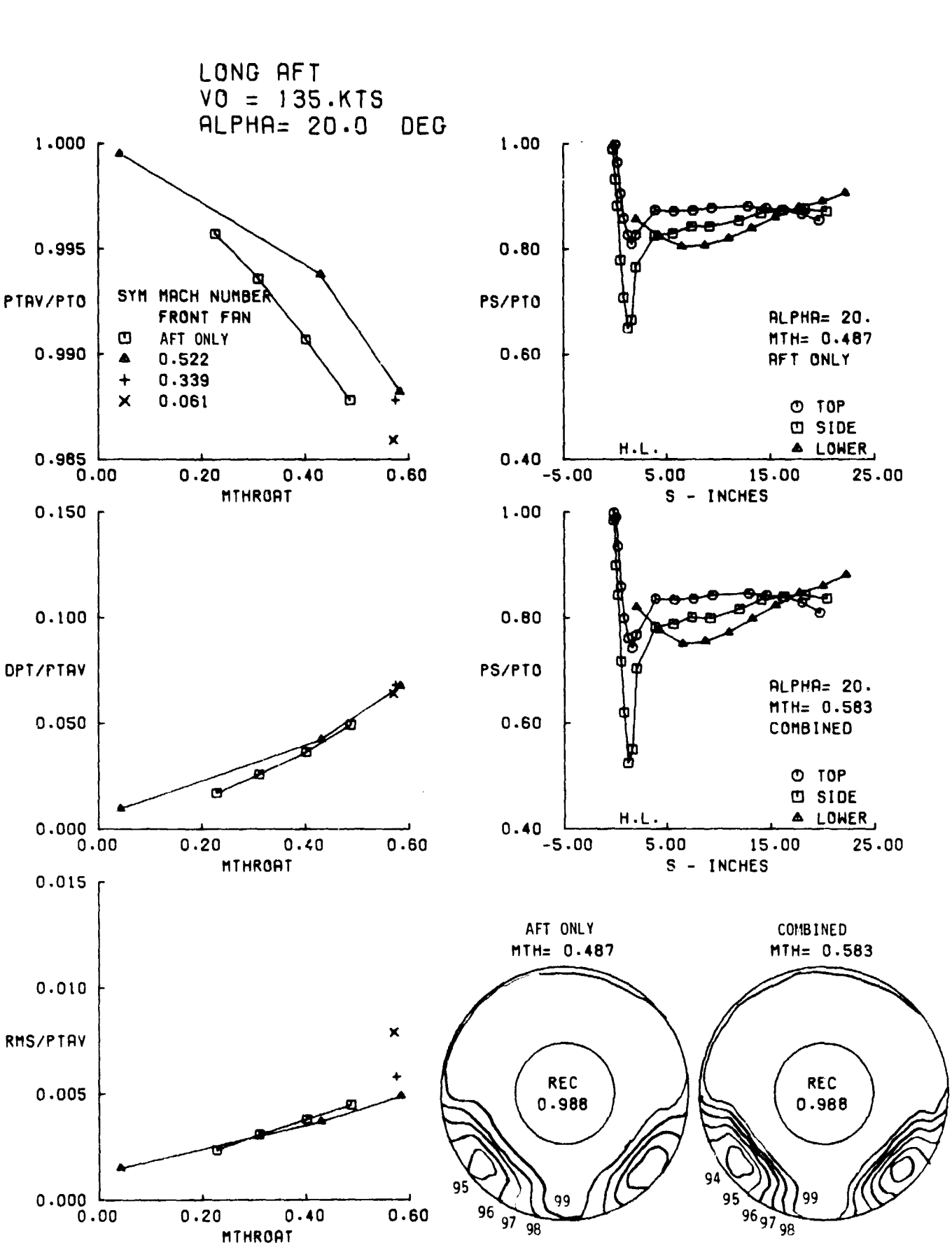

FIGURE 25c. LONG AFT INLET PERFORMANCE AT V_o = 135 KNOTS, α = 20°.

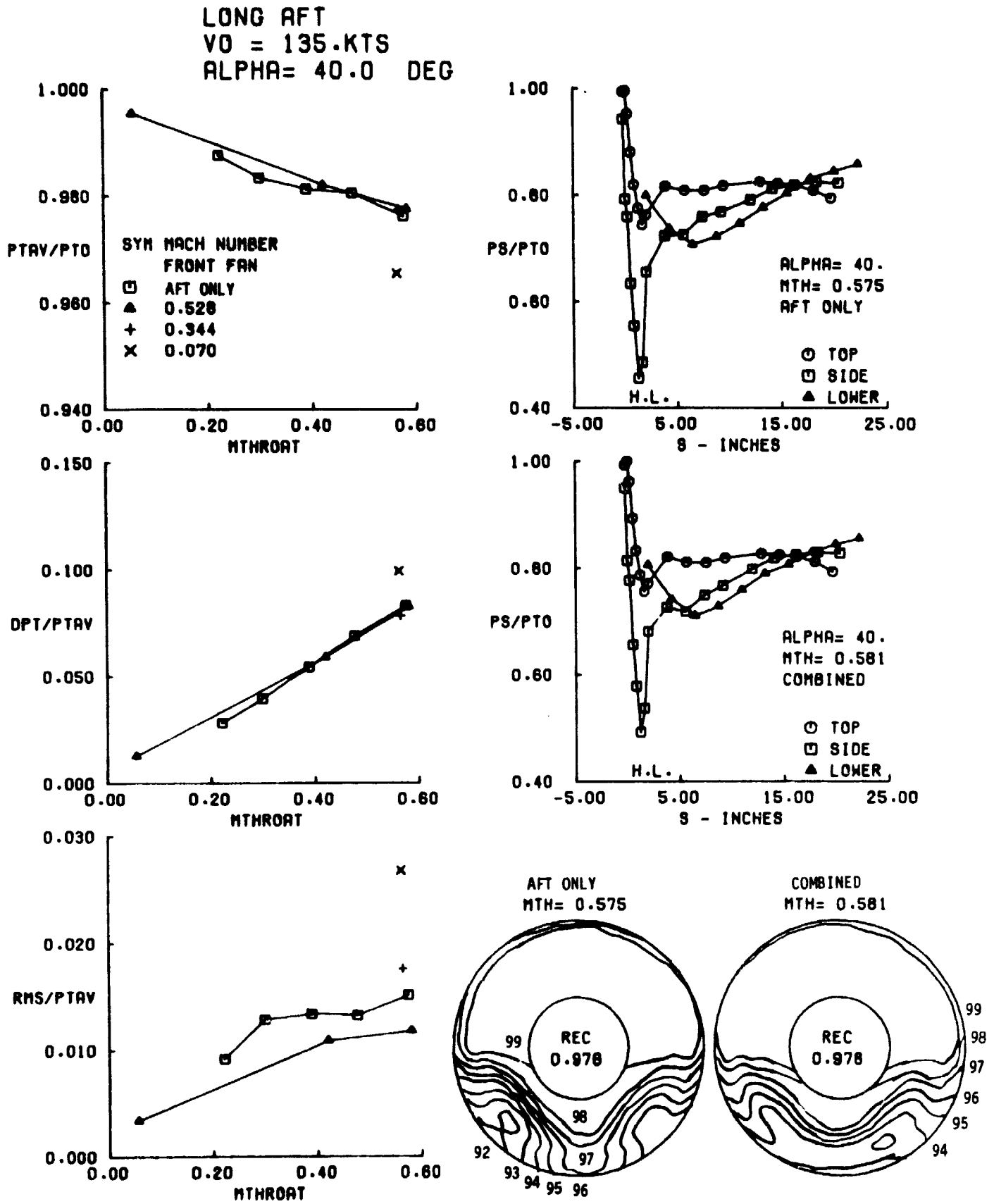

FIGURE 25d. LONG AFT INLET PERFORMANCE AT V_0 = 135 KNOTS, α = 40°.

pressure distributions and fan face contour maps are very similar. The contour maps are highly symmetrical. This pattern is repeated for Vo = 35 and 85 knots, Figure 23 and 24, throughout the angle-of-attack range. For the Vo = 135 knots case, the front inlet beneficial effects decrease with increasing angle-of-attack, Figure 25.

Supply Pipe on Side

Clean Long Aft Inlet performance with the front fan air supply pipe on the side is presented in Figure 26 to 29. These data are for tunnel operating conditions of Vo = 0, 35, 85, and 135 knots and angles-of-attack of -10, 0, 20, and 40^0. Again the presence of an operating front fan improves the aft inlet performance. The effect of the front fan air supply pipe is clearly evident in the contour maps at Vo = 35 knots (Figure 27), Vo = 85 knots (Figure 28), and Vo = 135 knots (Figure 29). Also note that the average pressure recovery is also lower for the combined inlet data at Vo = 85 and 135 knots.

6.2.1.2 Long Aft Inlet with Vortex Generators and Simulator Shaft

The front inlet fan is driven by a shaft that extends through the aft inlet duct. A stationary shaft was installed to simulate the front fan drive shaft, Figure 10. Test results for this long aft inlet configuration, including presence of vortex generators, are shown in Figures 30, 31, 32, and 33. The pressure recovery and distortion levels are slightly lower than for the clean long aft inlet; compare Figures 22 and 30, 23b and 31b, 24b and 32a, etc. However, the pressure recovery and distortion levels are again slightly higher for the combined aft inlet than for the isolated aft inlet. The low pressure region extending to the centerbody still persists in the bottom quadrant.

6.2.2 Short Aft Inlet

The short aft inlet isolated versus combined performance comparison data are given in Figures 34 through 41. Fillets were faired onto the inlet lip corners in an attempt to improve high angle-of-attack performance of the short aft inlet. See sketch on Page 15. These results are shown in Figures 42 through 45.

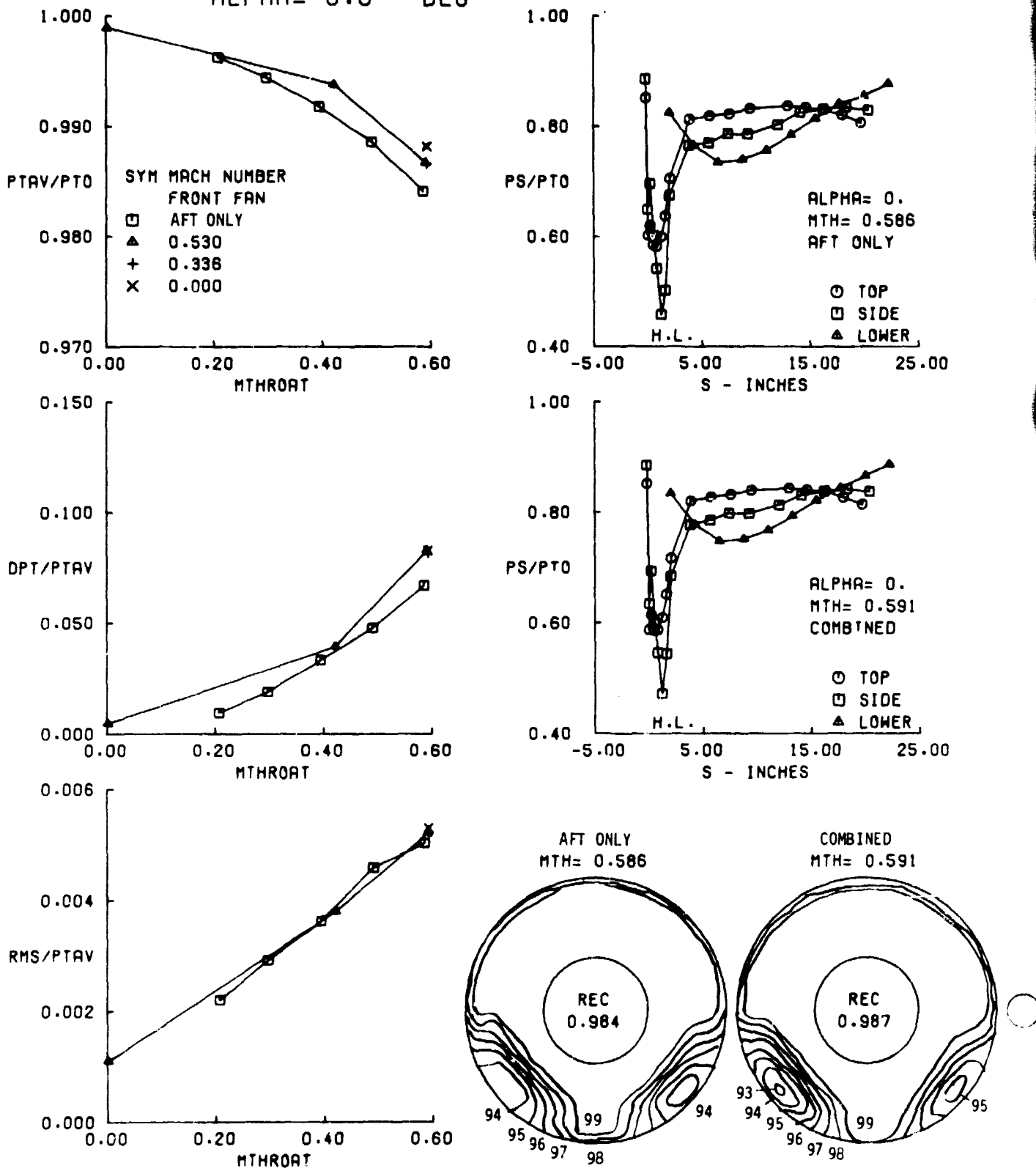

FIGURE 26. LONG AFT INLET PERFORMANCE (SIDE PIPE) AT V_o = 0 KNOTS.

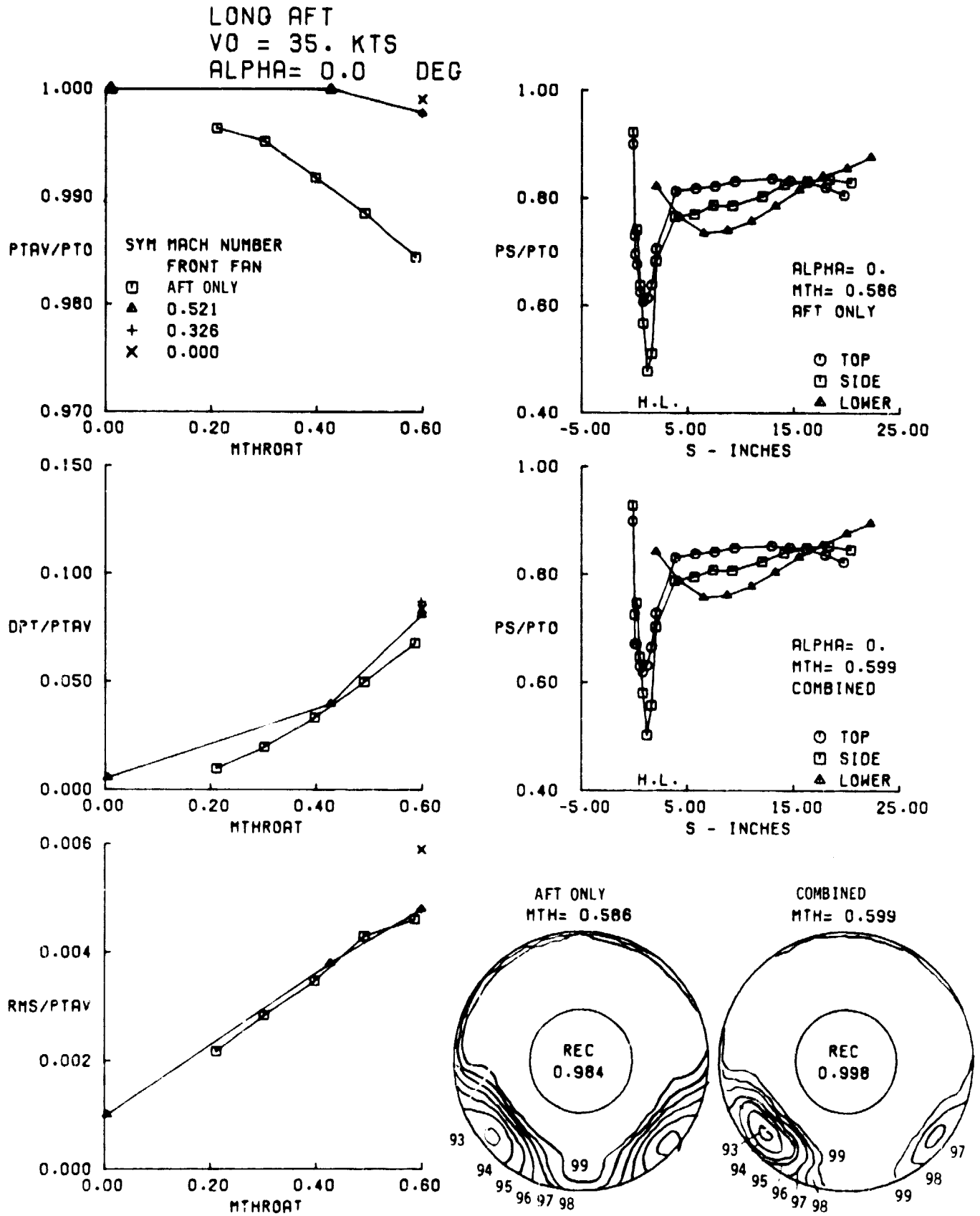

FIGURE 27a. LONG AFT INLET PERFORMANCE (SIDE PIPE) AT V_o = 35 KNOTS, $\alpha = 0^o$.

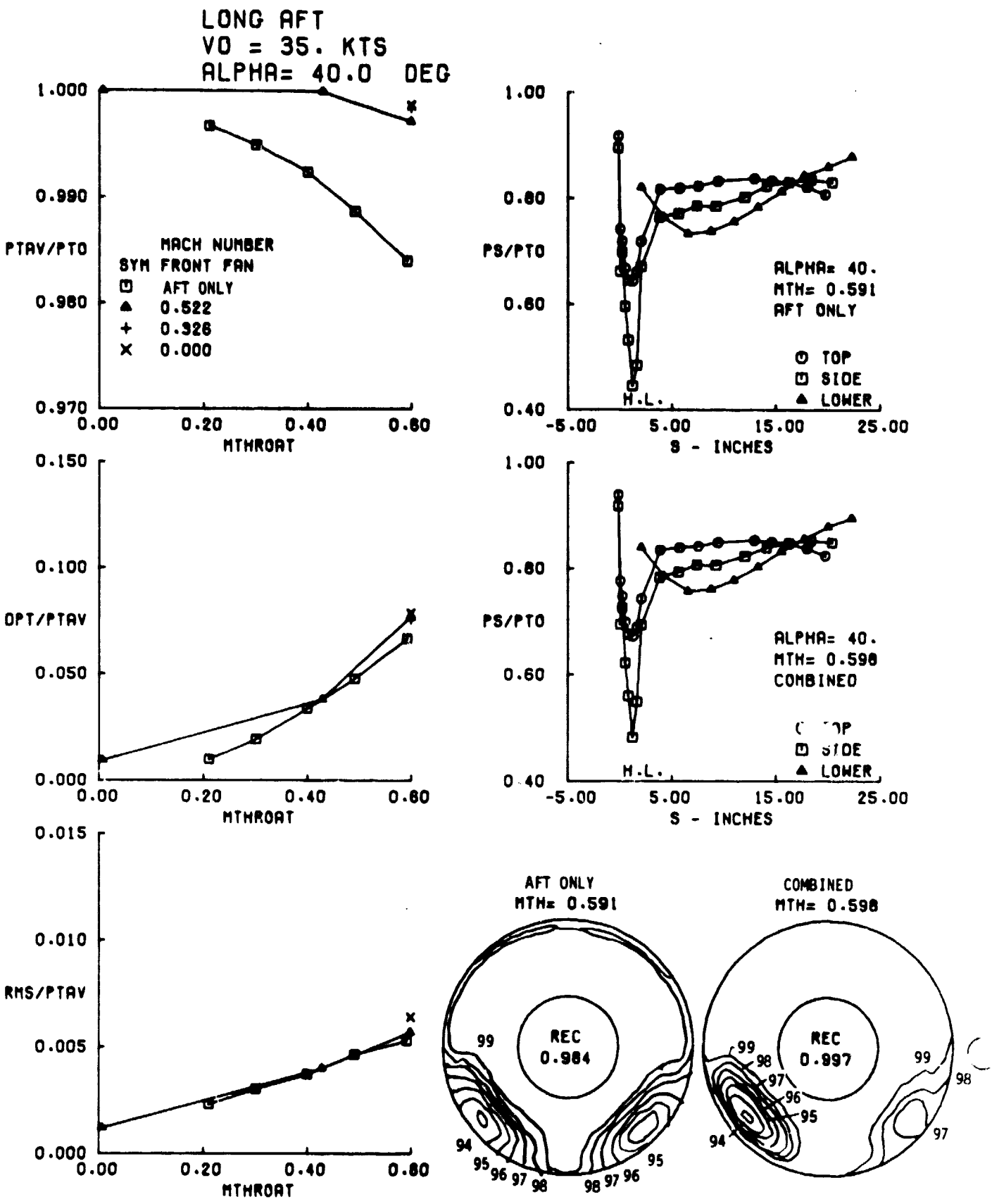

FIGURE 27b. LONG AFT INLET PERFORMANCE (SIDE PIPE) AT V_o = 35 KNOTS, α = 40°.

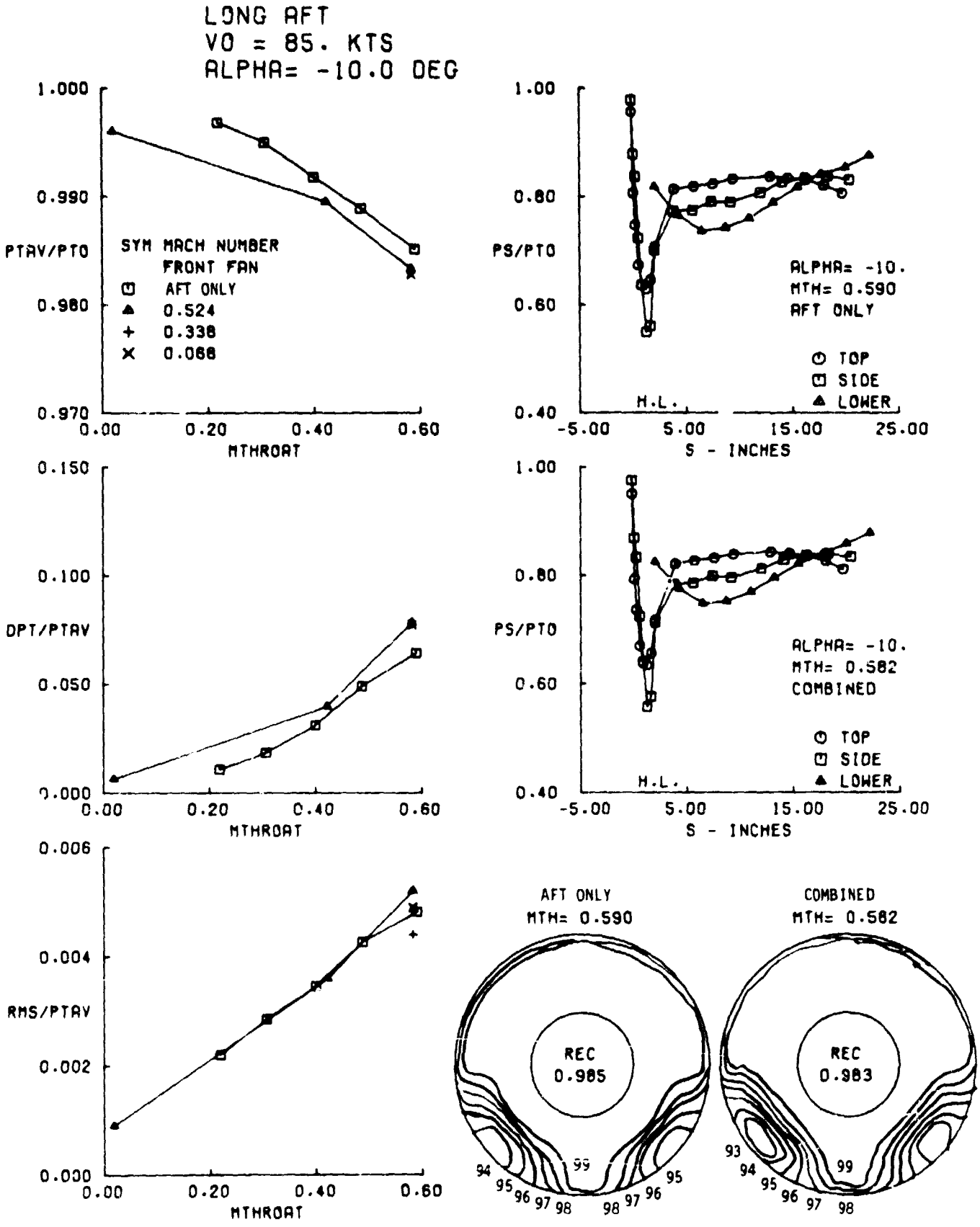

FIGURE 28a. LONG AFT INLET PERFORMANCE (SIDE PIPE) AT V_o = 85 KNOTS, α = -10°.

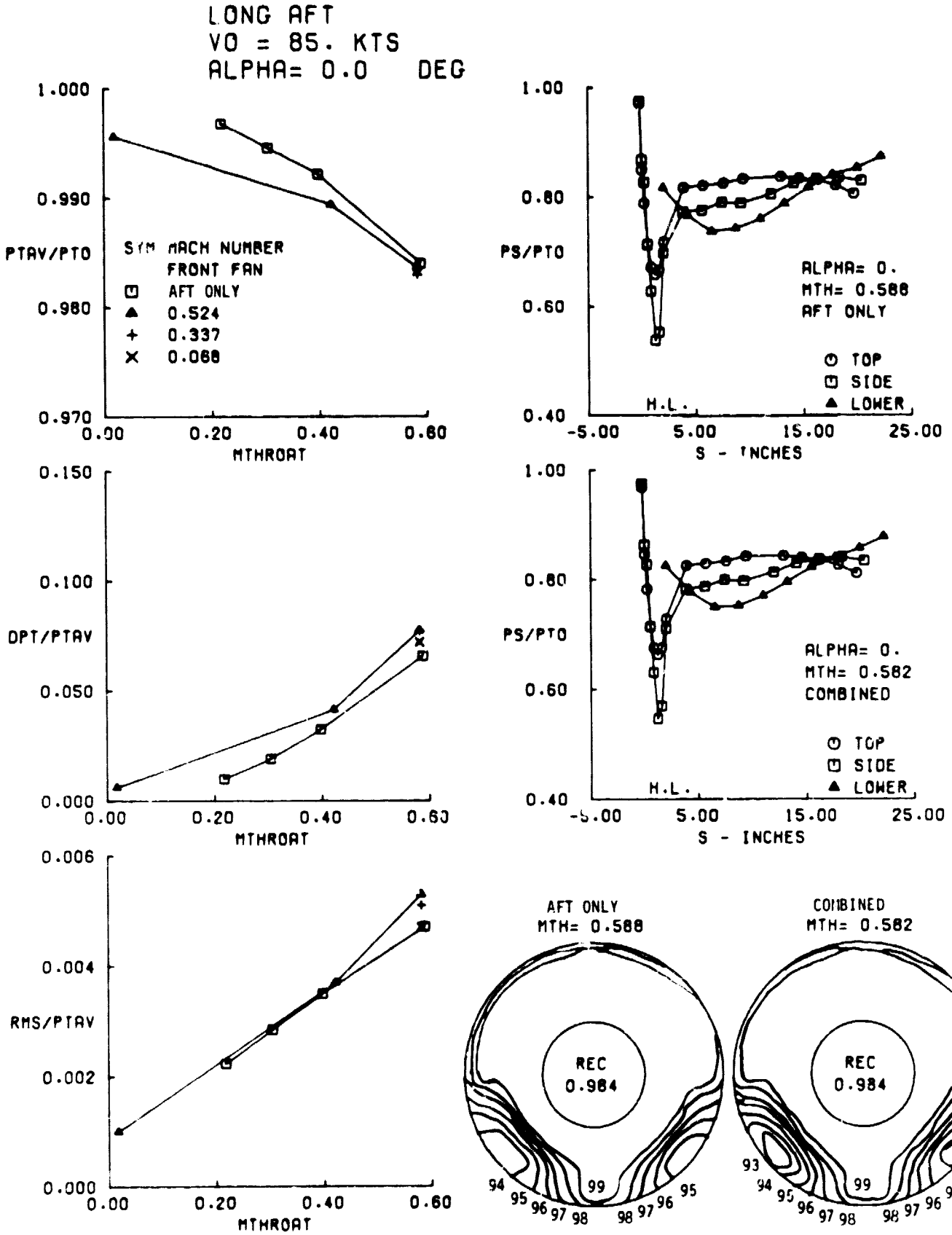

FIGURE 28b. LONG AFT INLET PERFORMANCE (SIDE PIPE) AT V_o = 85 KNOTS, $\alpha = 0^o$.

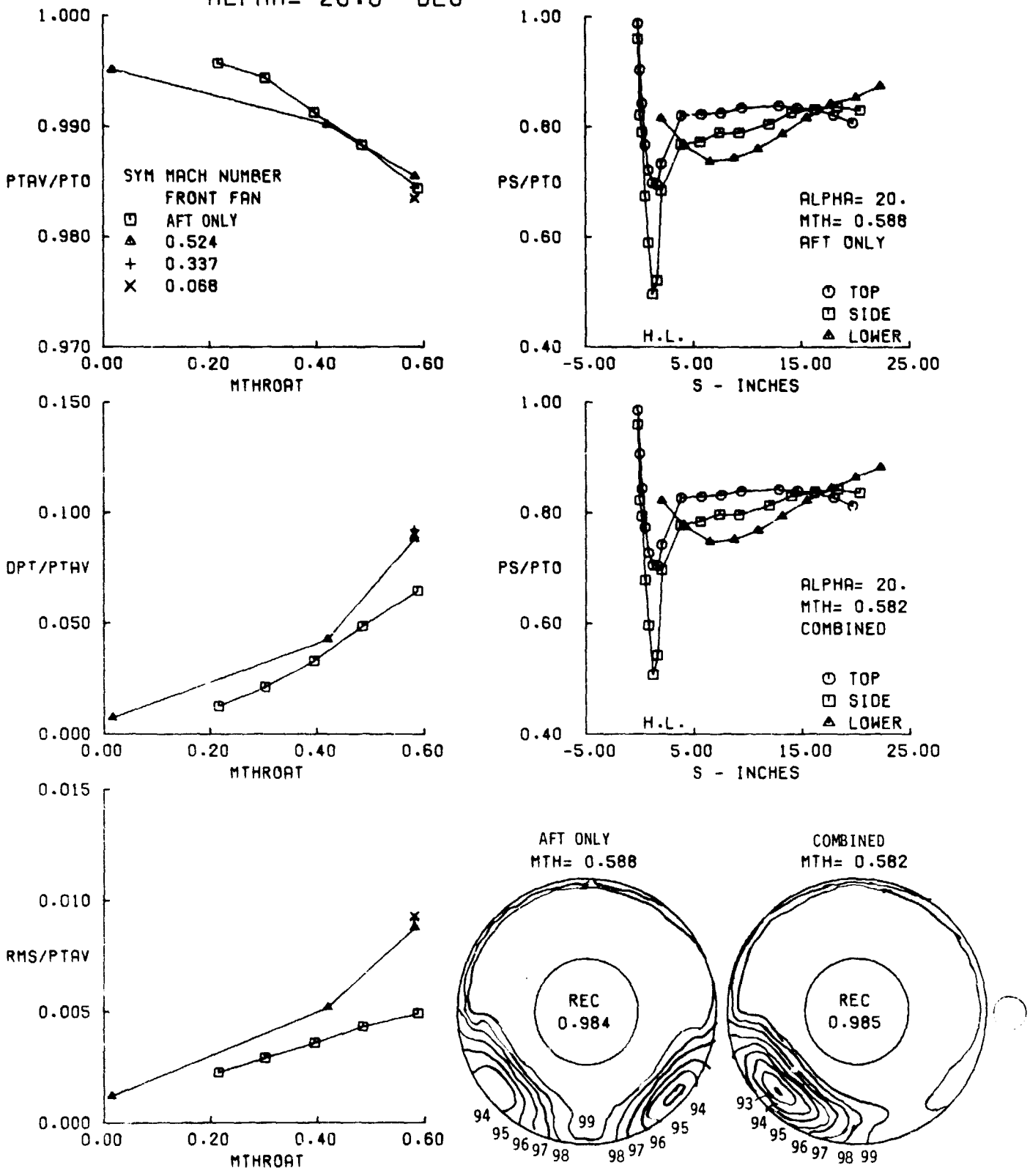

FIGURE 28c. LONG AFT INLET PERFORMANCE (SIDE PIPE) AT V_0 = 85 KNOTS, α = 20°.

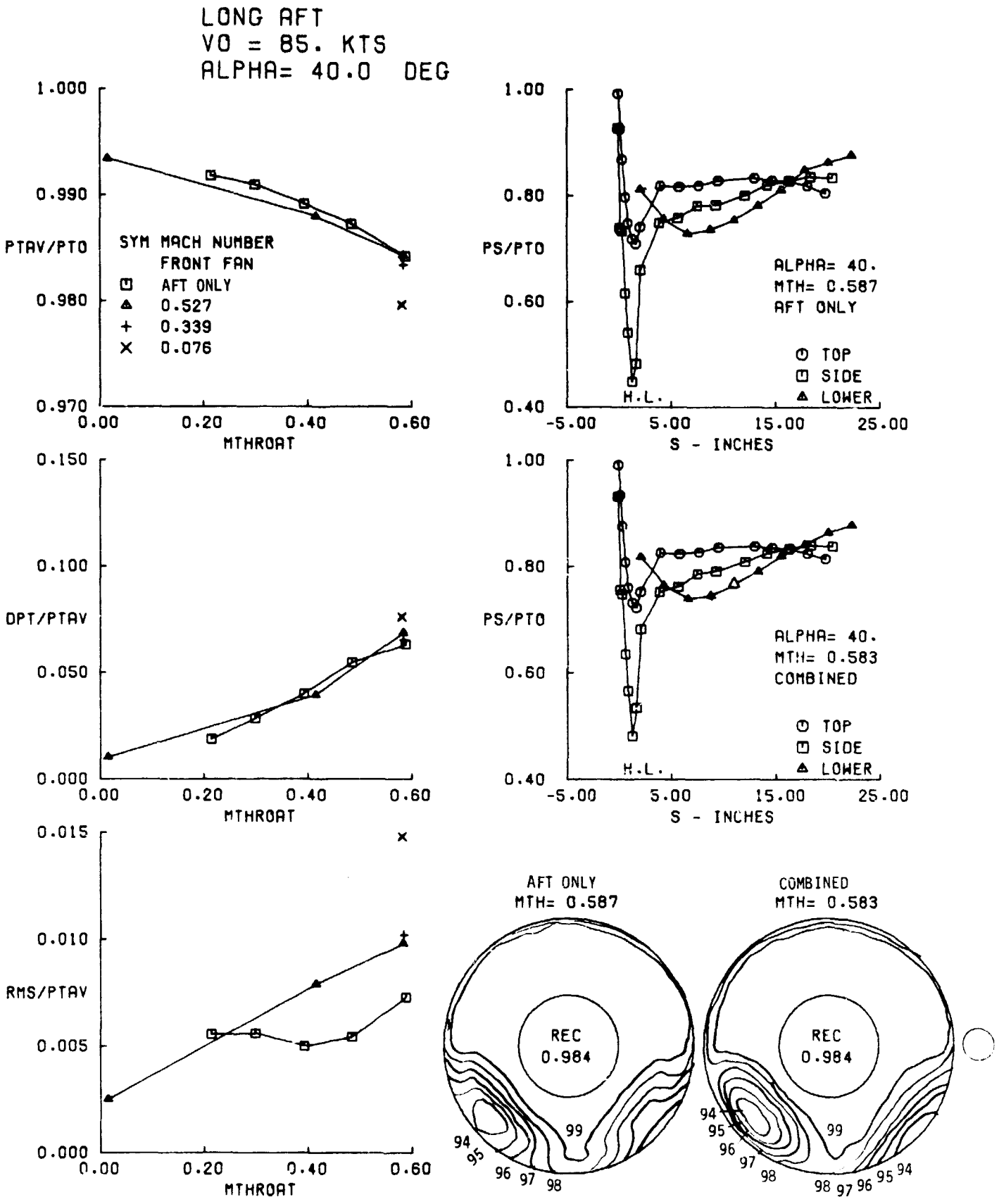

FIGURE 28d. LONG AFT INLET PERFORMANCE (SIDE PIPE) AT V_o = 85 KNOTS, $\alpha = 40^o$.

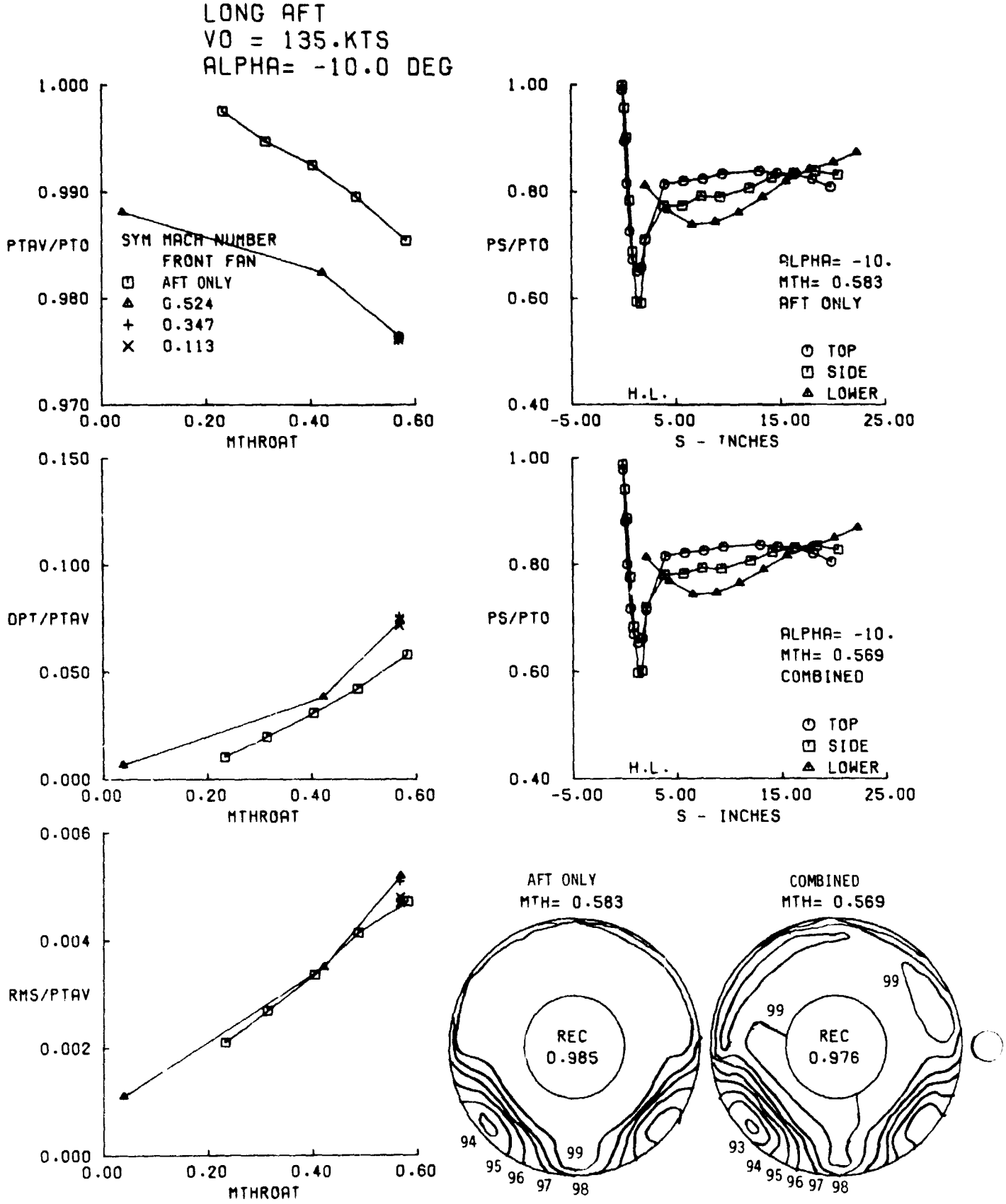

FIGURE 29a. LONG AFT INLET PERFORMANCE (SIDE PIPE) AT V_0 = 135 KNOTS, α = -10°.

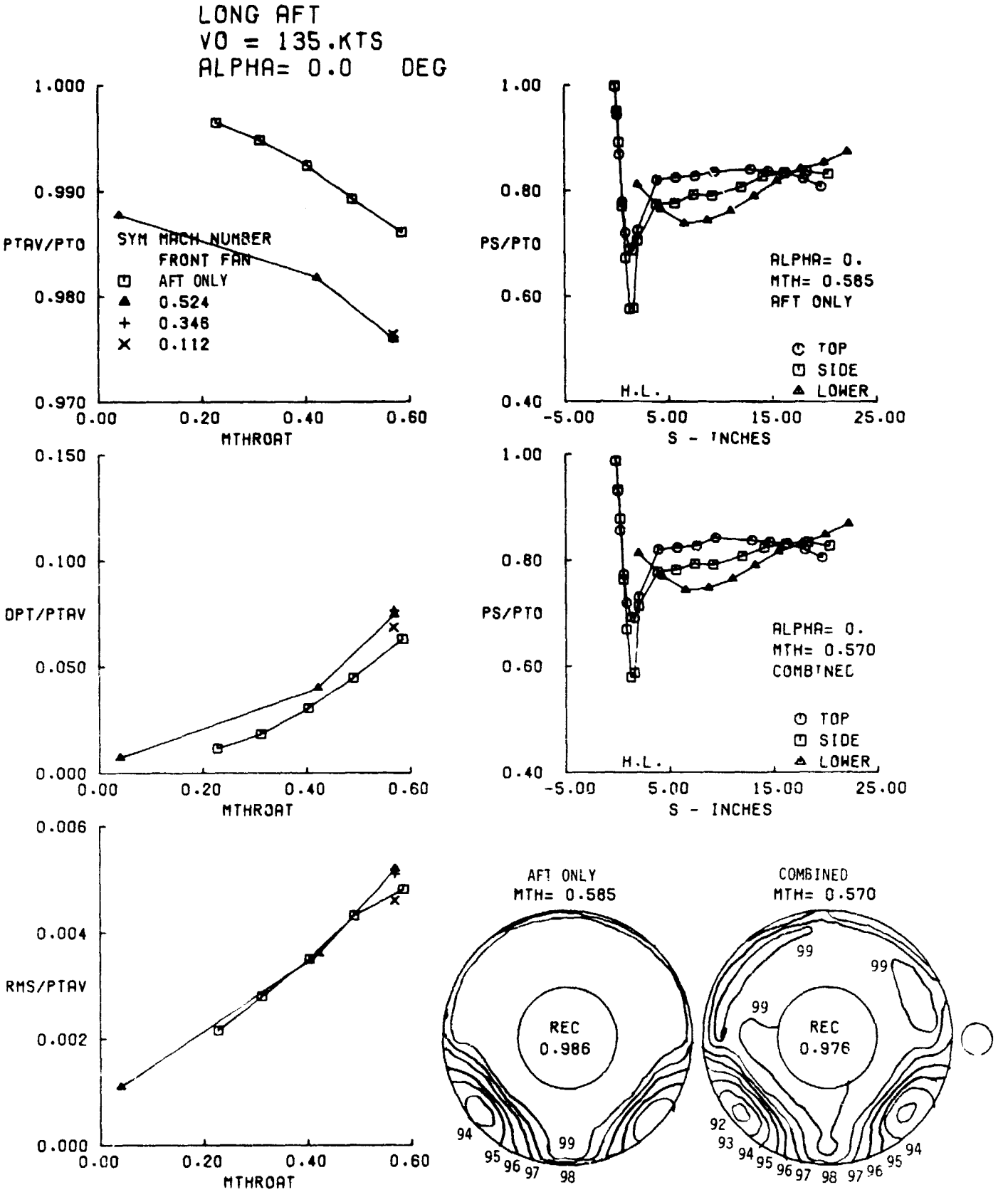

FIGURE 29b. LONG AFT INLET PERFORMANCE (SIDE PIPE) AT V_o = 135 KNOTS, $\alpha = 0^o$.

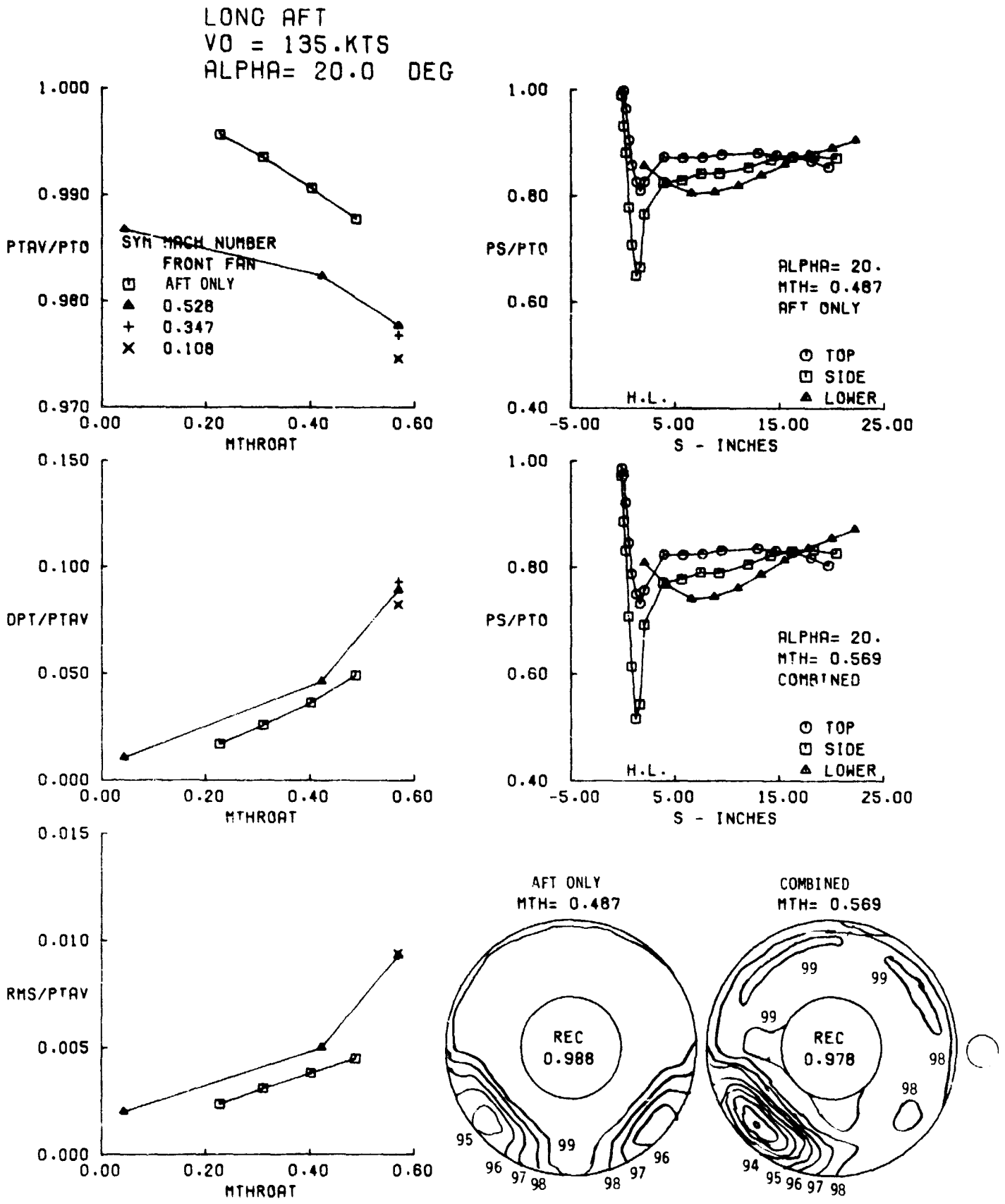

FIGURE 29c. LONG AFT INLET PERFORMANCE (SIDE PIPE) AT V_o = 135 KNOTS, $\alpha = 20^o$.

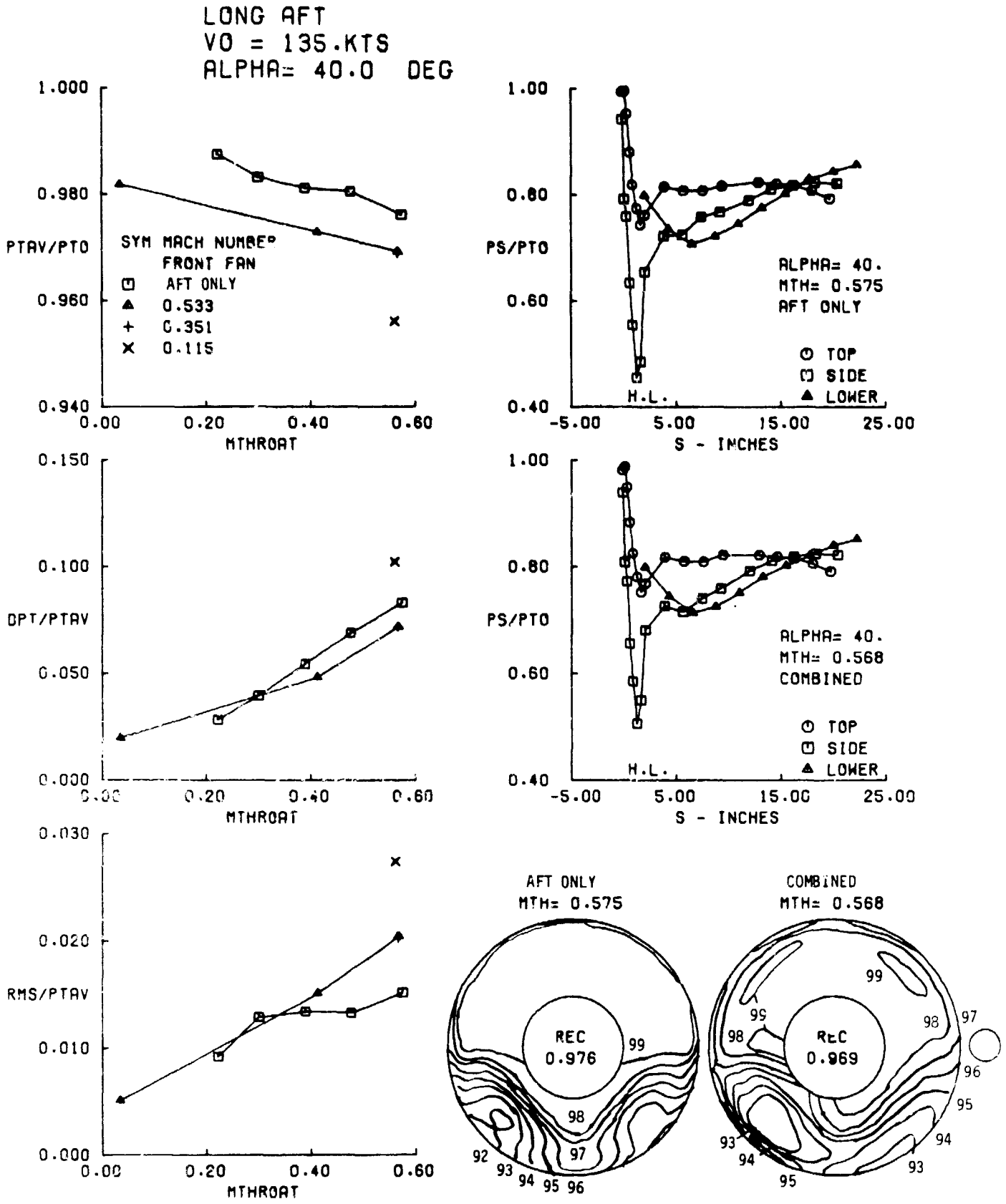

FIGURE 29d. LONG AFT INLET PERFORMANCE (SIDE PIPE) AT V_0 = 135 KNOTS, $\alpha = 40^0$.

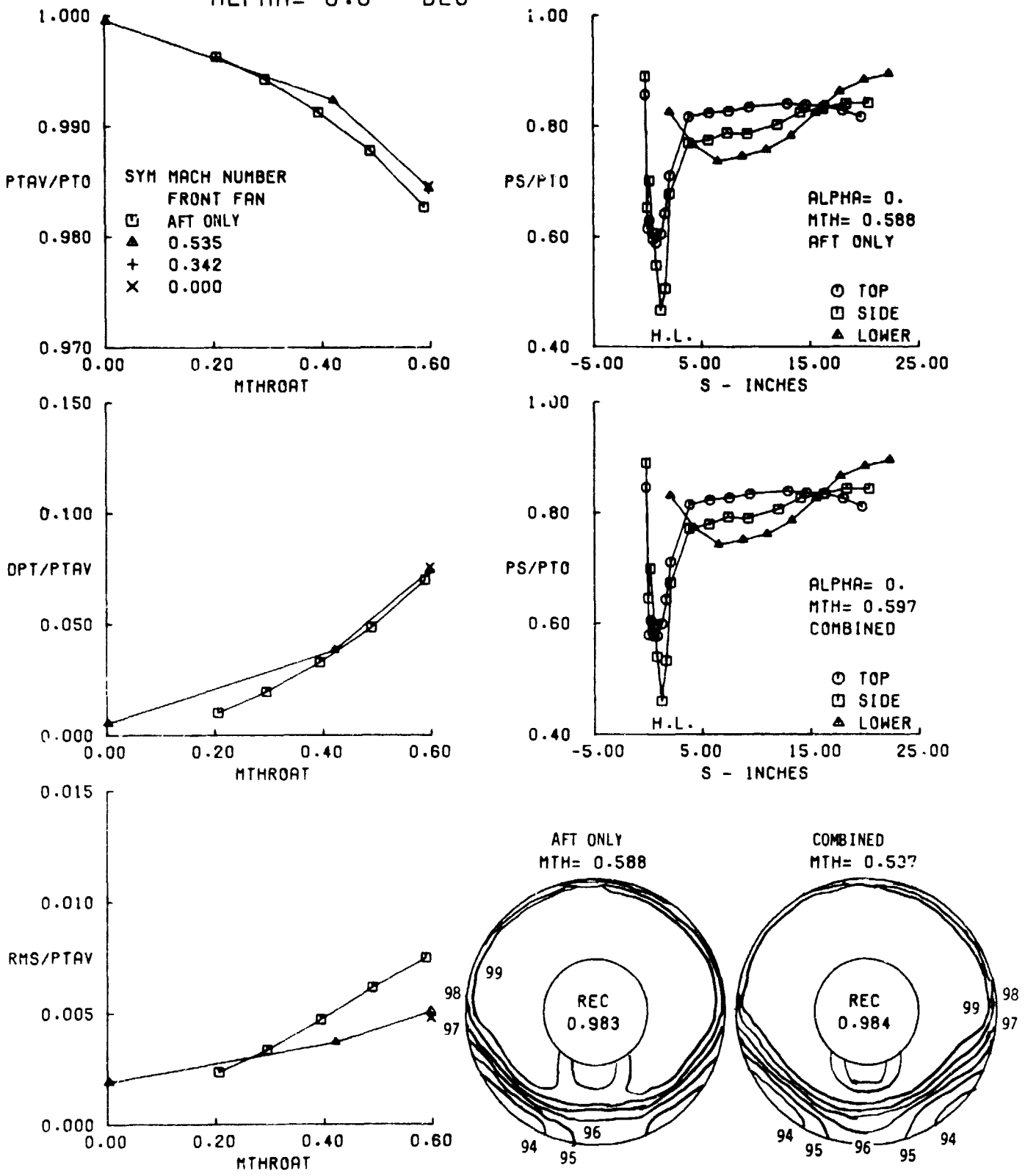

FIGURE 30. LONG AFT INLET WITH VORTES GENERATORS AND SHAFT SIMULATOR PERFORMANCE AT V_0 = 0 KNOTS

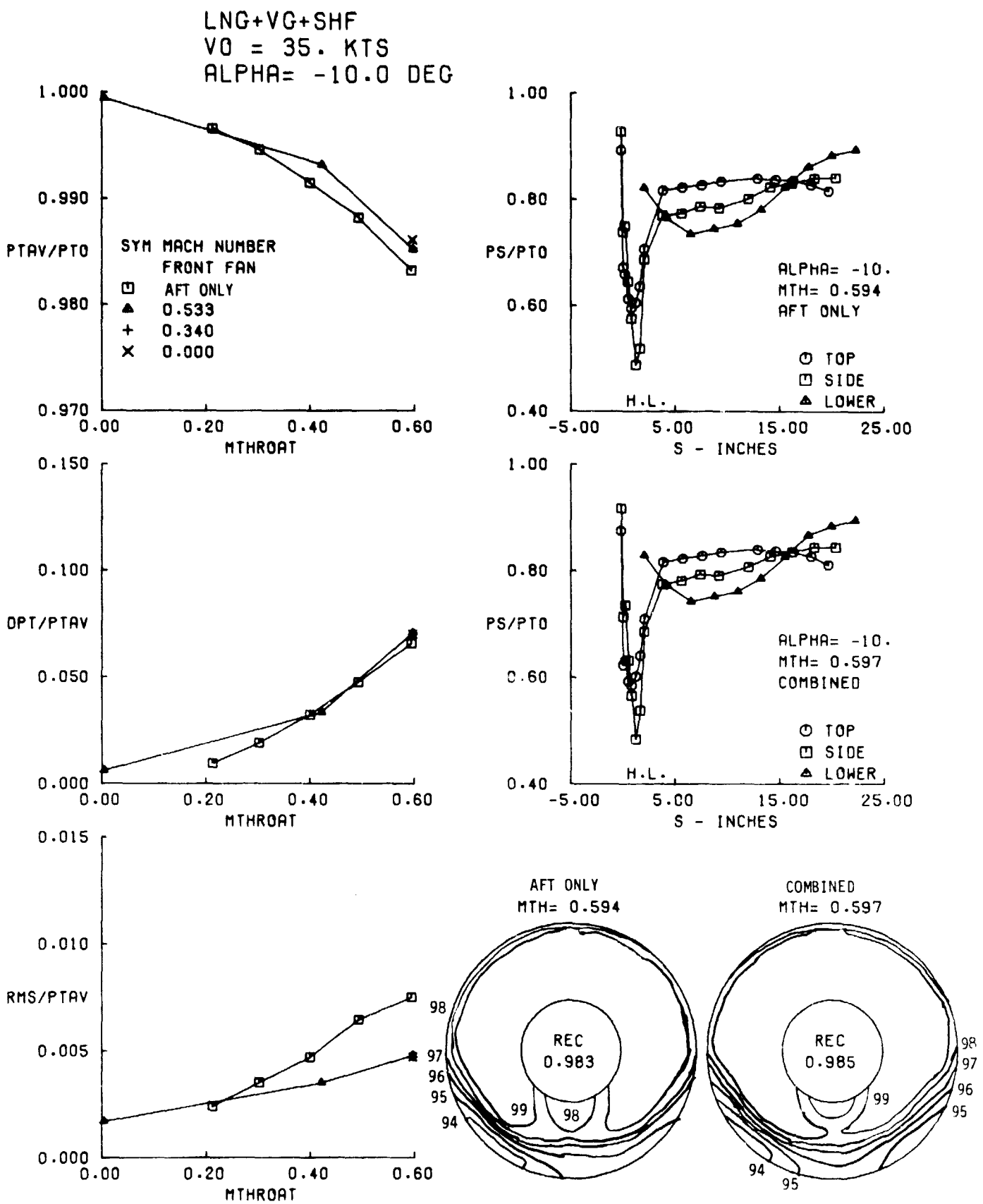

FIGURE 31A. LONG AFT INLET WITH VORTEX GENERATORS AND SHAFT SIMULATOR PERFORMANCE AT V_0 = 35 KNOTS, α = -10°

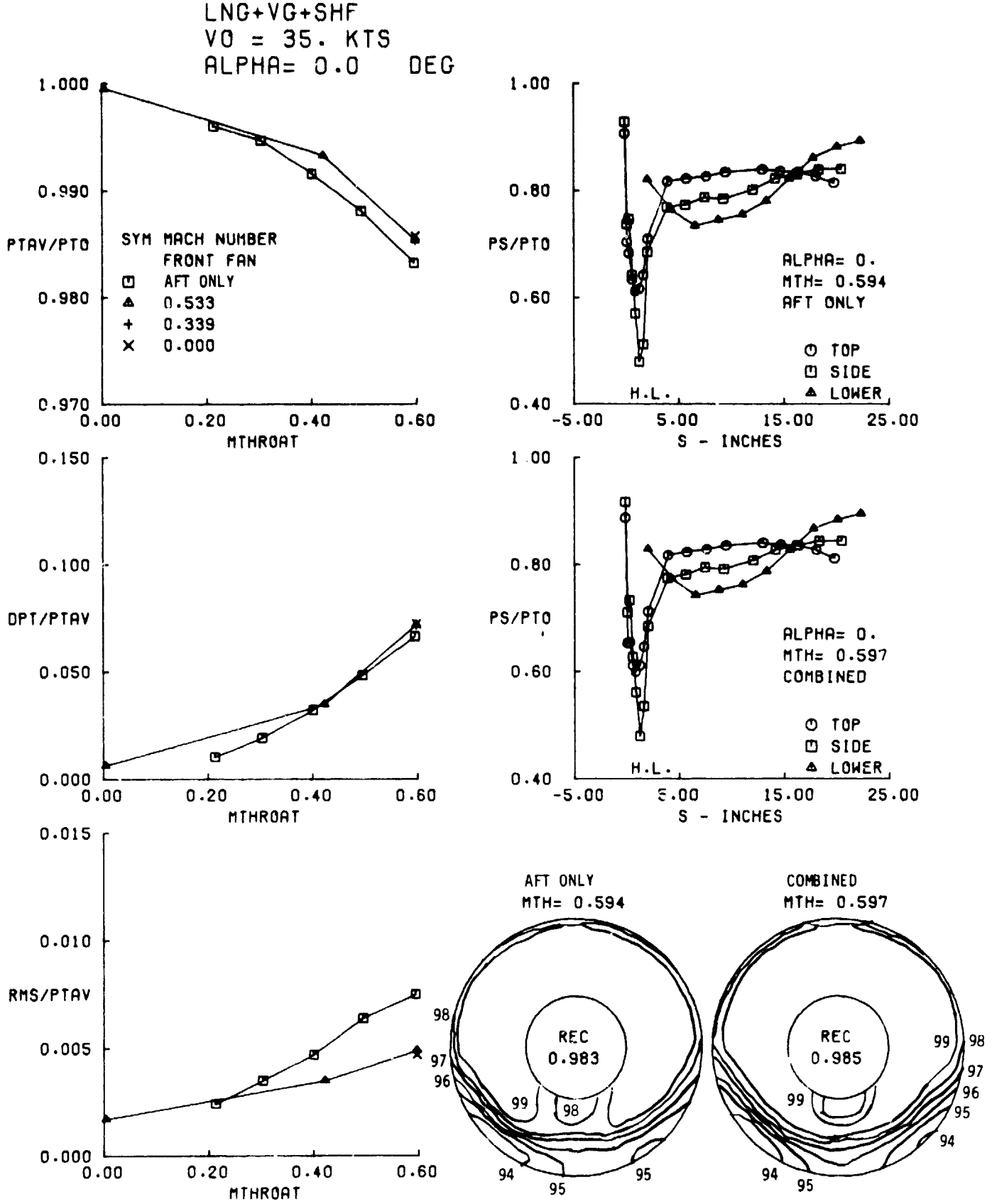

FIGURE 31B. LONG AFT INLET WITH VORTEX GENERATORS AND SHAFT SIMULATOR PERFORMANCE AT V_0 = 35 KNOTS, = 0^0

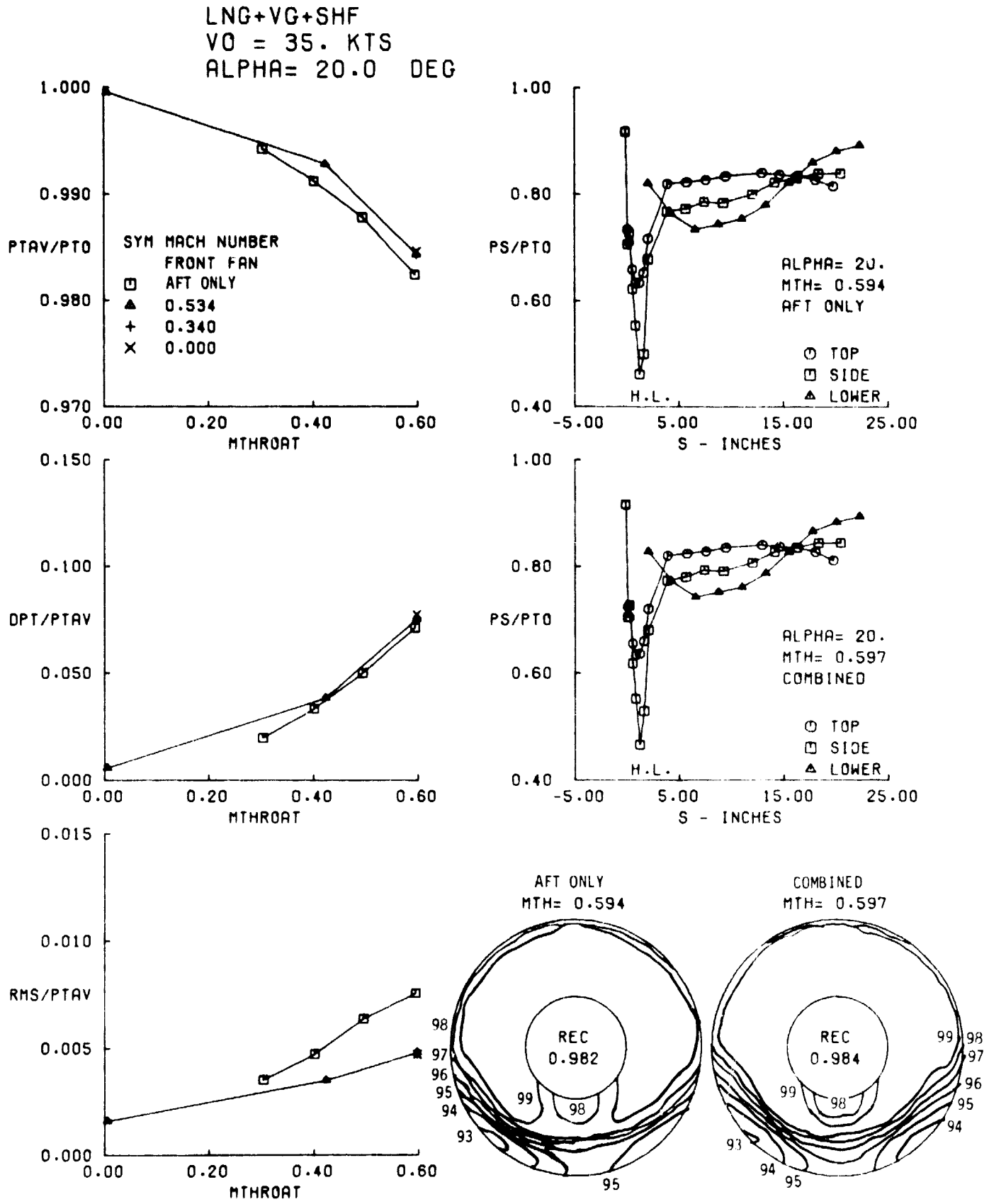

FIGURE 31C. LONG AFT INLET WITH VORTEX GENERATORS AND SHAFT SIMULATOR PERFORMANCE AT V_0 = 35 KNOTS, α = 20°

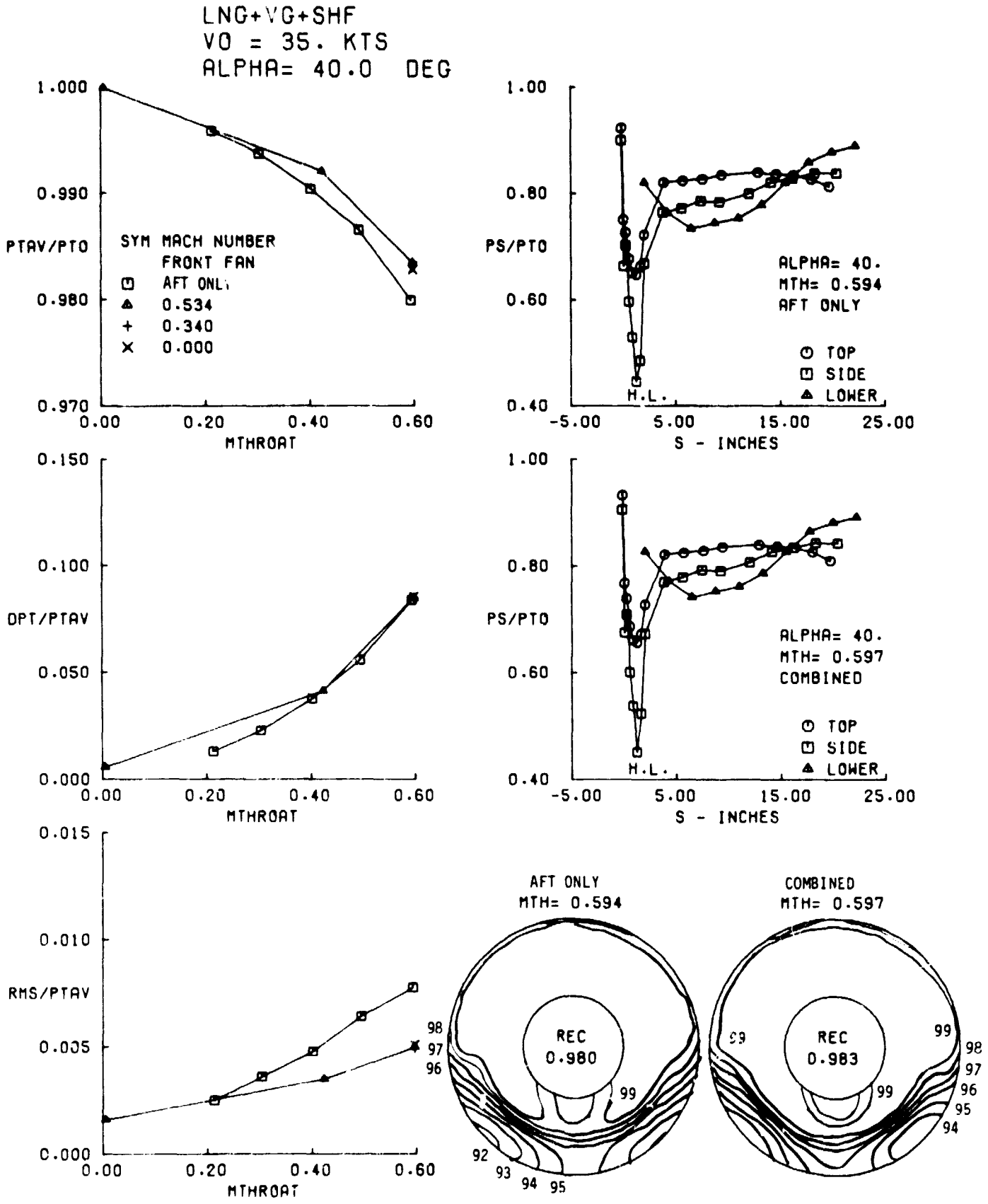

FIGURE 31D. LONG AFT INLET WITH VORTEX GENERATORS AND SHAFT SIMULATOR PERFORMANCE AT V_0 = 35 KNOTS, α = 40°

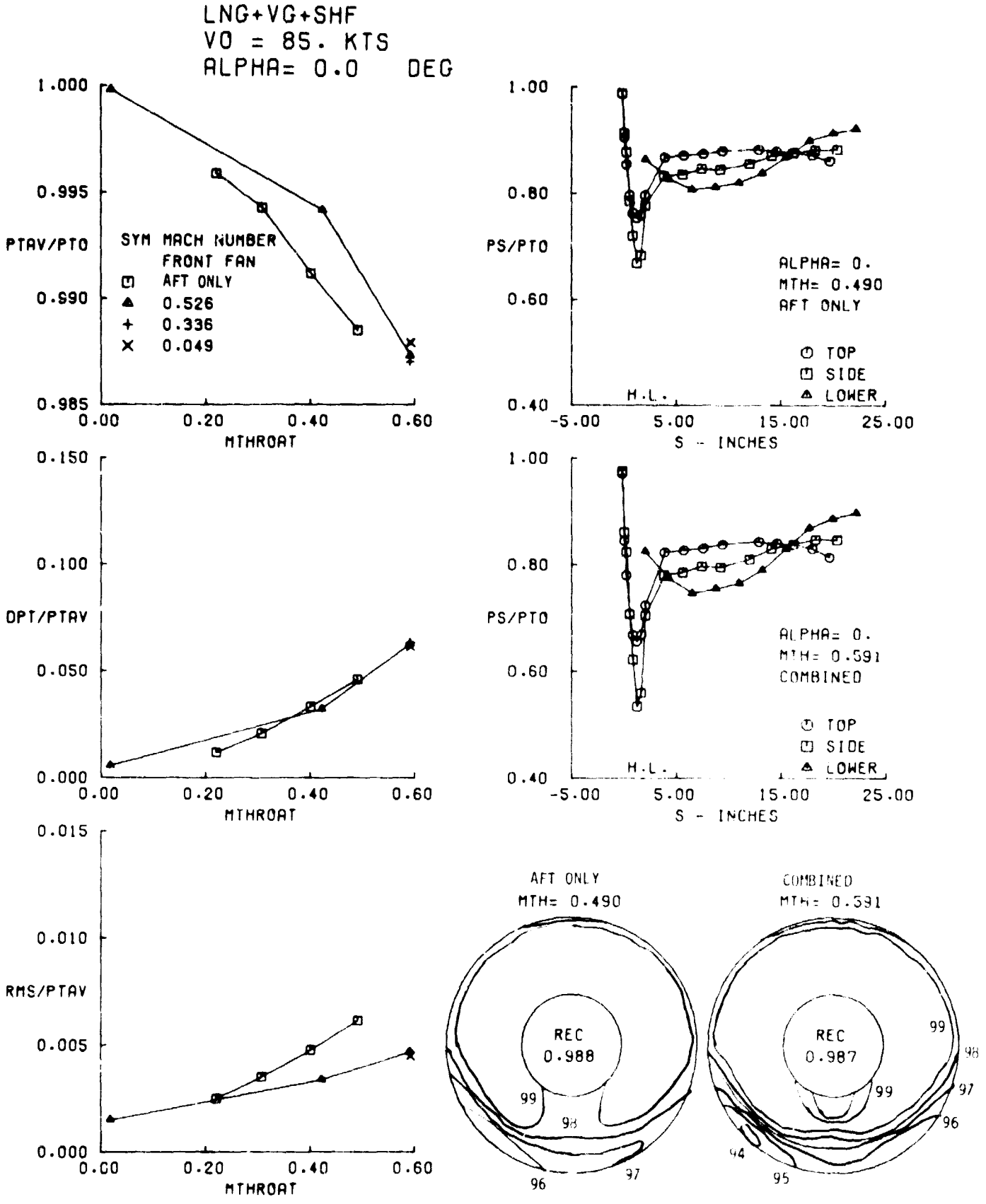

FIGURE 32A. LONG AFT INLET WITH VORTEX GENERATORS AND SHAFT SIMULATOR PERFORMANCE AT V_0 = 85 KNOTS, $\alpha = 0^0$

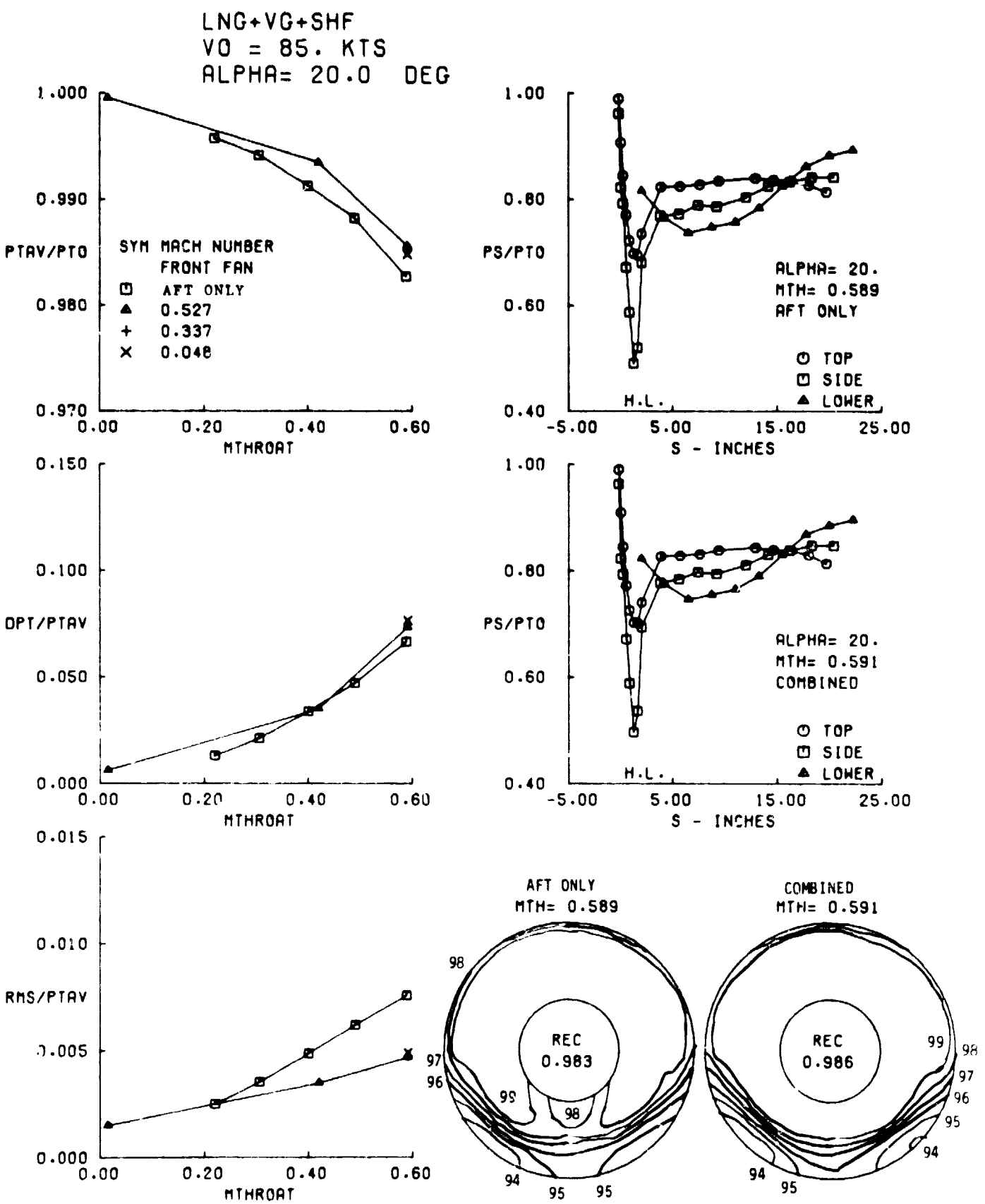

FIGURE 32B. LONG AFT INLET WITH VORTEX GENERATORS AND SHAFT SIMULATOR PERFORMANCE AT V_0 = 85 KNOTS, α = 20°

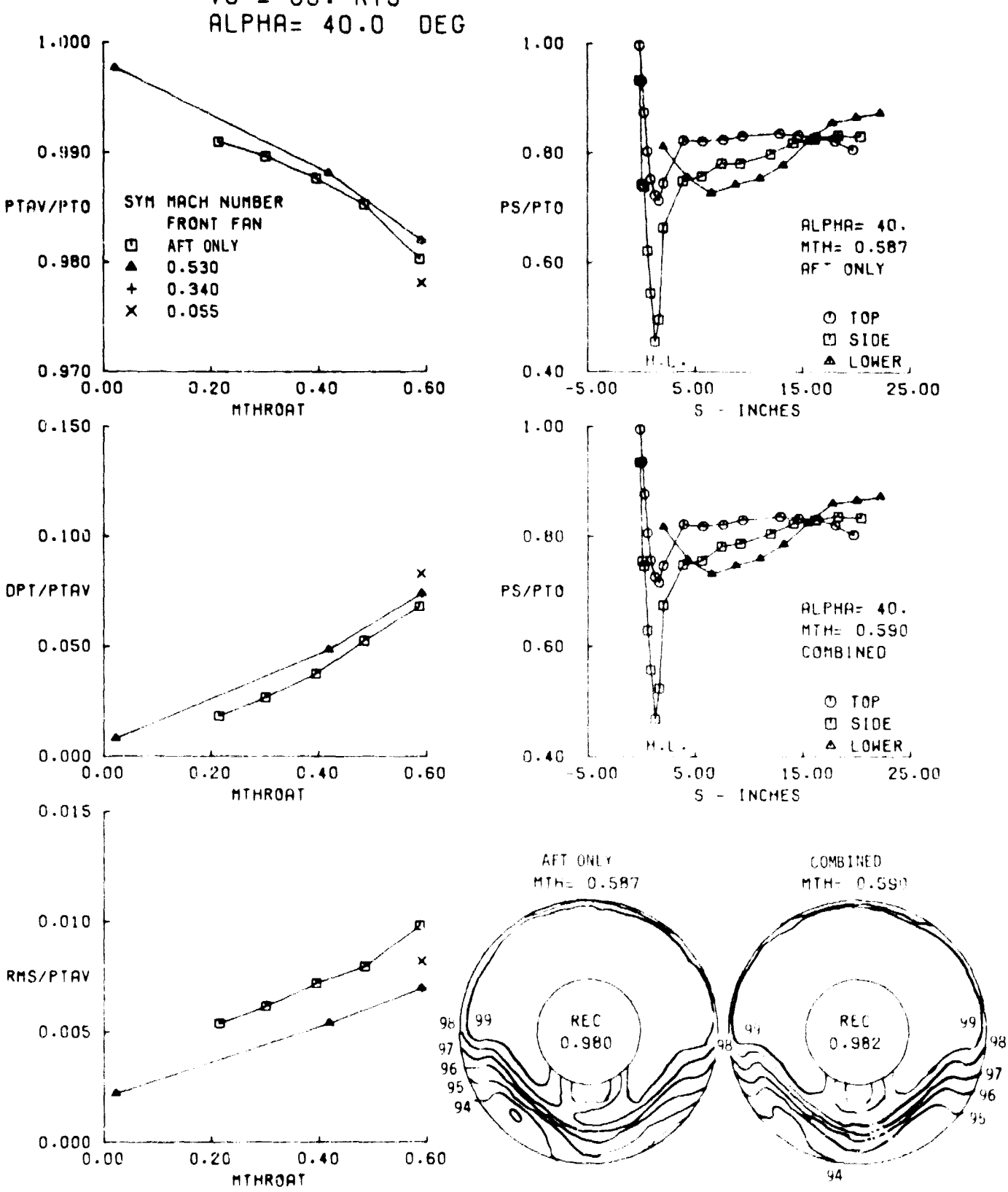

FIGURE 32C. LONG AFT INLET WITH VORTEX GENERATORS AND SHAFT SIMULATOR PERFORMANCE AT V_0 = 85 KNOTS, α = 40°

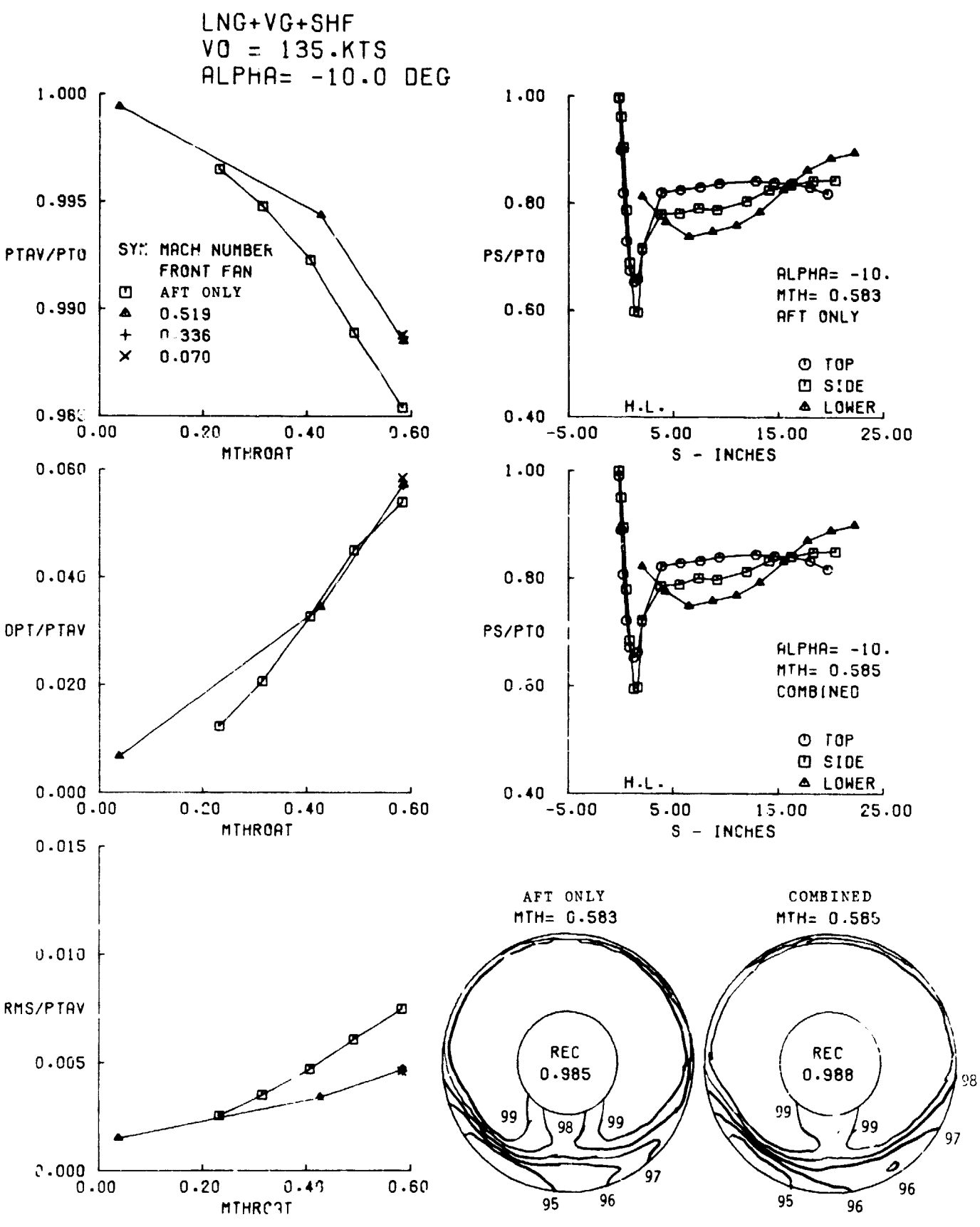

FIGURE 33A. LONG AFT INLET WITH VORTEX GENERATORS AND SHAFT SIMULATOR PERFORMANCE AT V_0 = 135 KNOTS, α = -10°

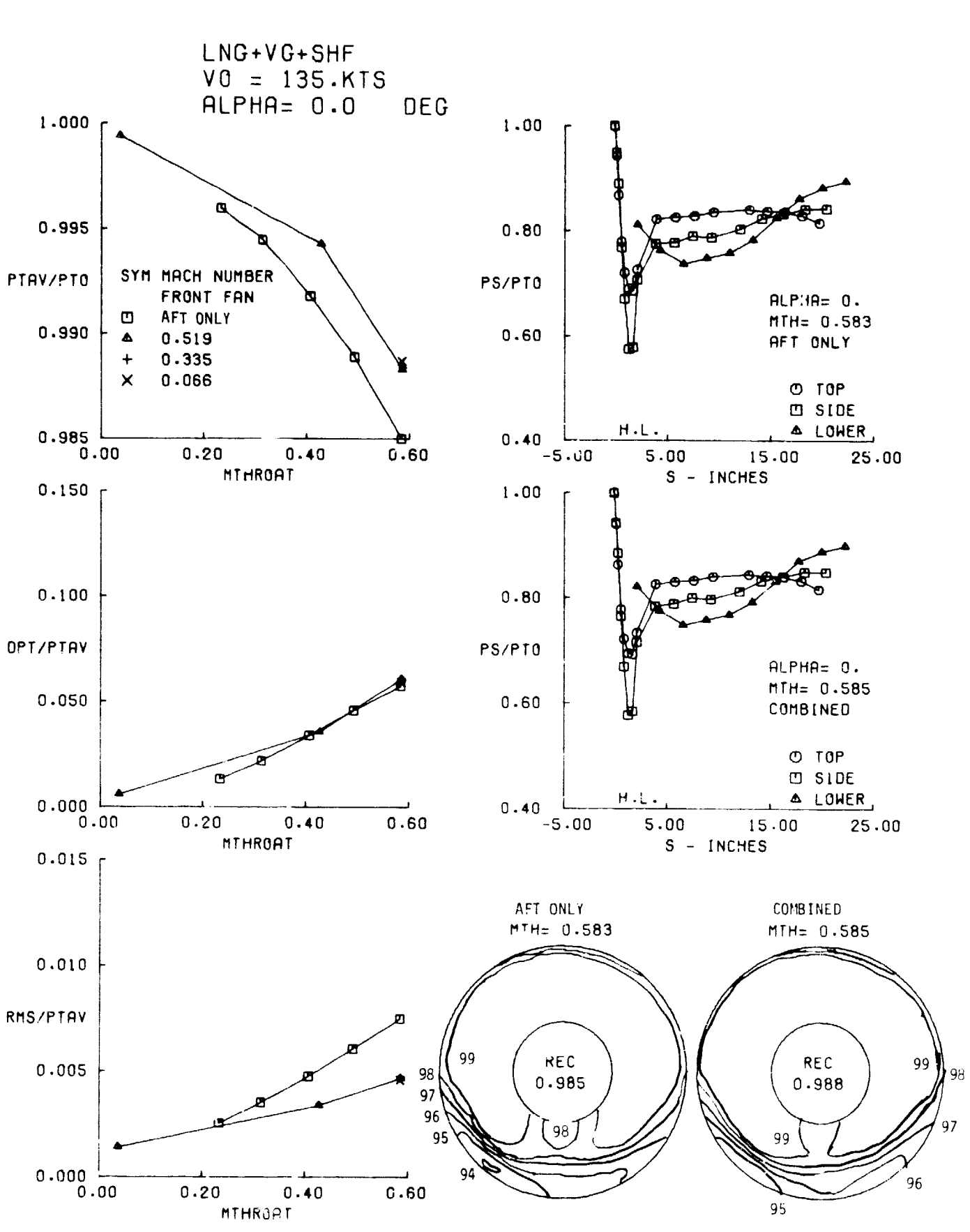

FIGURE 33B. LONG AFT INLET WITH VORTEX GENERATORS AND SHAFT SIMULATOR PERFORMANCE AT V_0 = 135 KNOTS, $\alpha = 0^0$

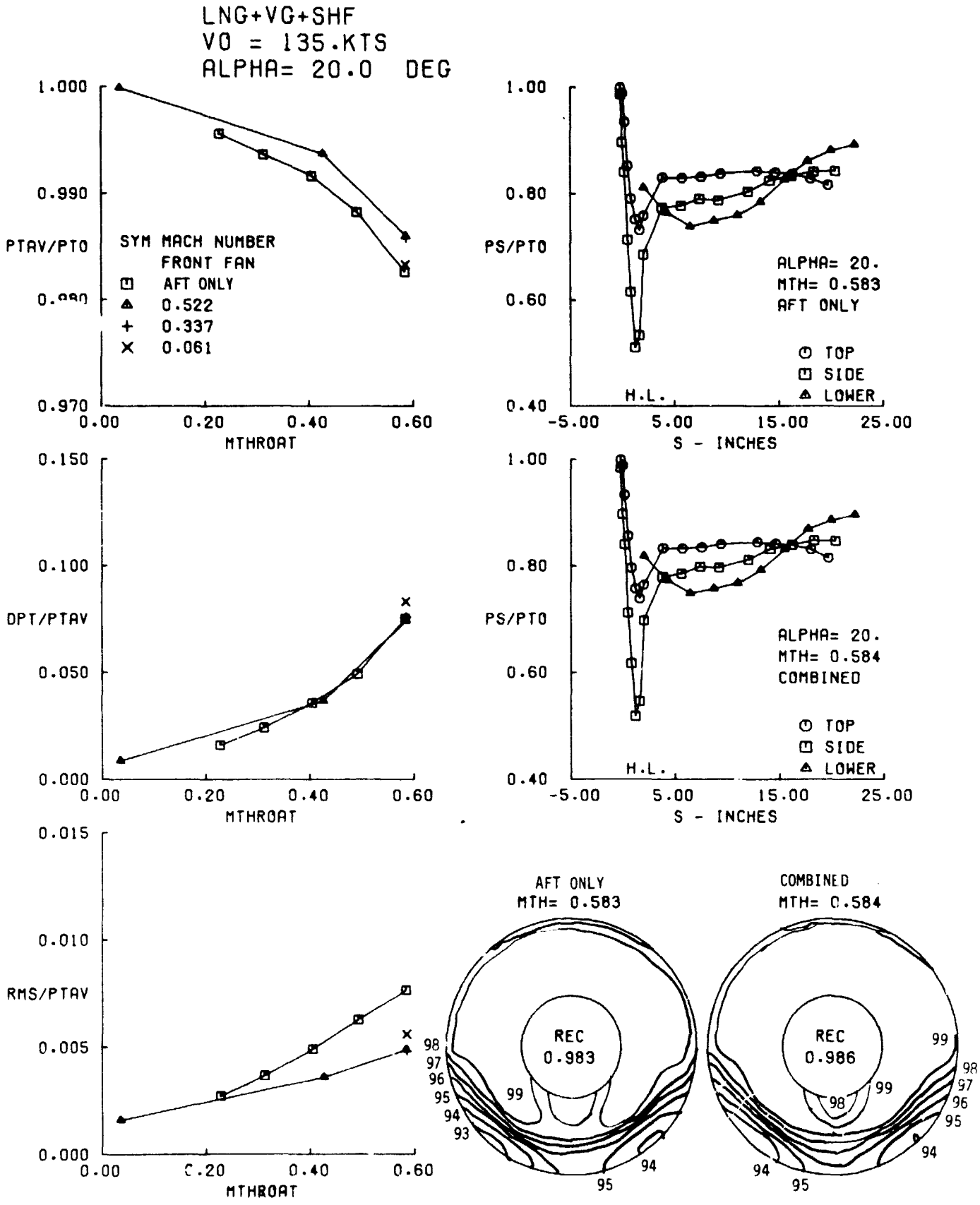

FIGURE 33C. LONG AFT INLET WITH VORTEX GENERATORS AND SHAFT SIMULATOR PERFORMANCE AT V_0 = 135 KNOTS, α = 20°

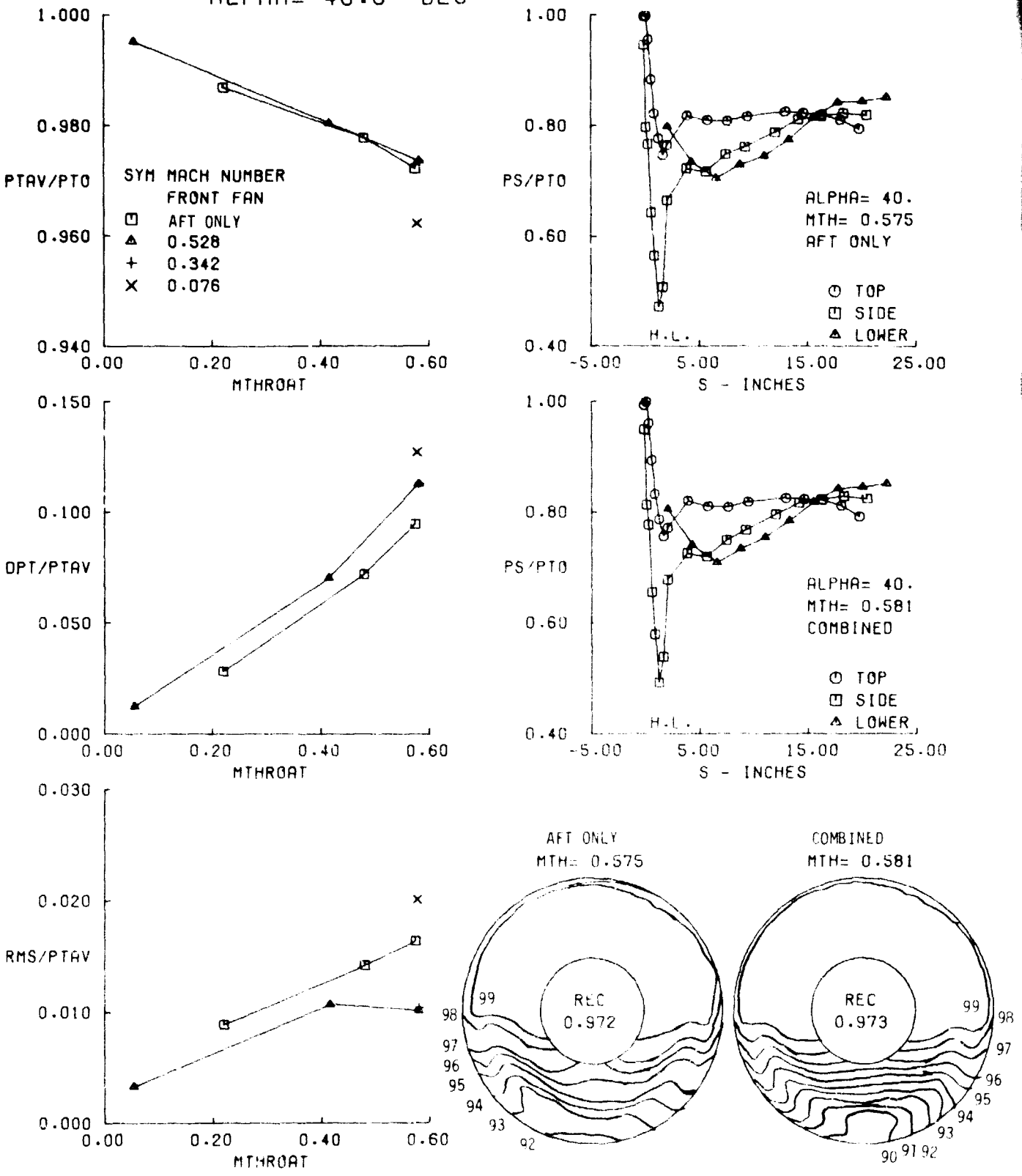

FIGURE 33D. LONG AFT INLET WITH VORTEX GENERATORS AND SHAFT SIMULATOR PERFORMANCE AT V_0 135 KNOTS, α = 40°.

The detailed inlet performance comparisons for the clean short aft inlet is presented in Figures 34 through 41. The front fan hot-air supply pipe was again located on the top of the nacelle and on the side of the nacelle. Results for each model configuration are presented next.

Supply Pipe on Top

The detailed clean short aft inlet performance is presented in Figures 34, 35, 36, and 37 for Vo = 0, 35, 85, and 135 knots (0, 18, 43.7, and 69.5 m/s). The static pressure distributions are plotted as a function of the surface distance from the lip hilite. For the lower ramp surface, the throat station was used as the reference point. The general trend continues for better pressure recovery for the combined aft inlet than the isolated aft inlet. The distortion levels are comparable to slightly higher. Also, the short aft inlet continues to be less dependent on airflow rate. Short aft inlet performance remains very high (.998+) except at the highest angles-of-attack.

Supply Pipe on the Side

Clean short aft inlet, with the front fan supply pipe located on the side of the nacelle, performance is presented in Figures 38,39, 40 and 41 for Vo = 0, 35, 85, and 135 knots (0, 18, 43.7, and 69.5 m/s). At the static condition, Vo = 0, the combined aft inlet recovery is better than the isolated inlet performance, Figure 38. Even at lower speed and angle-of-attack, this trend persists. However, at the higher speeds,Vo = 85 and 135 knots, the combined inlet performance is lower than the isolated inlet performance. This condition exists although the asymmetrical distortion pattern caused by the side mounted air supply pipe is not as severe as for the long aft inlet configuration.

6.2.2.2 Short Aft Inlet with Corner Fillets

The short aft inlet is more attractive from the standpoint of low speed, low angle-of-attack performance and system integration. However, the performance of the short aft inlet decays more rapidly at the high speed, high

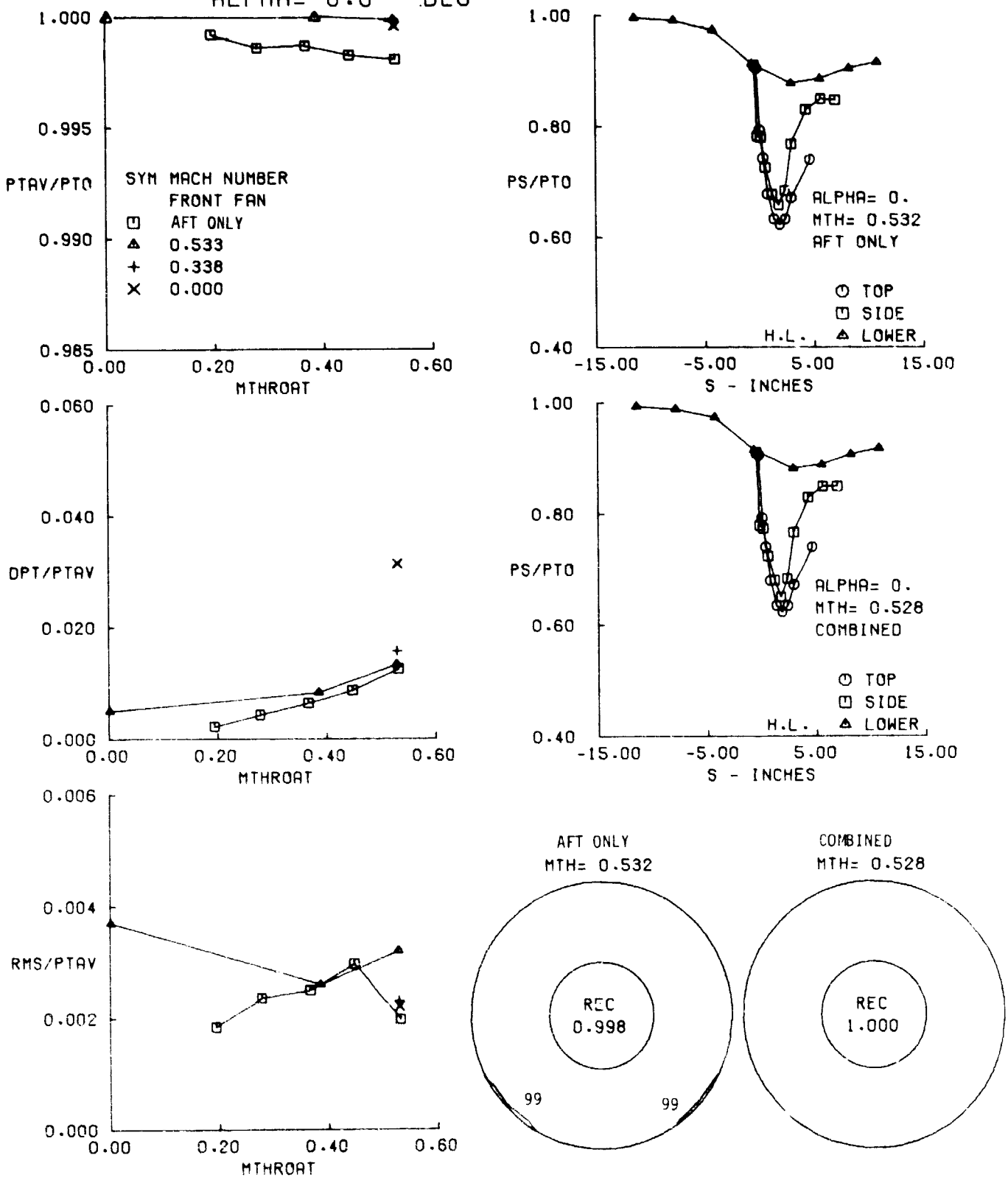

FIGURE 34. SHORT AFT INLET PERFORMANCE AT V_0 = 0 KNOTS

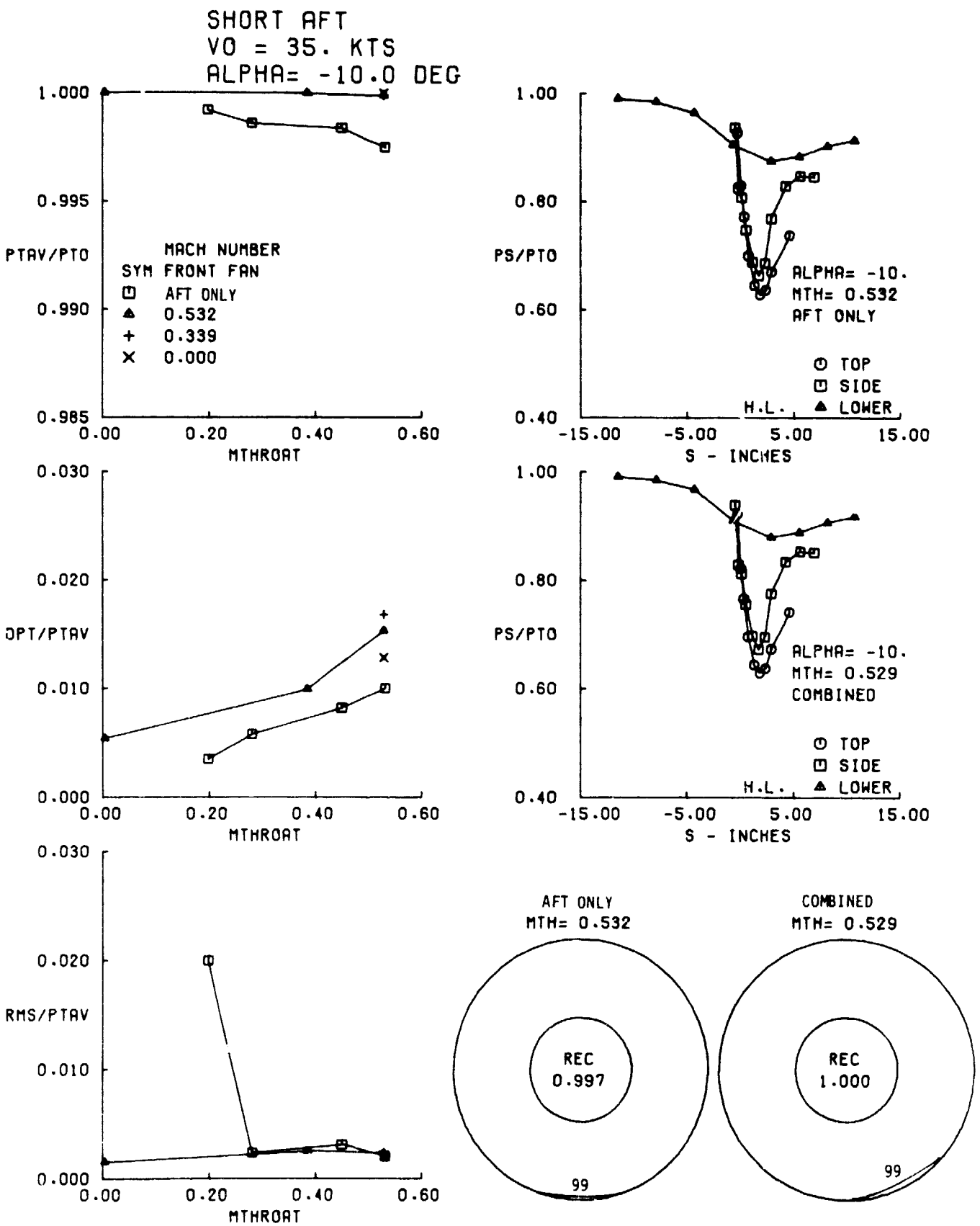

FIGURE 35A. SHORT AFT INLET PERFORMANCE AT V_0 = 35 KNOTS, α = -10°

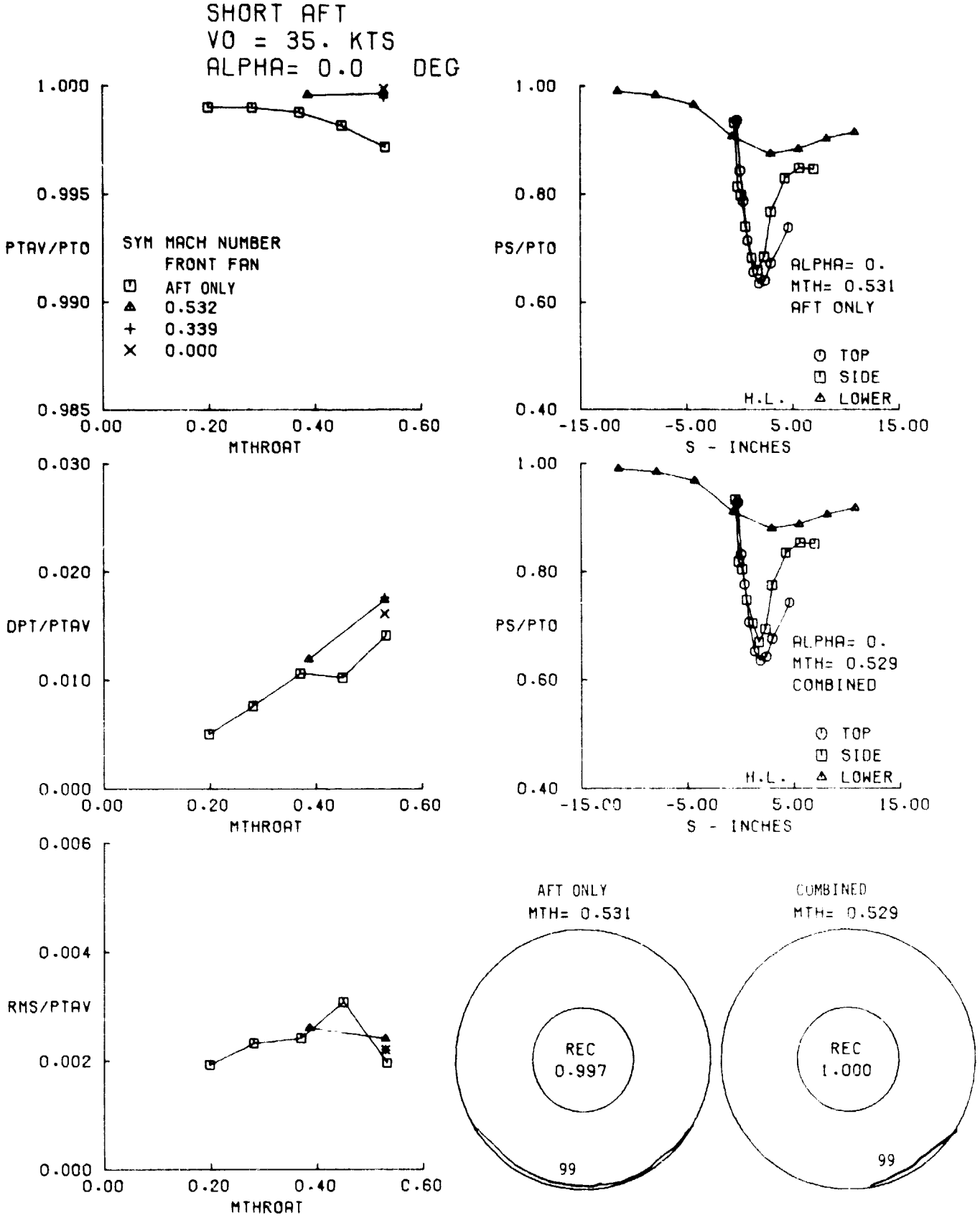

FIGURE 35B. SHORT AFT INLET PERFORMANCE AT V_0 = 35 KNOTS, α = 0°

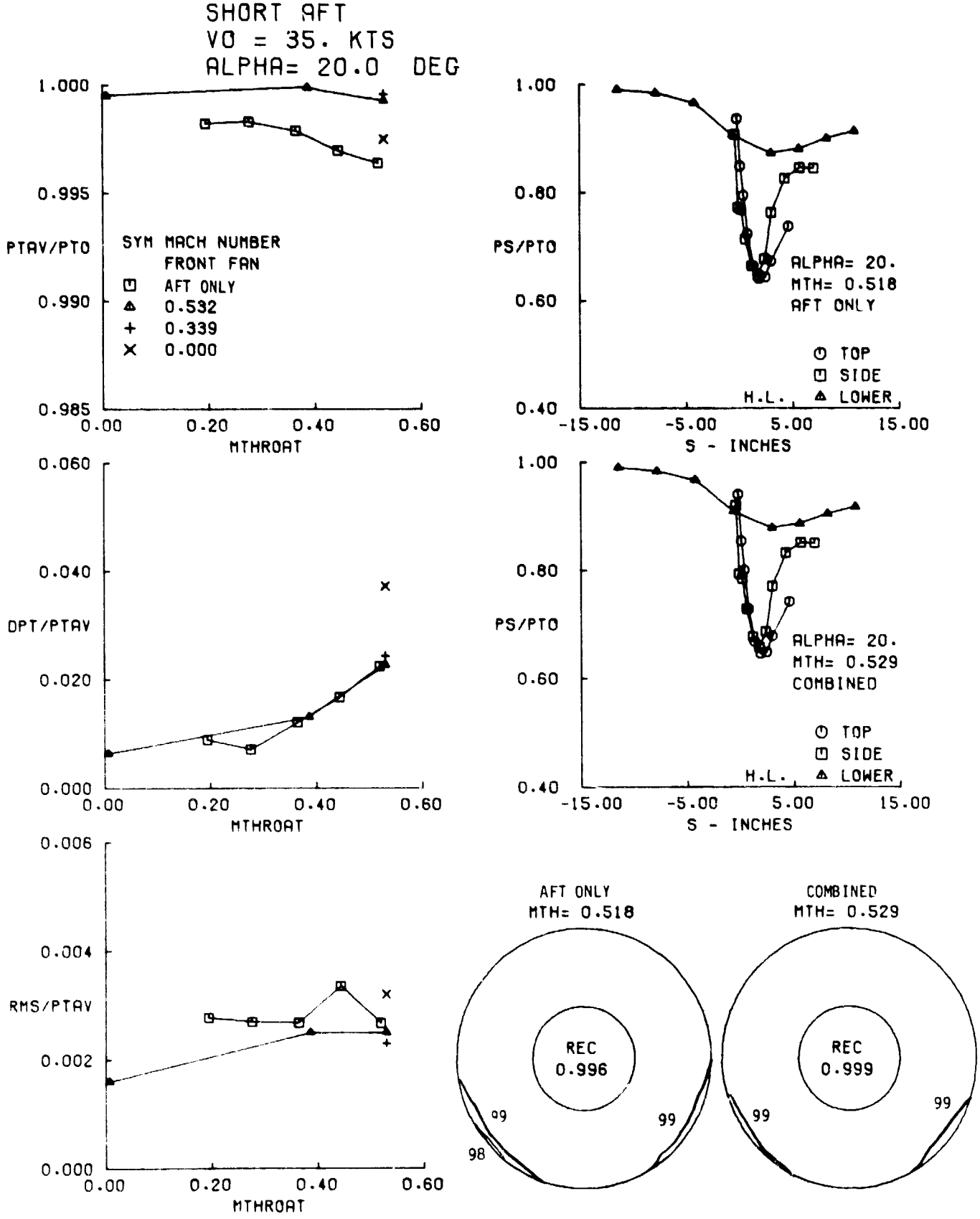

FIGURE 35C. SHORT AFT INLET PERFORMANCE AT V_0 = 35 KNOTS, α = 20°

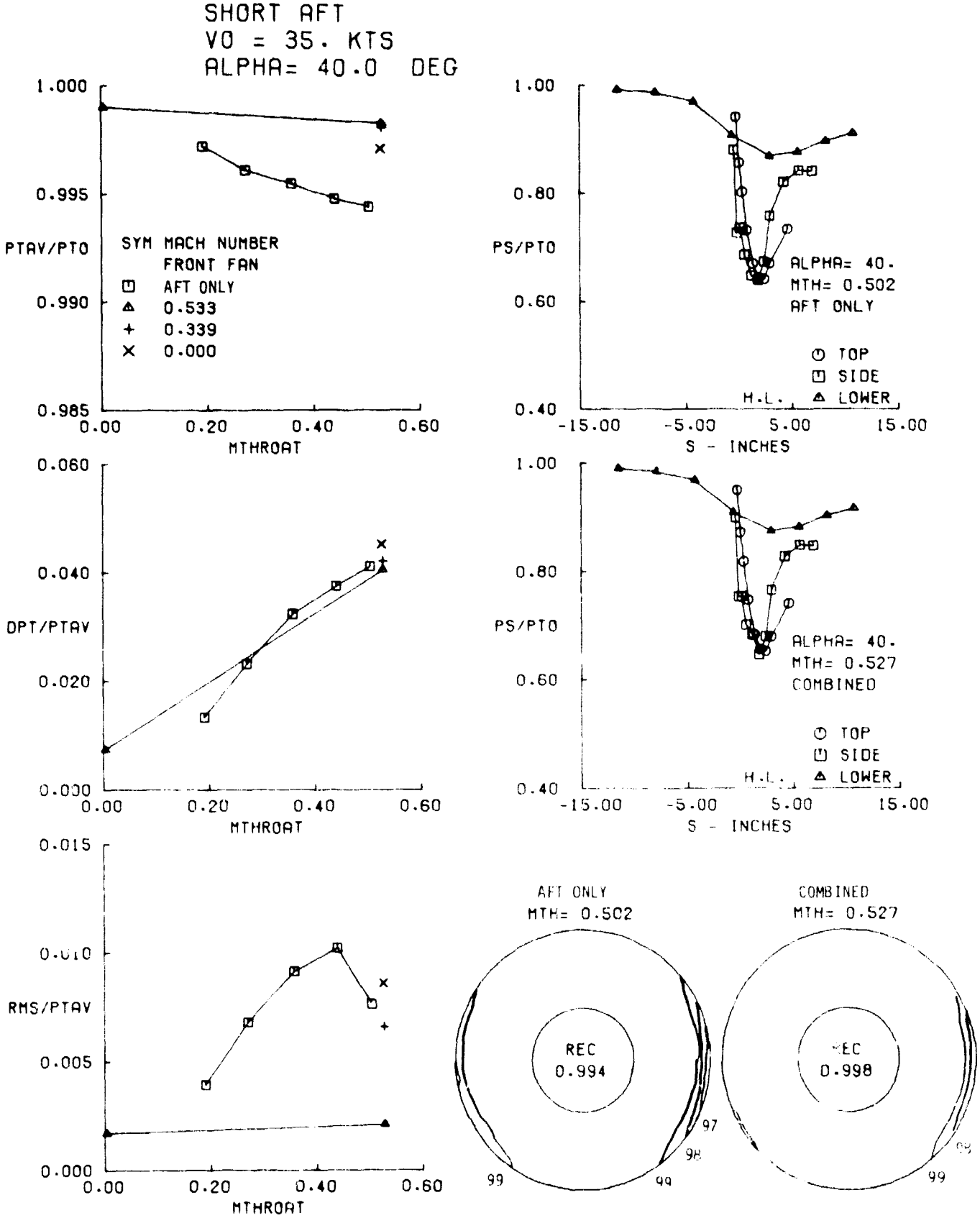

FIGURE 35D. SHORT AFT INLET PERFORMANCE AT V_0 = 35 KNOTS, α = 40°

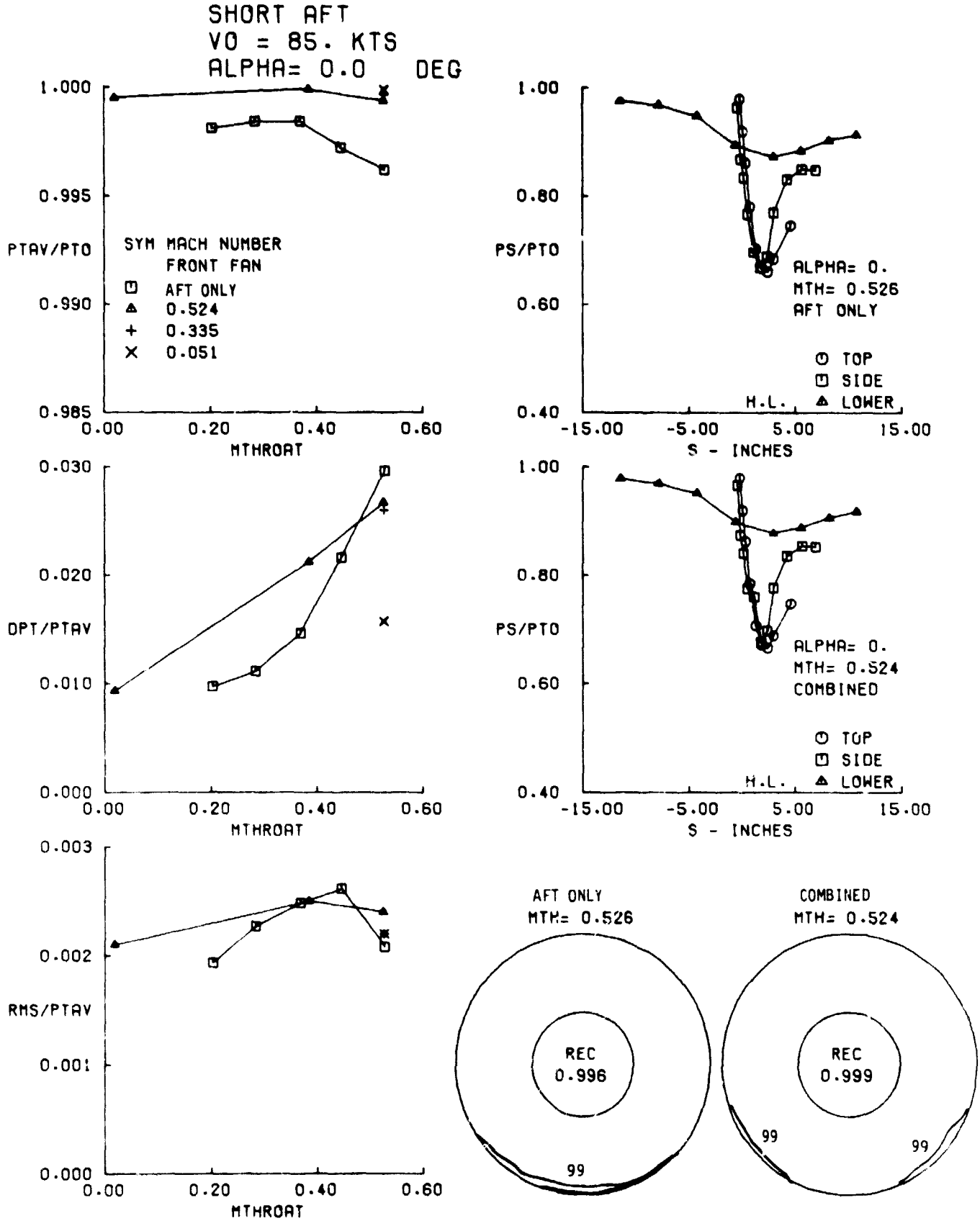

FIGURE 36A. SHORT AFT INLET PERFORMANCE AT V_0 = 85 KNOTS, $\alpha = 0^0$

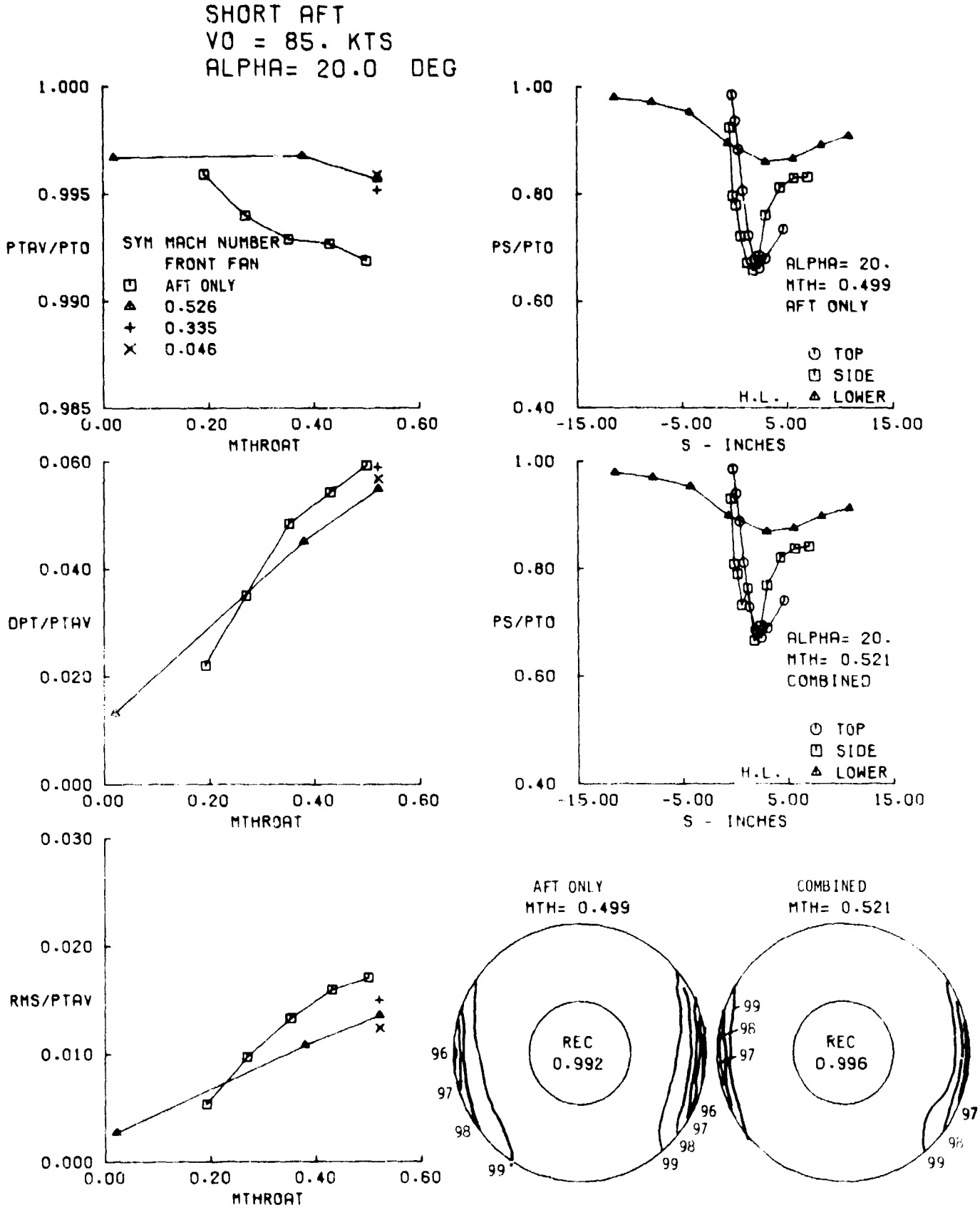

FIGURE 368. SHORT AFT INLET PERFORMANCE AT V_0 = 85 KNOTS, α = 20°

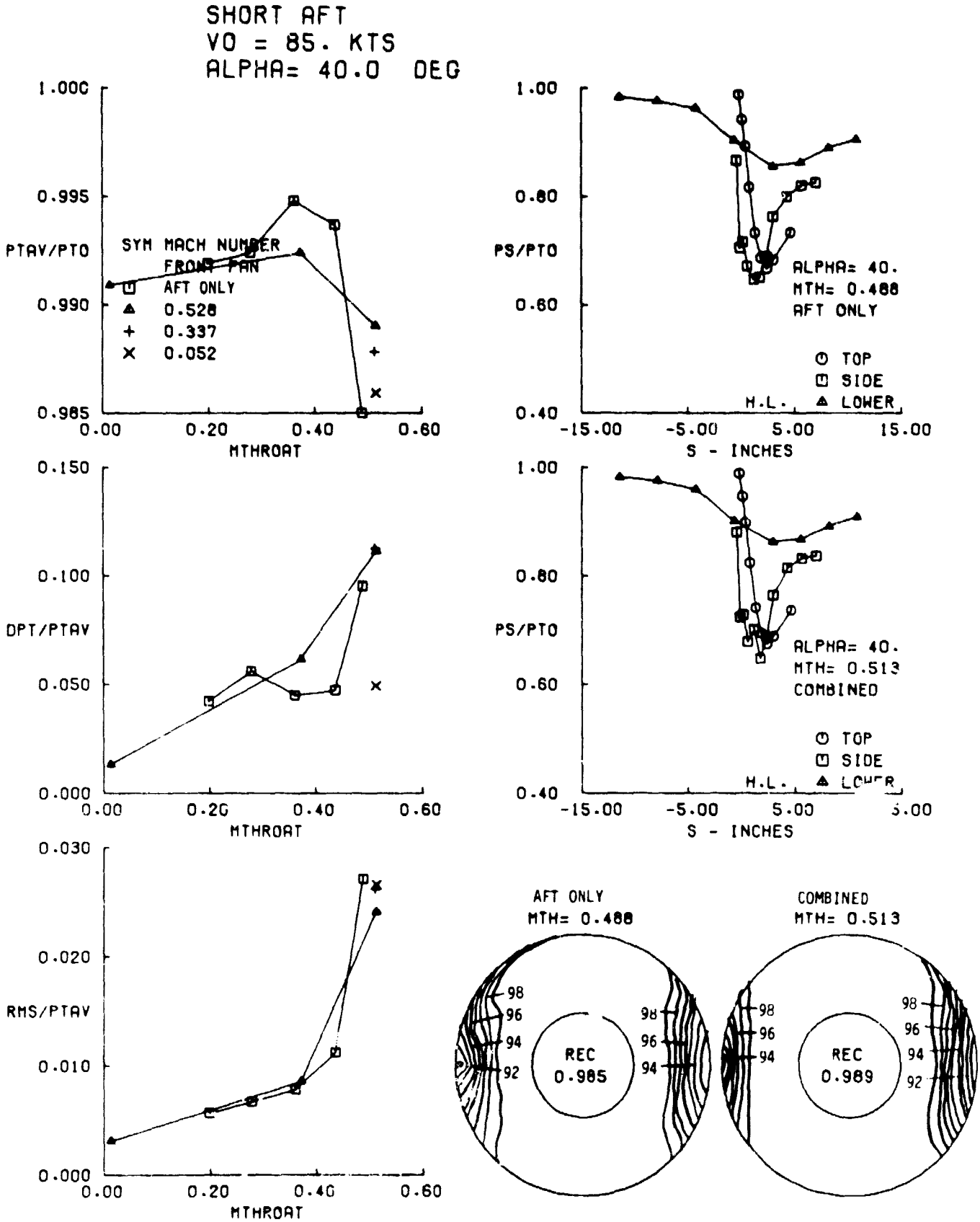

FIGURE 36C. SHORT AFT INLET PERFORMANCE AT V_0 = 85 KNOTS, α = 40°

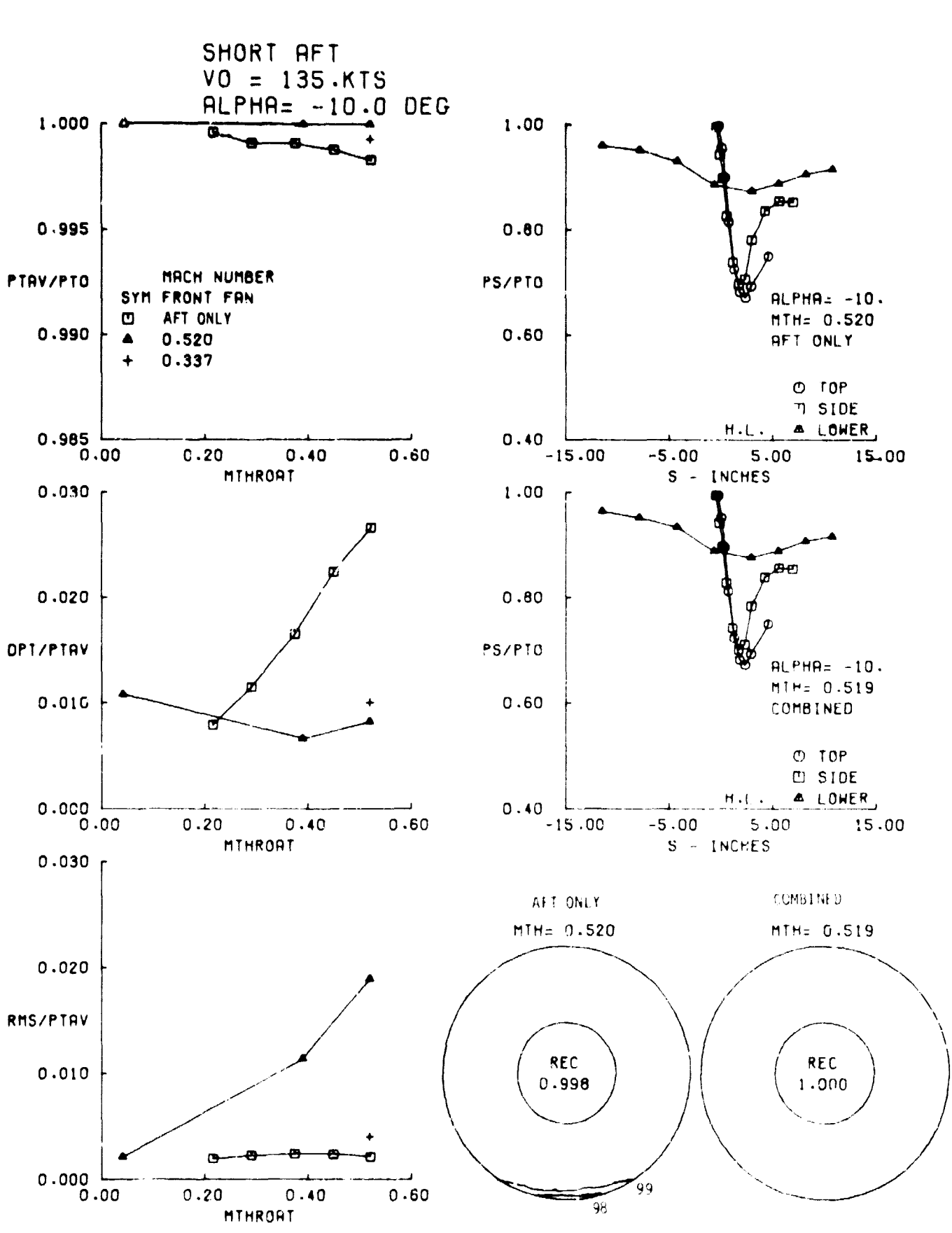

FIGURE 37A. SHORT AFT INLET PERFORMANCE AT V_0 = 135 KNOTS, α = -10°

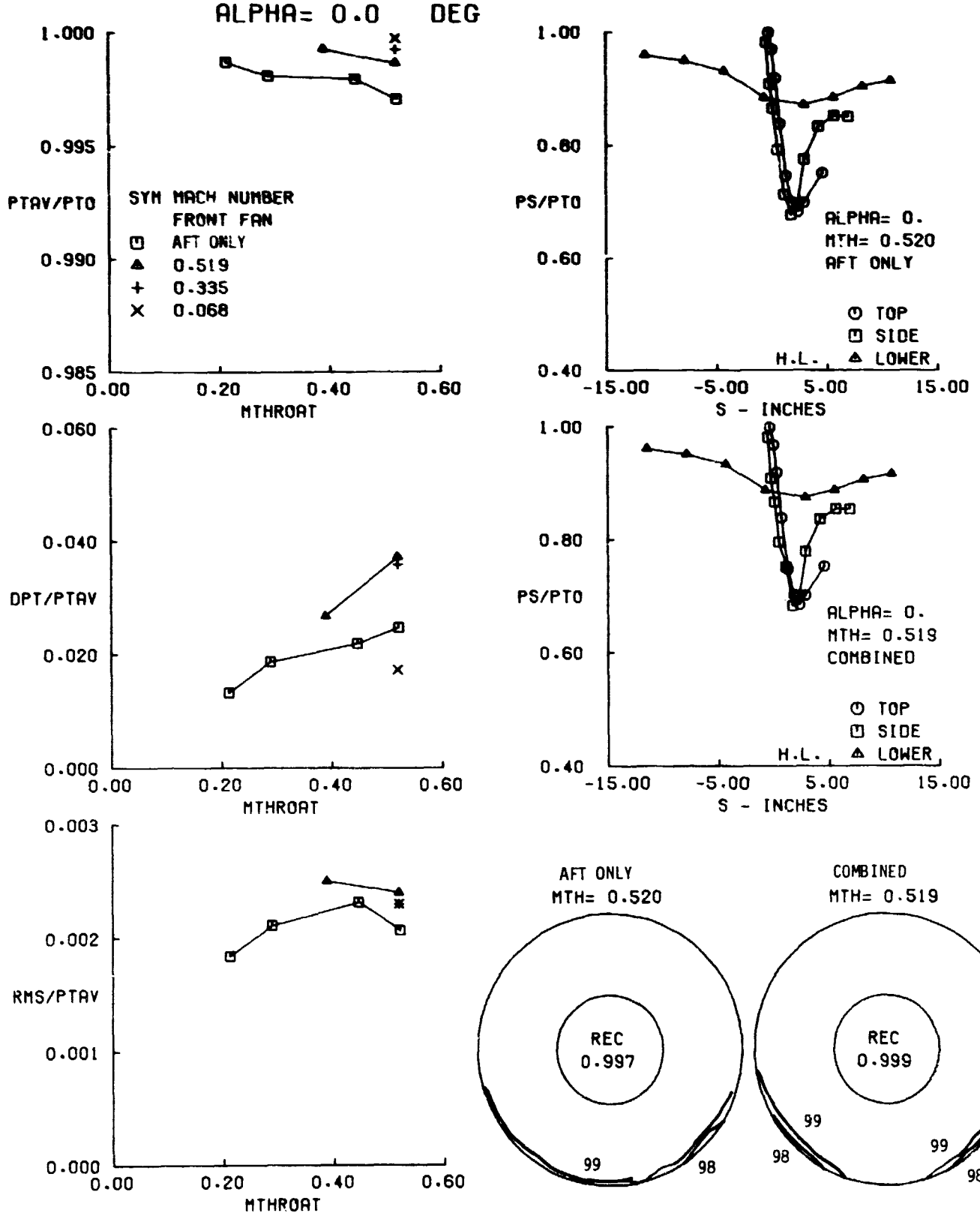

FIGURE 378. SHORT AFT INLET PERFORMANCE AT V_0 = 135 KNOTS, $\alpha = 0^0$

C - 2

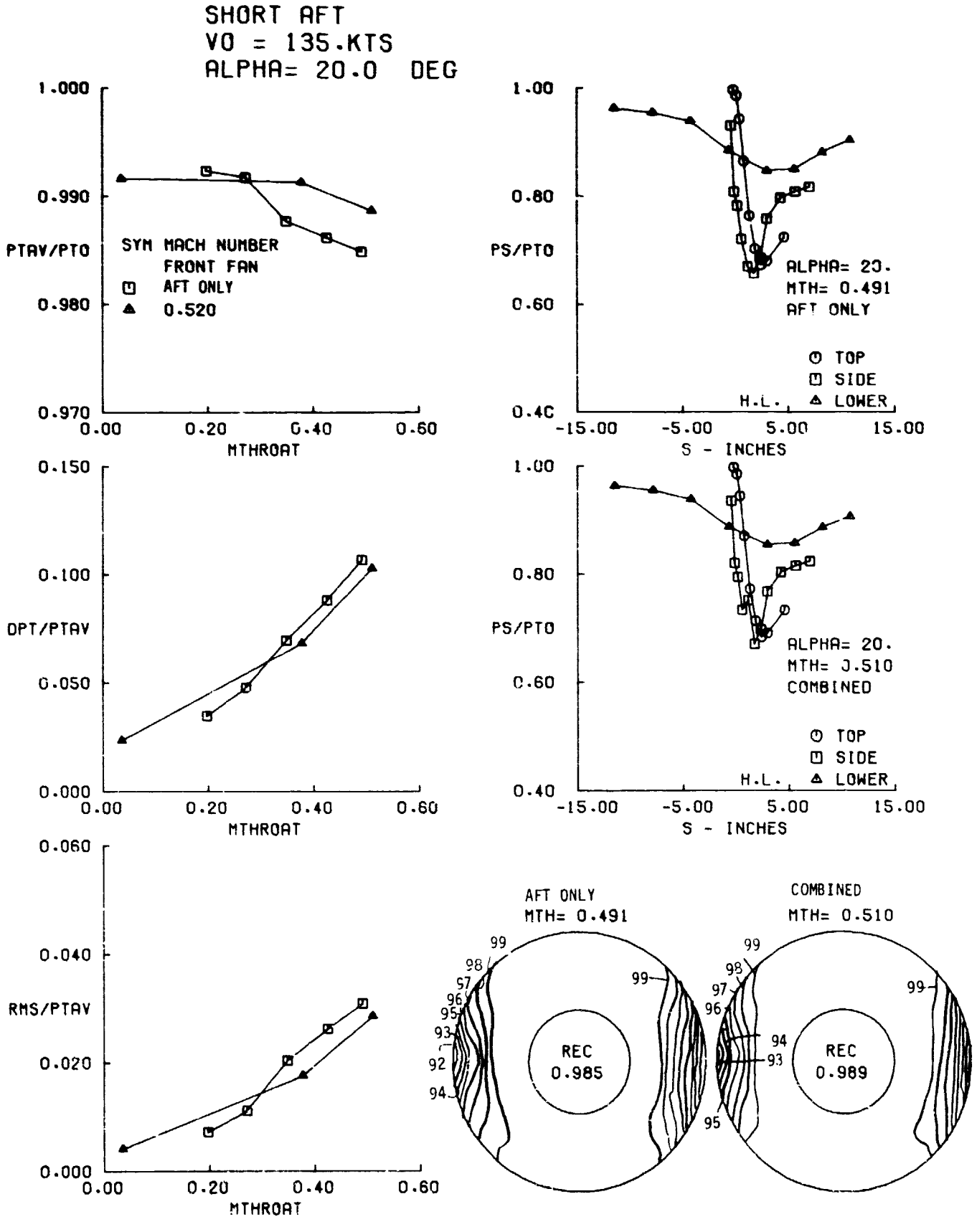

FIGURE 37C. SHORT AFT INLET PERFORMANCE AT V_0 = 135 KNOTS, α = 20°

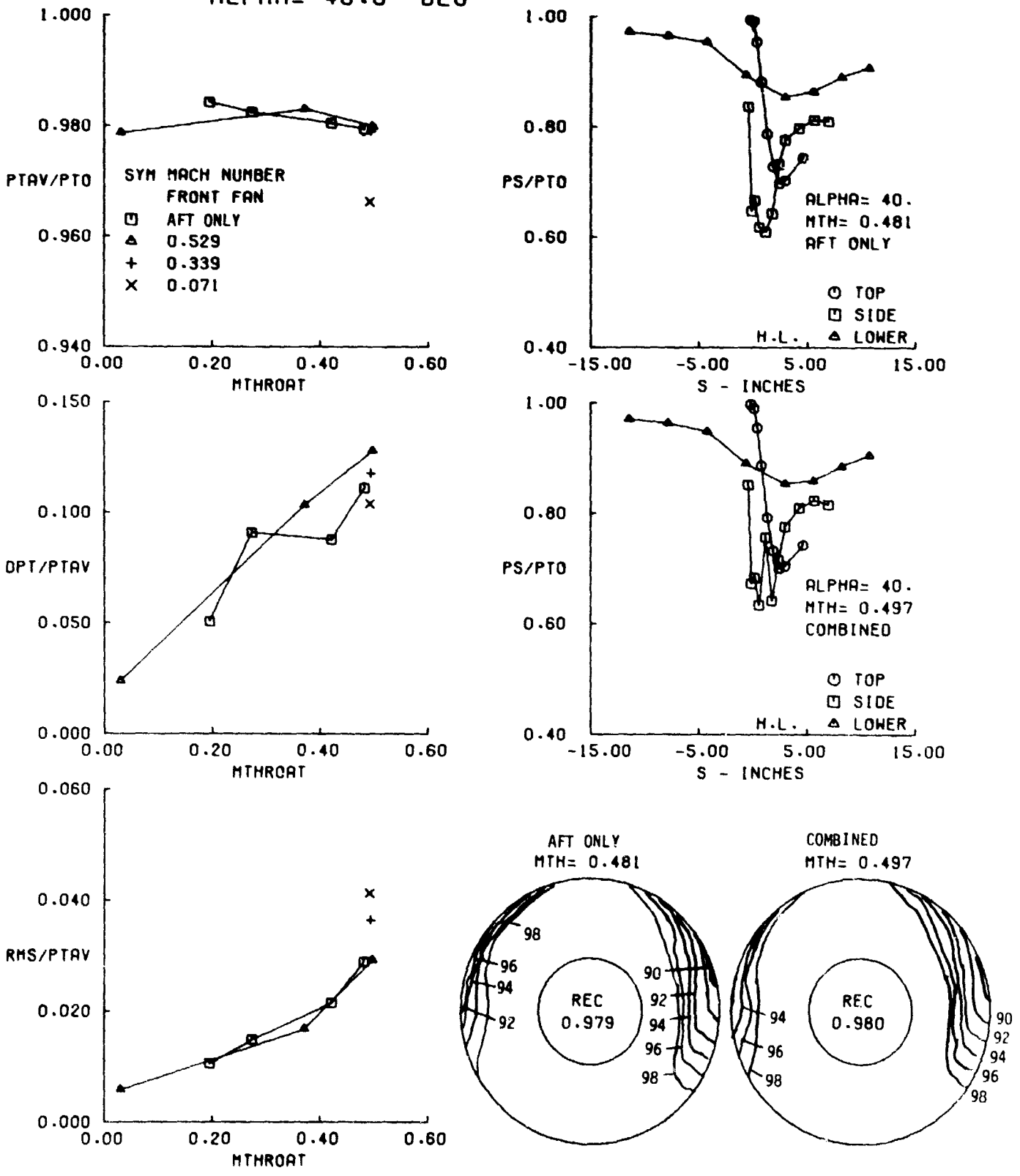

FIGURE 37D. SHORT AFT INLET PERFORMANCE AT V_0 = 135 KNOTS, α = 40°

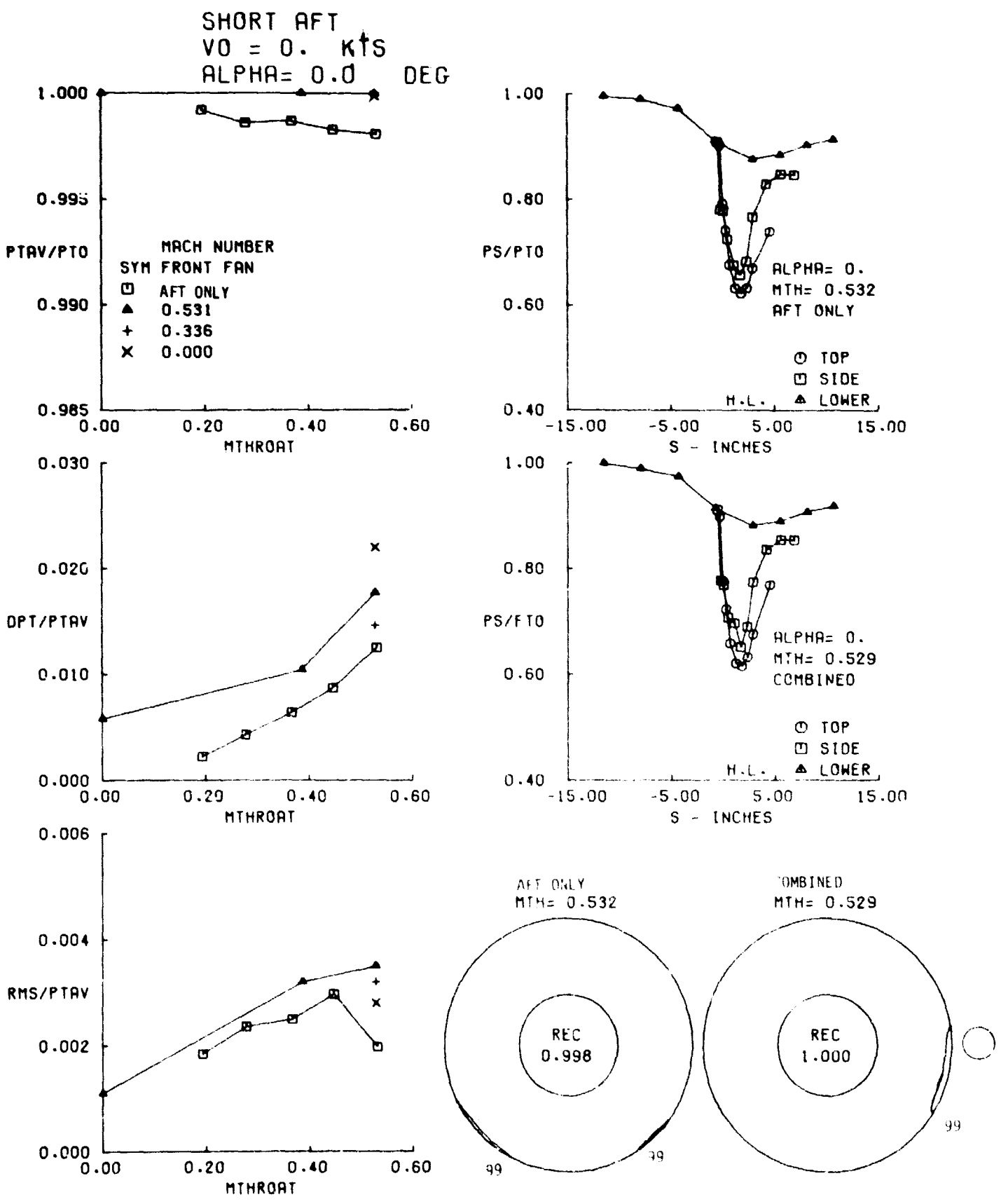

FIGURE 38. SHORT AFT INLET PERFORMANCE (SIDE PIPE) AT V_0 = 0 KNOTS

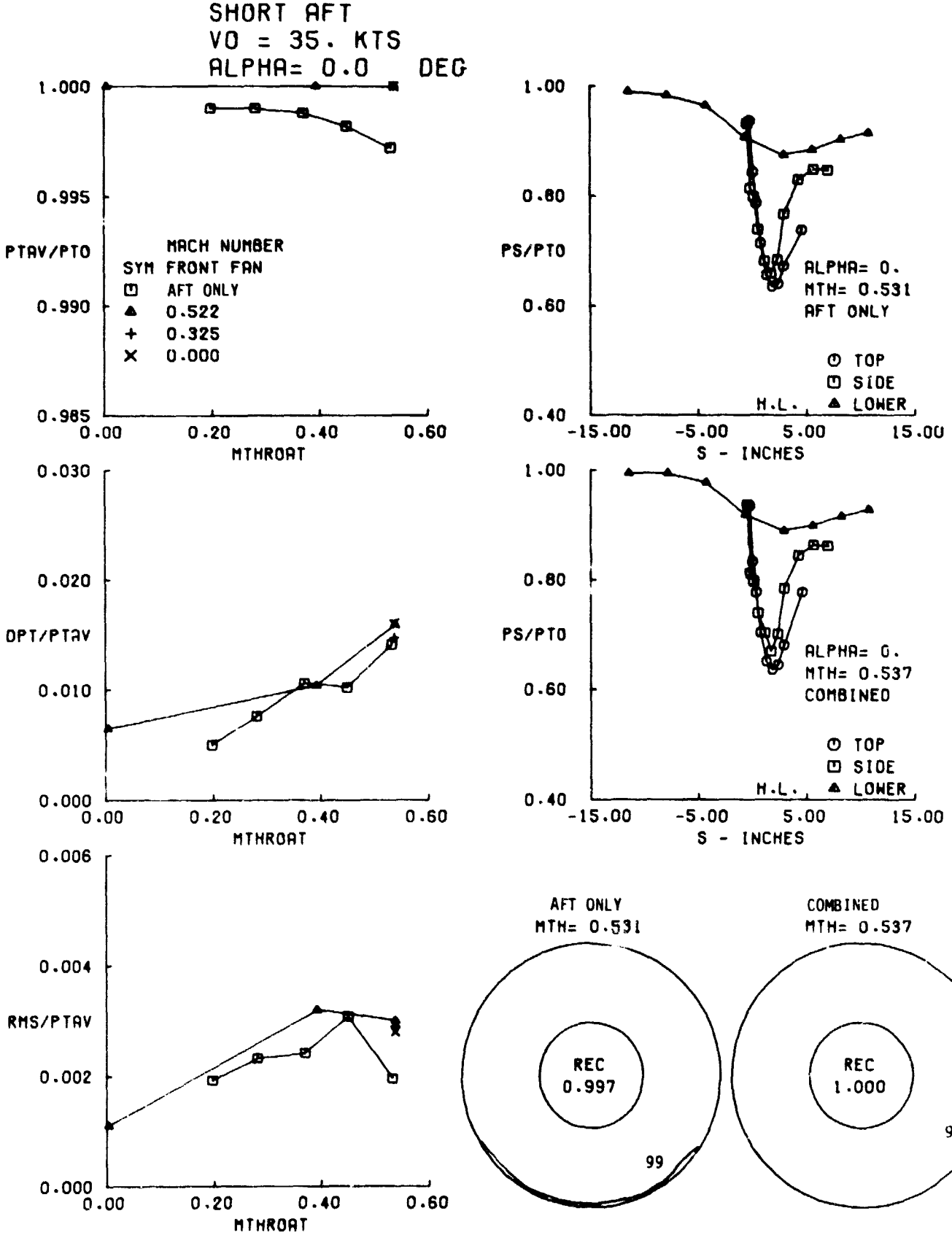

FIGURE 39A. SHORT AFT INLET PERFORMANCE (SIDE PIPE) AT V_0 = 35 KNOTS, $\alpha = 0^0$

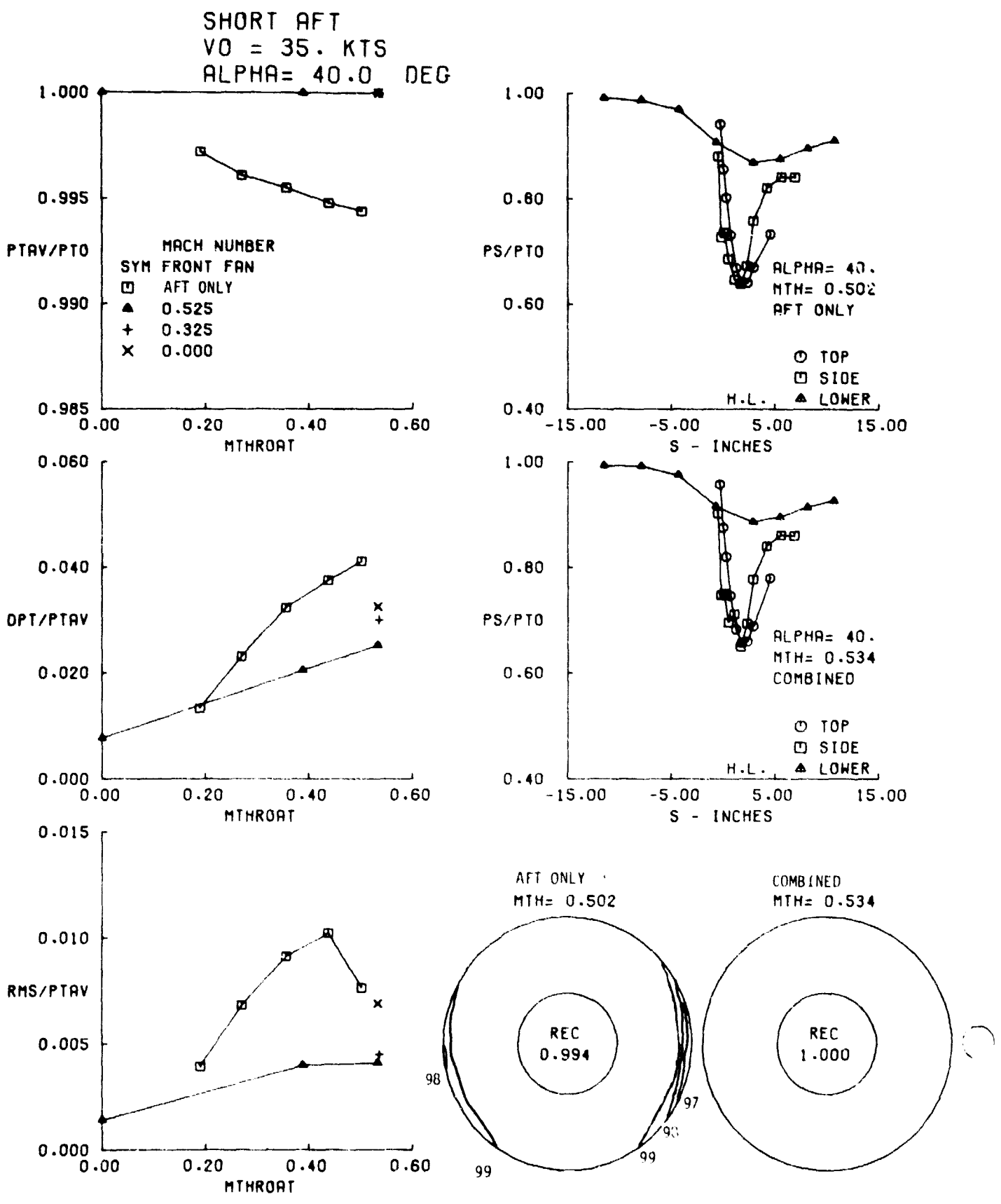

FIGURE 39B. SHORT AFT INLET PERFORMANCE (SIDE PIPE) AT V_0 = 35 KNOTS, $\alpha = 40^0$

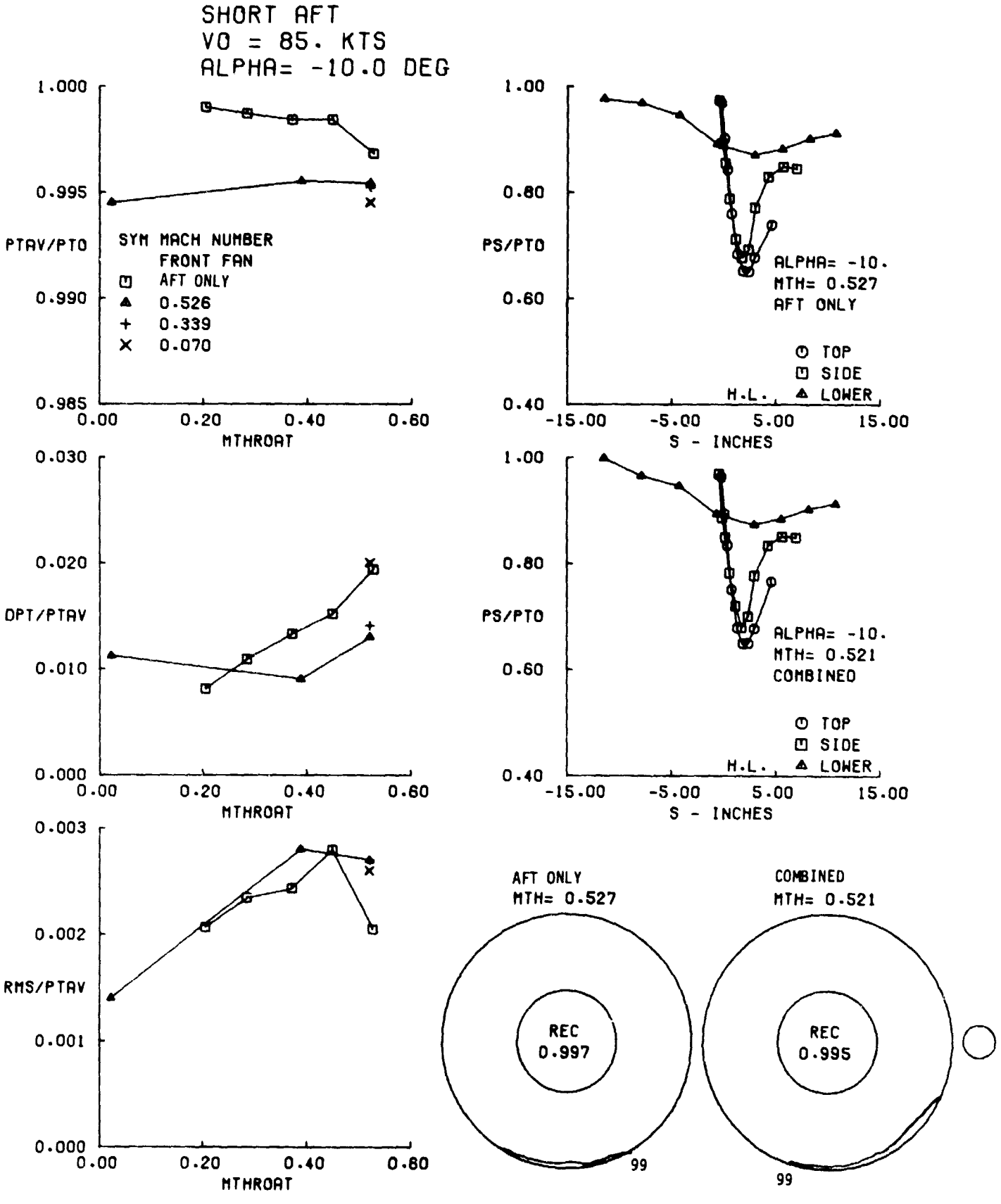

FIGURE 40A. SHORT AFT INLET PERFORMANCE (SIDE PIPE) AT V_0 = 85 KNOTS, α = -10°

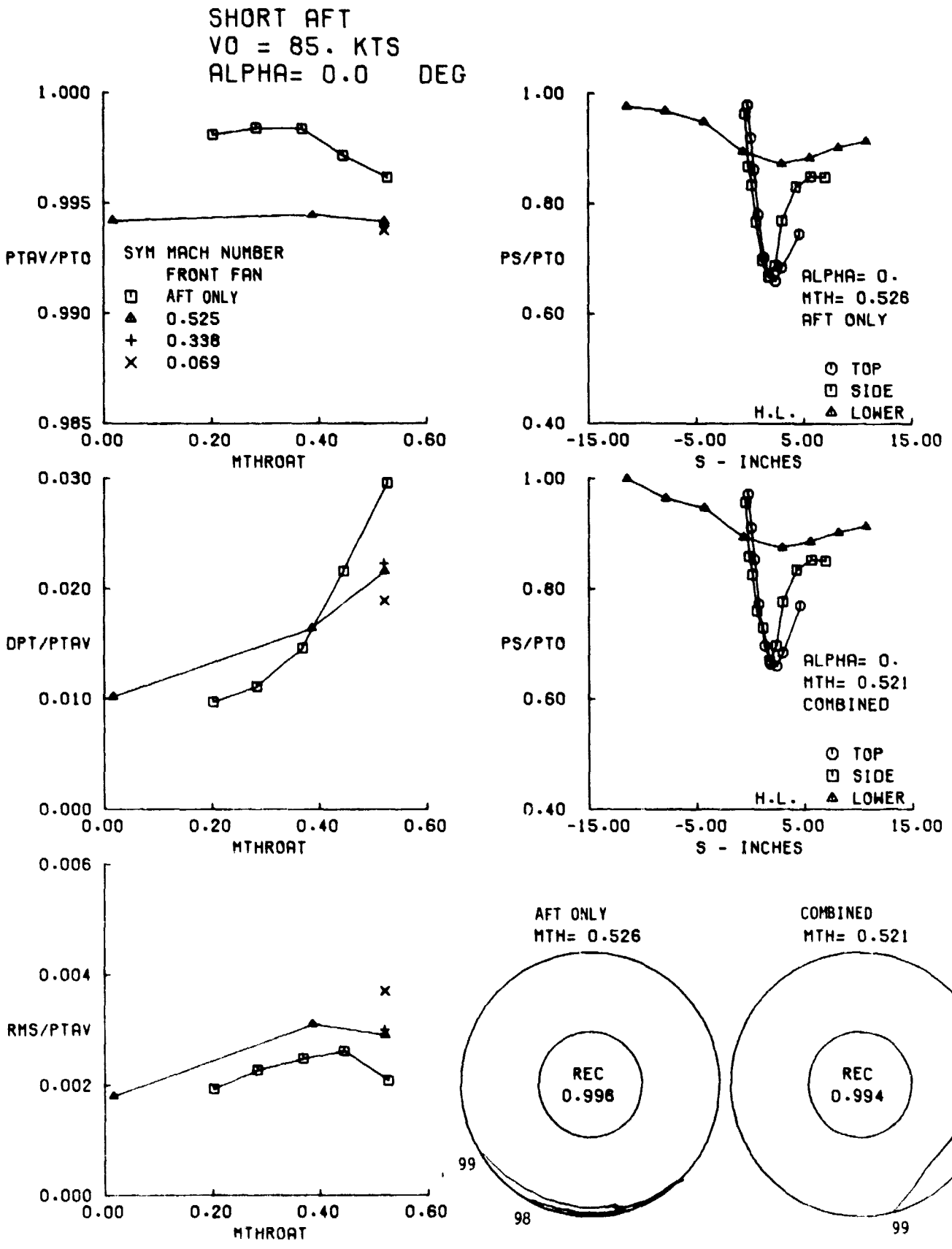

FIGURE 40B. SHORT AFT INLET PERFORMANCE (SIDE PIPE) AT V_0 = 85 KNOTS, $\alpha = 0^0$

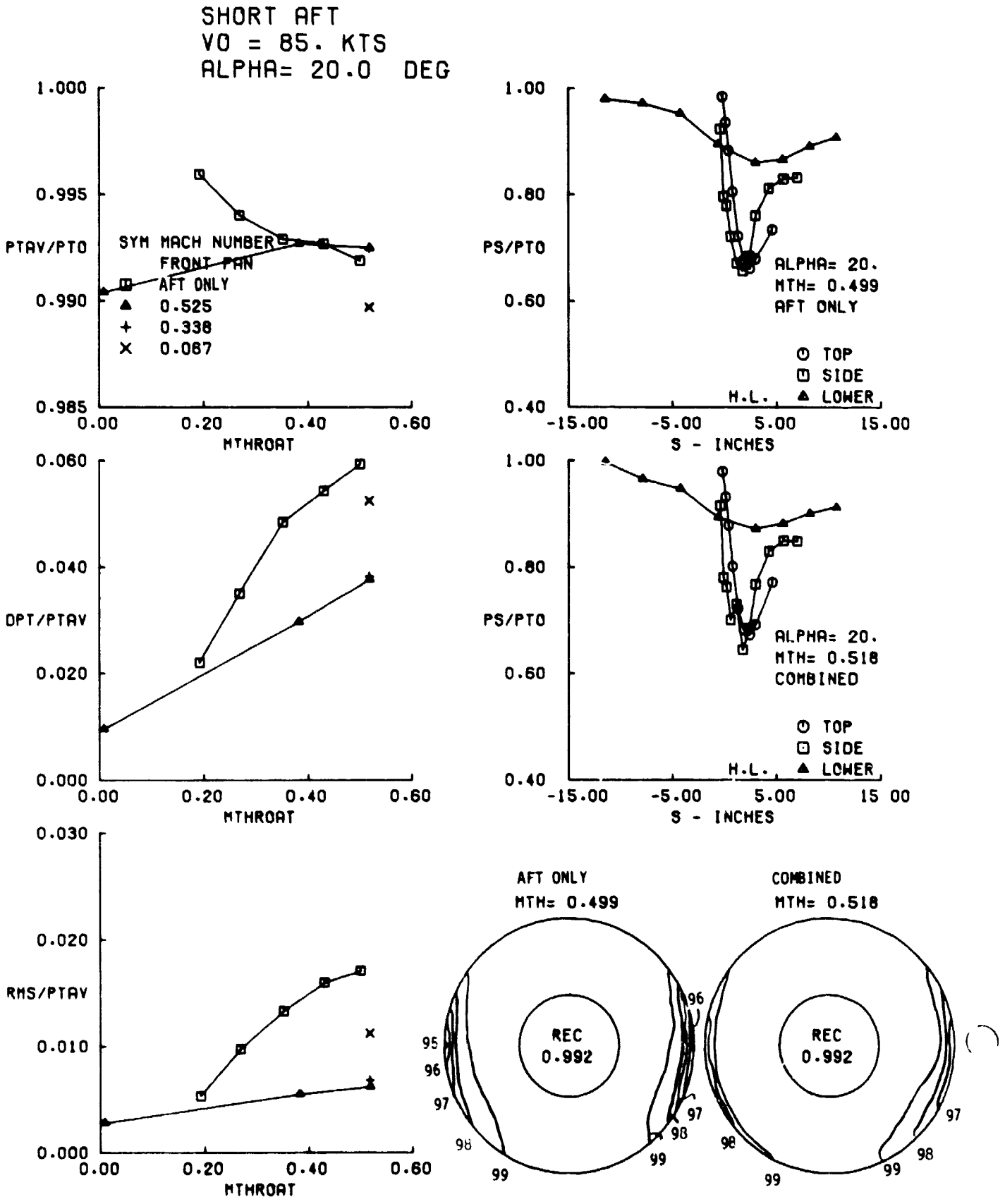

FIGURE 40C. SHORT AFT INLET PERFORMANCE (SIDE PIPE) AT V_0 = 85 KNOTS, α = 20°

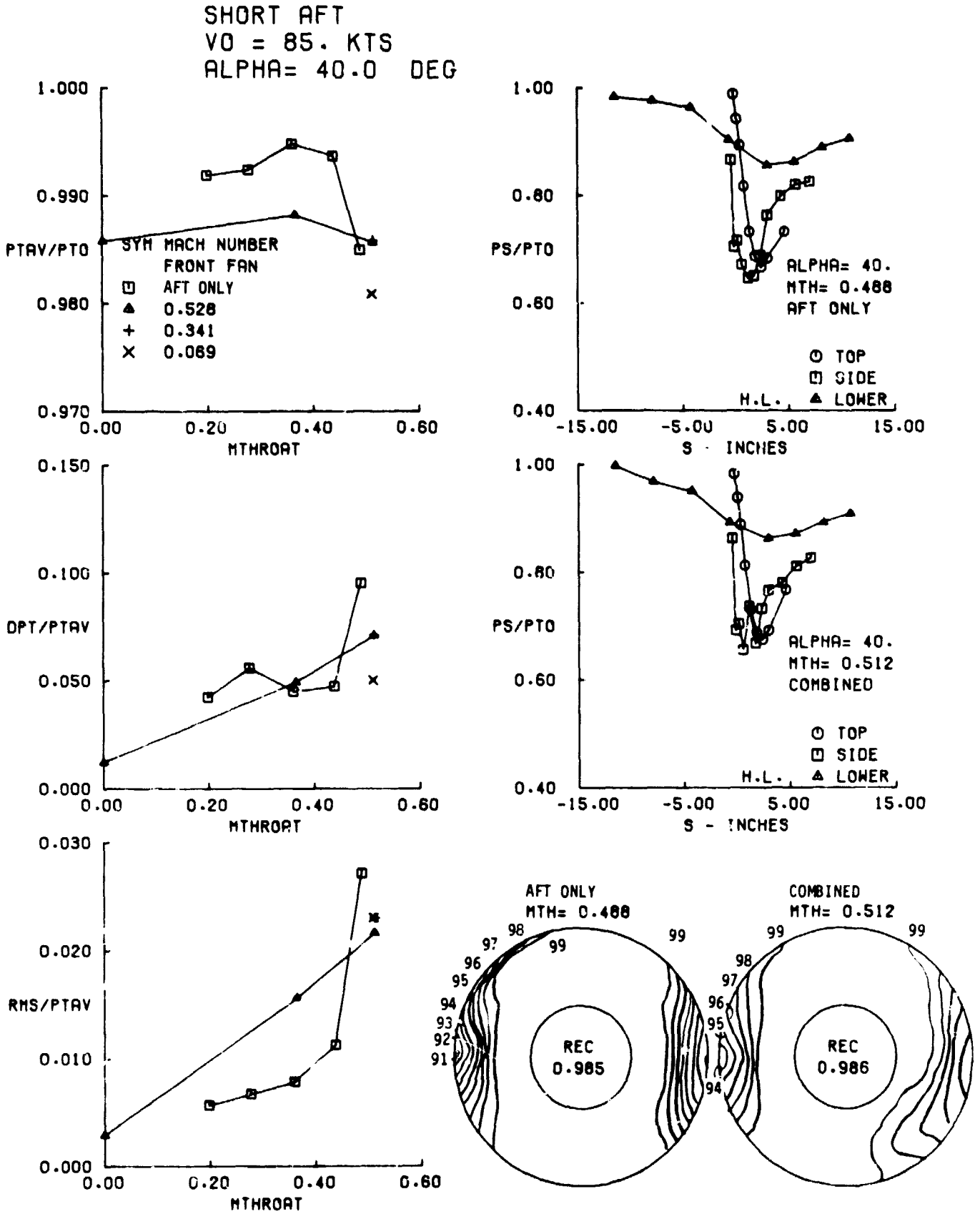

FIGURE 40D. SHORT AFT INLET PERFORMANCE (SIDE PIPE) AT V_0 = 85 KNOTS, α = 40°

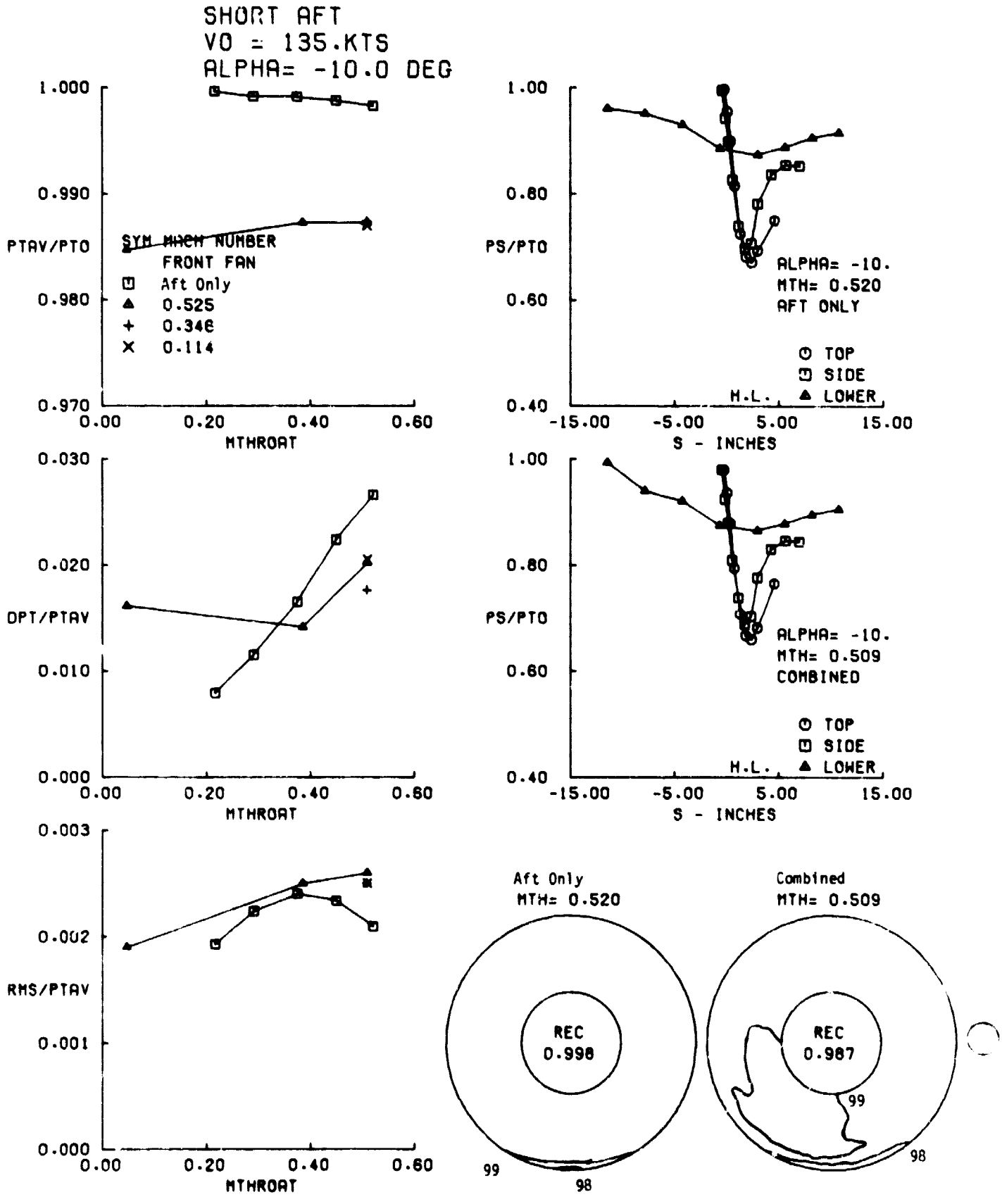

Figure 41A. Short Aft Inlet Performance (Side Pipe) at Vo = 135 knots, $\alpha = -10^{o}$

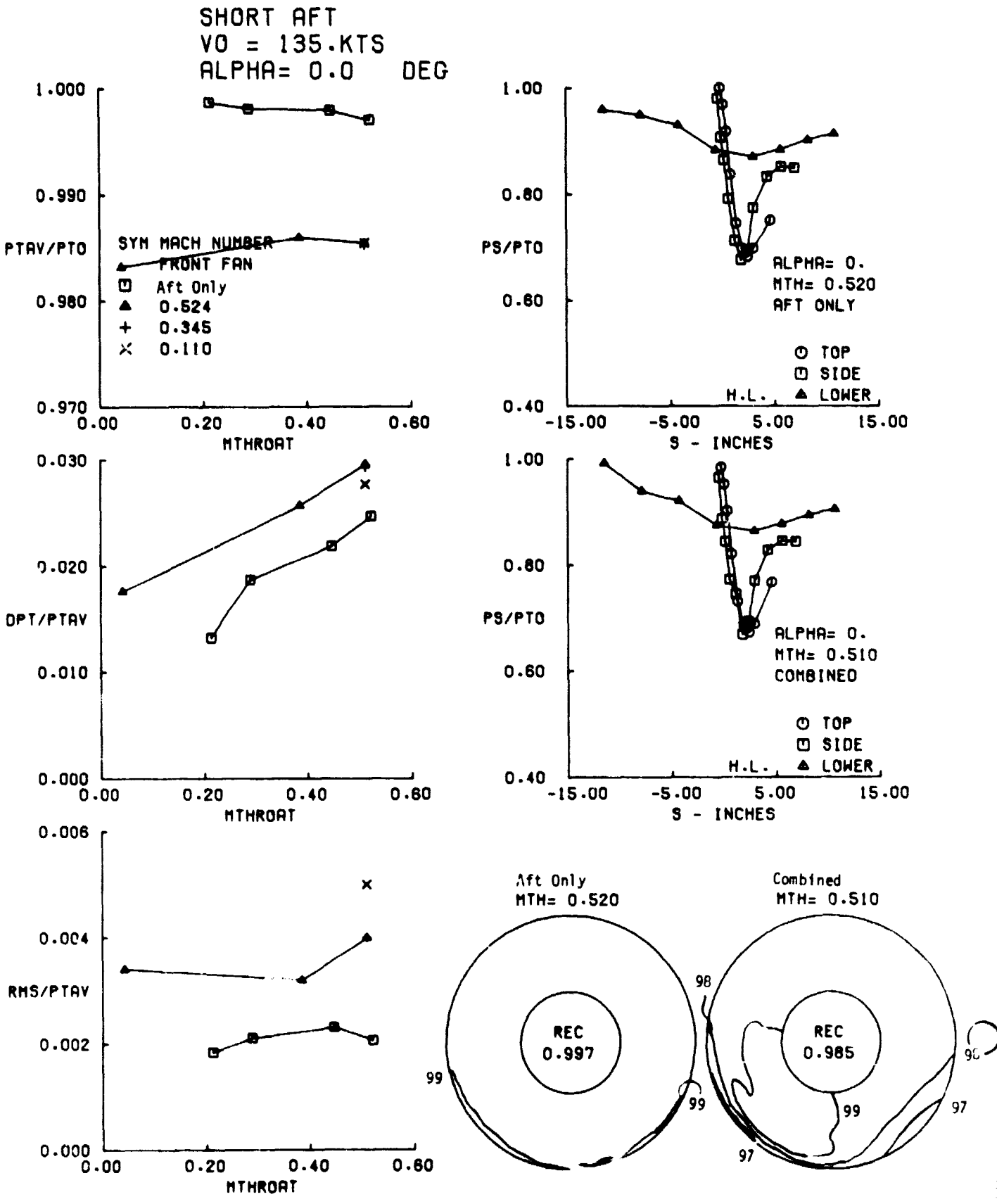

Figure 418. Short Aft Inlet Performance (Side Pipe) at Vo = 135 Knots, $\alpha = 0^{0}$

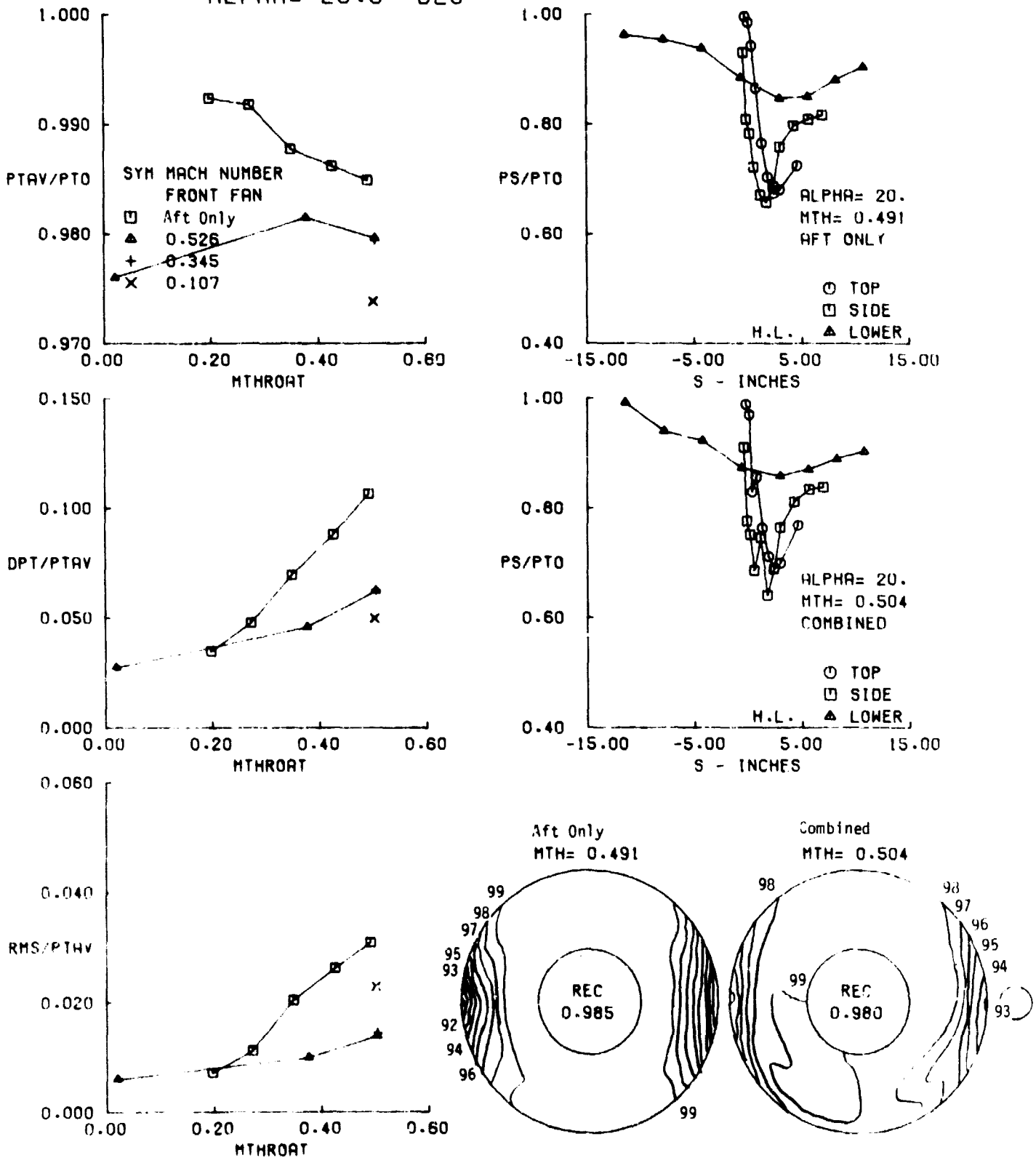

Figure 41C. Short Aft Inlet Performance (Side Pipe) at Vo = 135 Knots, $\alpha = 20^0$

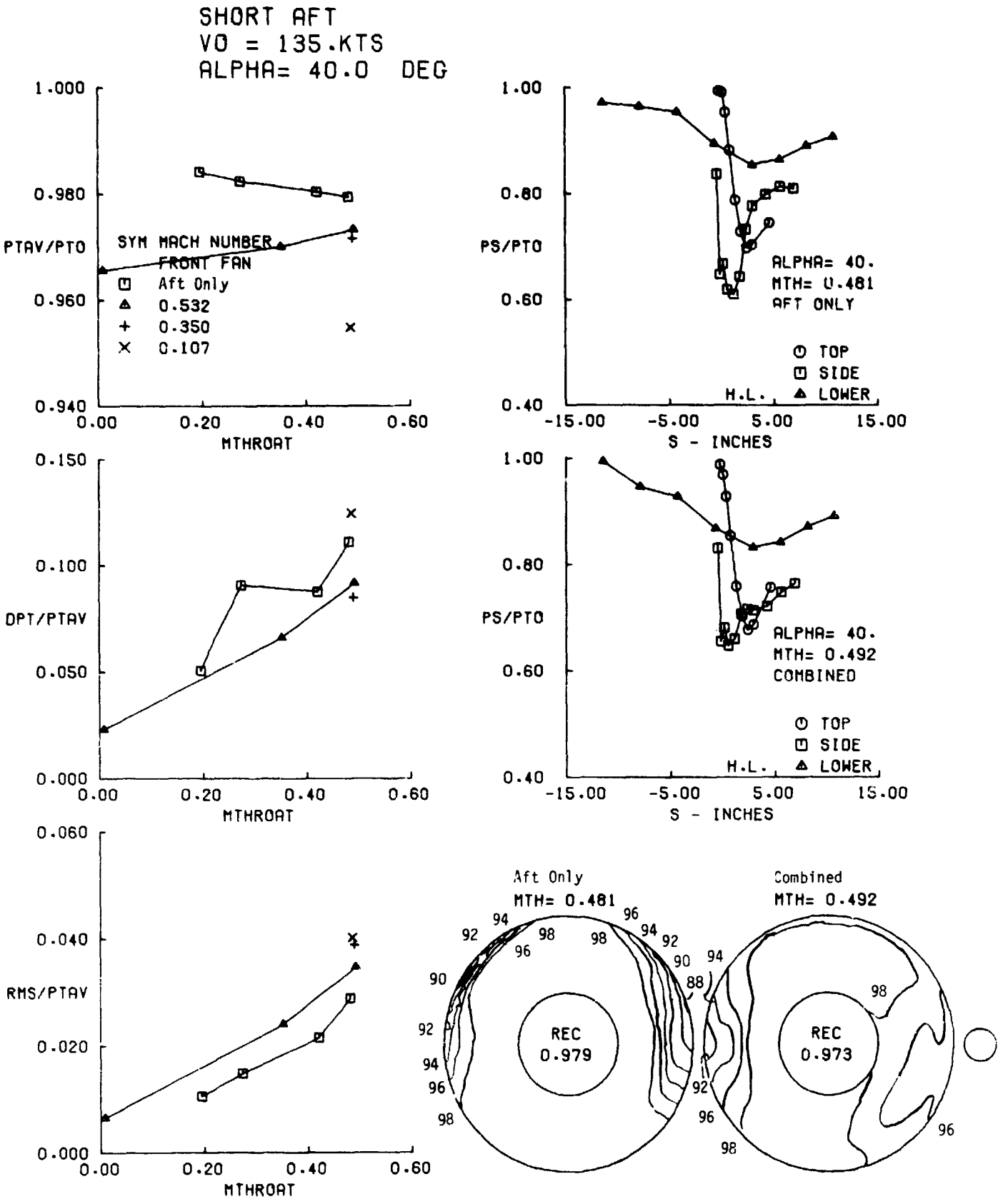

Figure 41D. Short Aft Inlet Performance (Side Pipe) at Vo = 135 Knots, $\alpha = 40^{o}$

angle-of-attack conditions. Therefore, fillets were added to the aft inlet lip corners as a means of improving the high speed, high angle-of-attack performance. The results are shown in Figures 42, 43, 44, and 45 for Vo = 0, 35, 95, and 135 knots (0, 18, 43.7, and 69.5 m/s). At Vo = 0 and 35 knots, Figures 42 and 43, the fillets appear to give better pressure recovery with little or no increase in distortion levels. The fan face pressure maps are essentially uniform. However, at the higher speeds, Vo = 85 and 135 knots, the performance decays below the isolated inlet levels, Figures 44 and 45. Note the performance levels for Figures 36a vs 44b; 37b vs 45b at $\alpha = 0^0$; and 36C vs 44d; 37d vs 45d at $\alpha = 40^0$. In summary, the corner fillets improve performance only in the low speed regime and are detrimental at the higher speeds.

6.2.3 Configuration Comparisons

Comparison in terms of total pressure recovery, distortion, and turbulence levels for two aft inlet configurations are presented in Figures 46 to 50. These data include freestream conditions of Vo = 0, 35, 85, 135, and 240 knots. These comparisons include angles-of-attack of 0 and 40 degrees. The model configurations compared are the clean long and clean short aft inlets, operating in an isolated environment and in a combined (with operating front inlet) environment.

Figure 46 shows the performance comparison for the static (Vo = 0) condition. The square symbol denotes isolated long aft inlet performance. The triangle symbol denotes isolated short aft inlet performance, which is considerably better both in absolute pressure recovery level and in its relative independence of air flow rate (M_{throat}). The combined long aft inlet (+) has an improved recovery over the isolated long and the combined short aft inlet (X) has the highest recovery. The distortion levels ($(P_{TMAX} - P_{TMIN})/P_{TAVG}$) are relatively unaffected by the presence or absence of the front fan for either long or short aft inlet, with the short inlet being better. The turbulence levels also are essentially all equal, with the short inlet yielding lower levels.

The combined inlets/aft inlet performance is based on front fan at full speed conditions.

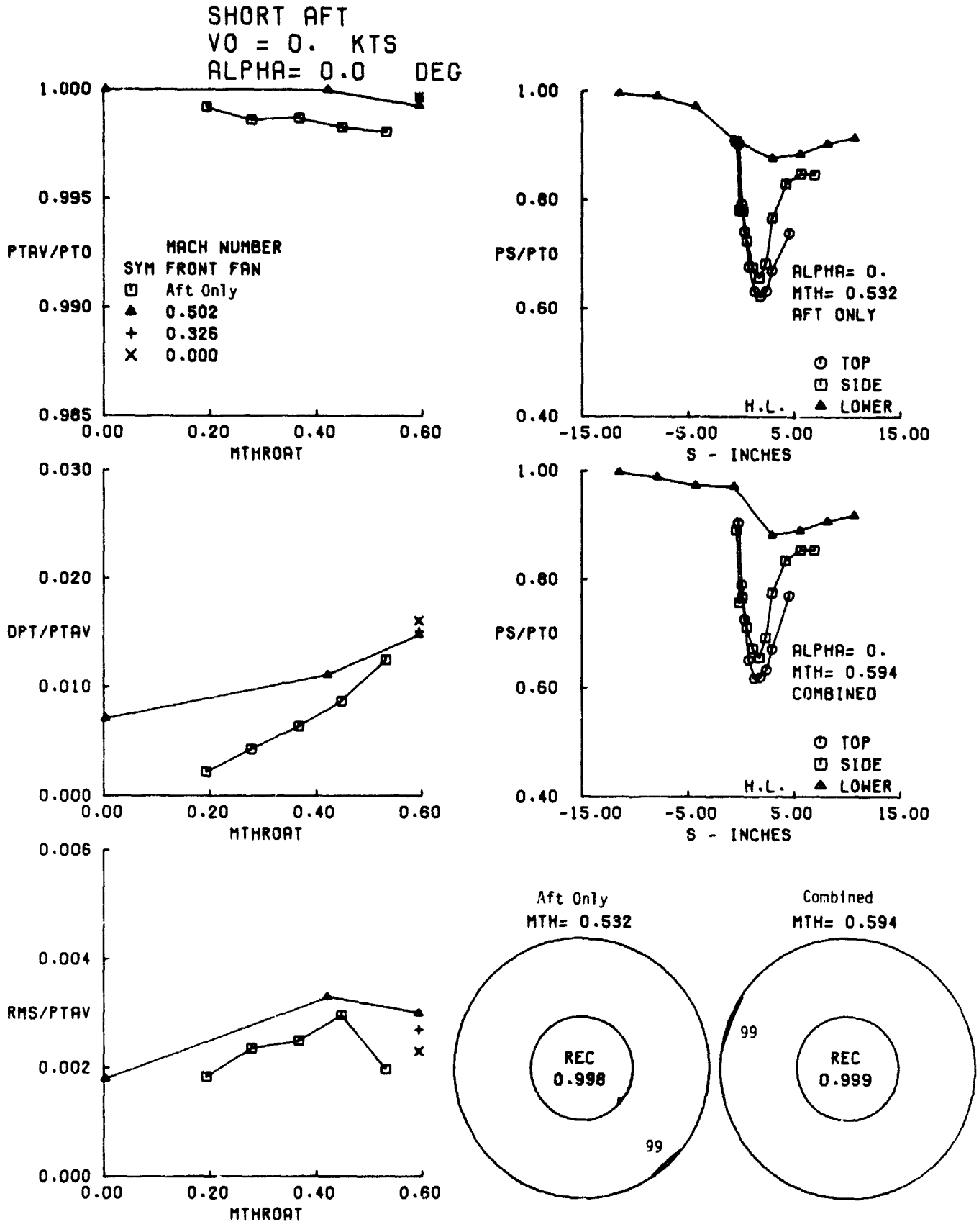

Figure 42. Short Aft Inlet with Corner Fillets Performance at Vo = 0 Knots

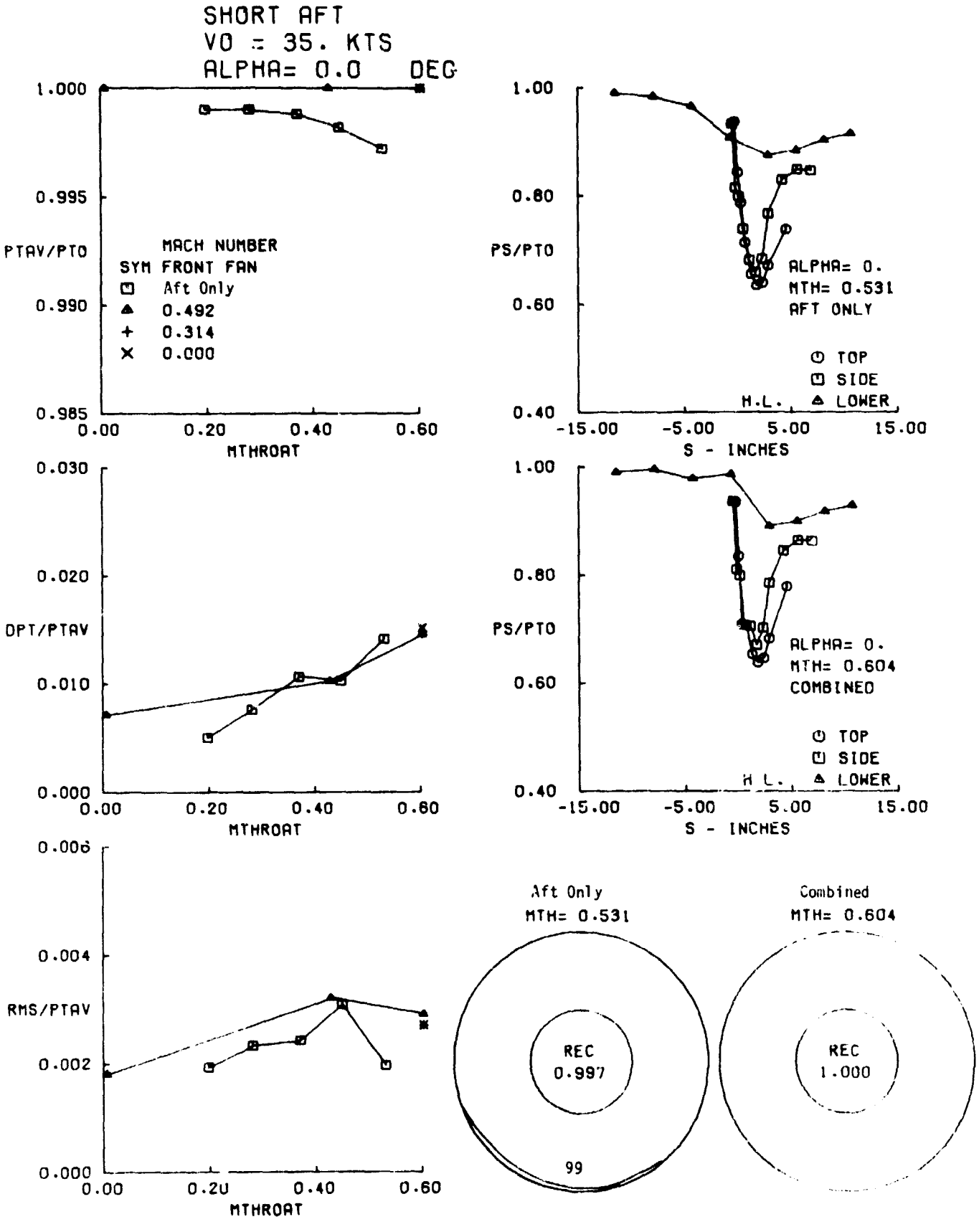

Figure 43A. Short Aft Inlet with Corner Fillets Performance at Vo = 35 Knots, α = 0°

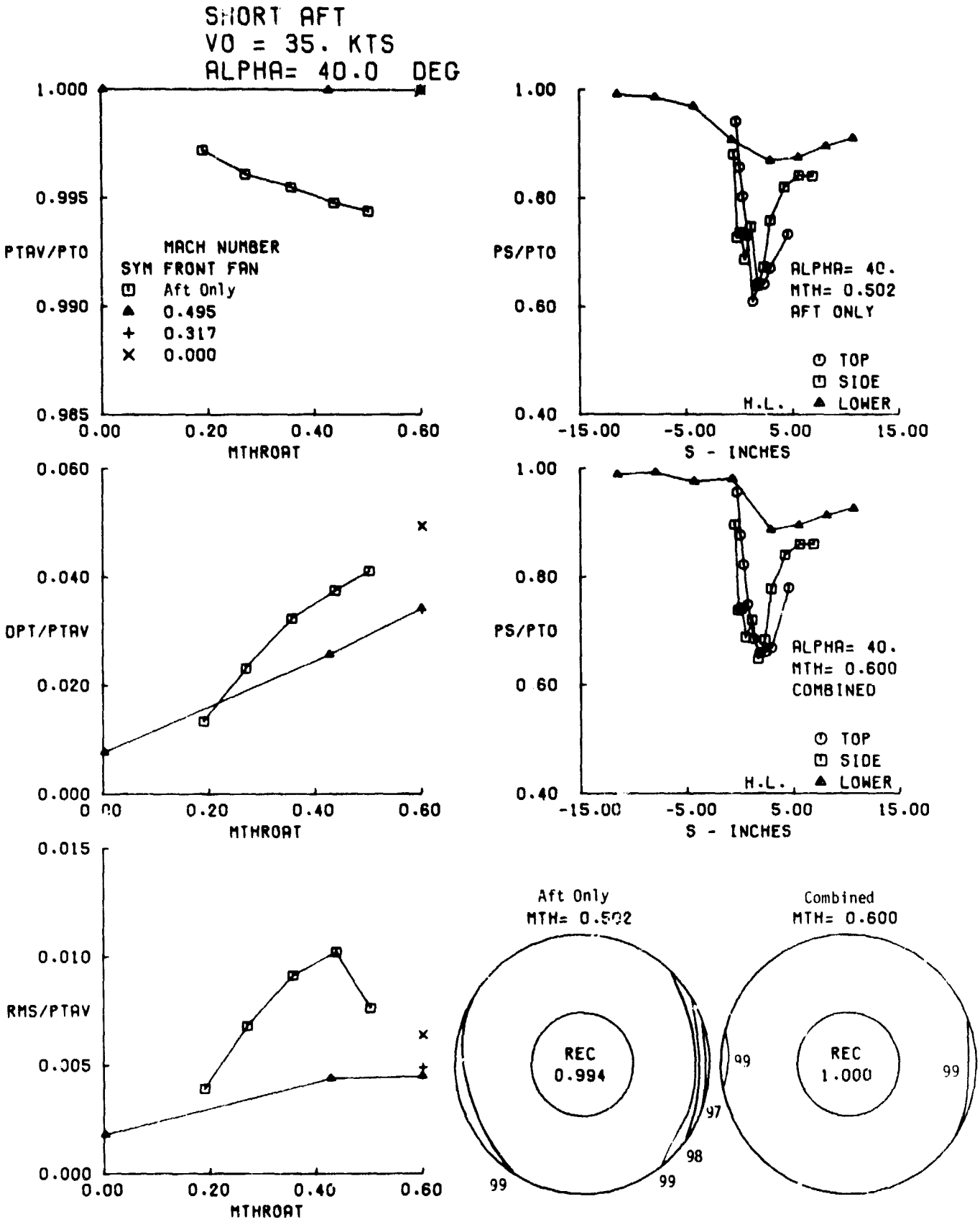

Figure 43B. Short Aft Inlet with Corner Fillets Performance at Vo = 35 Knots, $\alpha = 40^{0}$

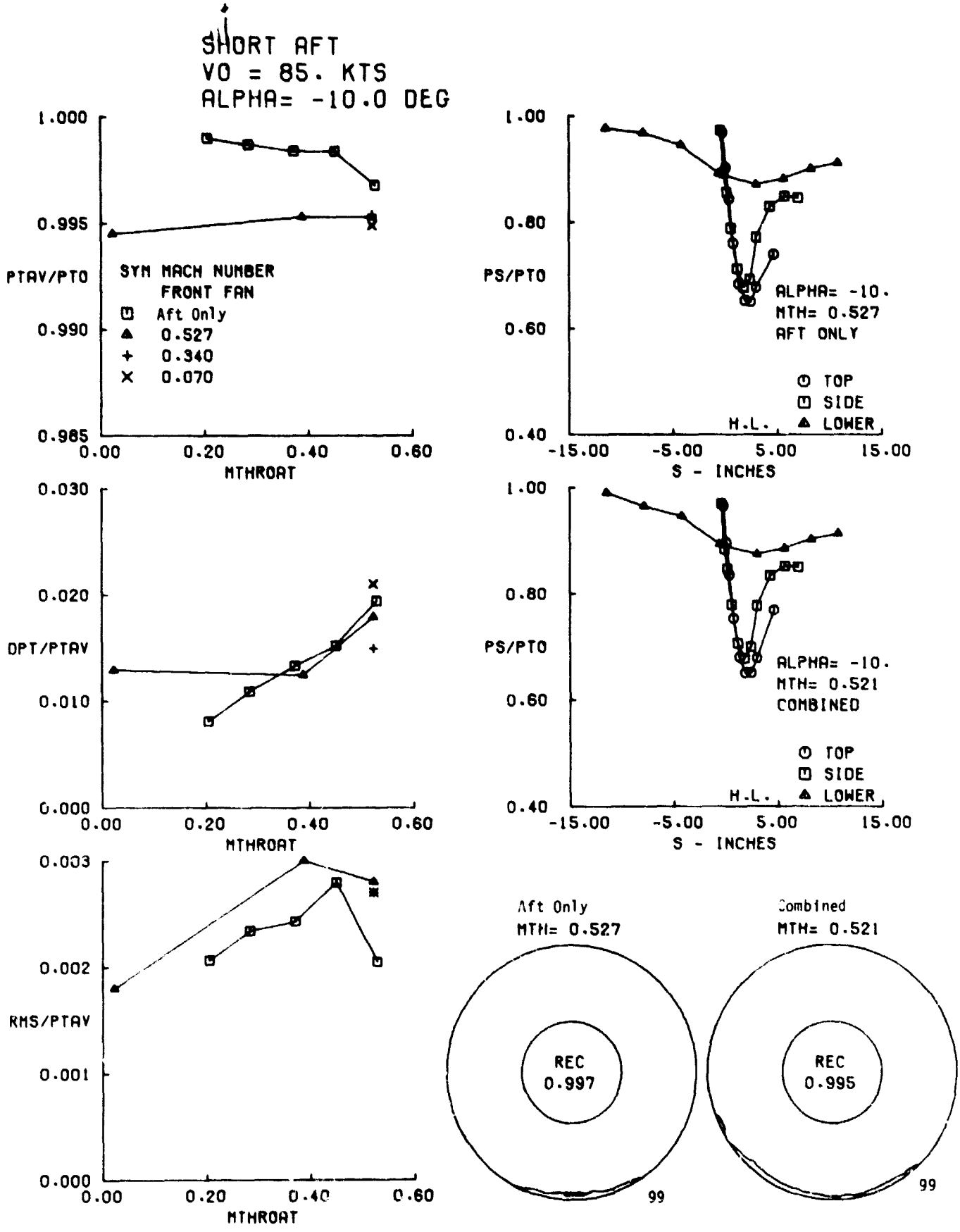

Figure 44A. Short Aft Inlet with Corner Fillets Performance at Vo = 85 Knots, $\alpha = -10^{o}$

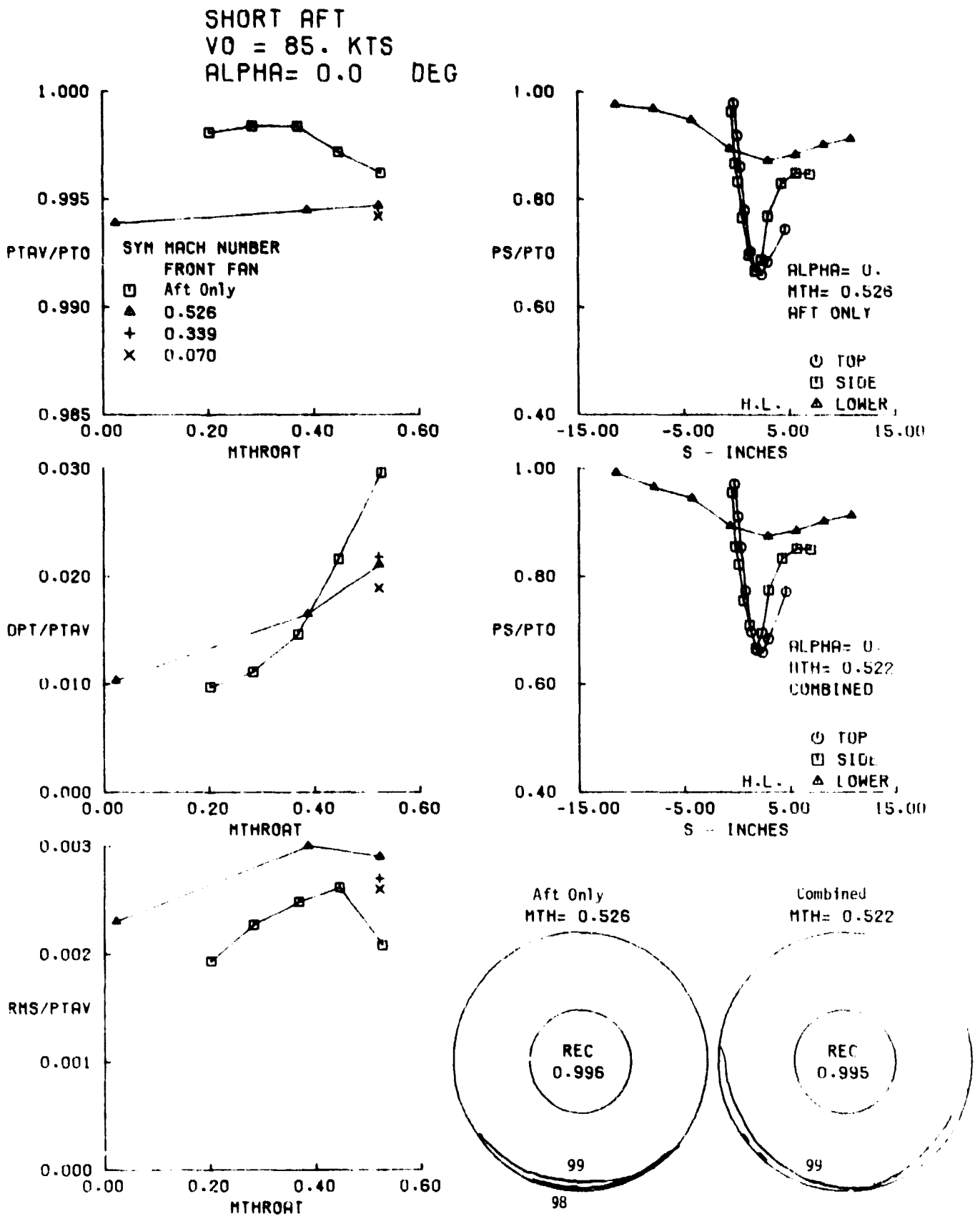

Figure 44B. Short Aft Inlet with Corner Fillets Performance at Vo = 85 knots, $\alpha = 0^0$

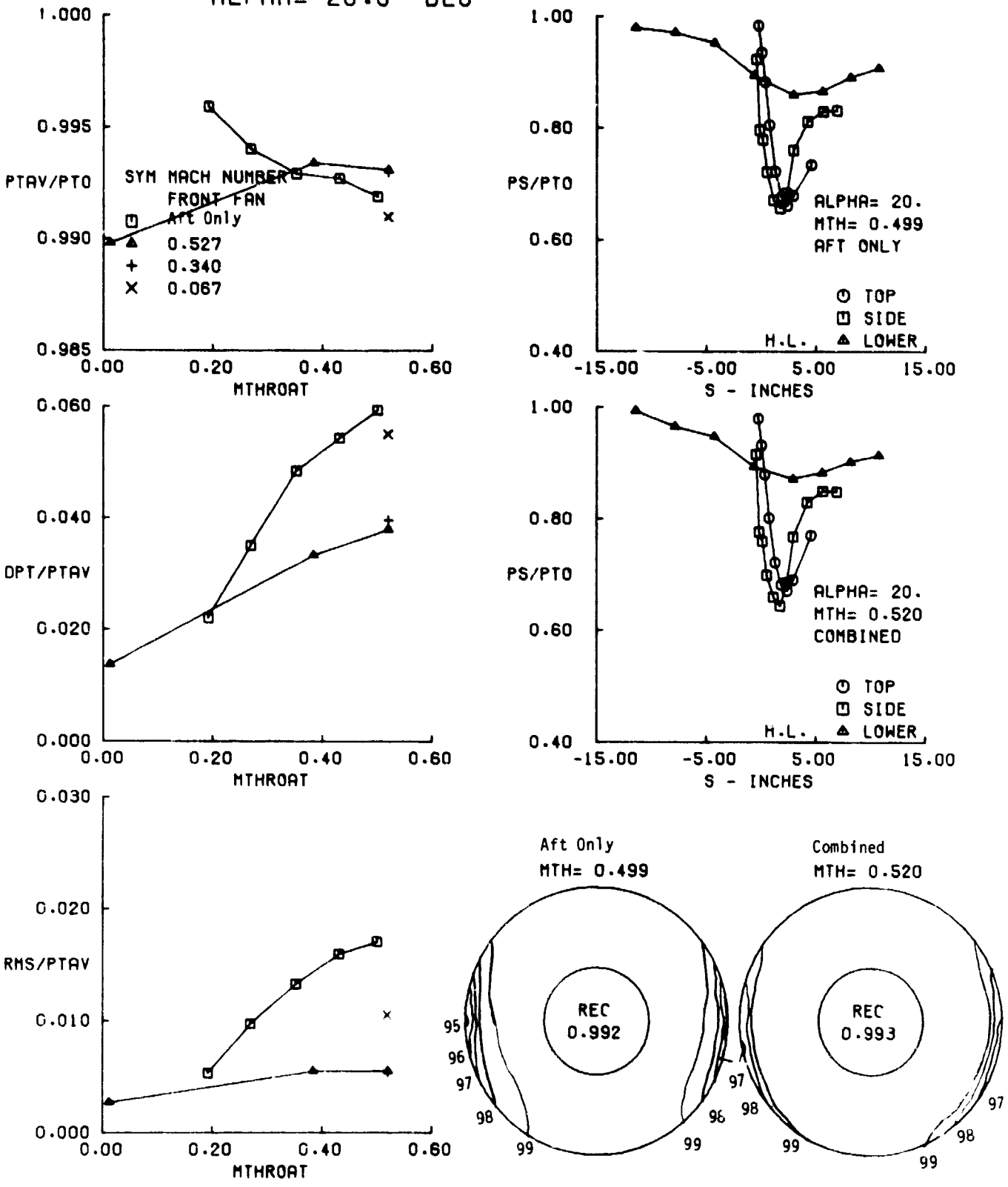

Figure 44C. Short Aft Inlet with Corner Fillets Performance at Vo = 85 Knots, $\alpha = 20^0$

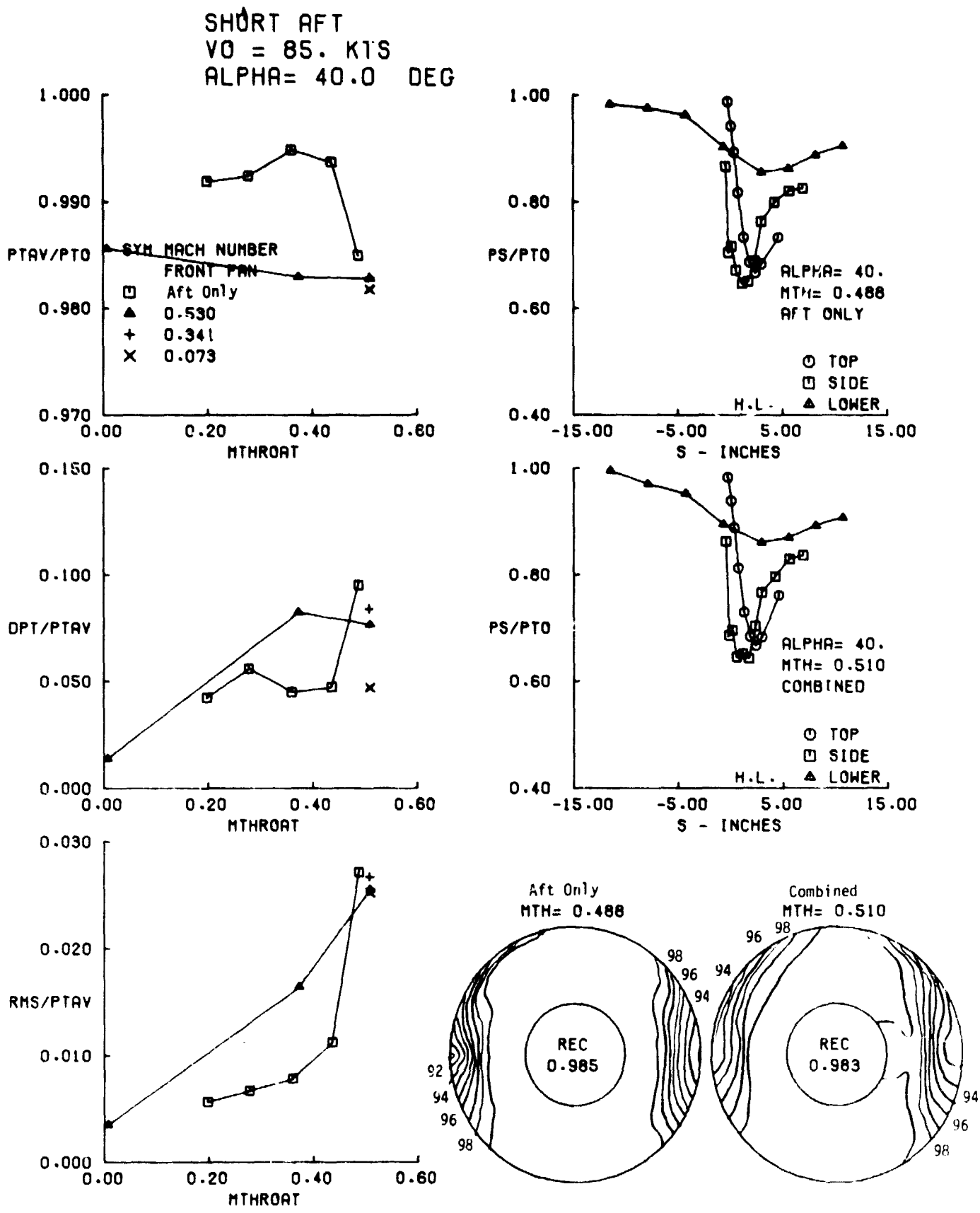

Figure 44D. Short Aft Inlet with Corner Fillets Performance at Vo = 85 Knots, $\alpha = 40^0$

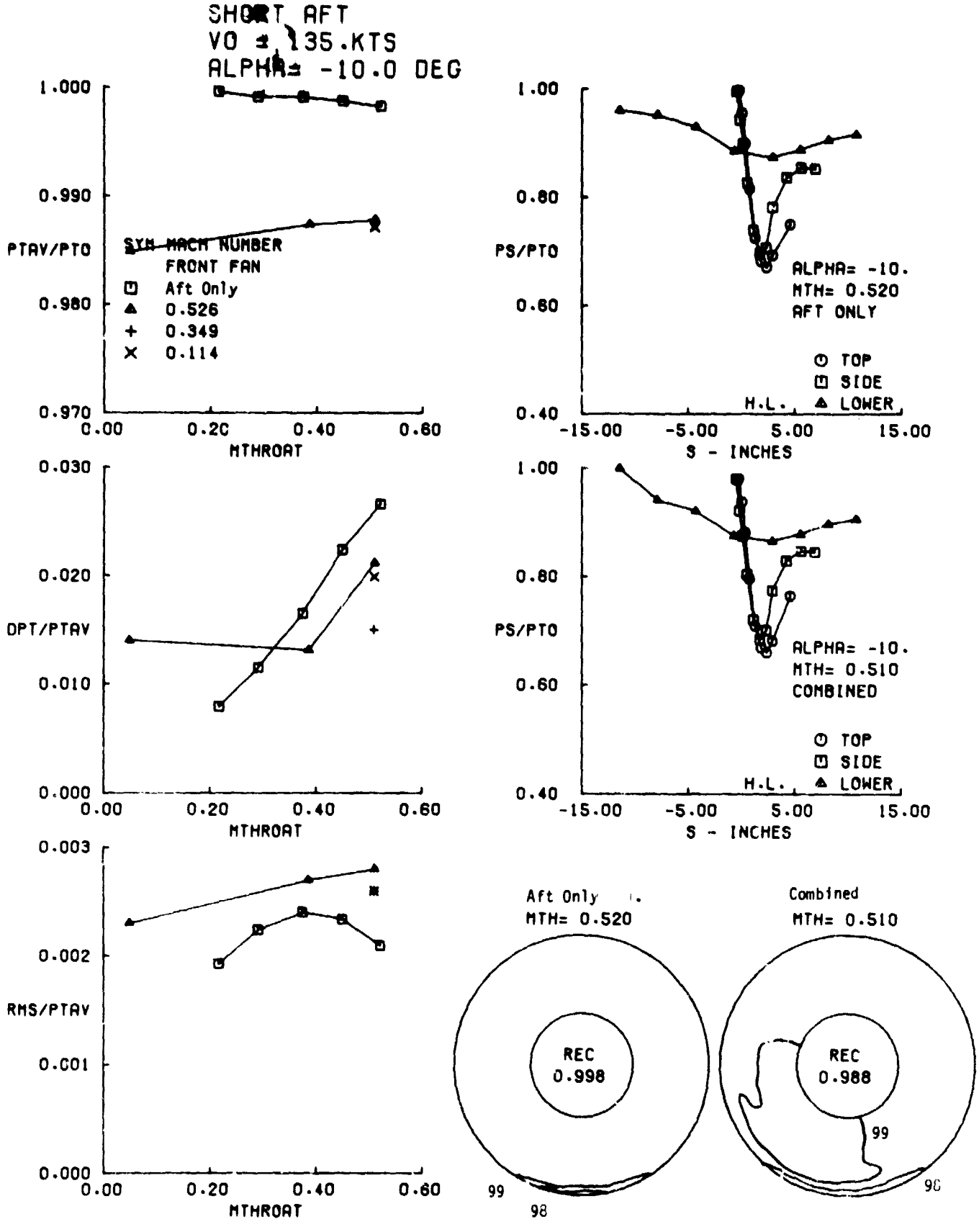

Figure 45A. Short Aft Inlet with Corner Fillets Performance at Vo = 135 Knots, $\alpha = -10^{o}$

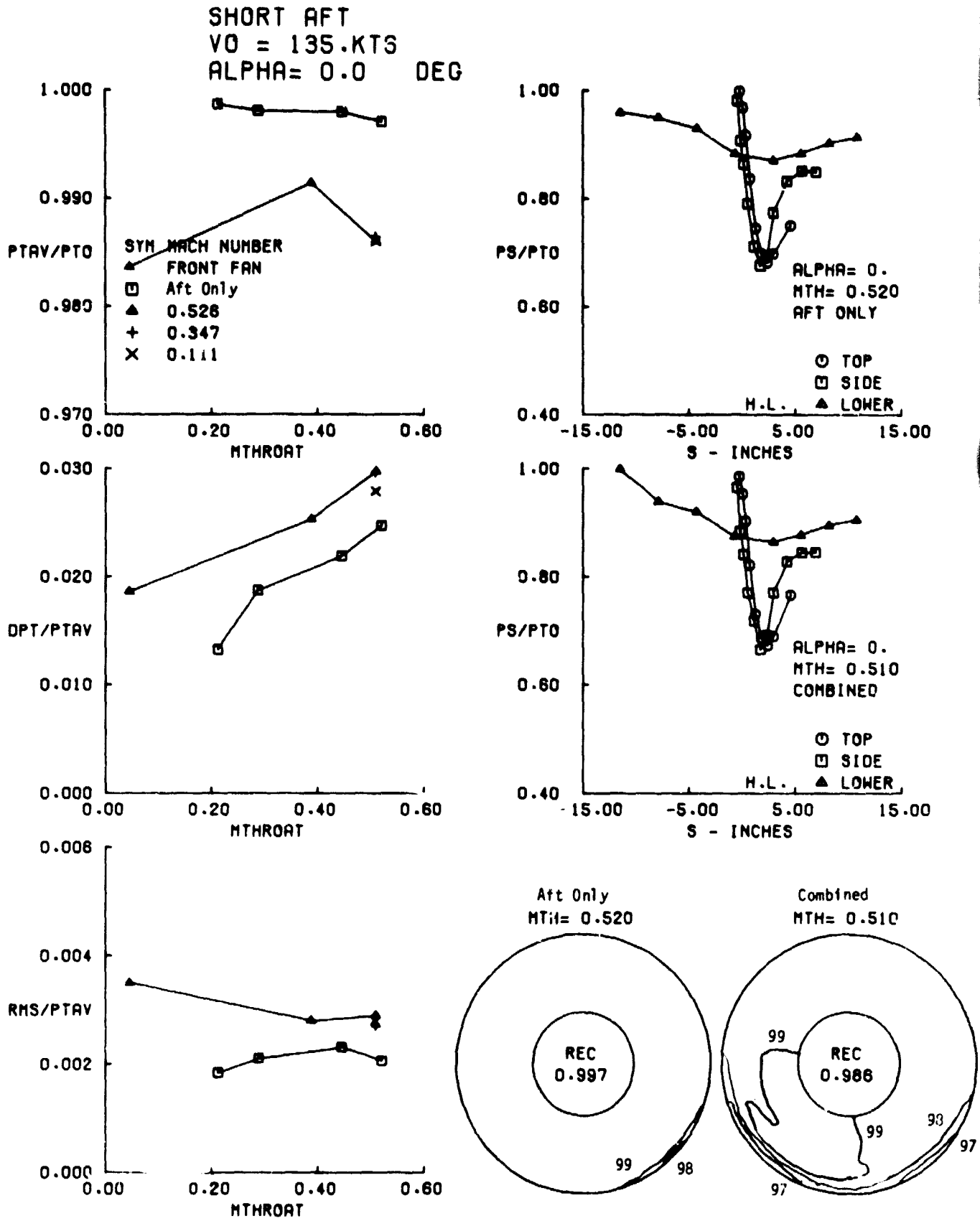

Figure 45B. Short Aft Inlet with Corner Fillets Performance at Vo = 135 Knots, $\alpha = 0^{o}$

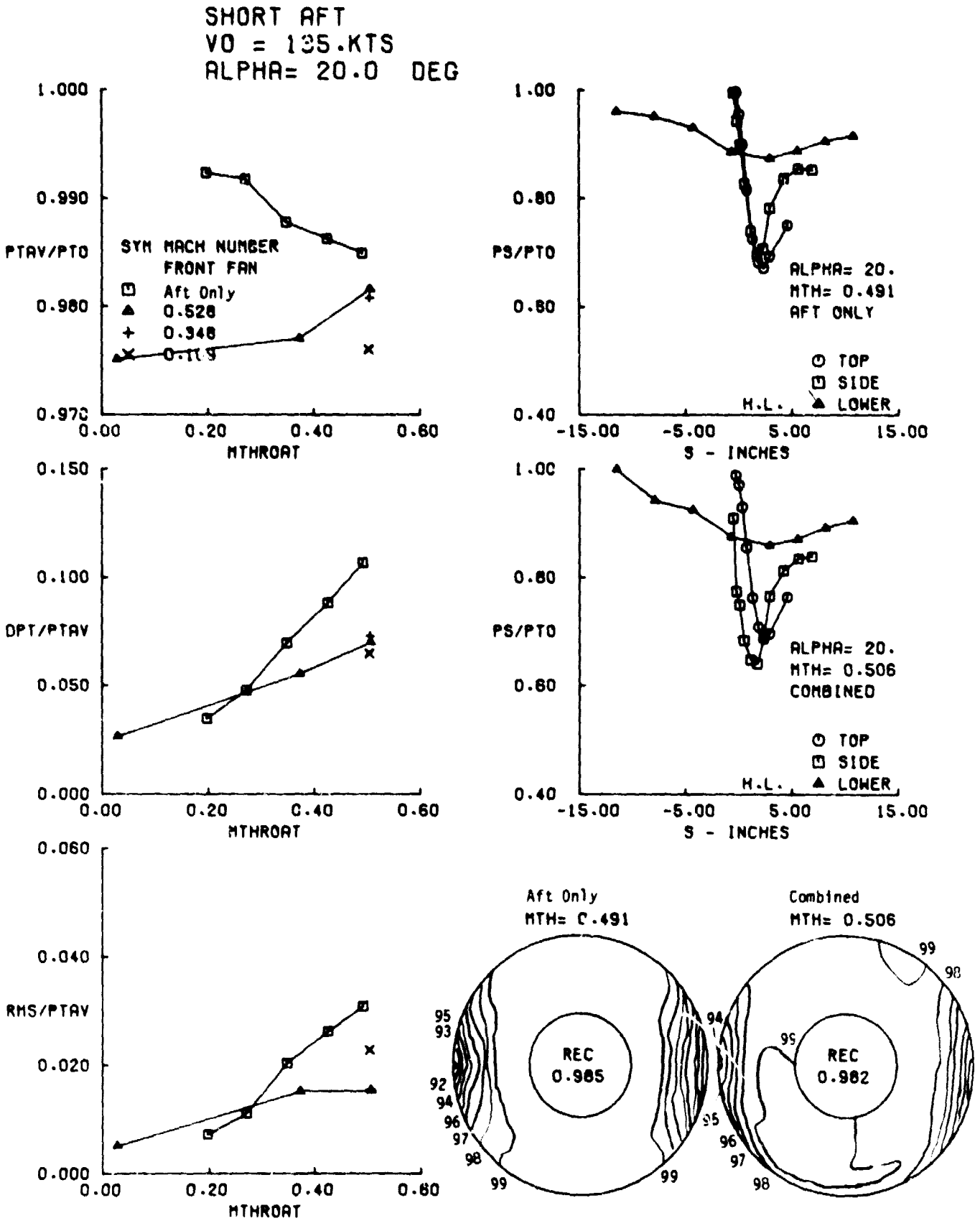

Figure 45C. Short Aft Inlet with Corner Fillets Performance at Vo = 135 Knots, $\alpha = 40^{o}$

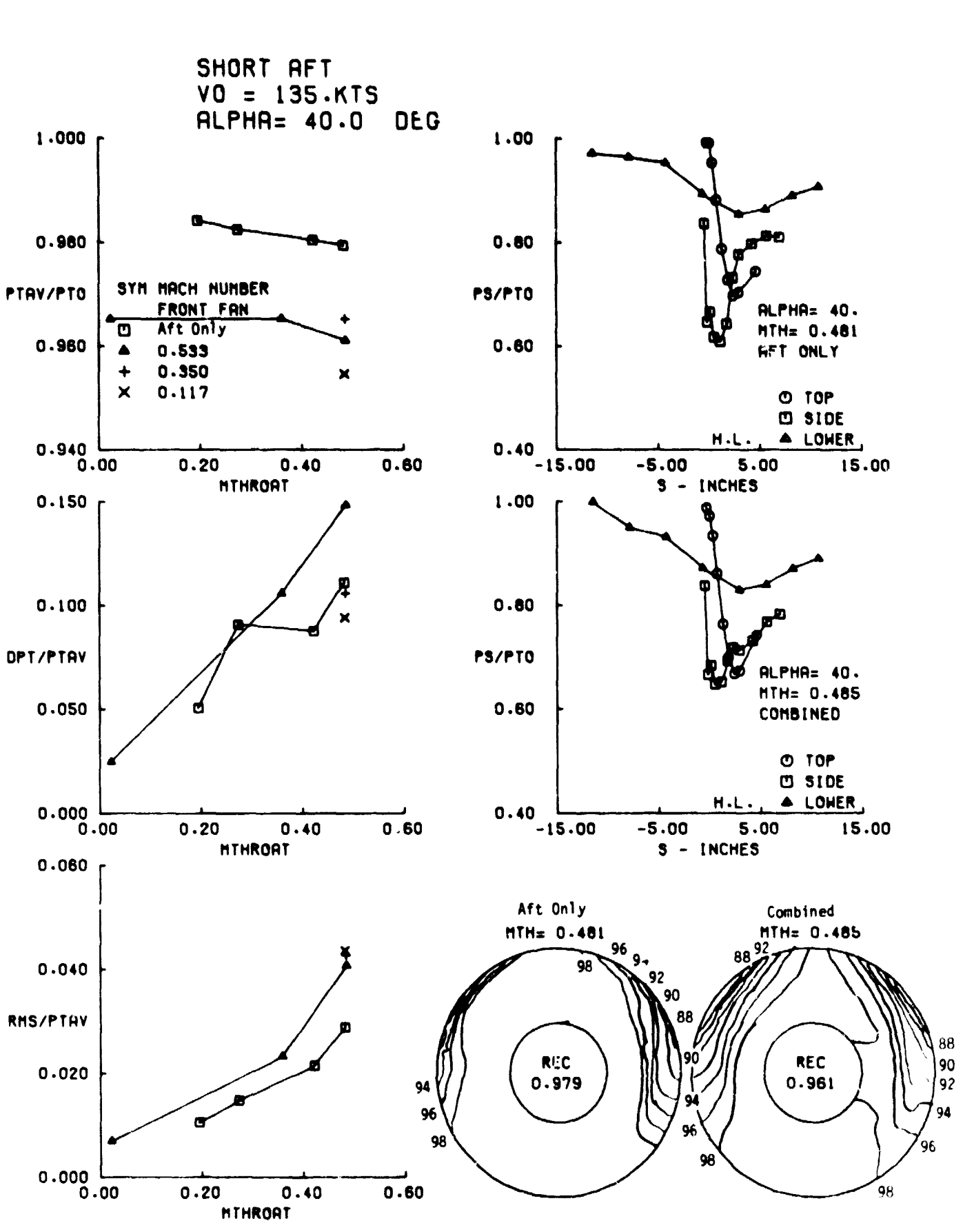

Figure45D. Short Aft Inlet with Corner Fillets Performance at Vo = 135 Knots, $\alpha = 40^0$

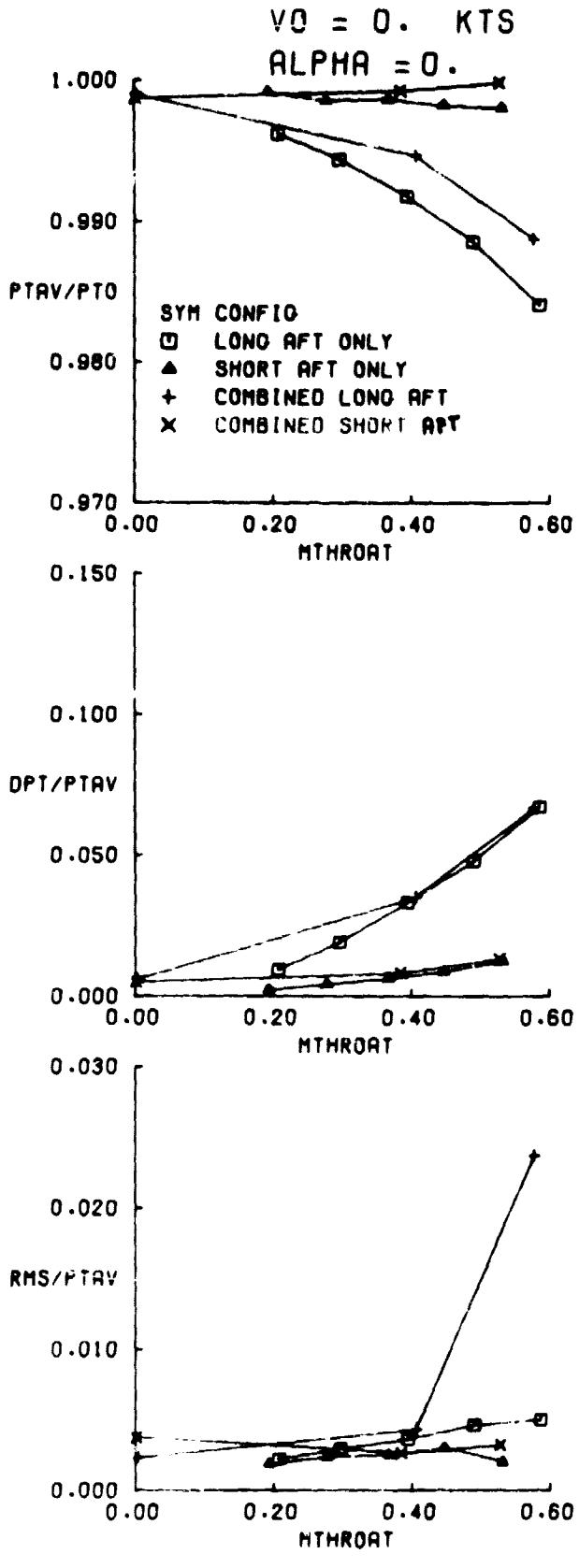

Figure 46. Performance Comparisons at Vo = 0 Knots.

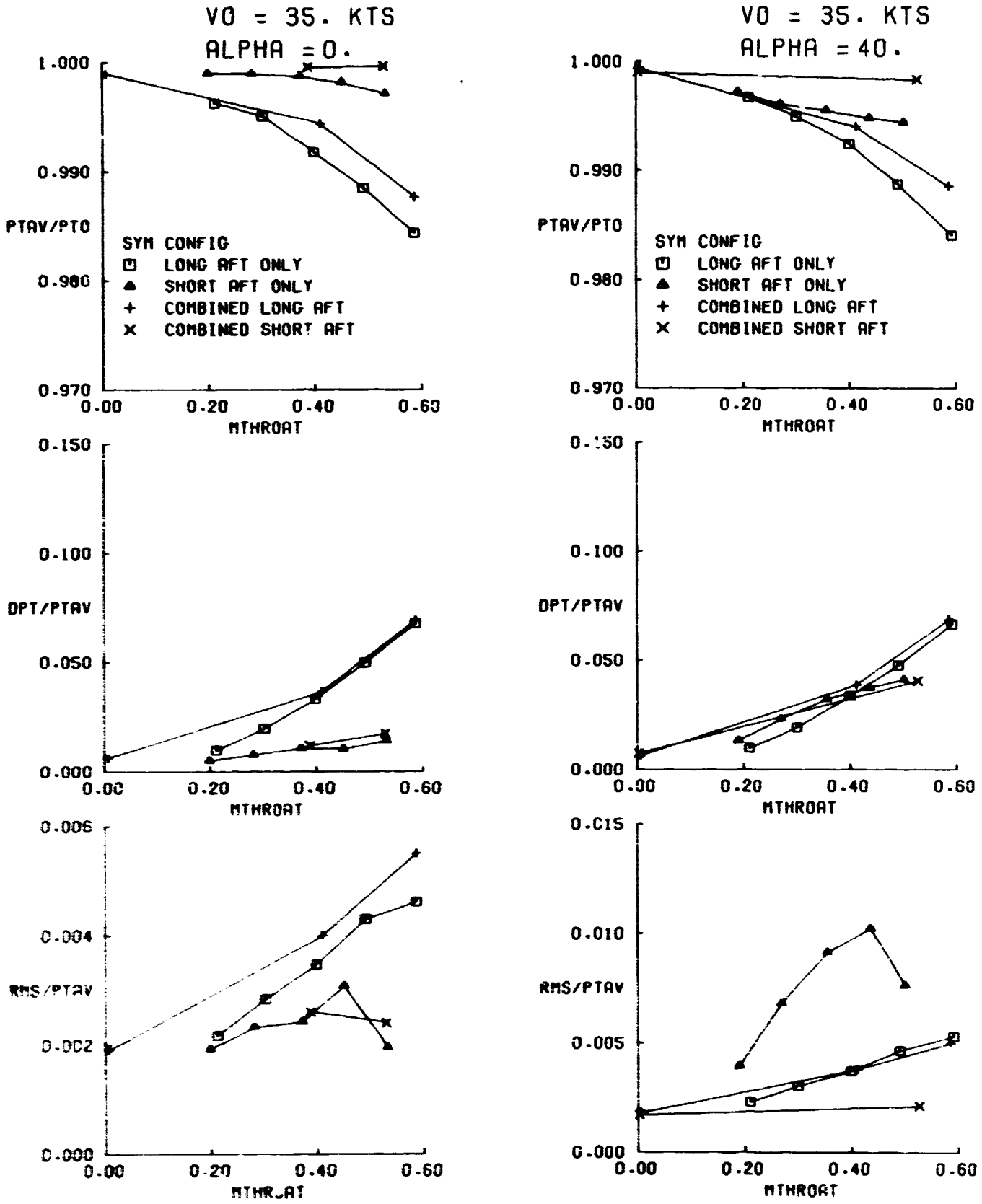

Figure 47. Performance Comparisons at Vo = 35 Knots.

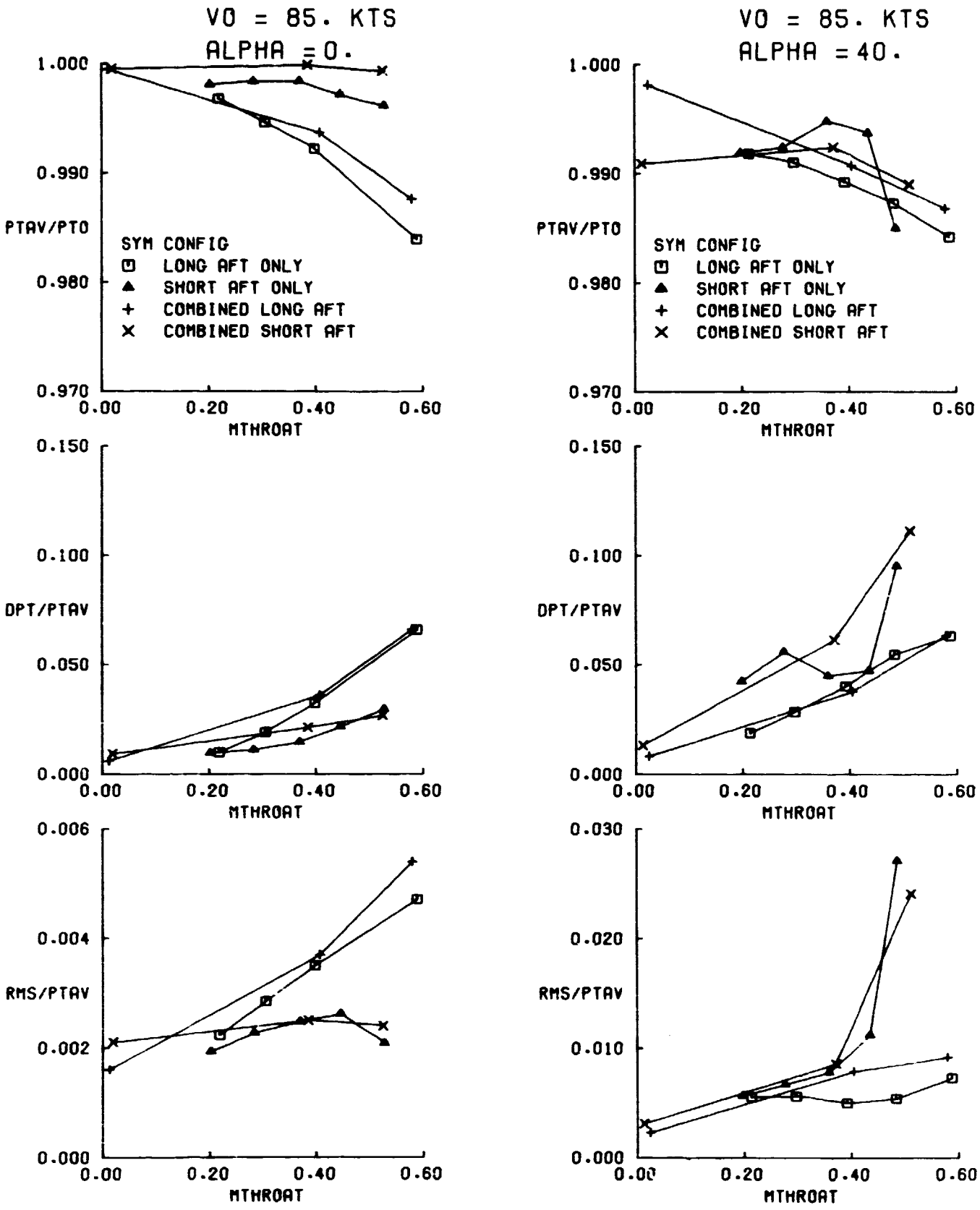

Figure 48. Performance Comparisons at Vo = 85 Knots.

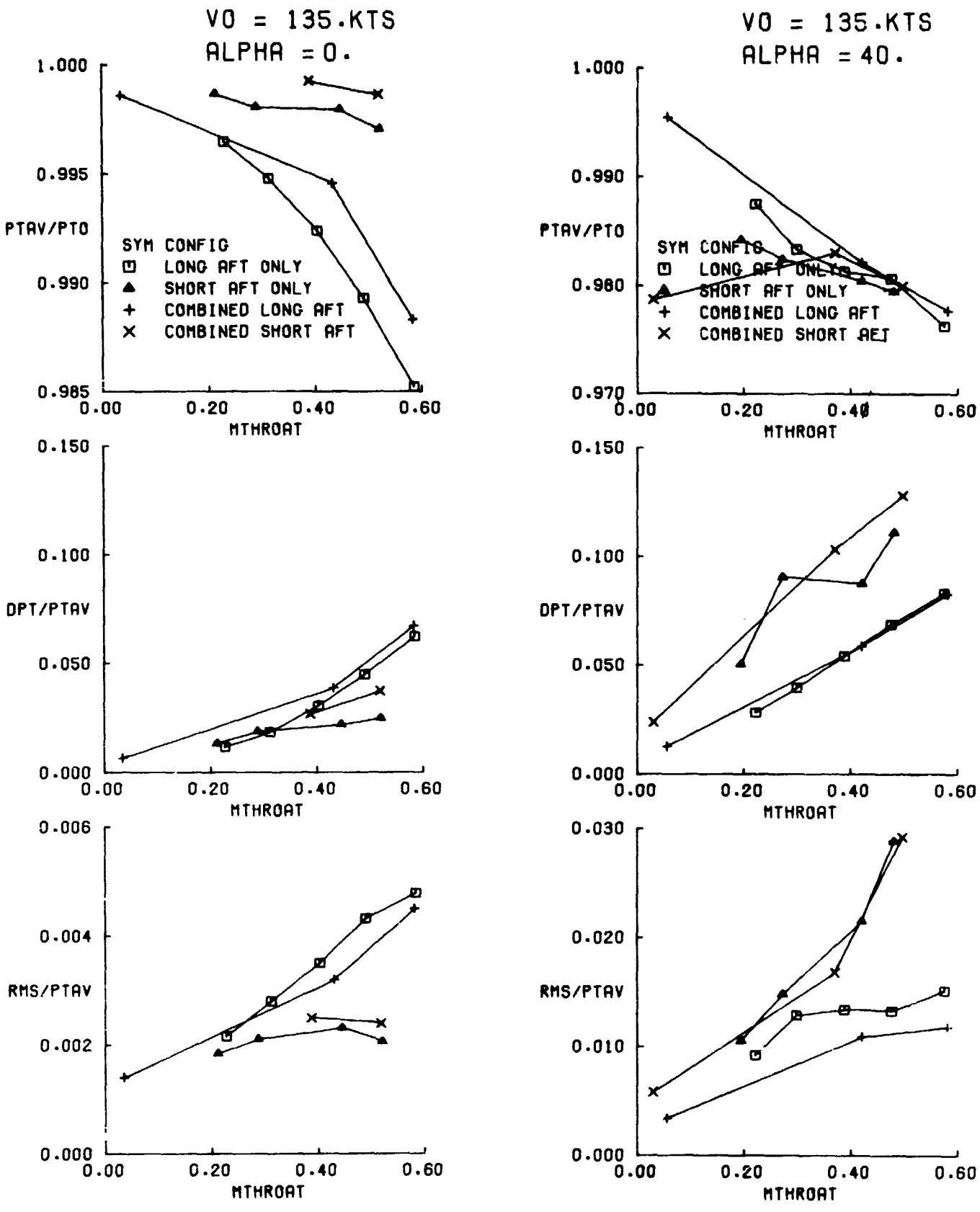

Figure 49. Performance Comparisons at Vo = 135 Knots.

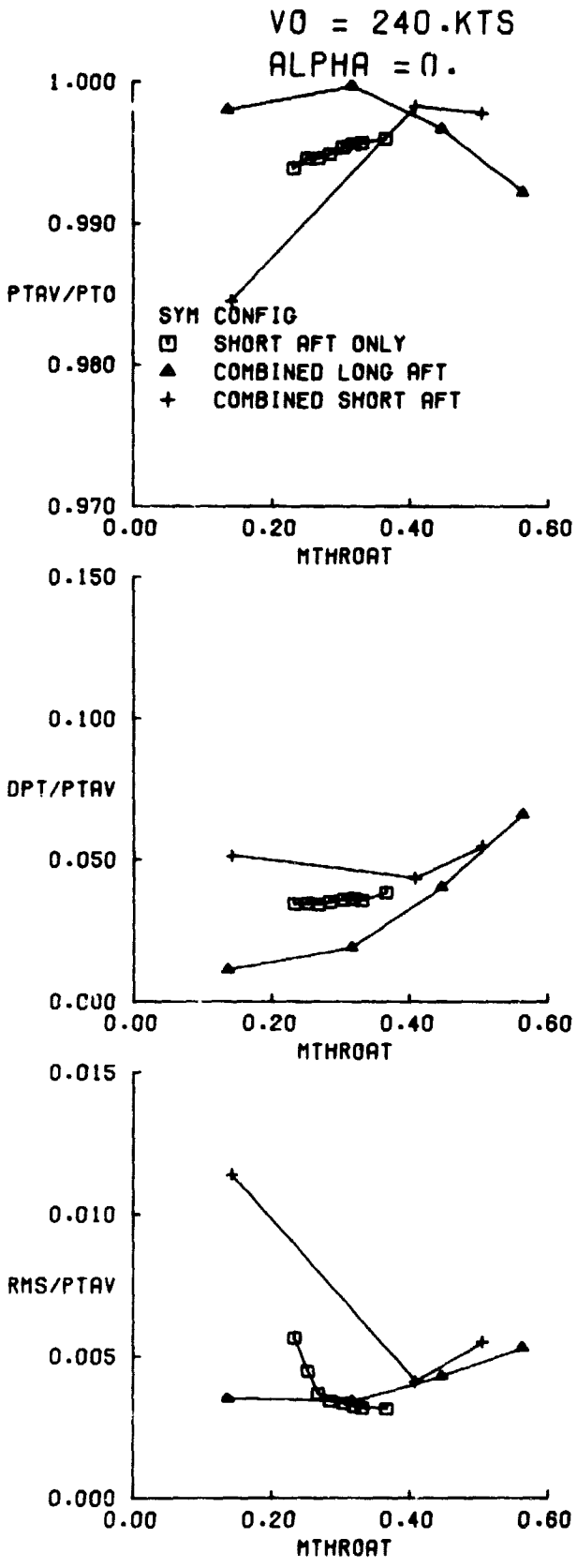

Figure 50. Performance Comparisons at Vo = 240 Knots.

Figure 47 shows configuration comparisons for Vo = 35 knots at α = 0^0 and 40^0. The short aft inlet yields the best performance, even at α = 40^0. Again, the presence of an operating front inlet improves the aft inlet pressure recovery levels. The pressure distortion and turbulence levels are essentially unaffected.

Similar results were obtained at Vo = 85 knots, Figure 48. However, the short aft inlet superiority decreases at high angle-of-attack (α = 40). This aft inlet advantage is completely lost at Vo = 135 knots and α = 40^0, Figure 49, whereas, the α = 0^0 data still show better performance for the short aft inlet.

Figure 50 shows limited configuration comparison data at a cruise condition of 240 knots. No cruise data are available for the clean long aft (isolated) configuration. The combined long aft inlet performance is better than the isolated short aft inlet and also appears to perform better at the lower flow rate. The short aft inlet tends toward separation - lower pressure recovery and higher distortion and turbulence levels - at reduced airflow.

6.3 Crosswind Test Results

The model was mounted on the sting 90^0 from the normal position to simulate a crosswind from the left of the nacelle. Tunnel air velocity was brought to 35 knots. However, secondary circulation in the tunnel, caused by fan exhaust impingement on the solid tunnel walls, prevented a meaningful test. In order to sweep fan exhaust downstream, tunnel air velocity was increased to 120 knots. Severe flow separation at the upwind lip caused fatigue failure of many small total pressure probes. Data from these tests are not published herein, since the aerodynamic conditions of the nacelle were dominated by fan exhaust until unrealistically high crosswind velocities were simulated.

6.4 Combined Pitch and Yaw Test Results

The sting used for mounting the model in the wind tunnel, as illustrated in Figure 17, prevented simultaneous control of both pitch and yaw. To test the effects of combined pitch and yaw, the forward half of the model, containing the front fan and both inlets, was rotated forty-five degrees counterclockwise, viewing downstream in the tunnel. The forty-five

degree angle was dictated by bolt circle spacing. The new position of the model produced a simulated yaw of the nacelle to the left (crosswind component of relative wind was from the right). The pitch and yaw angles were equal, and were calculated simply as the sting angle multiplied by sine (or cosine) of the 45 degree rotation.

The results are presented in Figures 51 through 55. The data in Figures 51, 52, and 53 give aft inlet pressure recovery, distortion, and turbulence levels for three model configurations. These are long aft inlet (01A), short aft inlet (05A), and short aft inlet with nacelle strakes (07). In Figure 51, the performance data are presented as a function of aft inlet throat Mach number, for inlet attitudes from -7^0 to $+30^0$ combined pitch and yaw ($\alpha = \psi$) at a tunnel velocity of 85 knots. The best performance at high attitude angles is achieved by the short aft inlet with strakes. In Figure 52, the performance data are presented as a function of tunnel velocity. The best performance at zero degrees attitude ($\alpha = \psi$) angle is achieved by the short aft inlet. However, as the attitude angle increases, the short aft inlet with strakes performs better. Configuration performance comparisons are shown directly for $\alpha = \psi = 0$ and $\alpha = \psi = 30^0$ in Figure 53. All these data are with both front and aft fans at full speed or $M_{AF} = M_{FF} = 0.6$.

Figure 54 and 55 show aft fan face pressure contours for the three inlet configurations 01A, 05A, and 07. The data of Figure 54 are for zero degrees attitude ($\alpha = \psi = 0$). Only the conditions of 35, 85, and 135 knots tunnel velocity are shown. The presence of the strakes become evident at the higher velocities by the increased low pressure regions at the lower guadrants downstream of the inlet lip corners. The data of Figure 55 are for thirty degrees attitude ($\alpha = \psi = 30^0$). Again only the conditions of 35, 85, and 135 knots tunnel velocity are shown. The direction of the approach velocity vector is denoted in each plot. These fan face plots show that flow separation become severe at the windward corner, while flow improved at the leeward corner.

The test conditions of 30 degrees pitch and 30 degrees yaw are considered unrealistically severe, but valuable for a comparison of model configurations. Fuselage effects are expected to be especially important in this type of airplane operation.

6.5 Fan Blade Vibratory Stresses

Previous experience at LeRC has shown that fan blade vibratory stress is a qualitative, but very sensitive indicator of inlet airflow distortion. Apparently this is true only for fully cantilevered fan blades. The blades of the 12" fans used in this test are supported at the tips by small pins that engage into the tip turbine ring. This method of support suppresses all significant forced vibration of the blades. Strain gage readings (gages were mounted near the root of several fan blades) remained low and independent of distortion levels of the inlet, despite severe levels. The need for mid-span supports on the airplane fan blades could not be estimated, based on these results. A scale model fan is recommended for this purpose.

6.6 Nacelle Strakes

As indicated in the section 6.2.3, the short inlet required improvement near the corners in order to extend the good performance into a wider range of airspeed and angle-of-attack. Horizontal strakes were installed about 5 cm below the corners of the short aft inlet in order to block the high velocity local flow at the corners. The strakes were triangular pieces of 1-1/2 mm thick stainless steel sheet metal, resembling sharply swept-back delta wings, and were 15 cm wide by 36 cm long. These were tested at various conditions of airspeed and angle-of-attack. Plots comparing the strake effects with the basic short inlet are shown in Figures 51 to 55. Improvement, especially in distortion values are noticeable at the higher angles-of-attack. At lower angles, the strakes are slightly detrimental.

6.7 Lip and Throat Static Pressure Distributions

Figures 56 and 57 show comparisons of the static pressure circumferential distributions at the inlet lip and throat plane. Comparisons are presented between the clean long aft inlet, the clean short aft inlet, the short aft inlet with fillets, and the short aft inlet with strakes at nearly identical flow conditions - both front and aft fans at full speed. Figure 56 includes data at $\alpha = 0^0$ for forward speeds of 0, 35, 85, and 135 knots. Figure 57 includes data at $\alpha = 40^0$ for forward speeds of 35, 85, and 135 knots. The data are presented as the ratio of the local static pressure to

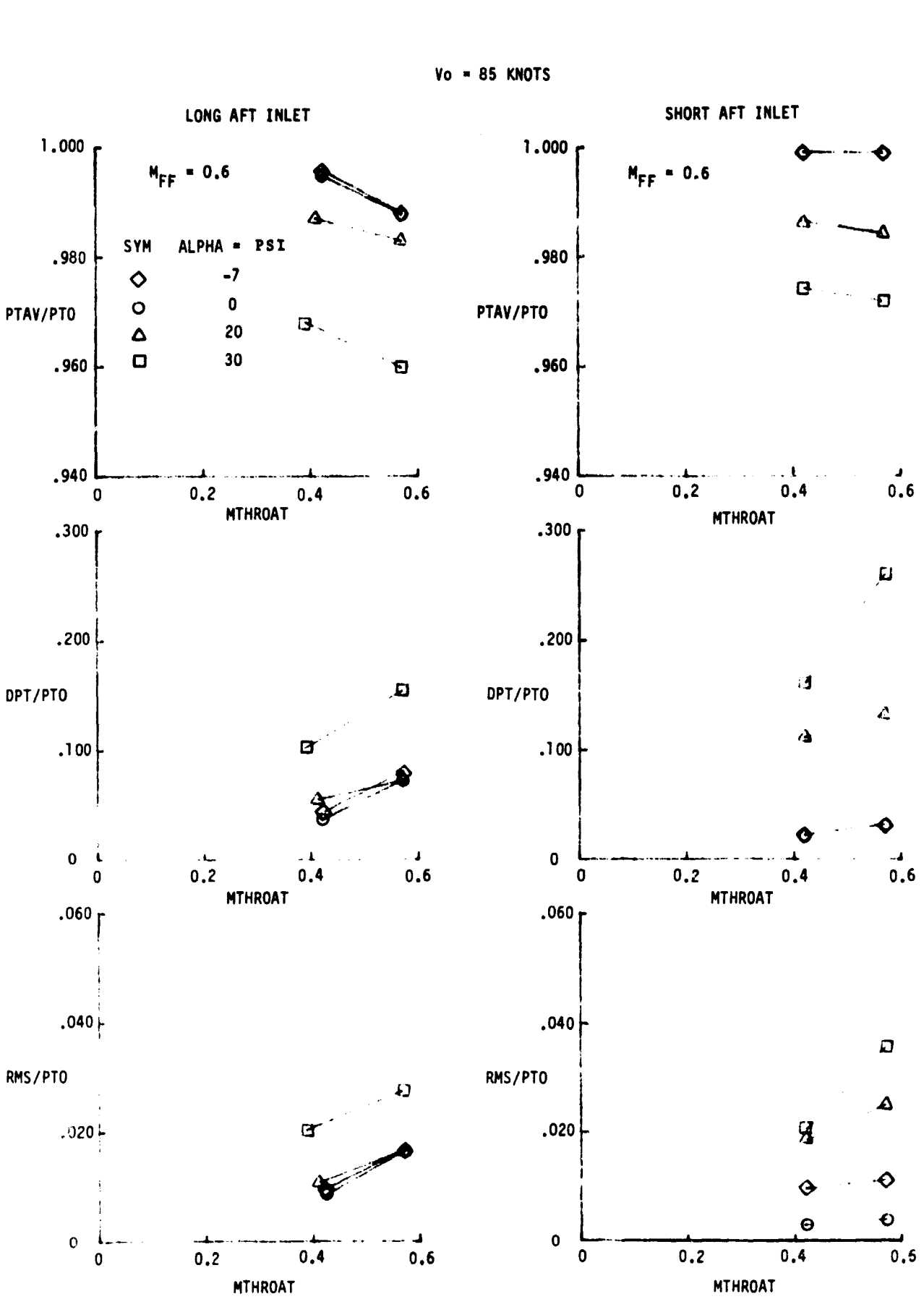

FIGURE 51A. AFT INLET PERFORMANCE IN COMBINED PITCH AND YAW, FLOW RATE EFFECT

Vo = 85 KNOTS

SHORT AFT INLET WITH STRAKES

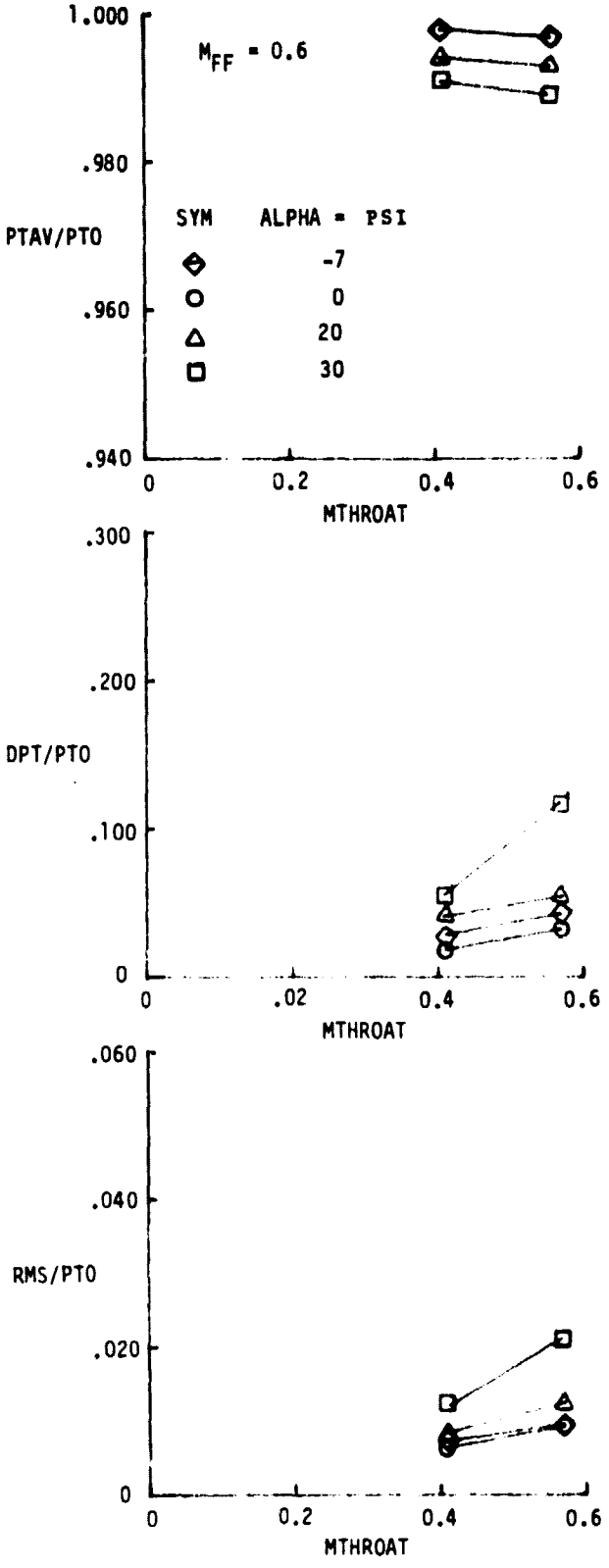

FIGURE 51B. AFT INLET PERFORMANCE IN COMBINED PITCH AND YAW, FLOW RATE EFFECT

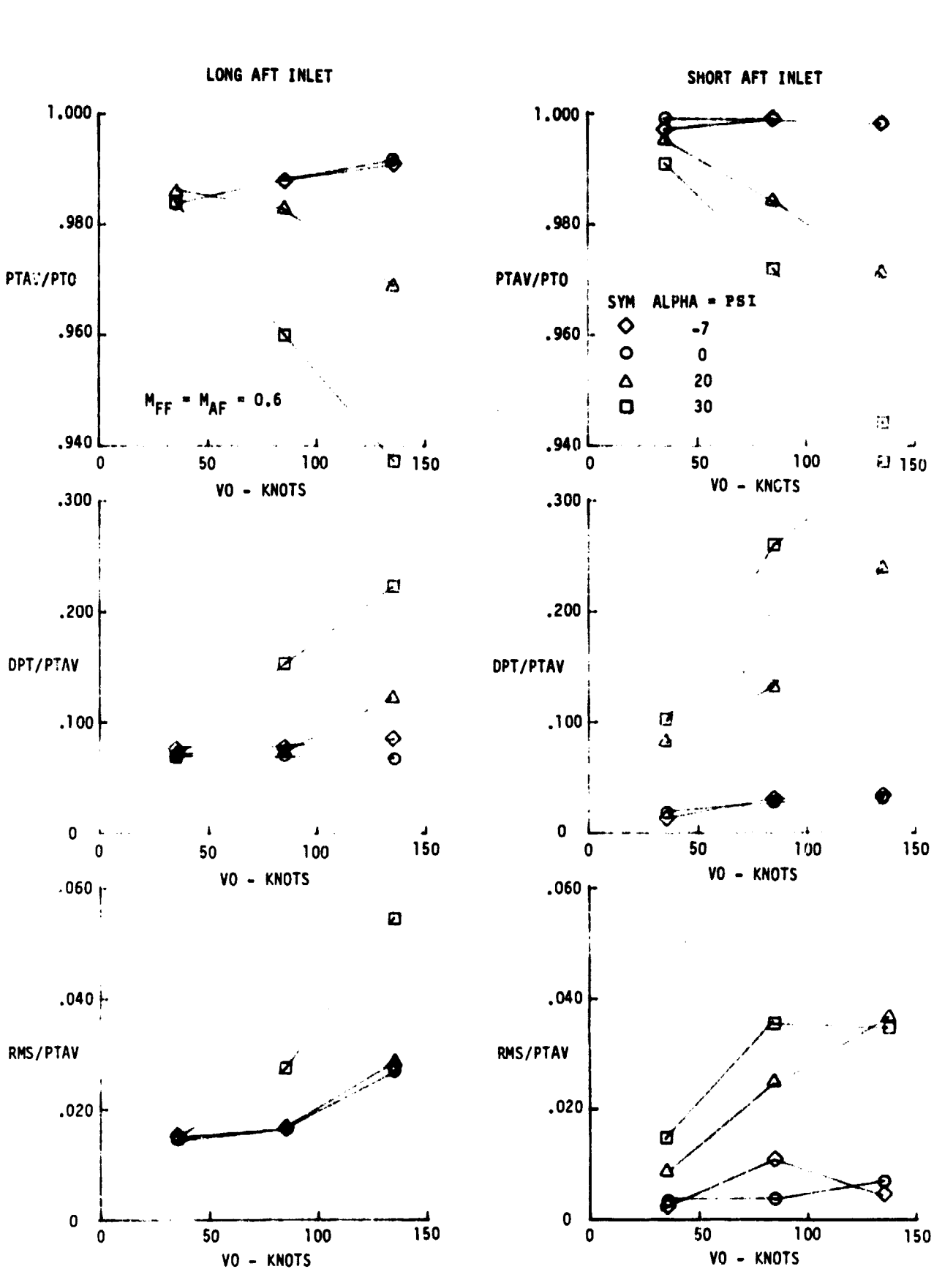

FIGURE 52A. AFT INLET PERFORMANCE IN COMBINED PITCH AND YAW, FREESTREAM VELOCITY EFFECT

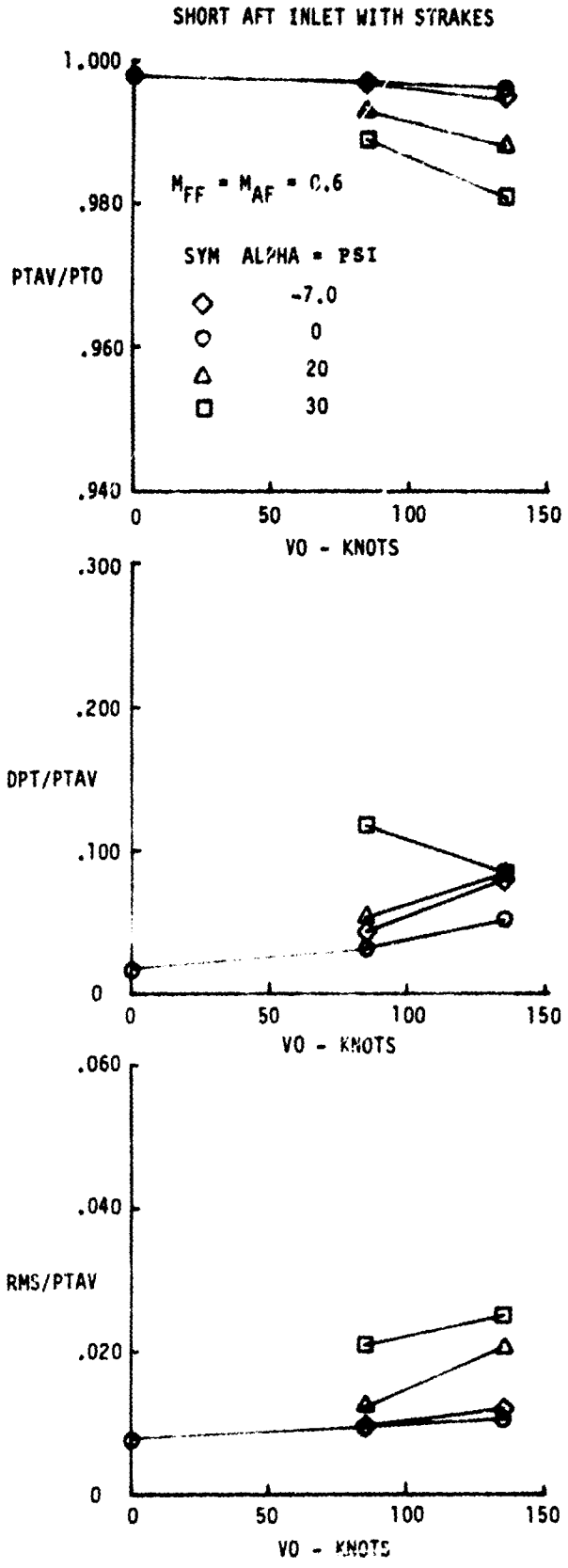

FIGURE 52B. AFT INLET PERFORMANCE IN COMBINED PITCH AND YAW, FREESTREAM VELOCITY EFFECT

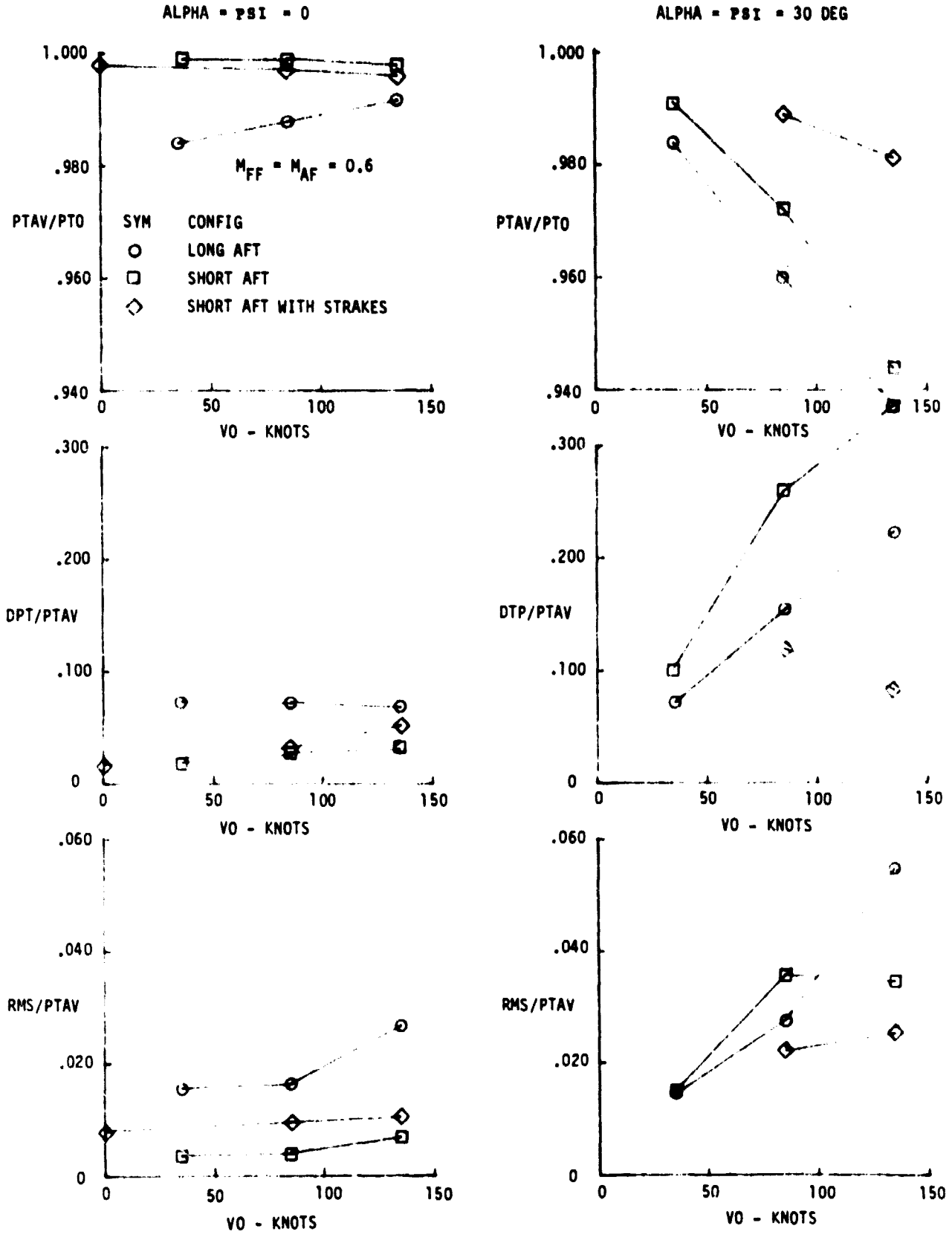

FIGURE 53. AFT INLET PERFORMANCE COMPARISONS IN COMBINED PITCH AND YAW

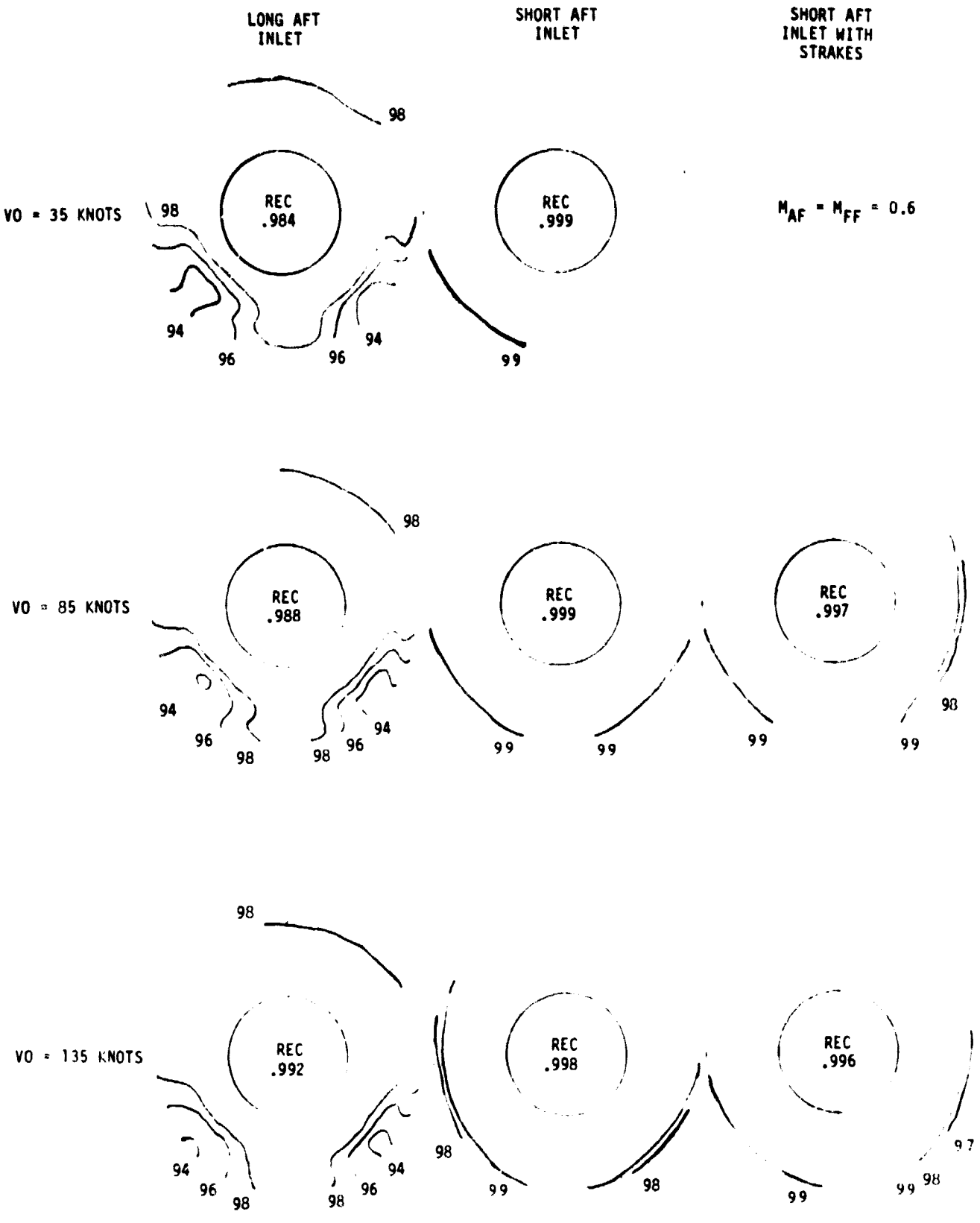

FIGURE 54. FAN FACE PRESSURE CONTOURS, CONFIGURATION COMPARISONS AT ZERO DEGREES ANGLE OF ATTACK

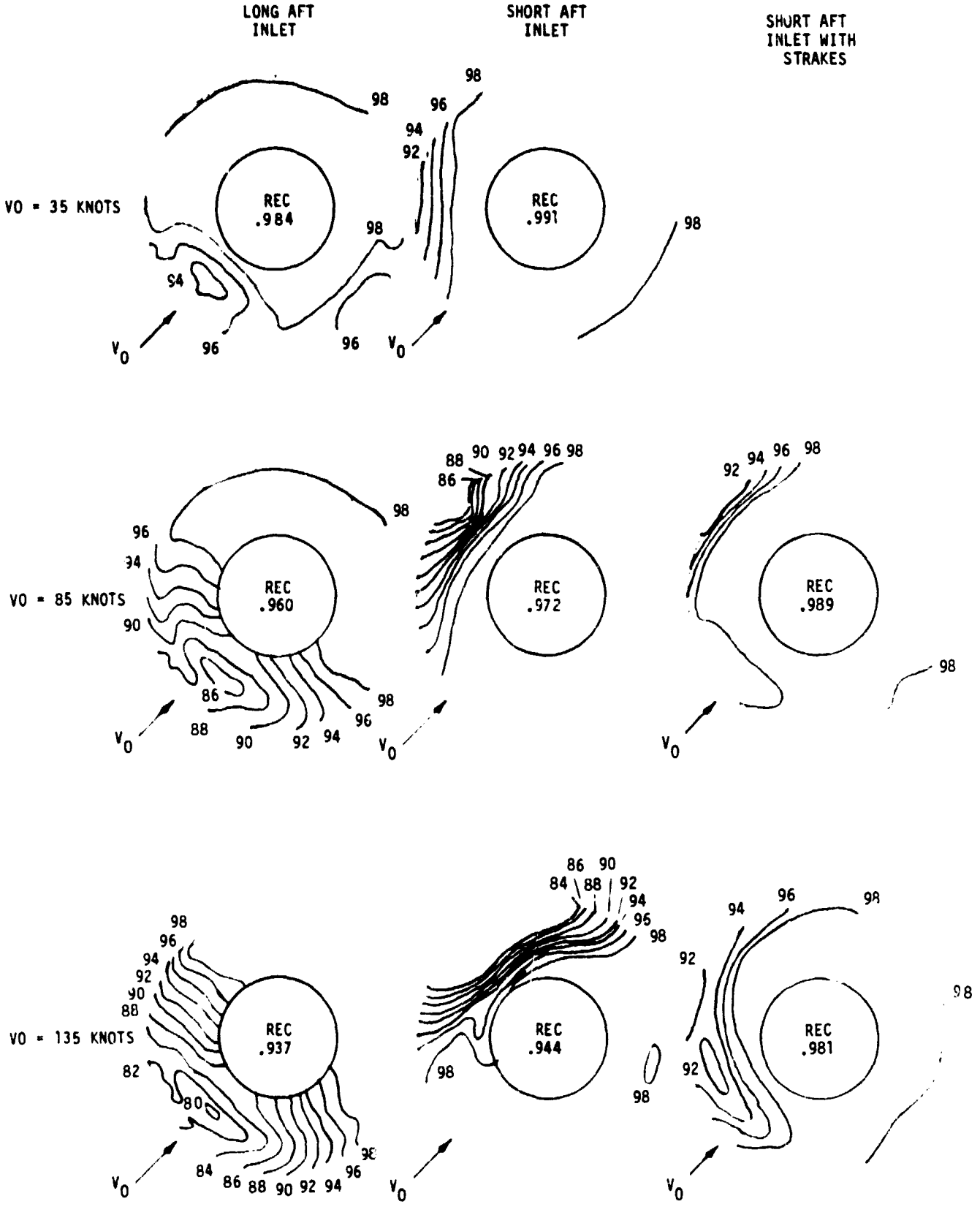

FIGURE 55. FAN FACE PRESSURE CONTOURS, CONFIGURATION COMPARISONS AT COMBINED PITCH AND YAW ($\alpha = \psi = 30^0$)

the freestream total pressure plotted as a function of the angle measured clockwise from the top of the inlet as shown in the inset in Figures 56 and 57. The static pressure data for each condition include distributions along the inlet lip inlite and the inlet throat. At $\alpha_i = 0^\circ$, the long aft inlet throat pressure distributions remain essentially unchanged. The highest lip loading occurs on the side lip ($\theta = 90^\circ$). The short aft inlet data, however, indicate that highest lip loading occurs further inboard. The lip loading for the long aft inlet is generally higher due to it having a lesser lip thickness.

6.0 Flow Visualization

To better understand the local flow pattern at the corners of the short aft inlet, two methods of flow visualization were used for several brief test runs. These results are discussed in Appendix A.

7.0 Conclusions and Recommendations

An approximately 0.25 scale model of Tandem Fan nacelle inlets designed for a U.S. Navy Type A (Subsonic Cruise) V/STOL aircraft configuration was tested in the NASA Lewis Research Center 10-by-10 foot (3.048 by 3.048 meter) wind tunnel. Twelve-inch (30.48 cm) tip driven turbofan simulators were used to provide the suction source for both the front and aft fan inlets. Model variables consisted of a long aft inlet cowl, a short aft inlet cowl, a front fan shaft simulator, diffuser vortex generators, short inlet lip corner fillets, and short inlet nacelle strake. Also, the model was mounted vertically in the tunnel to simulate crosswind conditions. Inlet pressure recovery, distortion, and inlet angle-of-attack limits were evaluated at tunnel velocities from 0 to 260 knots (0 to 133.5 m/s), angles-of-attack from -10 to 40 degrees and inlet flow rates from windmilling to thrust. Mach number of 0.6.

High inlet performance and stable operation were verified at all design forward speed and angle-of-attack conditions. The interface effects of an operating front inlet are beneficial to the aft inlet performance. The following conclusions can be made for the combined inlet tests:

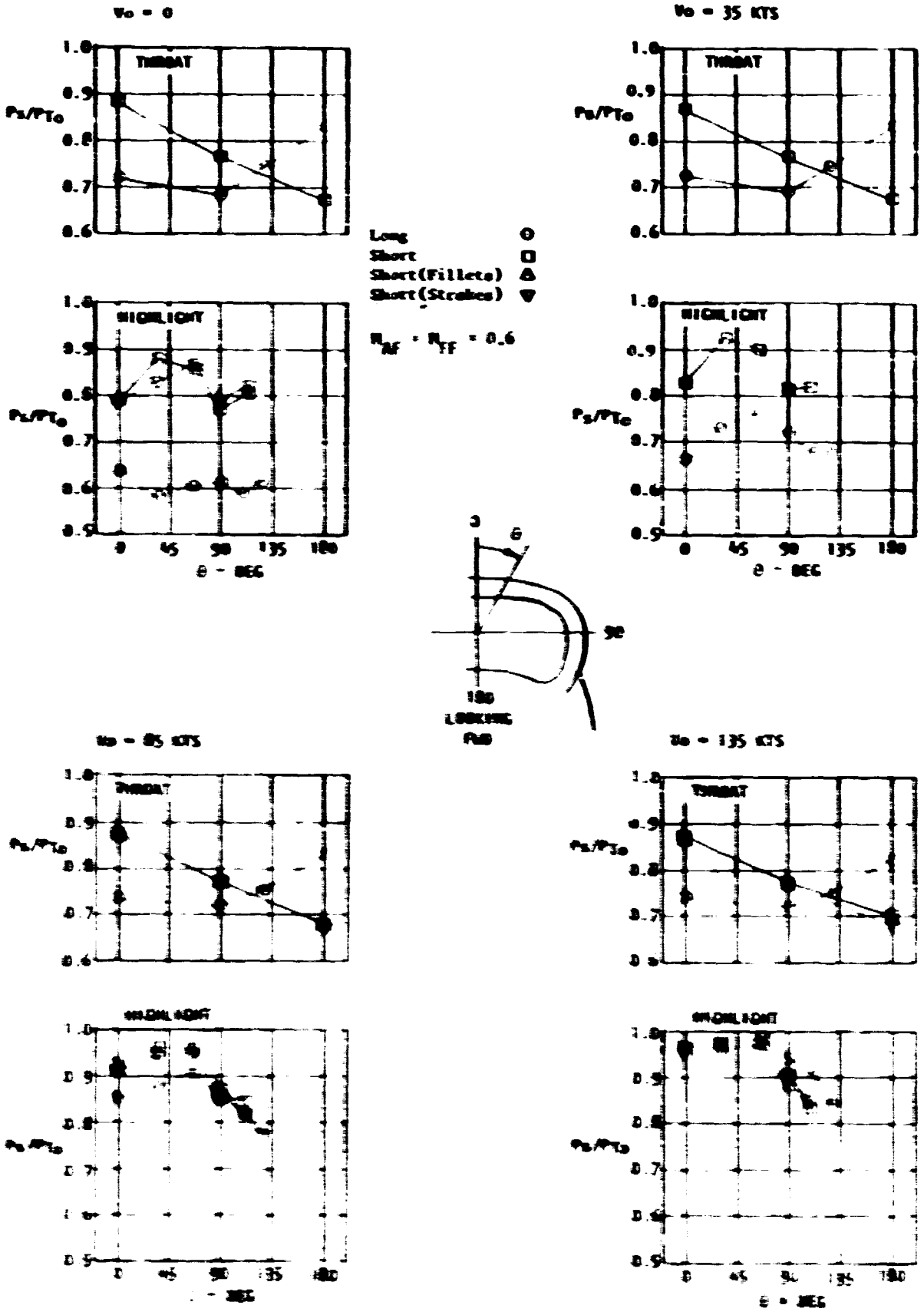
Vo = 0
Vo = 35 KTS
THROAT
HIGHLIGHT
Ps/Pto
θ - DEG
Long
Short
Short(Fillets)
Short(Strakes)
RAF = RFF = 0.6
LOOKING AFT
Vo = 85 KTS
Vo = 135 KTS

[illegible]

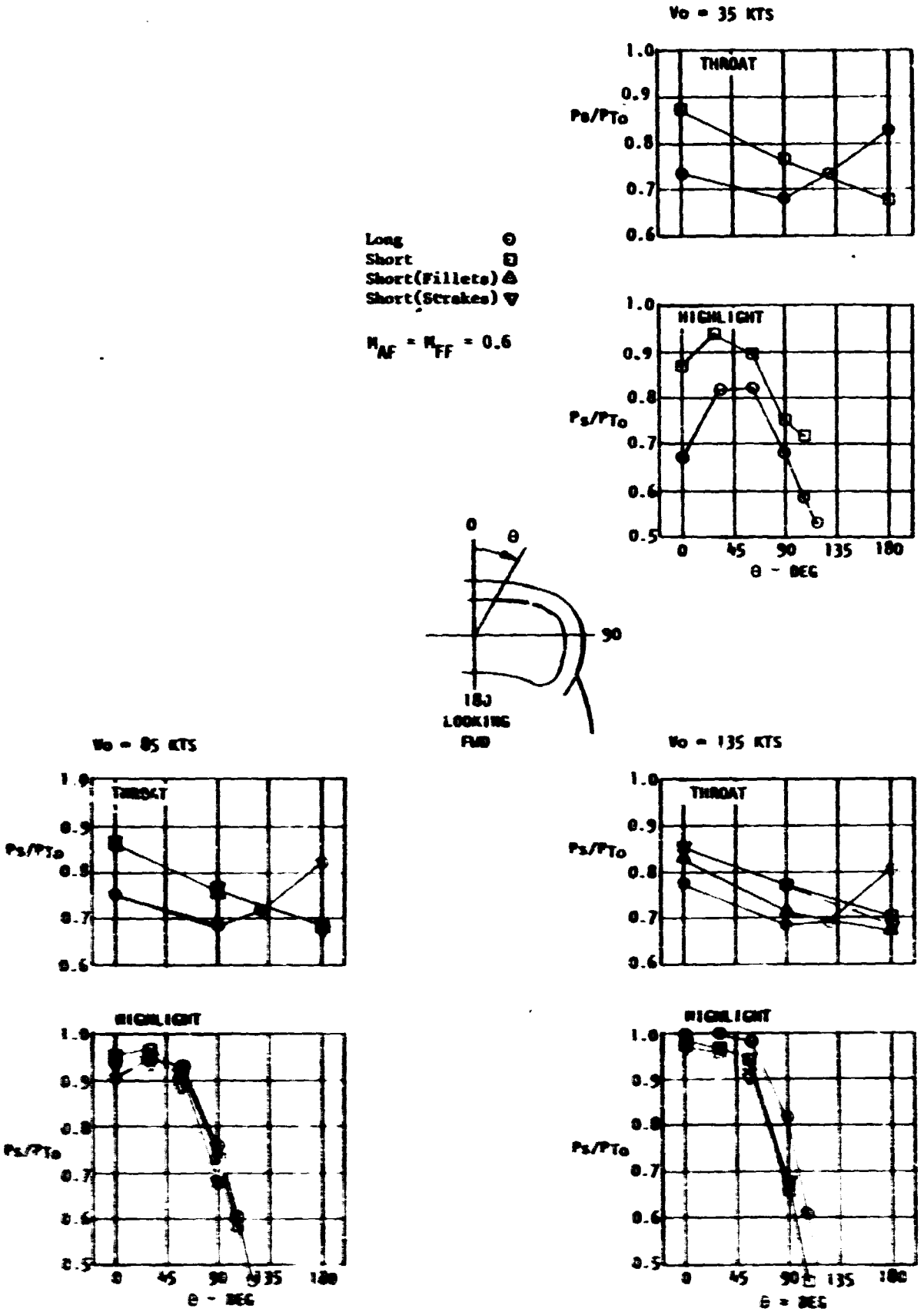

FIGURE 57. INLET CIRCUMFERENTIAL STATIC PRESSURE COMPARISONS, α = 40°

- Long aft inlet total pressure recovery is consistently around 99 per cent with distortion levels of less the 7 per cent.

- With the vortex generators and front fan shaft simulator, the long aft inlet pressure recovery is 98 per cent and distortion is approximately 7 per cent.

- The short aft inlet total pressure recovery is greater than 99 per cent except at Vo = 135 knots and α = 30 and 40 degrees. Distortion levels are less than 5 per cent except at Vo = 135 knots and $\alpha = 40^{0}$.

- With the corner fillets in place, the short aft inlet recovery decreases slightly with increasing forward speed and angle-of-attack.

- The crosswind part of the test was inconclusive because the nacelle recirculated flow interfered with the test section freestream conditions.

- The combined pitch and yaw results indicate that the windward side tends to separate while the leeward side flow tends to be improved.

- The fan blade vibrating stress portion of the test was also inconclusive because the twelve-inch fan model blades are supported on an outer ring also.

For the design conditions of speed and attitude, the Tandem Fan Nacelle inlets yield very good performance levels.

Based on the results of this test, it is recommended that the performance of the Tandem Fan nacelle inlets (especially the short aft inlet) be evaluated in a total nacelle model (including nozzles). Also, it is recommended that performance of the tandem fan nacelle be evaluated at vehicle cruise speeds.

REFERENCES

1. NASA Contract NAS3-21468, "Inlet Development for a Tandem Fan Propulsion System", 27 June, 1978.

2. "Low Speed Test of the Aft Inlet Designed for a Tandem FAn V/STOL Nacelle", W. W. Rhoades and A. H. Ybarra, NASA CR-159752 (Vought Technical Report 2-30320/0R-52360), February 1980.

3. "Effect of Entry-Lip Design on Aerodymanic and Acoustics of High-Throat-Mach Number Inlets for the Quiet, Clean, Short Haul Experimental Engine", NASA TMX-3222, B. A. Miller, May 1975.

4. "The Engine Inlet on the 747", ASME 69-GT-41, W. S. Viall, March 1969.

5. "Inlet Development for the L-500", J. P. Hancock, B. L. Hinson, AIAA 69-448.

6. "Experimental Optimization of Subsonic Inlet Design Parameters", A. H. Kraig, D. L. Motycka, B. J. Stewart, AIAA 66-690.

7. "A Combined Potential and Viscous Flow Solution for V/STOL Engine Inlets", A. H. Ybarra, W. W. Rhoades, N. O. Stockman, AIAA paper 78-142, January 1978.

8. "Design Report Model 1109-A 12-inch Tip-Turbine Fan TR77-101, Revision A", G. Linsker, Tech Development Incorporated TD-1109M, 4 February 1977.

9. "Fortran Program to Generate Engine Inlet Flow Contour Maps and Distortion Parameters", NASA TMX 2967, J. H. Dicus, February 1974.

10. "Flow-Direction Measurement with Fixed-Position Probes" NASA TMX-1904, T. J. Dudzinski and L. N. Krause, 1969.

APPENDIX A

Flow Visualization Studies

To better understand the local flow pattern at the corners of the short aft inlet, two methods of flow visualization were used for several short tests. The methods were paint streaks and tufts.

Artists oil pigments were mixed with penetrating oil to obtain a viscosity just high enough to ensure no flow under gravity forces alone. A number of paint spots were daubed on the model. Tunnel and fans were brought up to speed simultaneously at fixed angles of pitch and yaw. Tunnel and fans were operated for ten minutes, then shutdown, and still photographs were taken.

Three typical paint streak photographs are shown in Figure A-1, A-2, and A-3.

Figure A-1 shows paint patterns on and inside the short aft inlet after a test at 80 knots and 40 degrees angle-of-attack. Flow reversal is indicated just inside the corner. The higher surface velocities just ahead of the corner can also be visualized.

Figure A-2 was taken after identical test conditions, but with strakes installed. Note the lack of flow reversal inside the inlet corners. Small areas of flow separation (paint free areas) are visible inside the inlet sides. A strong vortex existed about 4 cm behind the strake trailing edge, another at the strake leading edge. Surface flow on top of the strake is forwards and outwards.

Figure A-3 shows the effects of 30^{0} combined pitch and yaw. Note the large area of separated flow (paint free area) just inside the upwind corner. At the nearer, downwind corner, surface velocities were low and flow spearation did not occur.

Tuft studies were conducted at a large variety of test conditions. The tufts illustrated flow direction and steadiness. Information was recorded on video cassette for later viewing. The informaion helped locate the strakes and provided helpful insights into the exterior and interior aerodynamic interactions.

Figure A1. - Paint streak patterns on short aft inlet after operation at 85 knots and 40° angle-of-attack, full fan speed.

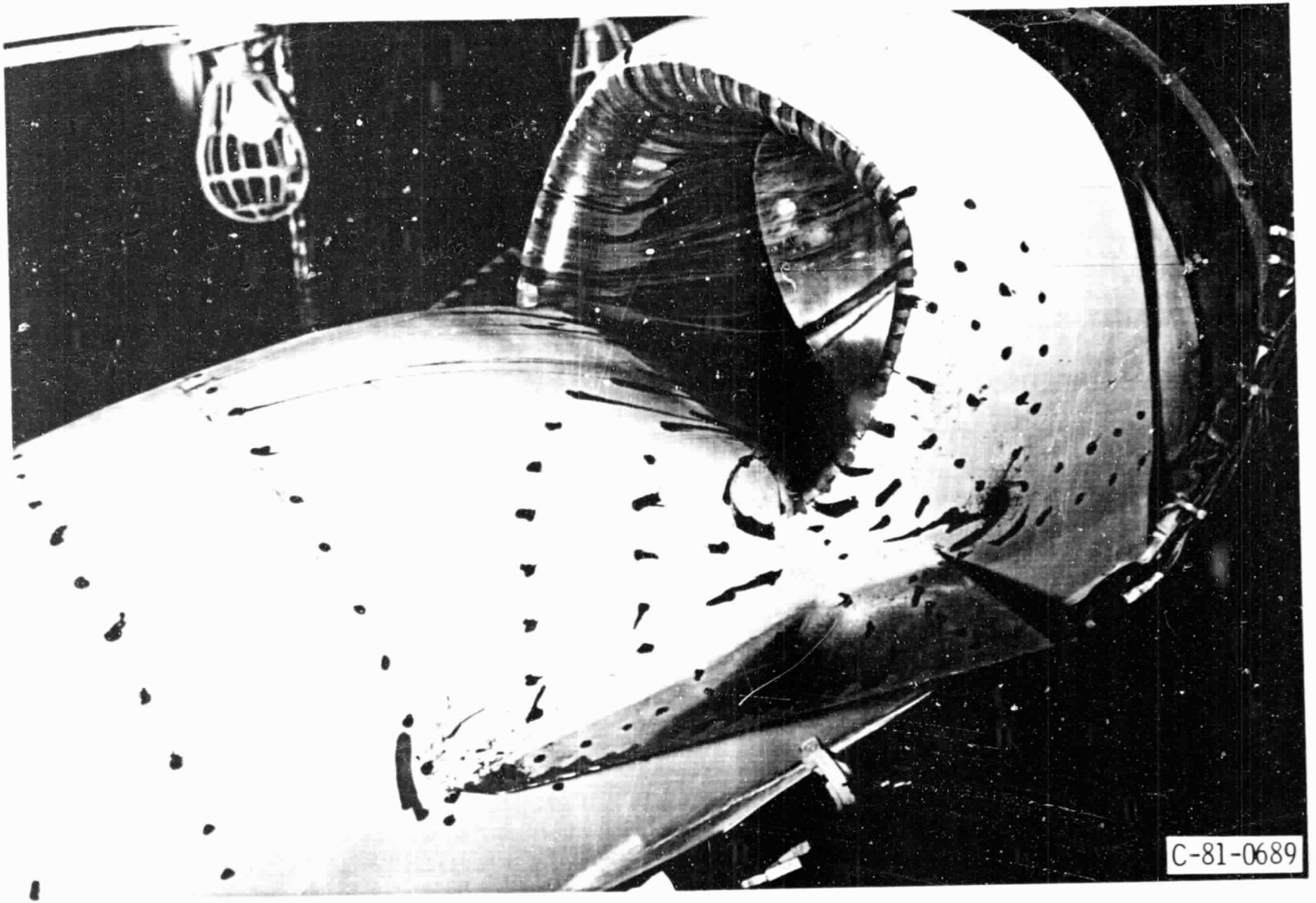

Figure A2. - Paint streak patterns on short aft inlet showing the effects of nacelle strakes. 85 knots and 40^{0} angle-of-attack.

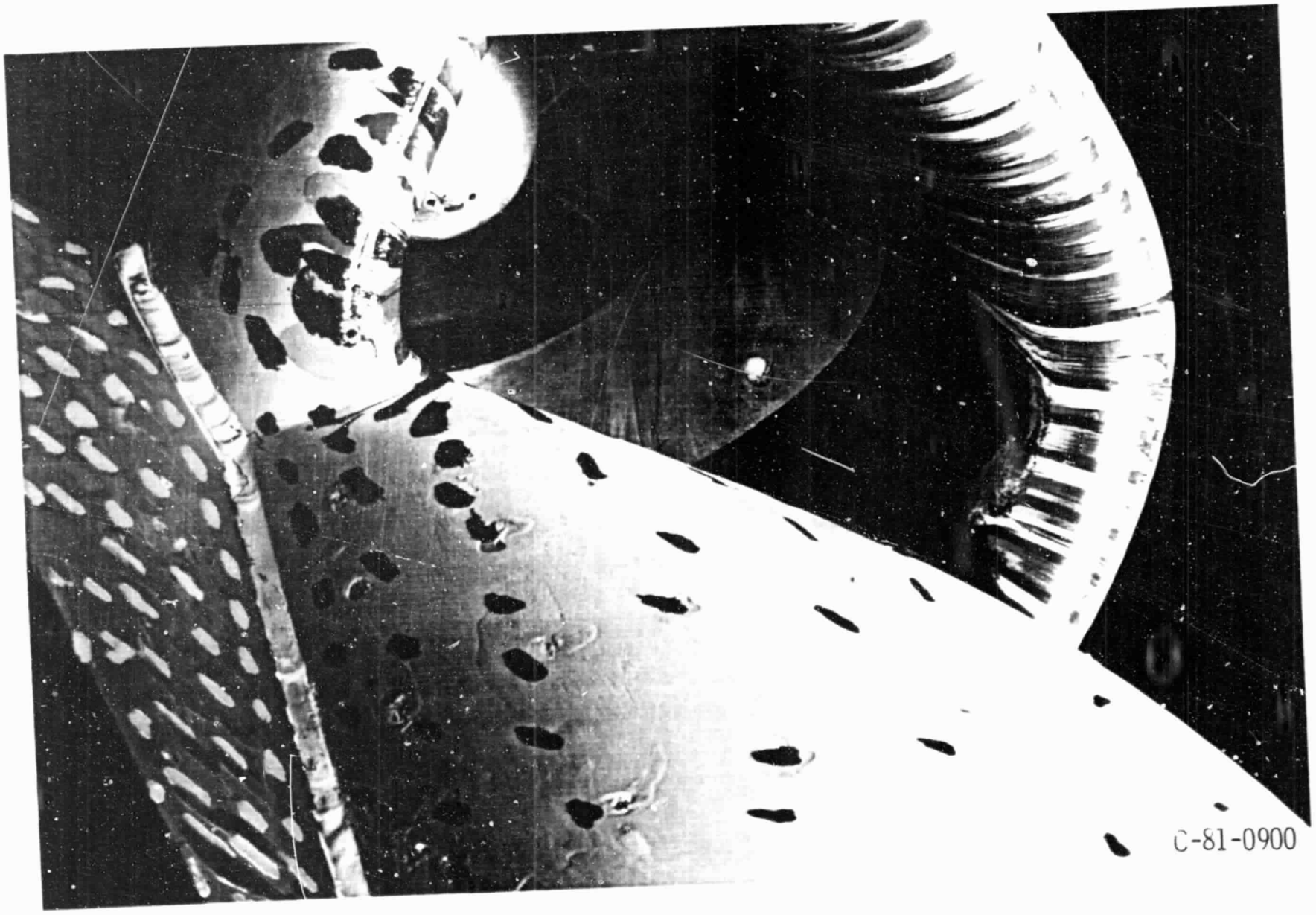

Figure A3. - Paint streak patterns on short aft inlet with nacelle strakes. Combined 30^{o} pitch and 30^{o} yaw at 85 knots. Far side of inlet was upwind.